USE OF ERI TO FIND THE SOURCE OF SALINE

IMPACTS IN EDMOND, OKLAHOMA

By

EMIKO KONISHI

Bachelor of Science in Geology

Oklahoma State University

Stillwater, Oklahoma

2004

Submitted to the Faculty of the
Graduate College of the
Oklahoma State University
in partial fulfillment of
the requirements for
the Degree of
MASTER OF SCIENCE
December, 2007

USE OF ERI TO FIND THE SOURCE OF SALINE

IMPACTS IN EDMOND, OKLAHOMA

Thesis Approved:

Dr. Todd Halihan

Thesis Adviser

Dr. James Puckette

Dr. Alex Simms

Dr. A. Gordon Emslie

Dean of the Graduate College

ACKNOWLEDGEMENTS

support through it all. His positive attitude and confidence in me always encouraged me

to accomplish this thesis.

TABLE OF CONTENTS

LIST OF TABLES

LIST OF FIGURES

LIST OF PLATES

CHAPTER I

INTRODUCTION

Large parts of the city of Edmond were in the past and are presently occupied by

oilfields. Because of the rapid growth of the city, the utilization of lands changed rapidly.

The change in the land use from petroleum production to residential use was a possible

cause of negative impacts on ground water in the residential areas. This thesis is a part of

a series of investigations conducted by Ground Water Protection Council, the Association

of Central Oklahoma Governments, and Oklahoma State University to assess the

relationship between ground water contaminations and previous and/or present oilfield

activities in Edmond, Oklahoma.

Problem Statement

The City of Edmond, Oklahoma has a history of petroleum exploration with two

prominent oilfields. The first petroleum field was the Edmond Field, which was

discovered in 1930 (GWPC, 2005) and the West Edmond Field was discovered in April

1943 (Swesnik, 1952). While these petroleum fields were profitable for the city growth,

they also brought negative impacts by producing large amounts of brine as a production

byproduct. At that time, some brine was disposed in surface saltwater evaporation pits.

After major production declined in these production areas, these properties were rapidly replaced mainly by residential and commercial areas with the rapid development of the city and the increase of population. Ground water problems were recognized in the Thunderhead Hills Addition and its neighborhoods. The private domestic water wells in the area are impacted with chlorides. Although the source(s) of brine contamination have not been verified, the previous and/or present oilfield activities are one suspected source(s) of the high chloride concentrations in those water wells in the Thunderhead Hills Addition and its surrounding.

Location of Study Area

The City of Edmond is located in Oklahoma County, Oklahoma in the central part of the state (Figure 1.1). A series of surveys was conducted at the central part of the city, within Section 29, and 32 of Township 14 North, Range 2 West in Oklahoma County, Oklahoma. This study especially focuses on the Thunderhead Hills Addition and its surrounding areas since salt water contamination has been found in several private water wells in the area.
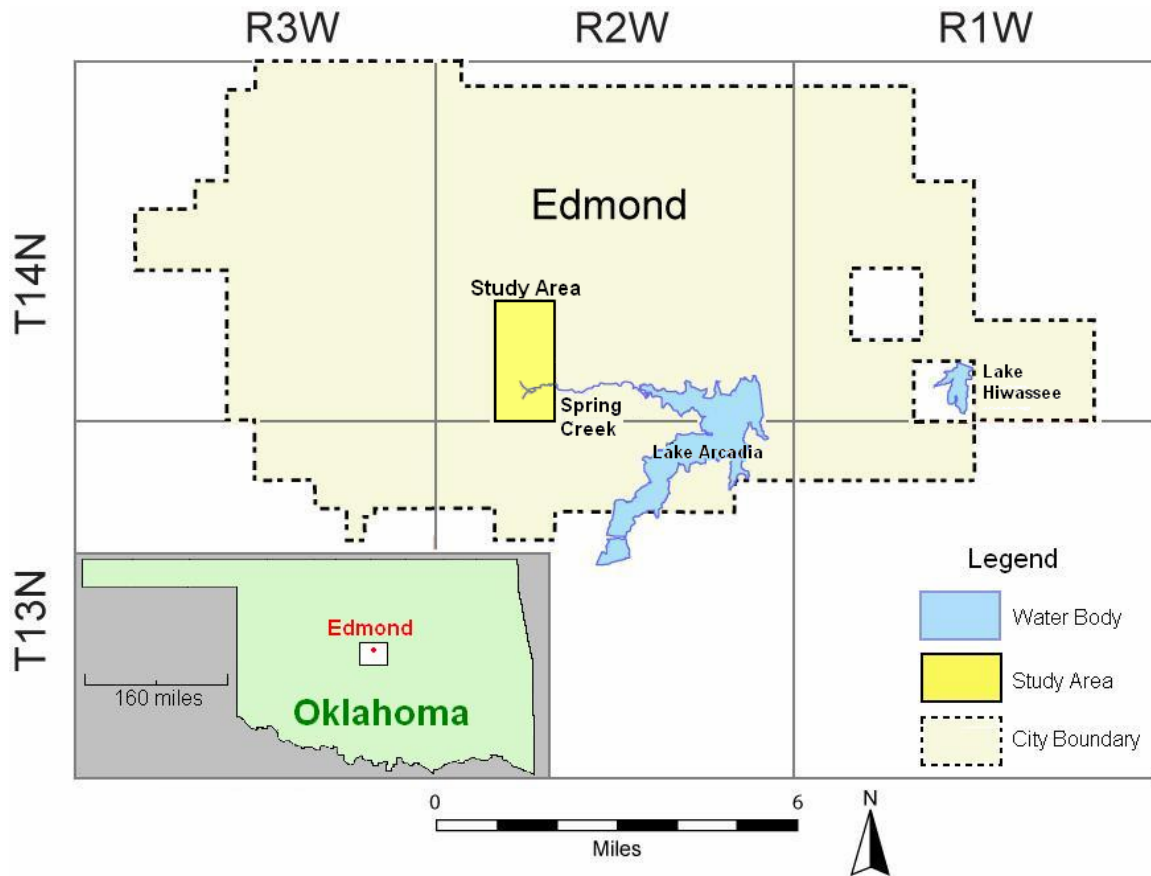
Figure1.1: Location Map of Study Area
A series of ERI surveys was conducted at the central part of the city, within Section 29, and 32 of Township 14 North, Range 2 West in Oklahoma County, Oklahoma.

Purpose and Objectives of Investigation

The main purpose of this study is to determine how efficiently advanced electrical resistivity imaging (ERI) techniques can delineate the extent and cause of ground water impacted by previous and/or present oil field activities, specifically surface saltwater disposal pits and the piping that is used as part of these systems. The project will be conducted by collecting and analyzing ERI data collected as multielectrode surface surveys. The main objectives of study are the following:

1. Delineating the extent of salt water contamination at depths of up to 60 meters (200 feet) using the ERI method. The ERI surveys provide an ability to visualize

the vertical and horizontal coverage of a saltwater plume by measuring resistivity differences in the subsurface.

2. Generating two dimensional electrical resistivity forward models using AGI EarthImager 2D^{TM}. The forward models will aid to distinguish the resistivity images that are influenced by underground utilities and/or petroleum pipes generating electrical noise, the resistivity images that are influenced by old petroleum pipe(s) with leaking brine, and the resistivity images that are influenced by brine in isolation.

Hypothesis

As stated previously, the primary purpose of the study is to determine the efficiency of advanced ERI techniques using combination of field data and 2D resistivity models to delineate the area of ground water brine intrusion, which may be caused by previous and/or active petroleum activities. The ERI surveys took place in urban area with multiple utility lines. Several active and abandoned petroleum pipe lines are buried near the survey lines besides the utility lines. These underground objects can affect ERI interpretation. To provide a scientific framework appropriately interpret the presence of pipe lines and their status as competent or leaking, the following hypothesis was tested:

Pipe interference in ERI images can be quantified through forward modeling and applied to field data through a-priori inversion modeling to evaluate the effect of pipes to determine if they were leaking.

The forward models are employed to determine anticipated pipe patterns in ERI datasets. A pipe(s) will be arranged in several ways to examine the electrical resistivity

4

behaviors in different scenarios. The results of the forward models will be applied into the a-prior inversion models of actual field data with known and unknown pipe locations.

Limitations of Study

The limitations of this study mainly occur due to the field accessibility, the field barriers, and the electrical resistivity data with depth. The failure of the field accessibility arises from landowners limiting property access. The rearrangement of the survey lines frequently occurs on account of natural or anthropogenic barriers such as houses, fences, and dense forests. In addition to the field constraints, subsurface geological conditions cause difficulties in interpreting the field data. Those drawbacks occur under the following circumstances:

(1)   if the top soil is very conductive, and any deeper salt signals are very weak.

(2)   and if the top layer is very resistive, and any deeper salt signals are very weak

In this particular study site, situation two seems to be a typical problem due to the extremely dry and resistive soil in the study area.

CHAPTER II

REVIEW OF LITERATURE

As stated previously, the main purpose of the study is to determine the efficiency of advanced ERI techniques to delineate the extent of ground water impacted by previous and/or present oil field activities in the presence of obvious metallic interference. Knowledge of the regional geology and hydrogeology is necessary since the local geologic conditions can influence the electrical resistivity properties and its interpretations. It is also important to be familiar with basic resistivity theory before performing and interpreting ERI. Numerous investigations that applied ERI surveys to the study of salinity problems have been conducted. Evaluation of these previous investigations will aid in understanding different hypotheses that exist. Therefore, the purpose of this chapter is to improve the range of knowledge and ideas by analyzing prior research studies and theoretical articles.

Regional Geology and Hydrogeology

The rocks exposed in the Central Oklahoma consist of consolidated Permian sedimentary rocks and unconsolidated Quaternary alluvium and terrace deposits. The Permian sedimentary rocks of the Central Oklahoma include siltstones, sandstones, and shales (Christenson and Havens, 1998; Edwards, 1992; Wood and Burton, 1968). The Quaternary alluvial and terrace deposits overlying the Permian units contain lenses of

clay, silt, sand, and gravel (Christenson and Havens, 1998; Edwards, 1992; Wood and Burton, 1968).

The geologic units cropped out within the ERI survey area are Quaternary alluvial deposits and the Permian Garber Sandstone. In addition to the two significant geologic units within the survey area, basic features of four stratigraphic units exposed at the surface adjacent to the study area will be presented briefly. In ascending order, the four stratigraphic units exposed at the surface adjacent to the study area are: Wellington Formation, Garber Sandstone, Hennessey Group, and alluvial and terrace deposits. Due to the similarity in their lithological characteristics, the Garber Sandstone and Wellington Formation can be interpreted as one single unit, the Garber-Wellington (Edwards, 1992; Roberts and Spitz, 2001; Wood and Burton, 1968).
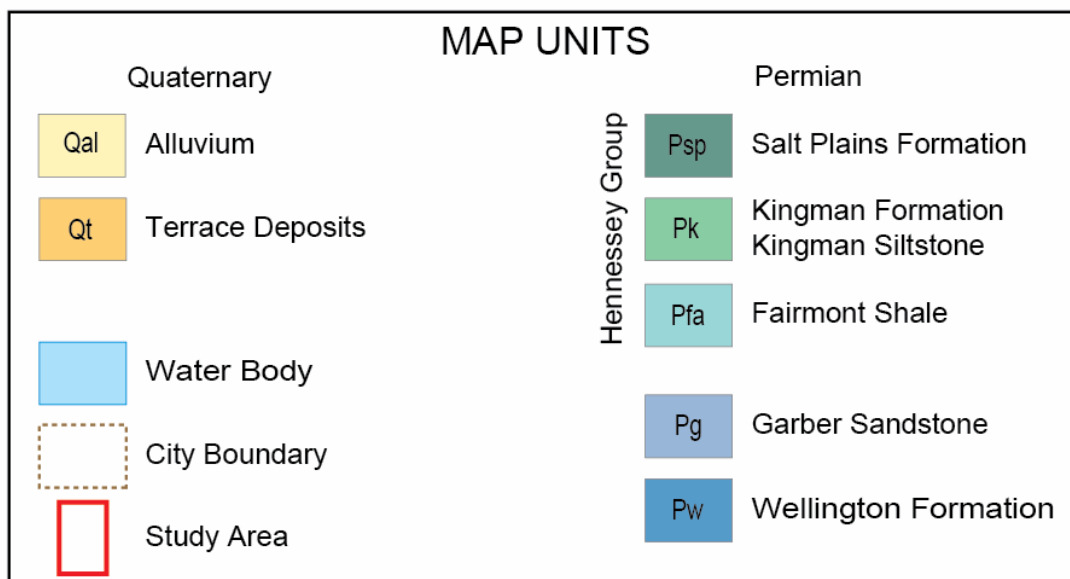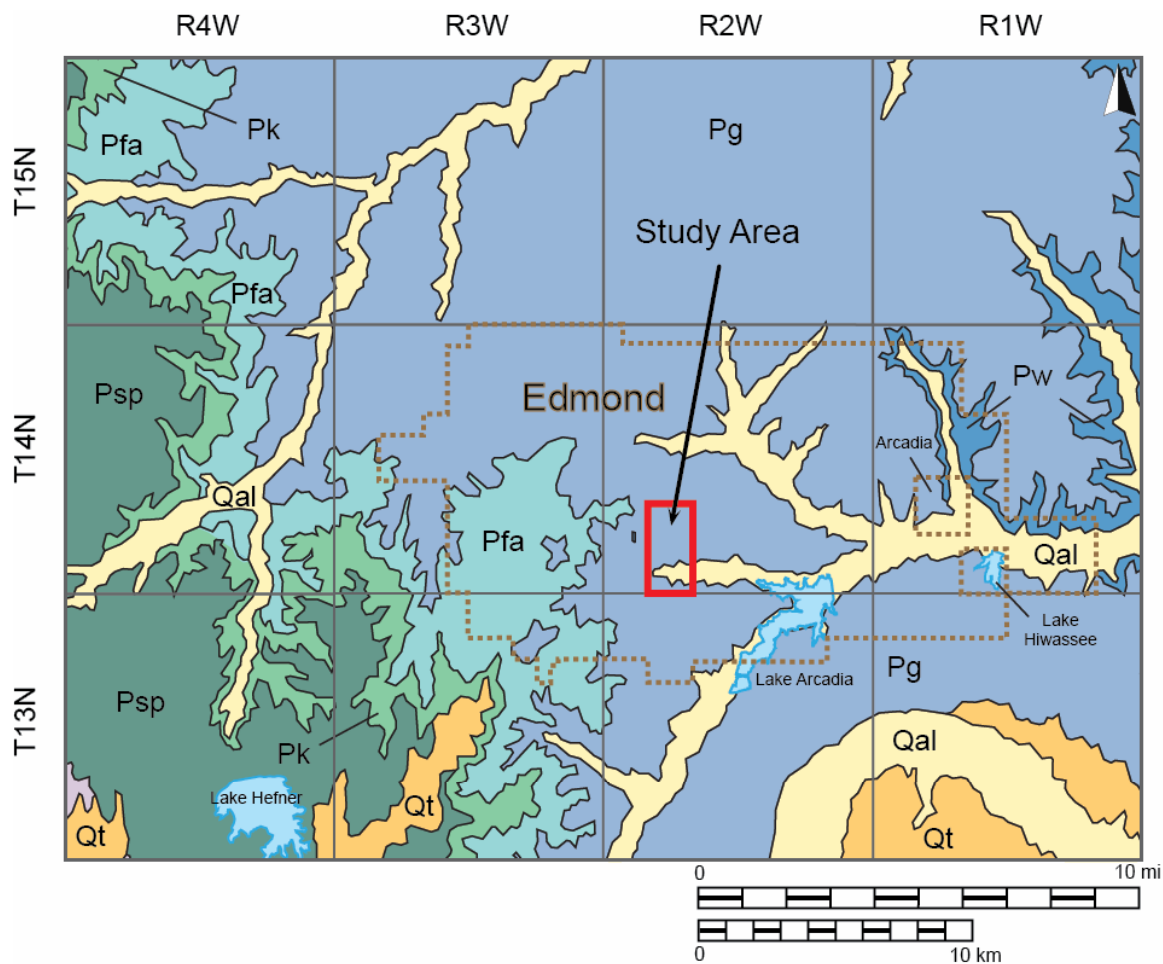
Figure 2.1: Geologic Map of Study Area (after USGS 1998)

<u>Permian Rocks</u>

The Permian rocks are the oldest exposed rocks in the study area. The Permian rocks are characterized by predominantly red-colored, lenticular beds of fine-grained, cross-bedded sandstone interbedded with siltstone and mudstone (Christenson and Havens, 1998; Wood and Burton, 1968). Their depositional environment represents a fluvial-deltaic environment, and the lithological variations within distances are significant (Christenson and Havens, 1998).

Garber Sandstone and Wellington Formation

The Garber Sandstone is the predominant exposed geologic unit within the study area, Section 29 and 32-T14N-R2WIM, Oklahoma County, Oklahoma (Figure 2.1). The Garber Sandstone and the Wellington Formation are oriented in a north-south direction from north of Logan County to Cleveland County and range 6 to 20 miles wide east to west. Although the bed thicknesses of 1.5 m (5 ft) or less are commonly observed in these units, the thickness of each stratigraphic section can range from 45 to 150 m (150 to 500 ft) near the Oklahoma City area (Christenson and Havens, 1998; Christenson et al., 1992; Heran et al., 2003; Wood and Burton, 1968). The Garber Sandstone and Wellington Formation consist primarily of deep-red to reddish-orange, massive cross-bedded fine-grained sandstone, which are irregularly interbedded with chert and mudstone conglomerates, siltstone, and/or red-brown shale (Christenson and Havens, 1998; Heran et al., 2003; Wood and Burton, 1968). The sandstone layers contain subangular to subrounded very-fine to fine quartz grains (Wood and Burton, 1968). The cementation of Garber Sandstone and the Wellington Formation is very weak. A fine red

mud is the most common cement type in the Garber Sandstone and Wellington Formation. However calcite, dolomite, and barite cements are also found in some sandstone beds (Wood and Burton, 1968). In general, the shale beds consist of nonlaminated and white to dark red shale. The shale in the Wellington Formation has clayish and stocky shale with conchoidal fracture while the shale in the Garber Sandstone has silty or sandy shale (Wood and Burton, 1968).

Hennessy Group

The Permian Hennessy Group lies within the southwest portions of the study area, portions of Townships 13 and 14N-R3W, and Townships 13 and 14N-R2W, Oklahoma Country, Oklahoma (Figure 2.1). The Hennessey Group consists primarily of red-brown shale with a few siltstone and fine-grained sandstone beds (Heran et al., 2003; Roberts and Spitz, 2001; Wood and Burton, 1968). Formations belonging to the Hennessey Group near the study area include: Salt Plains Formation, Kingman Formation (Kingman Siltstone), and Fairmont Shale. The Salt Plains Formation and the Fairmont Shale near the study area are dominantly red-brown blocky shales and orange brown siltstones (Heran et al., 2003). The Salt Plains Formation in the Oklahoma City area can reach thicknesses as great as 60 m (200 ft), whereas approximately 10 m (30 ft) of thickness is common for the Fairmont Shale. The Salt Plains Formation and the Fairmont Shale consists predominantly of shale. However, shale is less common in the Kingman Formation (Kingman Siltstone). The Kingman Formation comprises mainly even beds of orange-brown to greenish-gray siltstone with fine-grained sandstone and smaller amounts

of red-brown shale as thick as 10 m (30 ft) near the Oklahoma City area (Heran et al., 2003).

Quaternary Deposits

The Quaternary alluvial and terrace deposits overlie the Permian rocks in or adjacent to the stream drainages near the study area. The terrace deposits in the Oklahoma City metropolitan area consist of unconsolidated and lenticular beds of sand, silt, clay, and gravel. Thickness varies from a few feet to 100 feet with an average thickness along major streams near Oklahoma City metropolitan area is approximately 50 feet (Heran et al., 2003; Wood and Burton, 1968).

The alluvial deposits are exposed in the southern portion of study area. The alluvial deposits expand along the modern channels, flood plains, and low terraces along the major streams and their distributaries. These deposits mainly comprise sand silt, clay, and lenticular beds of gravel (Edwards, 1992; Heran et al., 2003; Wood and Burton, 1968). Their thicknesses range from 30 to 100 feet with the average thickness along minor streams of about 25 feet (Heran et al., 2003).

Hydrogeology of the Central Oklahoma

The Central Oklahoma aquifer, located in the central Oklahoma provides water supplies for the Oklahoma City metropolitan area and its surrounding cities (Figure 2.2). The Central Oklahoma aquifer underlies approximately 8,000 square kilometers (3088 square miles), which includes all or portions of Cleveland, Lincoln, Logan, Oklahoma, Payne, and Pottawatomie Counties (Christenson and Havens, 1998). The Central

11

Oklahoma Aquifer is made up of all Permian sedimentary rocks and the Quaternary alluvial and terrace deposits (Christenson and Havens, 1998; Edwards, 1992; Roberts and Spitz, 2001; Wood and Burton, 1968). Although the Hennessey Group and the Quaternary alluvial and terrace deposits contain some water, the Garber Sandstone and Wellington Formation, known as the Garber-Wellington Aquifer yields the most substantial volumes of drinking water in Central Oklahoma (Roberts and Spitz, 2001).
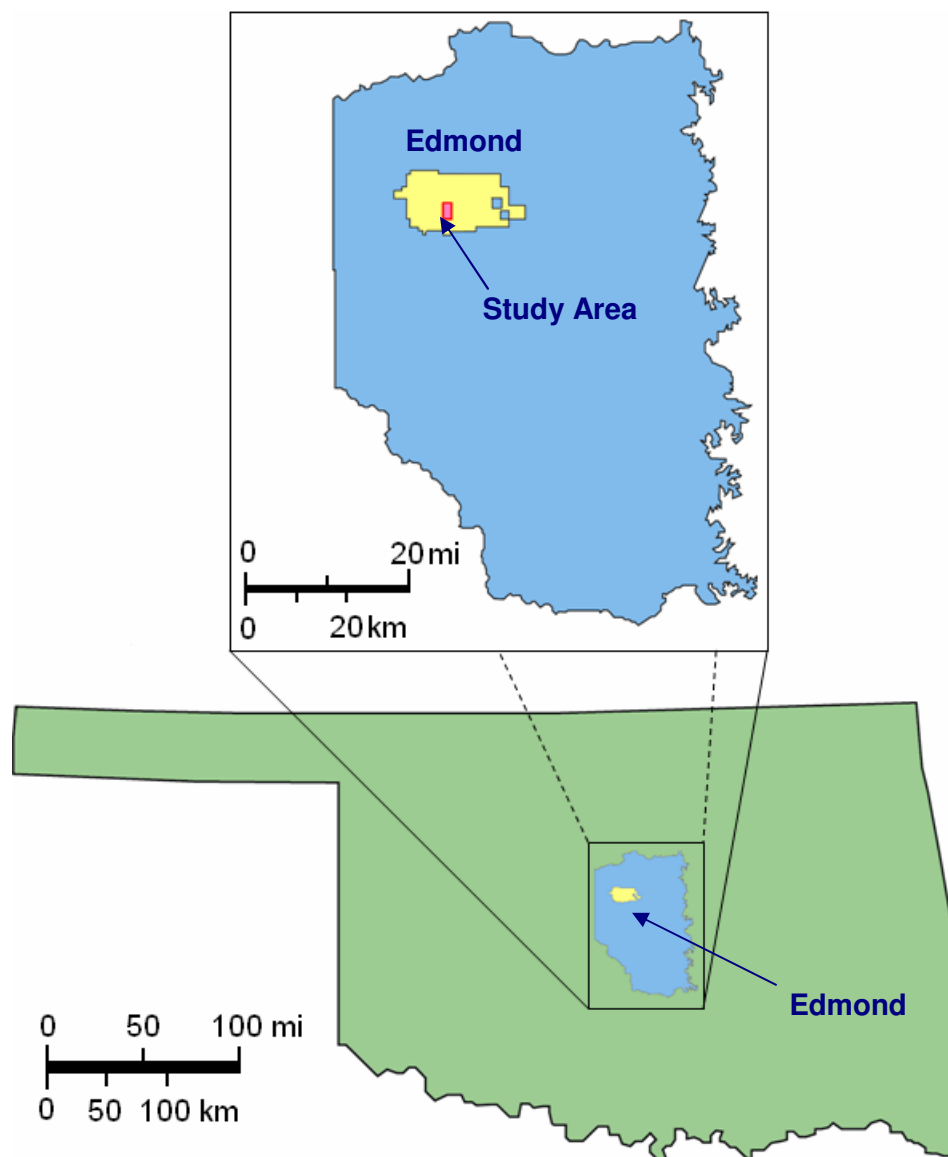
Figure 2.2: Location Map of Central Oklahoma Aquifer (after Christenson and Havens, 1998)

Development of Electrical Resistivity

Electrical resistivity and/or conductivity studies have evolved and been employed to study electrical properties of rocks and materials in the subsurface. One of the earliest recorded electrical conductivity studies in geology related fields have been performed by Gray and Wheeler in 1720 and Watson in 1746 (Jakosky, 1950; Van Nostrand and Cook, 1966). Gray and Wheeler measured electrical conductivities of various rocks, and Watson ascertained that the ground conducts electricity (Van Nostrand and Cook, 1966). The next recorded series of earth electrical property studies have been done by Robert W. Fox in 1830 (Van Nostrand and Cook, 1966). He discovered the existence of natural electrical currents within sulfide ore deposits and successfully measured the electrical current between his copper plate electrodes (Van Nostrand and Cook, 1966). Several advanced experiments based on Fox's discovery had been performed by many scientists since Fox's first discovery. However, the early electrical conductivity and resistivity studies did not deal with quantitative approaches. The first successful experiments of application of direct currents to measure earth resistivity were conducted by Conrad Schlumberger in 1920 (Van Nostrand and Cook, 1966). Although the electrical resistivity/conductivity studies with a geological approach had been conducted in the early eighteenth century, the application of electrical resistivity methods came into wide use only after the advent of computing technology in the 1970's (Reynolds, 1997). The modern survey technologies provide faster data collection and better data quality. One of the advanced method examples is the Oklahoma State University proprietary Halihan/Fenstemaker technique, which can provide high-resolution subsurface ERI images (Halihan, et al. 2005).

Electrical Resistivity Method

Electrical resistivity is a geophysical investigation technique that allows the measurement of electrical properties of subsurface structures and subsequent interpretation of geological properties by introducing a direct current into the ground and measuring its electrical potential differences. Electrical resistivity is defined as an intrinsic electrical property of a material to oppose the flow of the electric current (Schwartz, 2003); meanwhile, resistance is a ratio of the voltage potential difference and the electrical current retardation which depends on inherent property of material and its physical geometry (Reynolds, 1997). According to Ohm's Law, resistance, R (Eq.1) and resistivity, ρ (Eq. 2) are defined by the following equations (Reynolds, 1997):

$$R = \frac{V}{I} \ [\Omega] \ (\text{Ohm's Law}) .... \text{(Equation 1)}$$

$$\rho = \frac{VA}{IL} \ [\Omega \cdot m] .... \text{(Equation 2)}$$

Where R is the resistance in ohms; V is the potential (voltage) difference in volts; I is the electric current passing through the material in amps; ρ is the resistivity in ohm-meters; A is the cross sectional area of the material in meters square; L is the length of the resistive material in meters.

In field surveys, the resistivity of geological properties is determined by measuring the electrical potential difference between electrodes, thus apparent resistivity can be calculated from the measured voltage drop (V), the electric current induced into the ground (I), and the geometric factor (K) which depends on the electrode configuration type (Schwartz, 2003) (Eq. 3):

$$\rho_a = K \frac{V}{I} \ [\Omega \cdot m] .... \text{(Equation 3)}$$

The electric current is commonly conducted through rocks and sediments by the pore fluids, clay minerals, and metallic minerals in the rocks and sediments (Reynolds, 1997; Schwartz, 2003). Because properties of same rock/sediment types (e.g. grain size, porosity, permeability, and clay mineral contents) can vary from locations to locations, the resistivity of geological materials is one of the most diverse physical properties (Kearey, et al., 2002; Reynolds, 1997) (Figure 2.3).
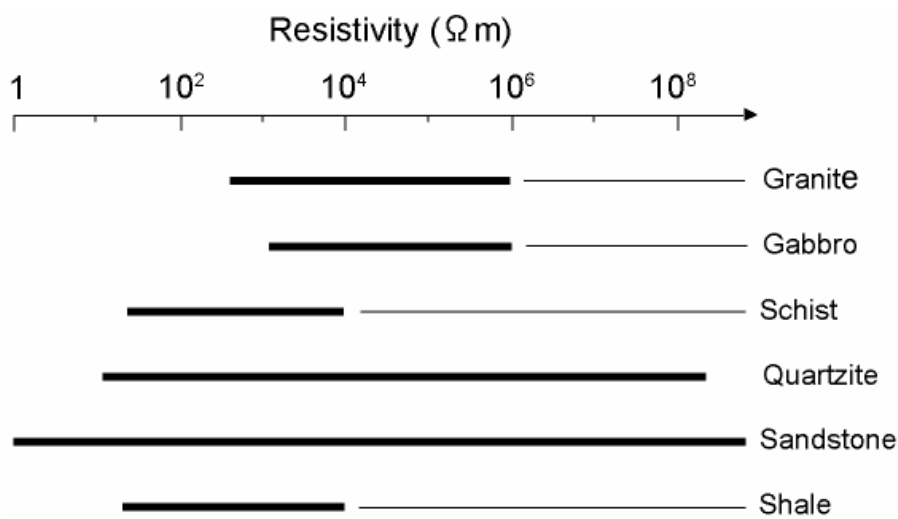
Figure 2.3: Approximate Range of Resistivity Values of Common Rocks (Kearey, et al., 2002)

Electrical Resistivity and Saltwater Contaminations

Numerous investigations that applied ERI surveys to the study of salinity subsurface problems have been conducted. These types of problems were intrusion of salt water near coastal areas, and surface disposal of saline wastes or other landfills, in addition to problems associated with petroleum production.

Koehler (1988) delineated ground water brine contamination using surface electrical resistivity. The electrical resistivity survey with Schlumberger array was conducted in a residential area which was located in the Walker Oil Field, Ottawa

County, Michigan. The 1 D electrical resistivity results of study indicated that the low resistivity zones were found within a sand and gravel aquifer, which was also supported the water quality data near the location.

Hibbs (1989) also examined ground water brine contamination in southeastern Hitchcock County, Nebraska using a combination of 1 D surface electrical resistivity survey, geochemical data, and seismic refraction data. In this investigation, a salt water disposal pit and other oilfield activities were evaluated as the suspected source of the contamination. The electrical resistivity method with the Wenner configuration was used near the salt water disposal pit and petroleum field. The electrode spacing was determined by a previous water table depth data. As a result, the lower resistivity area was found near the pit. This result was consistent with all resistivity survey lines with different spacing. Although the author believed that further study is necessary to obtain precise results due to the complexity of the aquifer system and the various sources of contaminants, the results of the electrical resistivity method showed that the leachate of brine water from the evaporation pit was one source of the contamination.

Direct current resistivity surveys were conducted on the coast of New Zealand to examine the applicability of the method for characterizing the saline and fresh water interface in a coastal aquifer (Wilson et al., 2004). The results indicated that the direct current resistivity traversing method was a useful tool to delineate the intrusion of saltwater in the coastal aquifer. The results were supported by water well water chemistry data. The significant contrast of saline and fresh water was detected even diffusive mixing involving as little as 1% seawater.

Whittecar, et al. (2005) applied electrical resistivity techniques and water chemistry data to delineate the extent of saltwater intrusion in the shallow aquifer surround a borrow pit lake, Lake Ballard. Dewatering during mining excavation operations near the shoreline of Portsmouth, VA drew saltwater intrusion into the local sandy coastal aquifer. The brackish water has contaminated Lake Ballard and several shallow wells near the lake for more than a decade after the mining operations were stopped. Twenty-seven Schlumberger resistivity soundings and two Wenner profiles measurements were obtained with various electrodes spacings. The investigations concluded that a moderately saline confined aquifer which is located beneath the lake and is connected to a deep depression on the bottom of the lake is the source of brackish water in the lake and surrounding area. With the help of previous limnological and geological studies, the electrical resistivity techniques could locate the relative distribution of brackish groundwater in the lake and the surrounding area.

Many studies using the electrical resistivity method successfully delineate saline plumes or discovered a source(s) of saline contamination. The electrical resistivity investigations dealing with environmental problems are often conducted with other methods to make better quality interpretations (Aristodemou and Thomas-Betts, 2000). The reason that other supplemental data are very important is because the electrical resistivity values of the earth materials are very diverse, and no definite value exists for each geological object (Kearey, et al., 2002; Reynolds, 1997).

CHAPTER III

METHODS

This chapter contains two sections. The first section will discuss the field equipment and its setup. The later section will concentrate on the analytical portion of the procedures which including processing of the field data and two-dimensional (2-D) electrical resistivity modeling.

Field Methods

The Electrical Resistivity Imaging (ERI) survey technique was selected as a primary sampling method in this investigation because of its portable, economical, and practicable advantages in an urban area. A total of 8 high resolution ERI surveys (ERI lines TH.A-TH.H) were conducted May 16, 2006 through March 21, 2007 in the vicinity of the Thunderhead Hills Addition, Edmond, OK, USA. The locations of the ERI survey lines were chosen based on the locations of previous and/or present petroleum field activities including saltwater evaporation pits, injection wells, and various types of petroleum pipe lines.

In addition to the ERI surveys, laser level surveying and magnetometer data were acquired along some ERI lines in order to enhance the ERI data interpretation. However, those field data were not taken with every ERI line, mostly because of accessibility limitations in the field.

ERI Data

ERI is a geophysical investigation technique that allows visualization of electrical properties of the subsurface structures by passing a direct current into the ground and measuring its electrical potential differences. An 8 channel resistivity meter with data storage (AGI SuperSting R8 IPTM) was applied in this investigation. Four cables with a total of 56 electrodes were connected to the resistivity meter through an electrode switchbox to collect and store subsurface electrical resistivity measurement data at depths up to 110 meters (360 feet). For this investigation, in addition to the 56 electrode cable, an 84 electrode cable was used in a survey line (TH.H) that was a common line with the Association of Central Oklahoma Governments (ACOG), who was conducting a concurrent study in the area.

Each specialized electrode contacted with the ground through a metal stake to measure the apparent resistivity of the subsurface beneath the survey line. Although metal stakes needed to be installed into the ground along a straight line and at equal intervals, the survey lines were often offset slightly due to the hindrance in the field (e.g. heavily wooded areas and fences).

The maximum spacing of the available cable was 10 meters (32.18 feet). The spacing between the electrodes was as large as field conditions allowed so that result of the electrical resistivity image penetrates sufficiently to observe the target depths of up to 60 meters (200 feet). In general, the maximum observable depth is approximately one-fifth of the total ERI line length (i.e. an ERI line of 56 electrodes with 10 meters spacing gives an ERI profile with a length of 55 meters). However, the field accessibilities and

barriers in the field often caused the limitations in the location and the spacing between the electrodes. Therefore, the ERI survey lines were frequently shorter than desired.

Once the survey line was laid out in the field, contact resistance tests were performed to monitor the condition of ground and electrodes. This test was performed by measuring the voltage between each designated electrode pair. In this investigation, a contact resistance of 2000 Ω or higher was considered poor. The poor contact resistance regularly occurred due to either a poor connection with electrode and metal stake connections or extremely dry soil. The latter was a common problem in this investigation. To solve this problem, saline water was poured over the base of metal stakes in order to provide better conduction between the dry soil and the metal stakes.

After all the electrodes met the acceptable range of the contact resistance, the Advanced Geosciences Inc. SuperSting R8 IP^{TM} collected data from the electrode array. The resistivity data acquisition and processing followed Oklahoma State University's Halihan/Fenstemaker 4.0 method to acquire significantly better quality data than other standard ERI techniques (Halihan and Fenstemaker, 2004). The details of each ERI survey line will be discussed in the following section.

TH.A Survey

The TH.A survey was conducted in a south (38°39'21.450"N, 97°26'5.220"W) to north (35°39'34.758"N, 97°26'9.067"W) orientation in a property east of Thunderhead Hills Addition on May 16, 2006 (Table 3.1; Figures 3.1; Plates 1-3). Due to a heavily wooded area in the field, the survey line TH.A was slightly shifted to southeast direction

at the middle of the survey line. The spacing between the electrodes was 8.0 m (26.3 ft), and the total length of the survey line is 440 m (1443.6 ft).

Figure 3.1: Photos from Electrical Resistivity Image TH.A
(A) Looking north from the south end (ERI electrode number1)
(B) Looking south from the north end (ERI electrode number 56)
(C) Looking north from the entrance to the wooded area
(D) Looking south from the entrance to the wooded area

TH.B Survey

On May 17, 2006, survey TH.B was conducted south to north orientation, to the north of Thunderhead Hills Addition, to the west of Johnson well #4 (Table 3.1; Figures 3.2; Plates 1-3). No major obstruction was found near the survey line. However, the area did not have enough space to extend the maximum cable length. The spacing between

the electrodes was 7.0 m (23 ft), and the total length of the survey line was 385 m (1263 ft).

Figure 3.2: Photos from Electrical Resistivity Image TH.B
(A) Looking north from the south end (ERI electrode number1)
(B) Looking south from the middle of the ERI line
(C) Looking south from the north end (ERI electrode number 56)

TH.C Survey

The TH.C survey was conducted west (35°39'29.496"N, 97°26'9.534"W) to east (35°39'28.22"N, 97°25'58.69"W) orientation in a property in the east of Thunderhead Hills Addition on May 18, 2006 (Table 3.1; Plates 1-3). Due to a heavily wooded area in the field and the property boundaries, the survey line TH.C could not extend the

maximum length of 550 m (1804 ft). The spacing between the electrodes was 5.0 m (16.4 ft), and the total length of the survey line was 330 m (902 ft).

TH.D Survey

The TH.D survey was performed west (35°39'20.082"N, 97°26'7.188"W) to east (35°39'19.416"N, 97°25'54.762"W) orientation in a property east of Thunderhead Hills Addition on June 8, 2006 (Table 3.1; Figure 3.3; Plates 1-3). The survey line TH.D was located on south of TH.C and almost parallel to the survey line. Due to very heavy woods in the field and the property boundaries, the available maximum spacing between the electrodes was 6 m (19.7 ft), and the total length of the survey line was 275 m (1083 ft).

Figure 3.3: Photos from Electrical Resistivity Image TH.D
(A) Looking east from the west end (ERI electrode number1)
(B) Looking east from the middle of the ERI line
(C) Looking west from the east end (ERI electrode number 56)

TH.E Survey

The TH.E survey was carried out along the north side of Faith Bible Church property on June 9, 2006 (Table 3.1; Figure 3.4; Plates 1-3). The orientation of the line was west to east direction. There were numerous utility lines near the survey line presenting at the surface. The survey line TH.E spacing was 6 m (19.7 ft), and the total length of the survey line was 275 m (1083 ft).

Figure 3.4: Photos from Electrical Resistivity Image TH.E
(A) Looking west from the west end (ERI electrode number1)
(B) Looking west from the center of the line
(C) Looking west from the east end (ERI electrode number 56)
(D) Johnson #2: Located about 15 m (4.6 ft) south of ERI line

TH.F Survey

On August 28, 2006, the TH.F survey was conducted west to east, in a property southeast of Thunderhead Hills Addition, along the spring creek (Table 3.1; Figure 3.5; Plates 1-3). Due to the natural and artificial boundaries (e.g. spring creek, wooded area, and property boundaries), the survey line TH.F could not reach the maximum length. The spacing between the electrodes was 7 m (23 ft), and the total length of the survey line was 385 m (1263 ft).
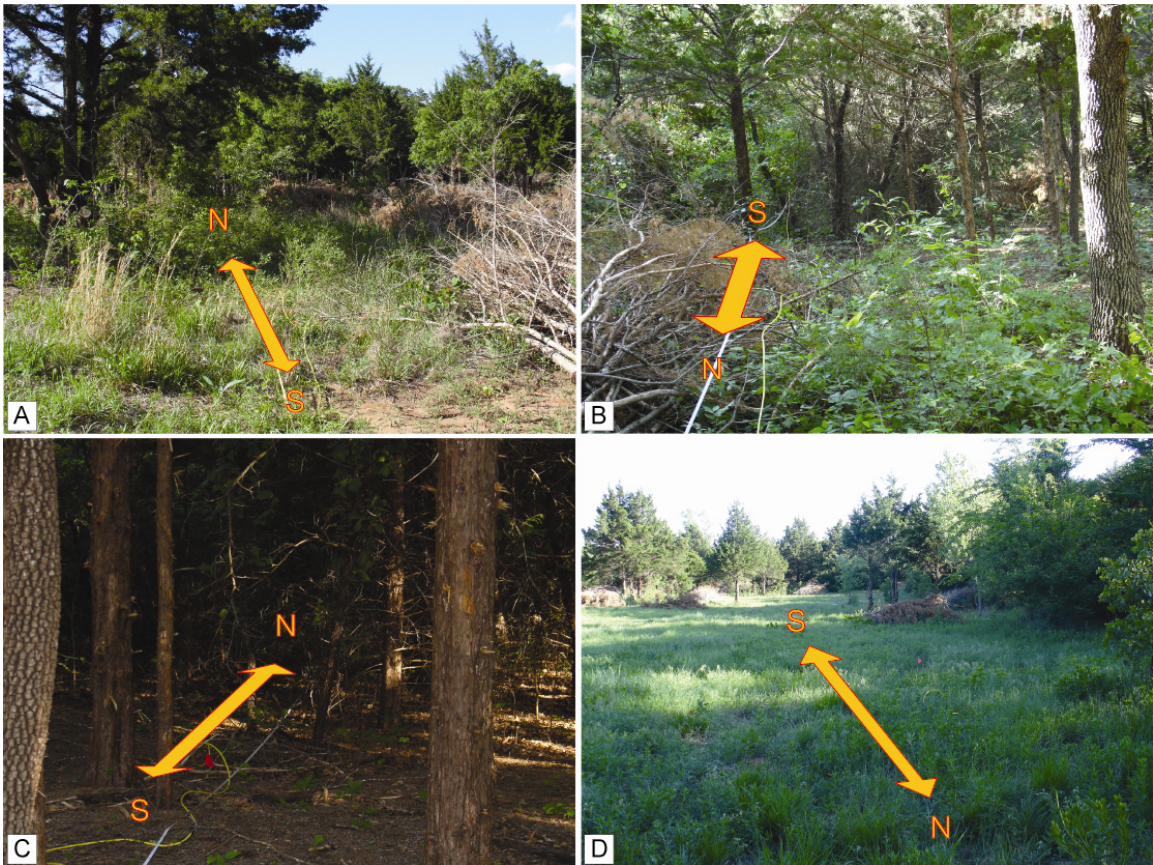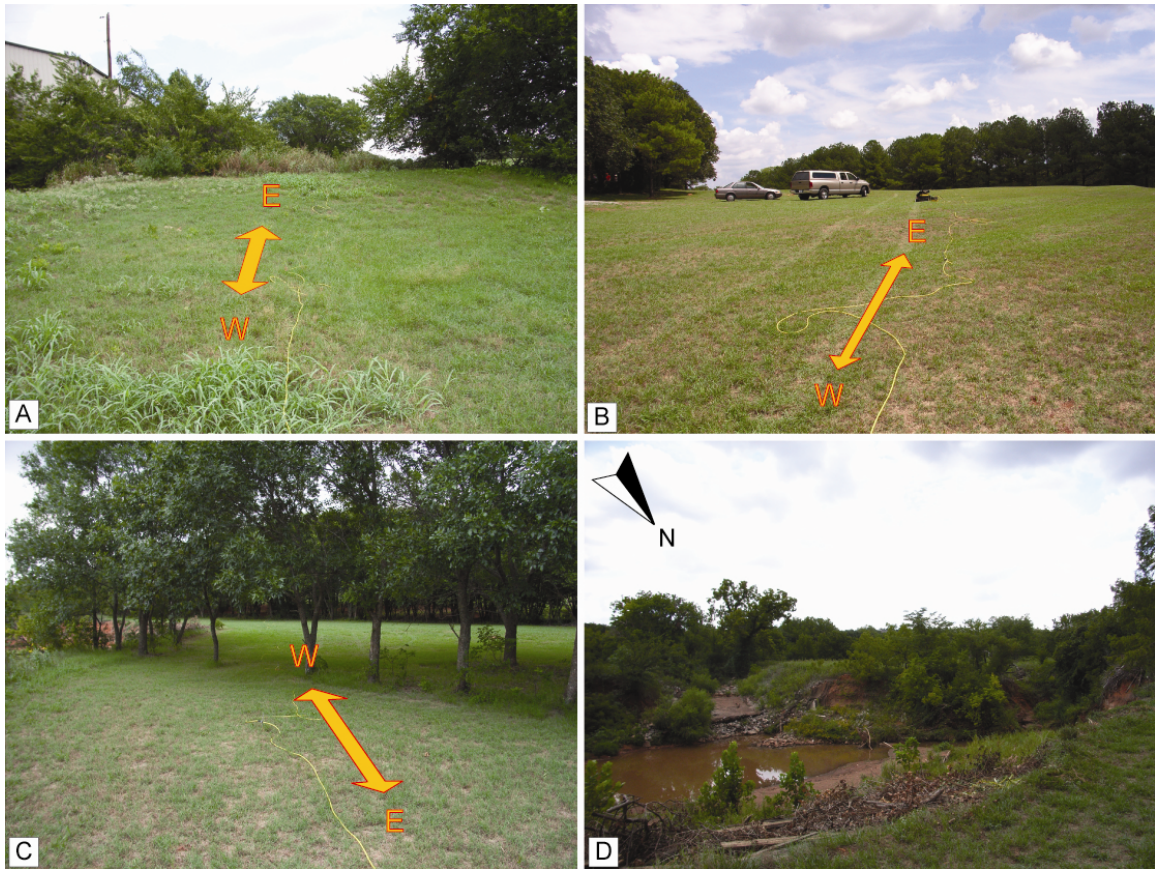
Figure 3.5: Photos from Electrical Resistivity Image TH.F
(A) Looking east from the west end (ERI electrode number1)
(B) Looking east from the center of the line
(C) Looking west from the east end (ERI electrode number 56)
(D) Spring creek adjacent to the ERI line

TH.G Survey

This survey was conducted south (35°39'14.3"N, 97°26'03.3"W) to north (35°39'33.3"N, 97°26'00.0"W), in a property in the east of Thunderhead Hills Addition on March 21, 2007 (Table 3.1; Figure 3.6; Plates 1-3). There was sufficient space to extend the full cable length of 550 m (1804 ft) in this property. Several buried petroleum pipe lines both parallel and perpendicular to the ERI survey line existed in this survey.

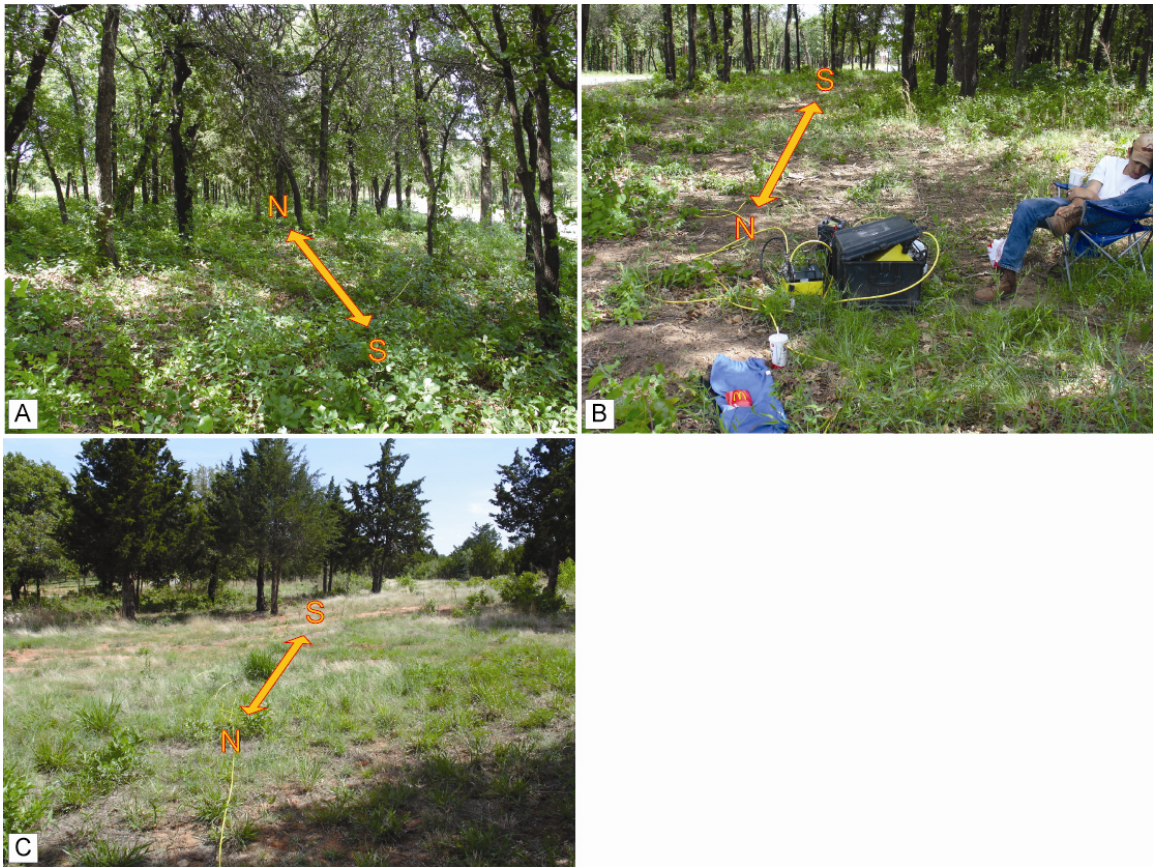**Figure 3.6: Photos from Electrical Resistivity Image TH.G**
(A) Looking north from the south end (ERI electrode number1)
(B) Looking south from the center of the line
(C) Looking south from the north end (ERI electrode number 56)
(D) Exposed metal pipe runs perpendicular to the ERI line

TH.H Survey (ACOG Common Line)

The TH.H survey was conducted along the south side of Faith Bible Church property on February 23, 2007 (Table 3.1; Figure 3.7; Plates 1-3). The orientation of the line was west to east direction. This survey line was a common line with Association of Central Oklahoma Governments (ACOG). The primary difference between TH.H survey line and other survey lines was the number of electrodes; the survey line TH.H had 84 instead of 56. This line was used a comparison between standard ERI methods employed

by ACOG (The Wenner array with standard inversion) and OSU proprietary methods
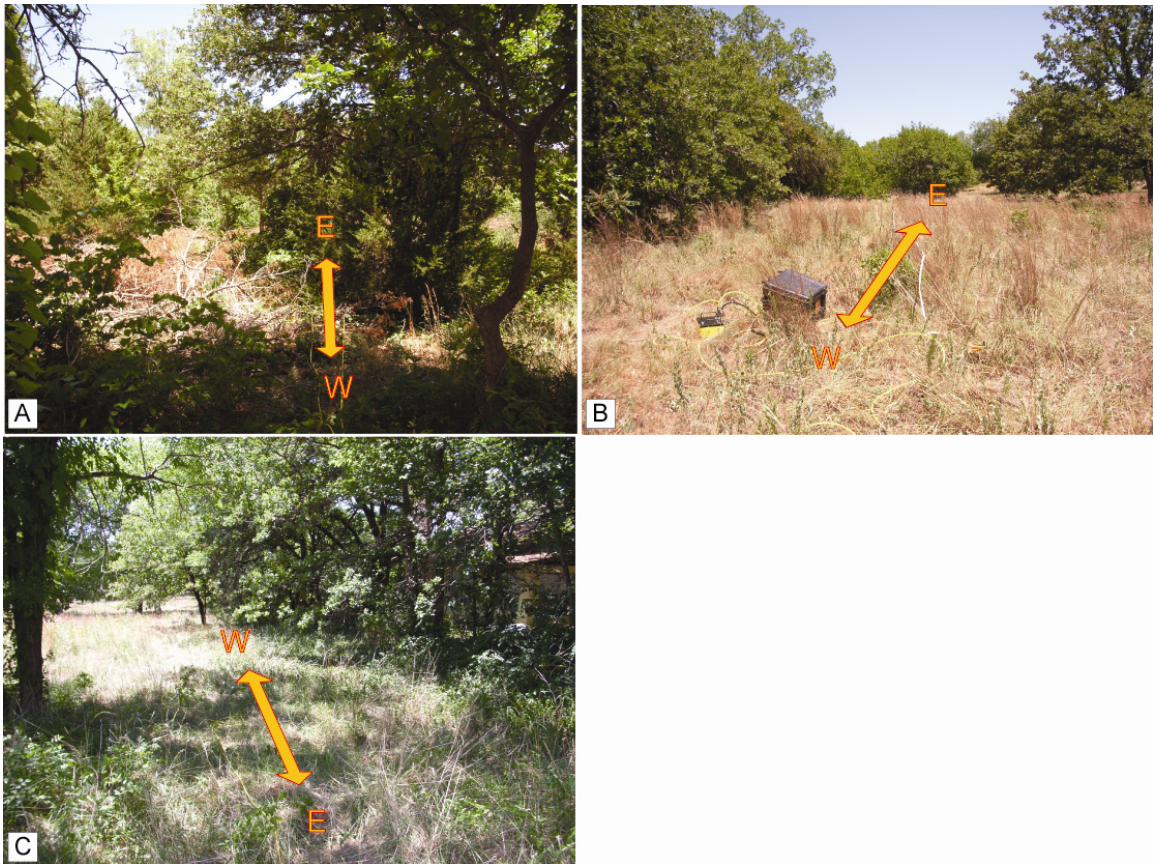
(Halihan/Fenstemaker v 4.0).

Figure 3.7: Photos from Electrical Resistivity Image TH.H
(A) Looking east from the west end (ERI electrode number1)
(B) Looking east from the center of the line
(C) Looking east from the east end (ERI electrode number 56)

ERI Name	Data Collection Date	Number of Electrodes	Spacing (m)	Spacing (ft)	Total Length (m)	Total Length (ft)	Line Orientation
TH.A	05/16/06	56	8.00	26.25	440.00	1443.57	S-N
TH.B	05/17/06	56	7.00	22.97	385.00	1263.12	S-N
TH.C	05/18/06	56	5.00	16.40	275.00	902.23	W-E
TH.D	06/08/06	56	6.00	19.69	330.00	1082.68	W-E
TH.E	06/09/06	56	6.00	19.69	330.00	1082.68	W-E
TH.F	08/28/06	56	7.00	22.97	385.00	1263.12	W-E
TH.G	03/21/07	56	10.00	32.81	550.00	1804.46	S-N
TH.H	02/23/07	84	3.35	11.00	278.28	913.00	W-E

Table 3.1: Field ERI Data Collection Summary

In addition to ERI surveys, other types of data collection methods were performed in order to enhance data quality and integrity. Those surveys supplemented the interpretation of ERI lines. Especially, the survey area was located on urban area, and it is hard to avoid utility pipes, cables, and power lines in subsurface.

GPS Data

Global positioning system (GPS) data were obtained to denote the start and end points of each survey line. The World Geodetic System of 1984 (WGS 84) datum projection was used on ERI survey lines TH.A, C, D, G, and H. The GPS data could not be obtained from the ERI survey lines, TH.B, TH.E, and TH.F due to equipment failure. The GPS data from those lines were estimated by information from the field notes. The start and end points of location data is shown on Table 3.2. All GPS data was converted from degrees, minutes, seconds to decimal degree.

ERI NAME	Start point (Electrode #1)		End Point (Electrode #56 or #84)	
	Latitude	Longitude	Latitude	Longitude
TH.A	35.655958°	-97.434783°	35.659655°	-97.435852°
TH.B*	35.663410°	-97.437867°	35.666912°	-97.437879°
TH.C	35.658193°	-97.435982°	35.657839°	-97.432969°
TH.D	35.655578°	-97.435330°	35.655393°	-97.431878°
TH.E*	35.661842°	-97.442575°	35.661754°	-97.438937°
TH.F*	35.649026°	-97.438750°	35.648319°	-97.434603°
TH.G	35.653972°	-97.434250°	35.659250°	-97.433333°
TH.H	35.659990°	-97.442570°	35.660150°	-97.439630°

Table 3.2: GPS Data of ERI Lines TH.A to TH.H

* indicates that the GPS data were estimated by information from the field note due to the unavailability of the GPS data during the field works.

Topographic Data

Laser level measurements were taken to obtain the topographic changes along some ERI lines where the topography along the ERI line was changing significantly. However, most of the lines did not conduct the surveying due to obstacles such as extremely heavy woods. Surveying was conducted along TH.G and TH.H survey lines.

Earth Magnetic Data

A proton precession magnetometer (Geometrix G856) was used as an aid to locate buried metal objects (e.g. utility and/or petroleum pipes) along ERI survey line TH.A (Figure 3.8). The previous investigation of TH.A survey showed that three pipe-like objects were possibly buried nearly perpendicular to the ERI line. A magnetometer survey was performed in order to provide supporting evidence. The magnetic field measurement was conducted on February 23, 2007. The location of ERI line was determined from the previous GPS data. The measurement was taken one meter interval along the TH.A from the north end to the south. The heavily wooded area and the south end of the ERI line were excluded due to accessibility limitations in the field.

Figure 3.8: Magnetometer Survey along the ERI Line TH.A

Analytical Methods

This section broadly contains two subsections. The first subsection describes ERI data processing. The raw data obtained in the field needed to be inverted before the final interpretation proceeded. Following the ERI data processing, the second subsection explains how forward models were constructed to quantify the pipe interference in ERI images, and then gives details how a-prior inversion models may be used to limit the effect of pipes to observe alternate conductive features in images.

ERI Data Processing

Data Inversion

The raw data of potential drop and electric current values measured in the field was calculated and converted to apparent resistivity. The apparent resistivity was inverted to 2D pseudosections using protocols developed by OSU (Halihan and Fenstemaker, 2004).

Error Reduction

The raw data was filtered before the final inversion for low signal (V/I < 10^{-6} ohms) or repeatability errors greater than 2%. Individual data points not fitting in the finalized resistivity model with an individual data error greater than 50% were excluded from the datasets in a trimming process. The Root Mean Square (RMS) error is a useful representative value to evaluate these outliers (AGI, 2004; Borradaile, 2003). In this study, most lines had 2-15% of the total dataset eliminated through filtering or trimming, and resulted in datasets with RMS errors of 4-9%. Lines C and E had significant noise and had nearly 50% data loss with RMS errors of 15%. Finally, line G which went right over several parallel petroleum pipes had data loss of 75% and a final RMS error of 17%.

ERI Color Scheme

The data sets collected in the field were contoured and plotted with various colors in the final 2-D ERI images. Each color represents a range of inverted electrical resistivity values in unit of ohm-meters ($\Omega \cdot$m). The region of cool colors (e.g. purple) indicates the area is less resistive (i.e. more conductive); the region of warm colors (e.g. orange) signifies that the area is more resistive (i.e. less conductive). As shown in Figure

3.9, the color scheme is gradated its colors from conductive to resistive as it goes from left to right. Because the magnitude of subsurface resistivity values was different from one site to another, the color scheme needed to be standardized for every one of the images to maintain the data integrity and avoiding misinterpretations. Over a single color range the scale is roughly linear, although the increments change from color to color.
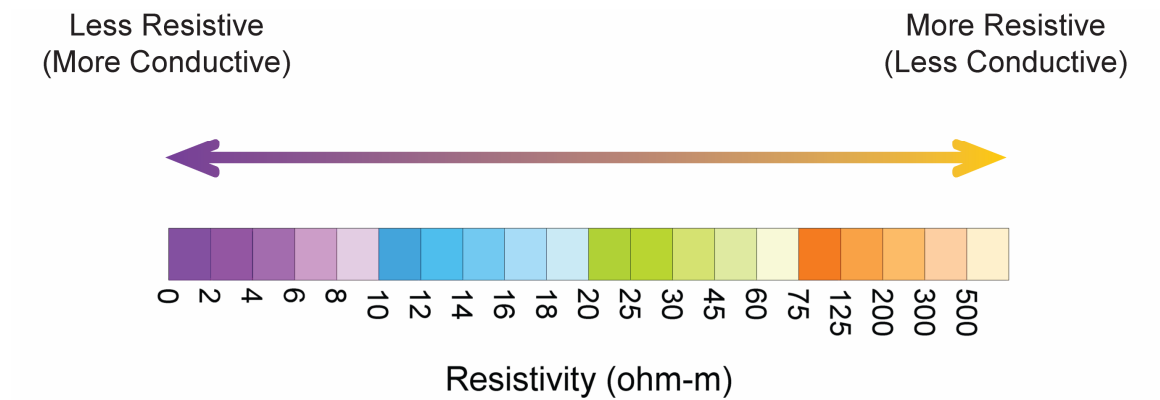
Figure 3.9: ERI Color Scheme

Electrical Resistivity Modeling

Since the ERI surveys took place in an urban area, to differentiate lower resistivity anomalies from saline contamination and the anomalies from utility lines in the subsurface was very problematic in this study. Generally speaking, utility or petroleum lines are buried close to the surface in most case. Although this fact can be an aid to distinguish between areas of saline impact and utility lines, this piece of information cannot fully solve the issue. Forward models were employed to determine patterns of buried man-made conductive objects. A model pipe was arranged in several ways to examine the electrical resistivity behaviors in different scenarios, and then, the results of the forward models were applied to an *a-priori* inversion model of to determine if the method may distinguish from known or unknown pipes to saline impact areas.

Forward Models

Two dimensional (2-D) electrical resistivity forward models were developed to quantify the pipe interferences in ERI images. AGI EarthImager 2D^{TM} version 1.7.4 was used to construct these 2-D forward models. For this study, roughly 8 different interference settings were applied to observe the noise behaviors in ERI images (Figure 3.10 and 3.11). In order to make the model as simple as possible, only one pipe and/or one brine location was placed in each model.
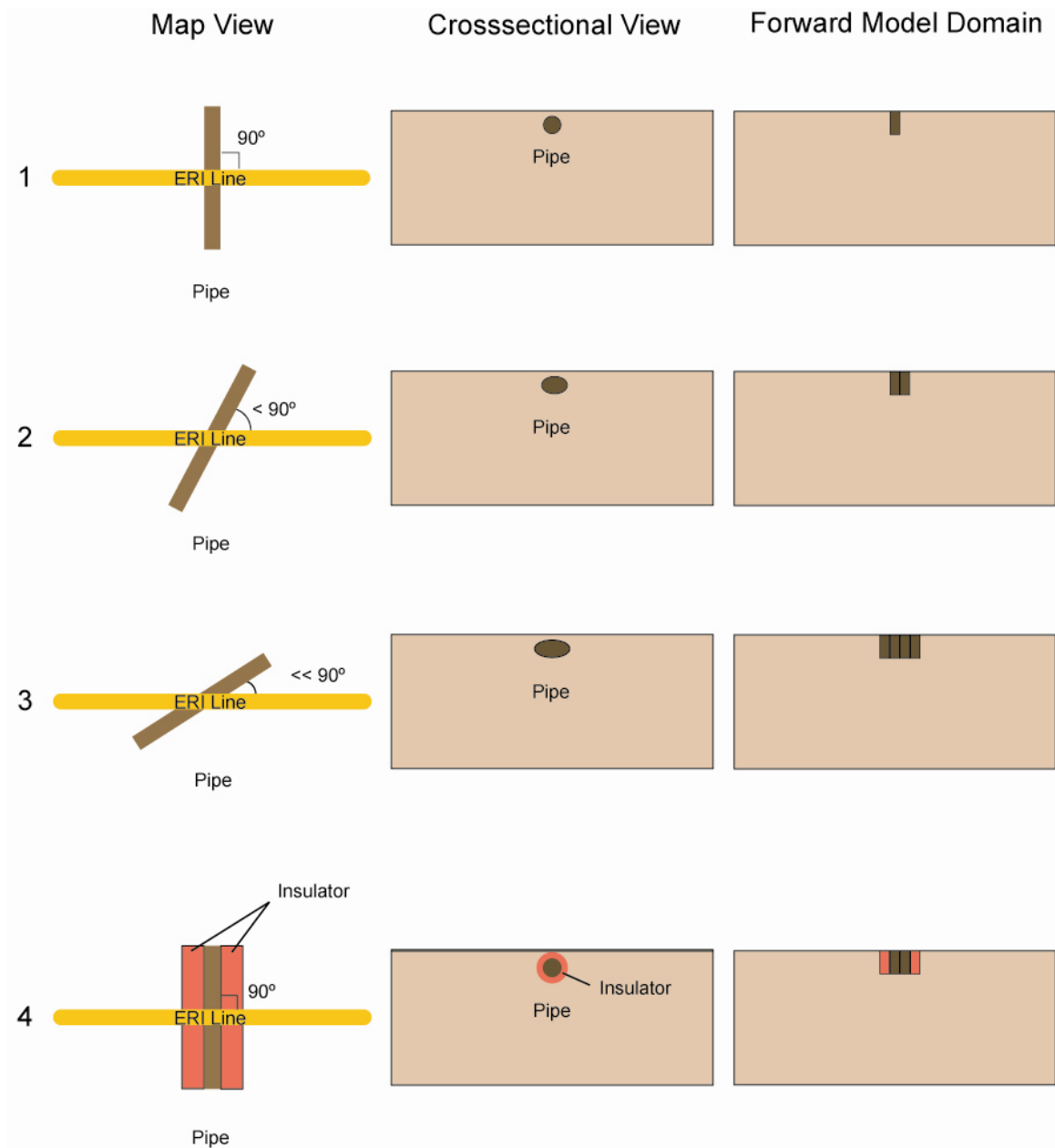
Figure 3.10: Forward Model Settings for Models 1 - 4

1. Single conductive pipe intersects with ERI line at 90 °

2. Single conductive pipe intersects with ERI line at low angle

3. Single conductive pipe intersects with ERI line at lower angle

4. Single conductive pipe surrounded by insulators intersects with ERI line at 90 °
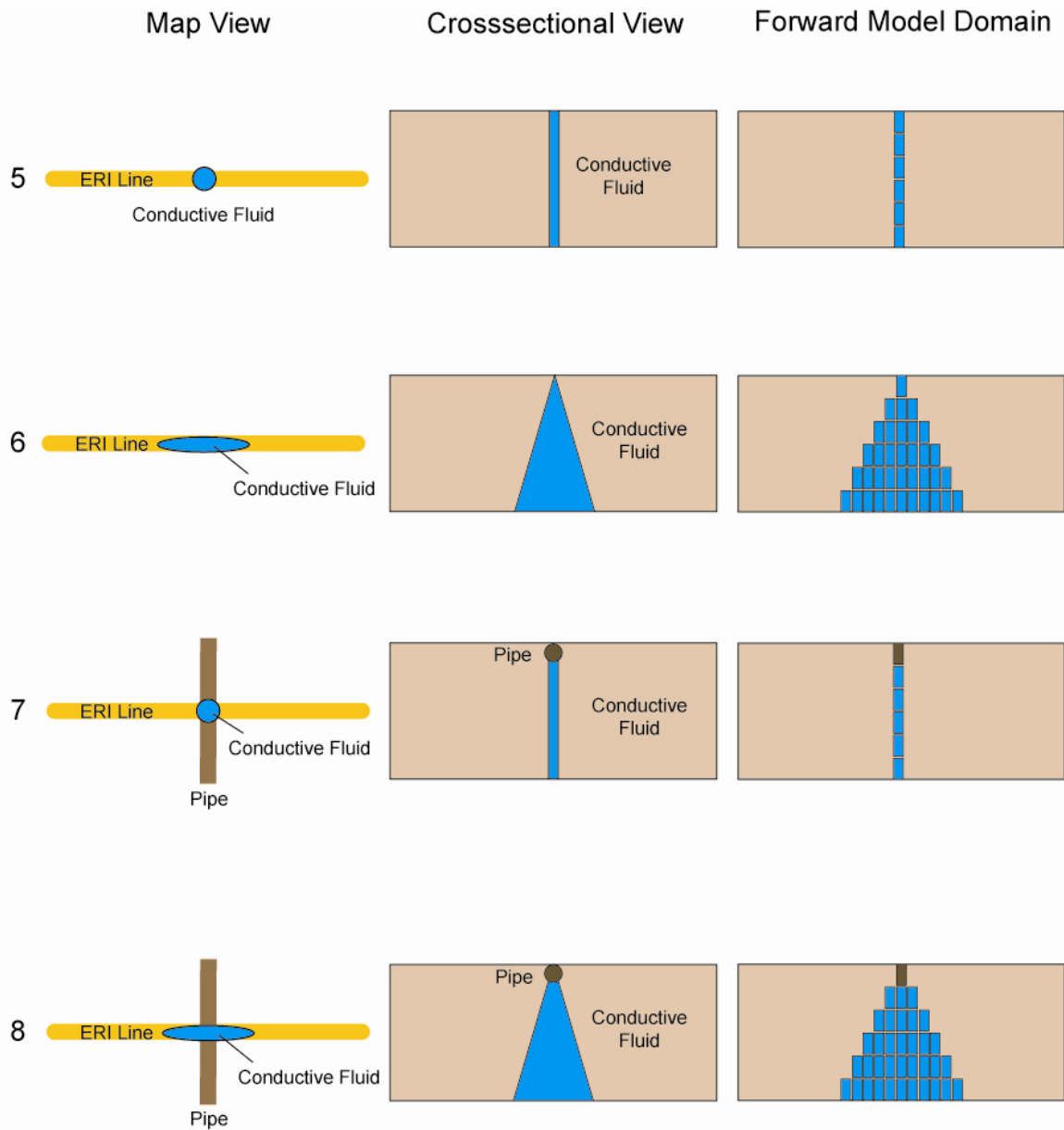
Figure 3.11: Forward Model Settings for Models 5 - 8

5. Conductive fluid (Straight) extending downward

6. Conductive fluid (Cone) extending downward

7. Conductive fluid (Straight) leaking from Single pipe intersecting with ERI line at 90 °

8. Conductive fluid (Cone) leaking from Single pipe intersecting with ERI line

The ERI background settings were provided based on the condition and results from the previous field surveys. The ERI background settings included; types of ERI arrays, a metal pipe size and location, ERI electrode spacing, background resistivity, and pipe resistivity. Two types of configurations were tested for comparison in the forward models: the Halihan/Fenstemaker techniques and the Wenner array with standard processing. The Halihan/Fenstemaker techniques were chosen because the field data were processed by this method. The Wenner array with standard processing techniques was also selected for comparison since it was a standard ERI technique and also used for the common line with ACOG (TH.H/TH.03). The metal pipe simulated in these forward models was placed in the top cell, and a cross section of a pipe was expressed as one conductive cell. The reasons of these assumptions were (1) the pipes in the study site were usually buried near the surface, and (2) general speaking, the diameter of those pipes was smaller than the resolution of the datasets (Figure 3.12).

Figure 3.12: an Exposed Petroleum Pipe Found near the ERI Line TH.G

The majority of electrode spacing lengths in the field experiments were between 5 and 10 meters (Table 3.1). A standard ERI electrode spacing for the forward modeling was set at 8 m (26.3 ft) because it is a whole number between 5 and 10 m (16.4 to 32.8 ft). According to the field survey results, a background resistivity of 50 to100 Ω·m was common in the study sites. Therefore, both resistivity values were tested as background resistivity values in each forward model. The pipe and/or brine were expressed as a conductive cell(s) whose dimension was one cell (4 meters in most simulations). The resistivity values of conductive objects in the subsurface were determined by lower resistivity anomalies from the resulting data of the field surveys, which were somewhere between 0 and 20 Ωm. Consequently, the resistivity values of 20, 10, 5, 2.5 and 1 Ωm were tested as a conductive object in each model.

Resistivity Forward Model 1 – Single Pipe

This model was the simplest model, which contained only one conductive cell located near the mid point of ERI line (Figure 3.13). This model simulated a case with an ERI line intersecting orthogonal to a buried pipe. Because of the nature of grid cells in the model, a conductive cell could not be located exactly in the mid point (220 m). To examine the variations of resulting images in different locations, the conductive cells were placed at both 218 m and 222 m. In addition to a forward model with 8 m spacing, this model was tested with 5 and 10 m spacing values to compare the differences in their results.
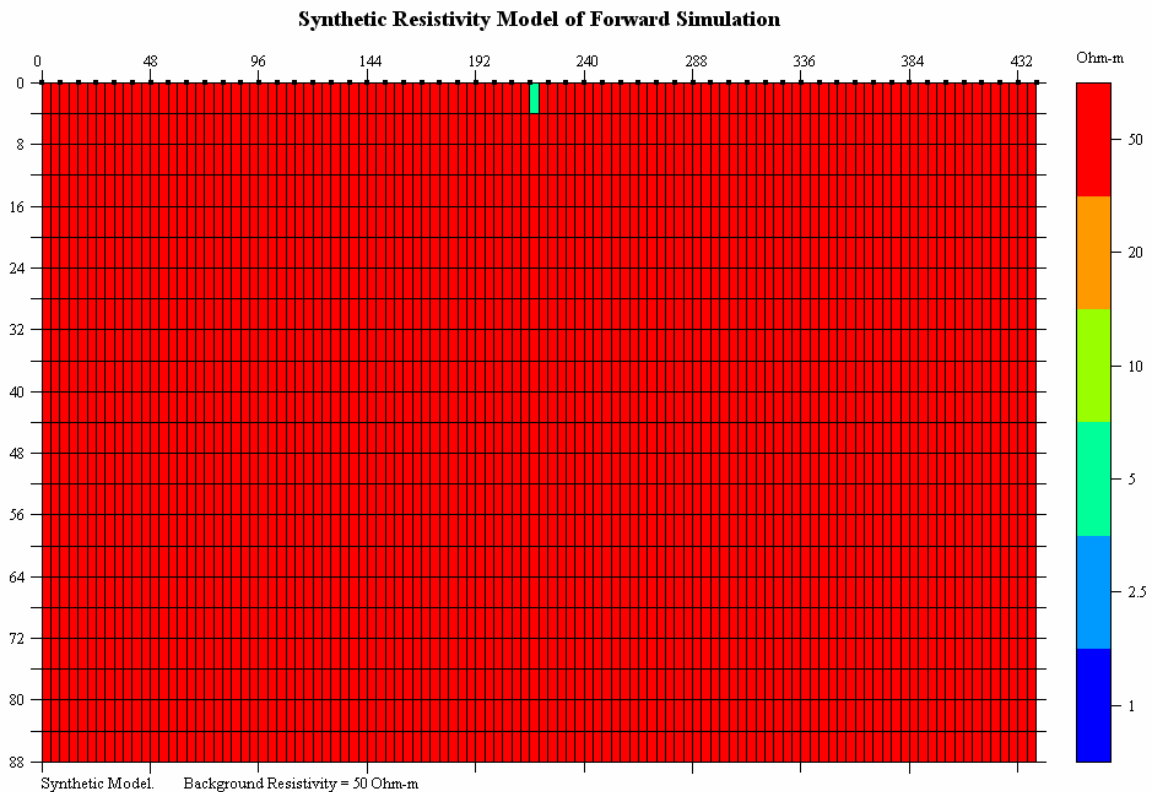
Figure 3.13: Resistivity Forward Model 1

Resistivity Forward Model 2 – Single Pipe at Small Angle

This forward model had two conductive cells at a distance of 218 and 222 m (Figure 3.14). This model simulated a case with an ERI line intersecting a buried pipe at an angle lower than 90°. The resistivity values of both cells were always the same in this model.
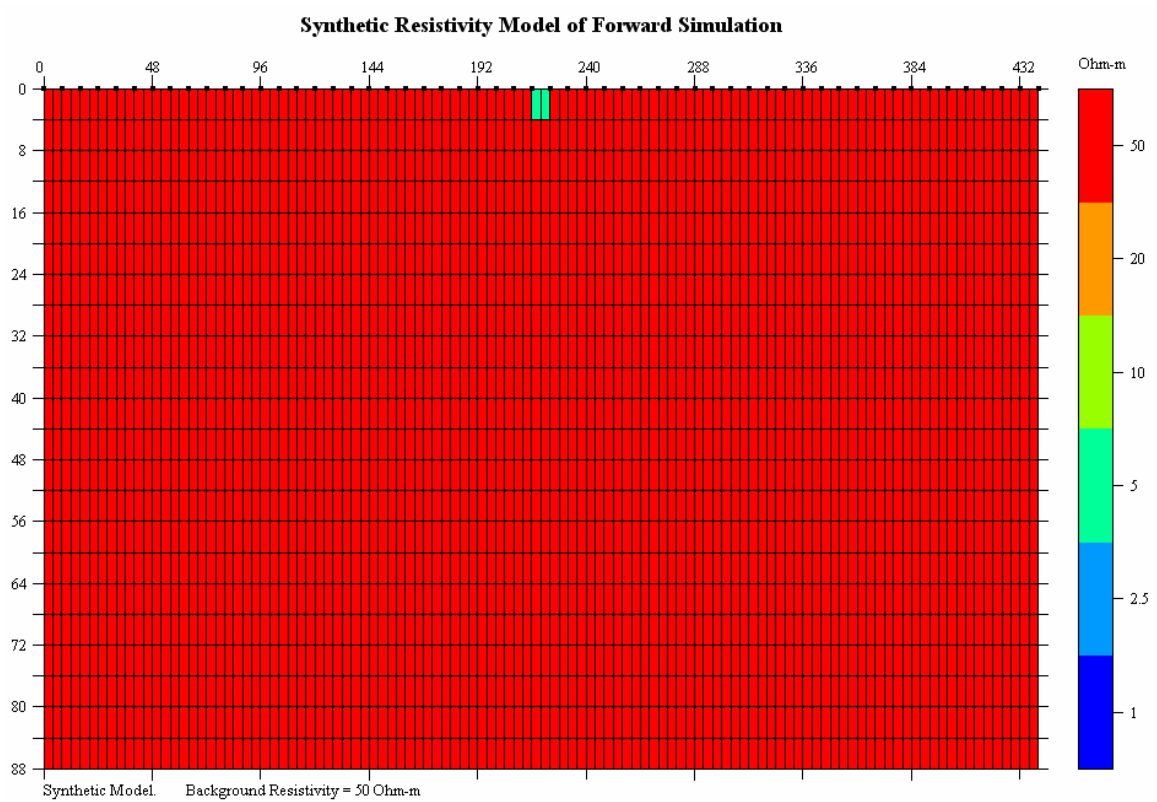
Figure 3.14: Resistivity Forward Model 2

Resistivity Forward Model 3 – Single Pipe at Low Angle

This forward model had four conductive cells at a distance of 214 to 226 m (Figure 15). The model was built to test a case with an ERI line intersecting a buried metal pipe nearly parallel by adding wider conductive cells. The resistivity values of both cells were the same in this model.
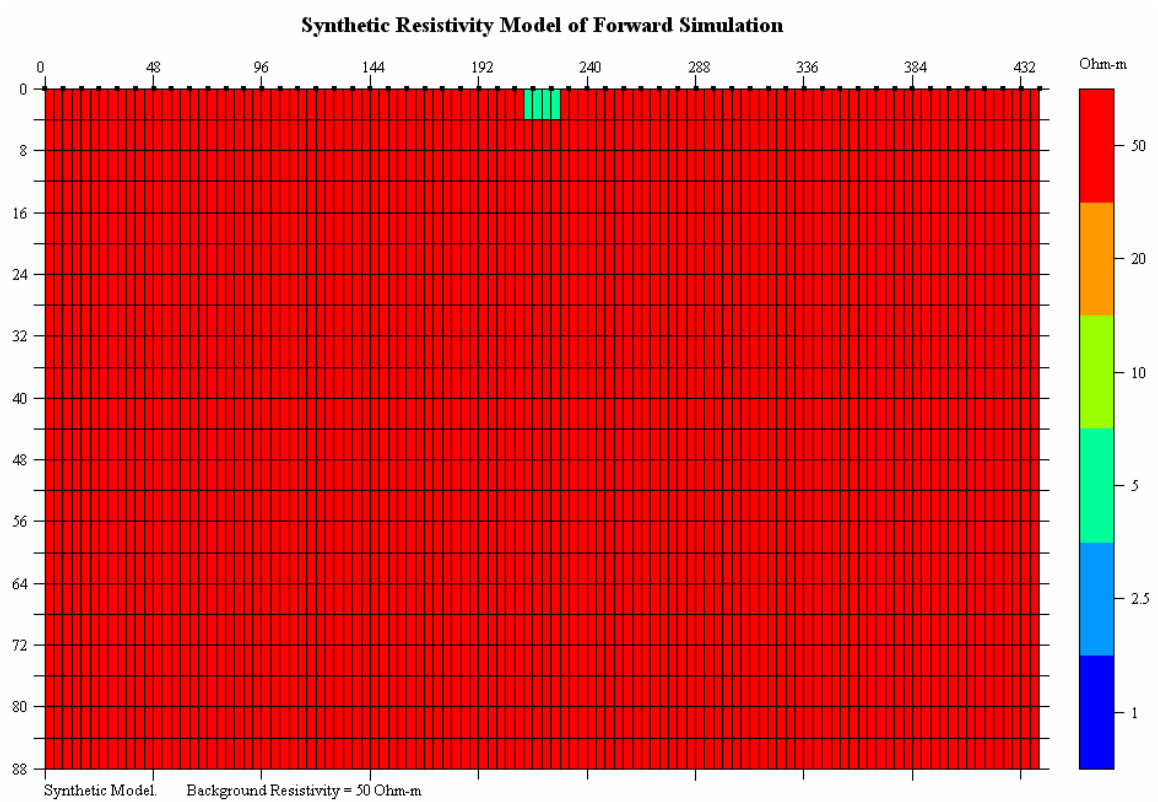
Figure 3.15: Resistivity Forward Model 3

Resistivity Forward Model 4 – Pipe with Surrounding Insulators

This forward model was similar to the resistivity model 3, and it is composed of one conductive cell placed at 218 m and four insulators located at 210, 214, 222, and 226 m (Figure 3.16). The different resistivity values of four insulators were tested, and they were 10, 100, and 1000 times the background resistivity values (i.e. if the background resistivity value is 50 Ω·m, then insulators with 500, 5000, and 50000 Ω·m were tested). The model simulated how a metal pipe which was surrounded by highly resistive materials had an effect on the ERI images.
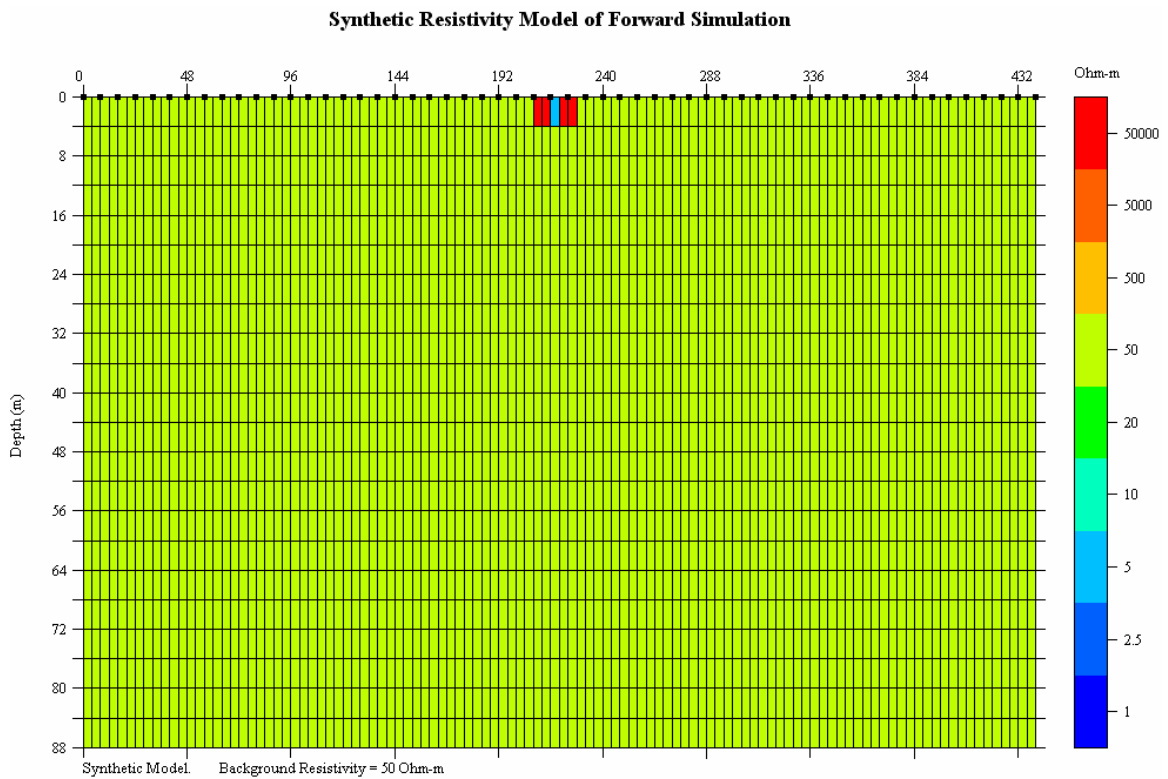
Figure 3.16: Resistivity Forward Model 4

Resistivity Forward Model 5 – Vertical Conductive Brine

This model simulated brine that was migrating downward. As showing in Figure 3.17, the resistivity value of the brine does not change with depth in this model. The location of the brine was placed at a distance of 218 m. This model did not contain any pipe unlike the resistivity forward model 6.
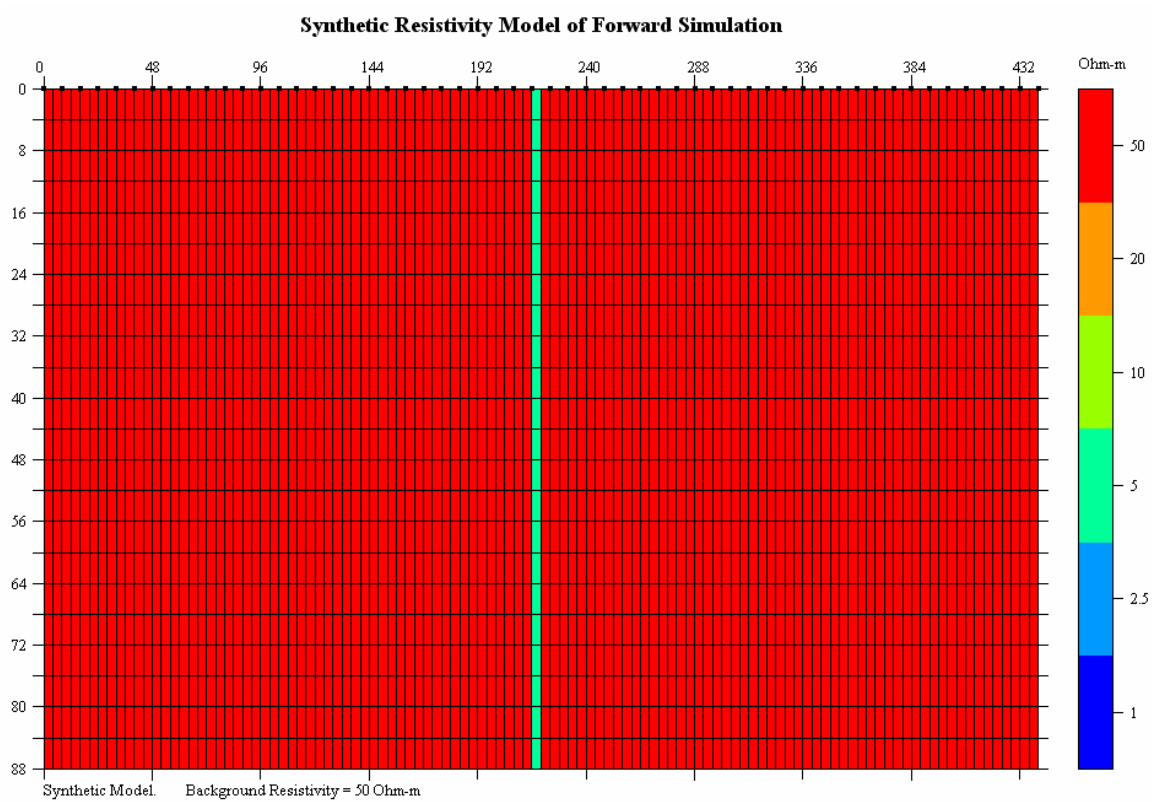
Figure 3.17: Resistivity Forward Model 5

Resistivity Forward Model 6 – Cone Shaped Brine

This model simulated brine that was migrating downward and generating a cone shape (Figure 3.18). Similar to the resistivity forward model 7, the resistivity value of the brine does not change with depth in this model. The location of brine was placed at a distance of 218 m. This model also did not contain any simulated pipe.
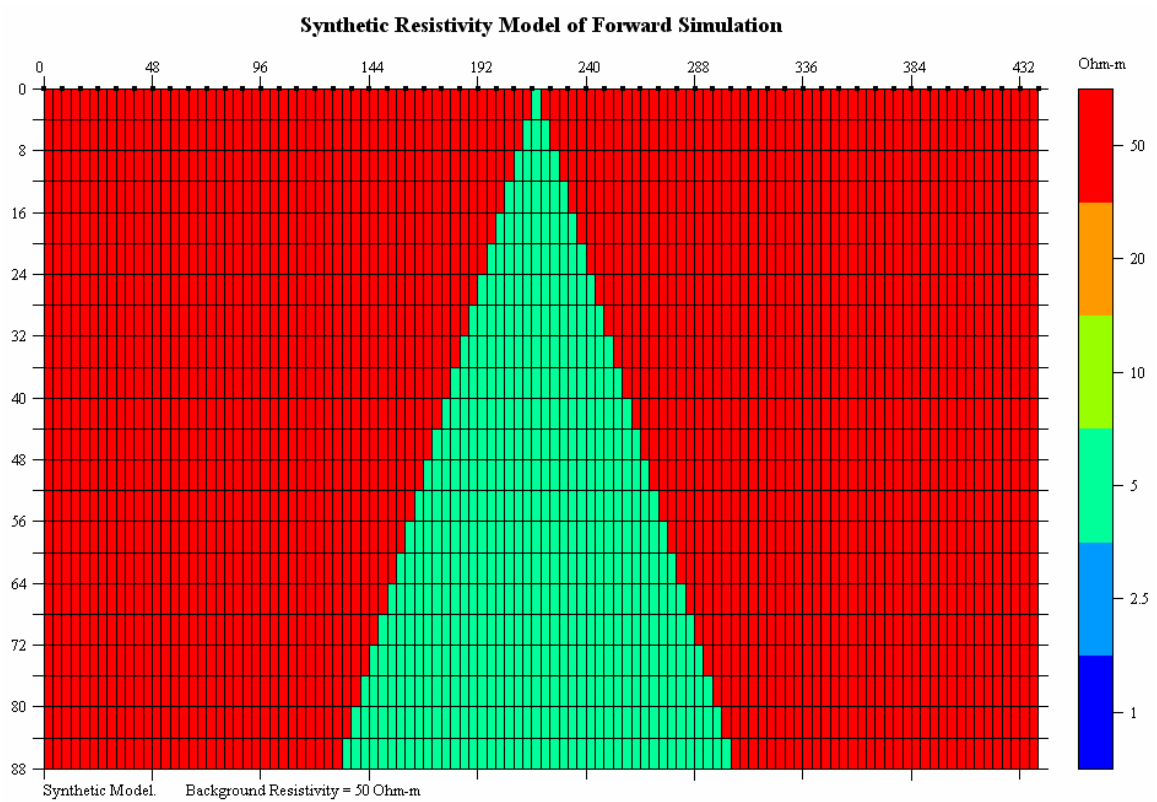
Figure 3.18: Resistivity Forward Model 6

Resistivity Forward Model 7 – Pipe with Vertical Brine

This model was combination of the resistivity forward model 1 and 5, and the shape of conductive area was similar to the resistivity forward model 5 (Figure 3.19). The top cell was set at lower resistivity values compared to the area beneath (e.g. the combination of conductive cells were 1 and 2.5 Ω·m, 2.5 and 5 Ω·m, 5 and 10 Ω·m, and 10 and 20 Ω·m). The model simulated a case which brine was leaking from a metal petroleum pipe.
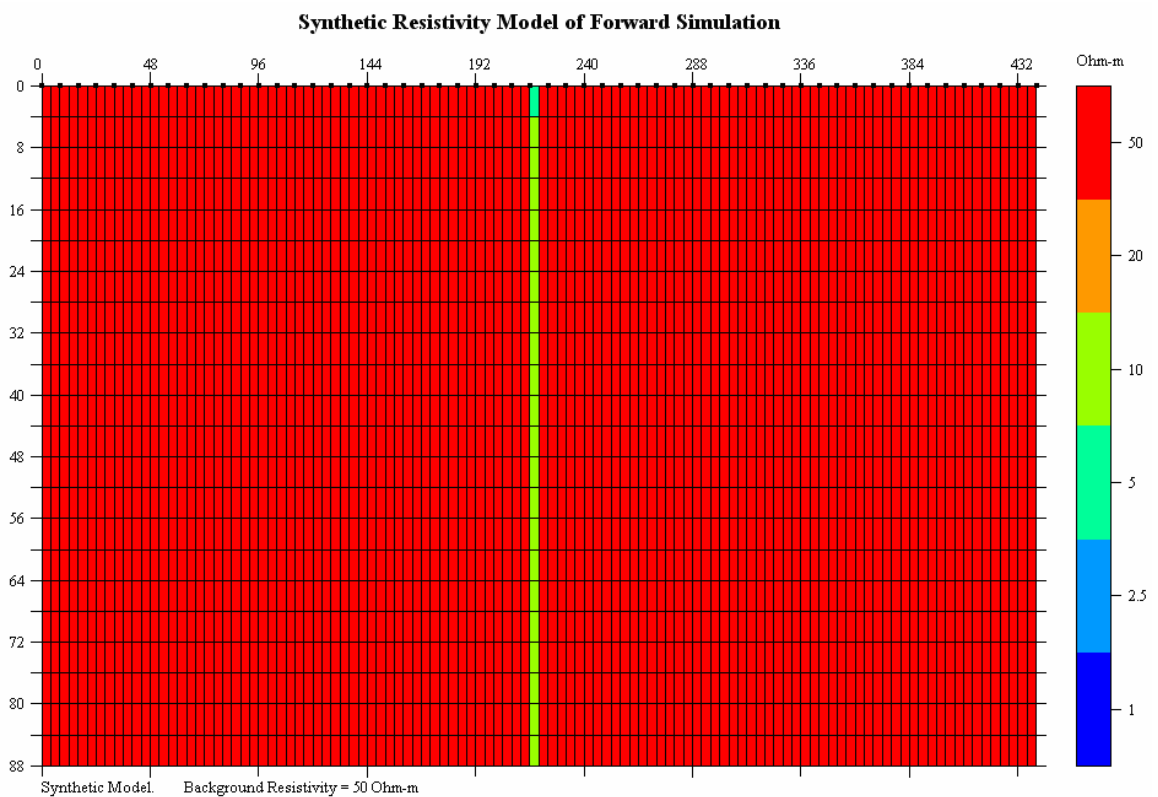
Figure 3.19: Resistivity Forward Model 7

The model simulated a case with brine leaking from a metal petroleum pipe and expanding at the bottom. This model was a combination of the resistivity forward model 1 and 6, and the shape of conductive area was similar to the resistivity forward model 6 (Figure 3.20). The top cell was set at lower resistivity values than the area beneath it (e.g. the combination of conductive cells were 1 and 2.5 Ω·m, 2.5 and 5 Ω·m, 5 and 10 Ω·m, and 10 and 20 Ω·m).
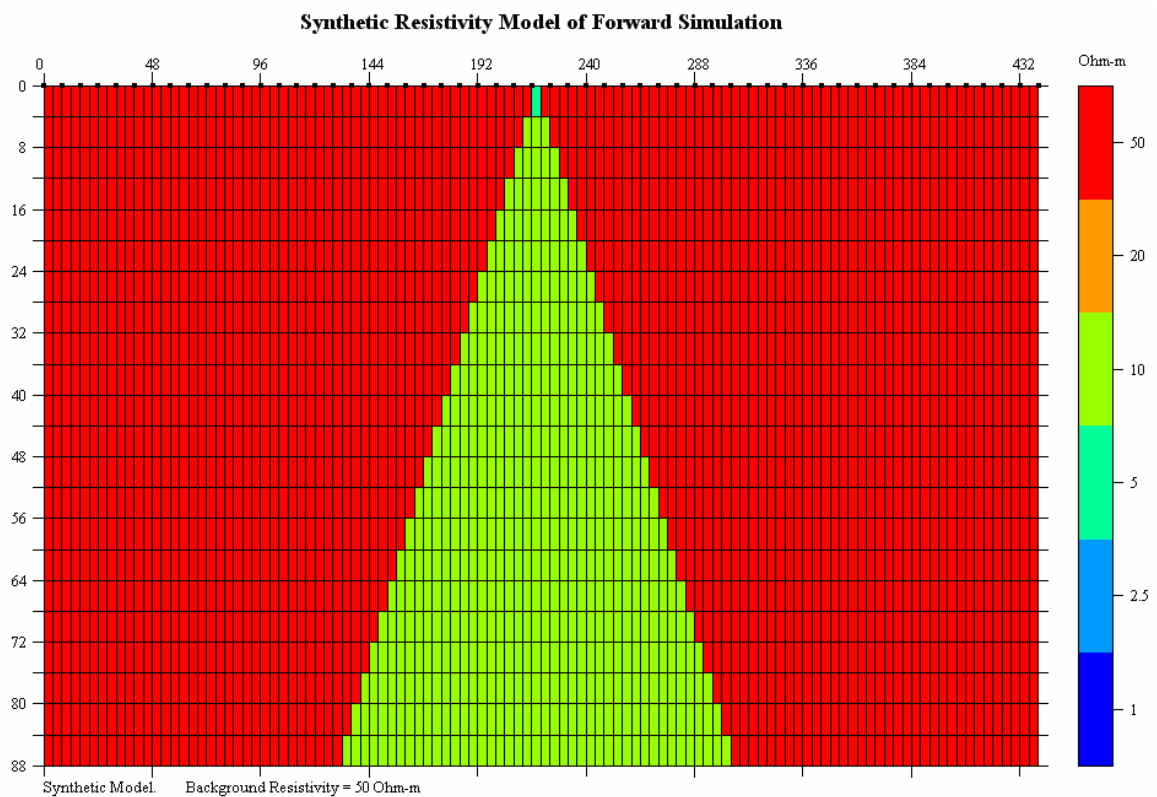
Figure 3.20: Resistivity Forward Model 8

A-priori Inversion Model

In addition to understanding pipe and/or brine behaviors by the results of forward models, the combination of forward models and 2-D electrical resistivity *a-priori* inversion models were employed as another approach to distinguish between areas of saline impact and utility lines. AGI EarthImager 2D^{TM} version 1.7.4 was also used to construct the 2-D *a-priori* inversion models. One *a-priori* inversion model was constructed based on the resistivity forward model 1 (Figure 3.13). The background resistivity of 50 and 100 $\Omega \cdot$m were used in these forward models. The resistivity values of a pipe and brine in the forward models were determined as 5 $\Omega \cdot$m and 10 $\Omega \cdot$m respectively. The pipe on the surface was placed at a horizontal distance of 218 m. Just as the previous forward models, both the Halihan/Fenstemaker techniques and the Wenner array were applied for the models.

In the *a-priori* inversion model, a pipe with various resistivity values was placed and examined how it behaves in terms of ERI images and resistivity values. First, the pipe resistivity value of 5 $\Omega \cdot$m were placed at the horizontal distance of 218 m, which was exactly the same resistivity value and the location as one used in the previous forward models. Subsequently, the resistivity values of pipe were changed from the value which used in the forward models. Those resistivity values of the pipe were ± 0.25 $\Omega \cdot$m, ± 0.5 $\Omega \cdot$m, ± 1 $\Omega \cdot$m, and ± 2.5 $\Omega \cdot$m of the original pipe resistivity value of 5 $\Omega \cdot$m.

XZ Model Data Processing

The resulting 2-D electrical resistivity images from the forward and *a-priori* inversion models could provide general trends for the pipe and/or brine interference in

the ERI images. To quantitatively evaluate the interferences and their behaviors, the inverted resistivity values were saved as X, Z, resistivity data files and were plotted numerically to determine the trends of each model.

The XZ model data represents horizontal distance (m), depth (m), and resistivity ($\Omega \cdot$m). The measurements of X values, the horizontal distance (m) values were obtained at 0, ¼ of the spacing, and then it increased to ½ of the spacing. The data points of depth (m) values, Z were taken as well as the X data points. The maximum observable depth in ERI varies depending on the type of array and the spacing of electrodes. The Z, the resistivity ($\Omega \cdot$m) values in the XZ model data file were taken at each depth and at each distance. Each XZ model file was plotted in three different graphs, which were vertical electrical resistivity profiles, horizontal electrical resistivity profiles, and vertically averaged horizontal electrical resistivity profiles. The vertical resistivity profile was the graphs of electrical resistivity values of the various pipe resistivity values at the model pipe domain (Figure 3.21). The graphs of the horizontal resistivity profile showed the electrical resistivity values along entire ERI line at the various depths which were first four data points from the surface (Figure 3.22). The graphs of vertically averaged horizontal electrical resistivity profile were similar to the horizontal electrical resistivity profile. The electrical resistivity values in the graphs were vertically averaged electrical resistivity values at the different depth of the same horizontal distance so that over all general trend of horizontal electrical resistivity could be observed (Figure 3.23).
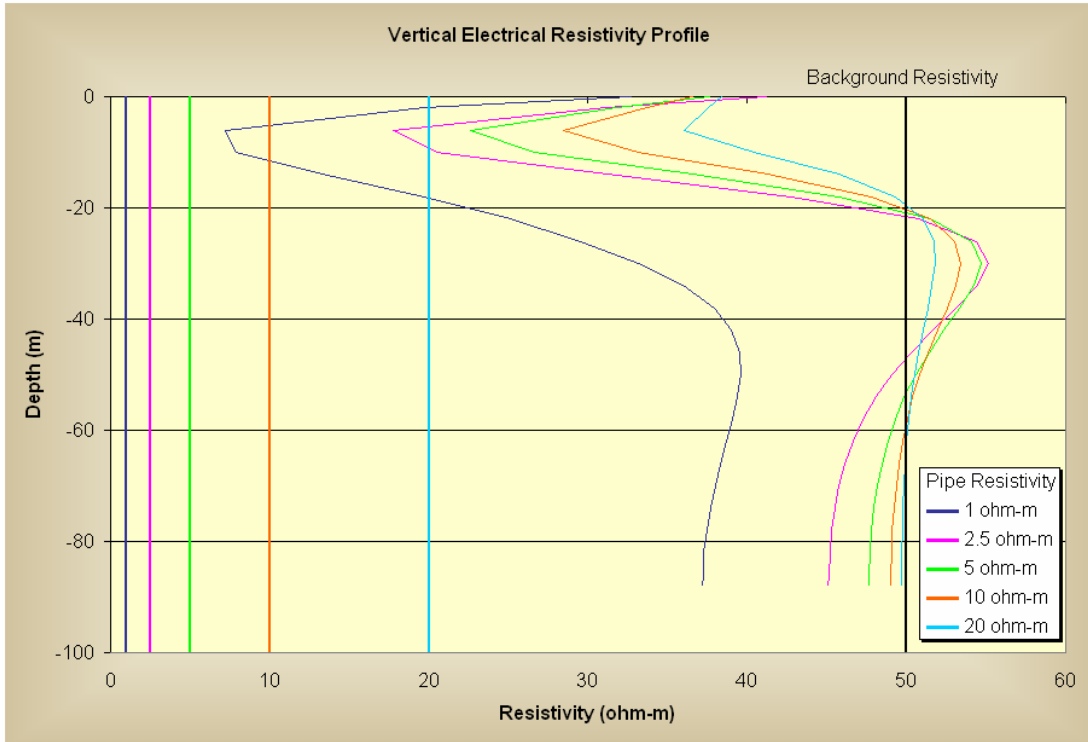
Figure 3.21: Example of the Vertical Electrical Resistivity Profile
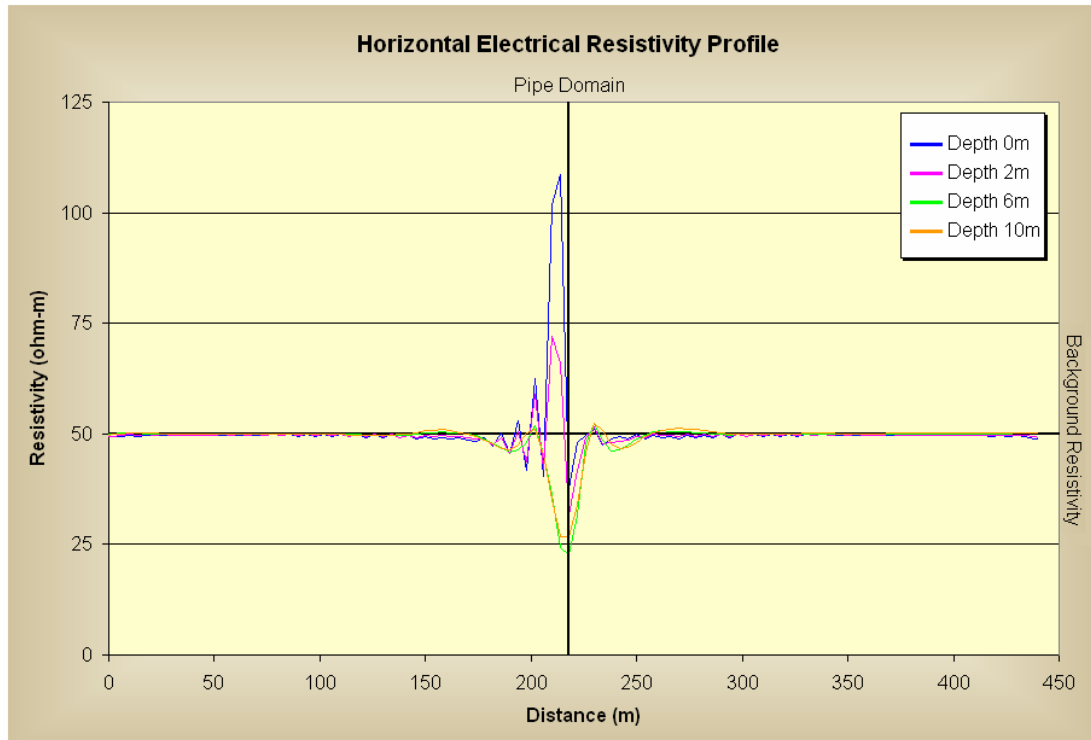
Figure 3.22: Example of the Horizontal Electrical Resistivity Profile
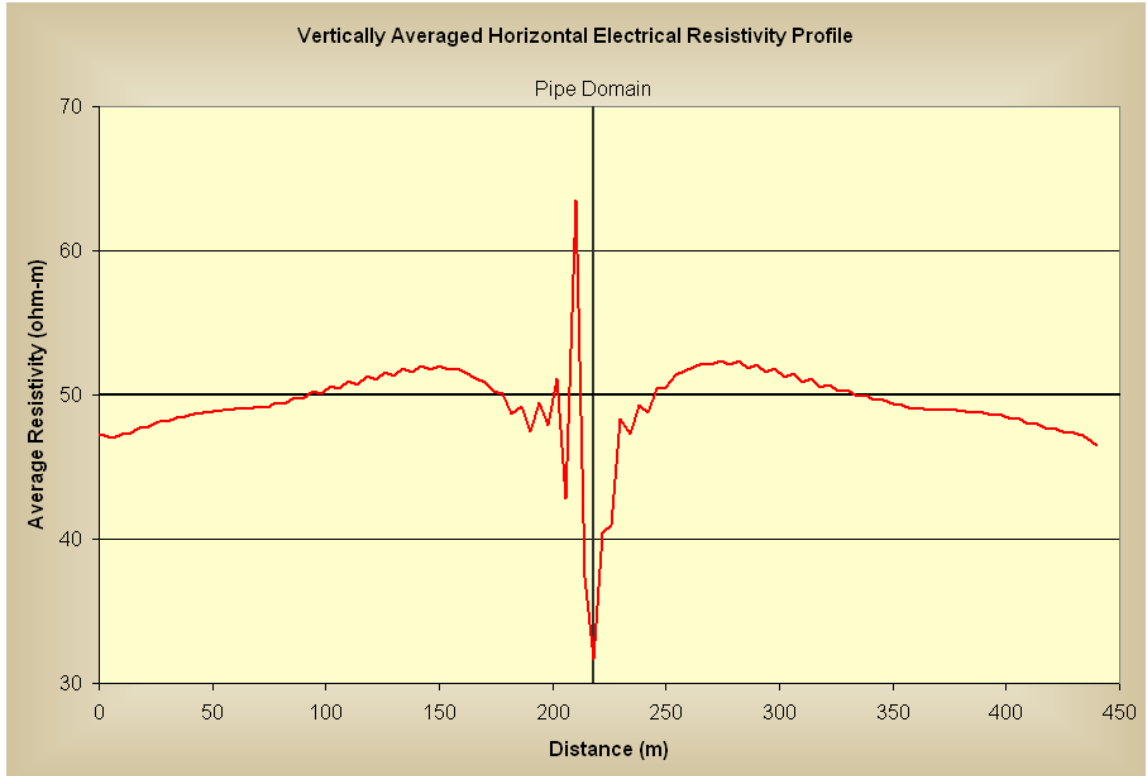
Figure 3.23: Example of the Vertically Averaged Horizontal Electrical Resistivity Profile

CHAPTER IV

RESULTS

A total of 8 ERI surveys and 1 magnetometer survey were conducted May 16, 2006 through February 23, 2007 in the vicinity of the Thunderhead Hills Addition. All ERI survey lines originated from either south or west. The Halihan/Fenstemaker techniques yielded high quality, high resolution 2-D ERI images of subsurface at the study site. The resulting ERI images of each 2-D ERI field survey are shown on Figure 4.1 to 4.8. As a part of the field work, each ERI survey line and notabl existing site features such as utility line locations, roads, and petroleum production systems were photographed during field data collection, except for survey line TH.C.

A total of 252 forward models were completed using both the Halihan/Fenstemaker and the Wenner techniques to compare and contrast the two different methods. Eight different model scenarios were applied in each technique to observe the noise behaviors in ERI images. In addition to the forward models, 36 *a-priori* inversion models were conducted based on the forward model 1.

Field Survey Results

Field results from the ERI data are presented followed by the line of magnetic data that was collected.

Several findings emerged through field surveys in this area. Low resistivity anomalies existed relative to surrounding materials, which indicated possible brackish water impacts were detected at relatively deep areas in the images. To detect the low resistivity anomalies at depth required the ERI lines to be extended as long as possible. In general, the maximum observable depth is approximately one-fifth of the total ERI line length. This requirement was problematic in the urban setting due to locations of utilities, property width, and scheduling issues relating to land owners. One of the biggest issues in this investigation was underground utility and petroleum pipes. Especially, a leaking metal petroleum pipelines which leaves an additional conductive signature in the ERI images can be confused from the conductive signature from a metal pipe itself. Many of the images contained significant horizontal and vertical signatures in electrical properties. Without a confirmation drilling program, the exact origins of most of the significant horizontal and vertical variations could not be substantiated in the field.

TH.A Survey

The background resistivity of this image was lower than the most of the other datasets. A higher resistivity layer were found at approximately 30 meters (100 feet) below the land surface, but the layer did not appear clearly in this image due to the color scheme. Several conductive features in TH.A survey were found at relatively shallow depth. The conductive features were located at 4 locations (~130 meters/~430 feet, ~215 meters/~705 feet, ~290 meters/~950 feet, and ~420 meters/~1380 feet). Three petroleum pipelines crossing the TH.A survey line correlated with these low resistivity anomalies.

The locations of pipelines were confirmed by subsequent magnetometer survey data and gas/petroleum pipeline markers found in the field after the ERI line survey was conducted (Figure 4.9). The conductive area at the north end of the ERI survey line from 400 meters to 550 meters (from 1300 to 1800 feet) did not have same appearance as the other pipeline anomalies. The location of a historic saltwater evaporation pit was estimated through aerial photos. It was mapped on the ERI image (Figure 4.1) and the magnetometer survey (Figure 4.10). The saltwater evaporation pit did not appear to affect the result of TH.A ERI survey. In the view of electrical properties, the saltwater evaporation pit appears to have no significant effects at this area. However, the result of magnetometer survey showed significantly lower anomaly approximately 10 meters (33 feet) north of the area of historic saltwater evaporation pit while the anomalies of pipes showed notable positive anomalies.

TH.B Survey

The background resistivity of this image was relatively consistent than the most of the other survey images. The resistivity values of this image were generally above 75 $\Omega \cdot$m which appeared as orange tones in the image (Figure 4.2). The resistivity values as low as 60 $\Omega \cdot$m existed in the shallow portion, which likely indicate changes in geological variations, some finer grained layers exist at approximately 12 meters (40 feet) depth at the south end of the image and at roughly 30 meters (100 feet) depth at the north end. Some lower resistivity anomalies were detected at a horizontal distance of 245 meters (800 feet) and at the vertical distance of 60 meters (200 feet). This indicates that possible

brackish fluid exists at depth. However, the lateral distance required for deeper ERI data was unavailable at this location.

TH.C Survey

A survey line TH.C was confronted with a noticeable number of petroleum related pipelines (Figure 4.3). These pipes were believed to be inactive and to have been drained over 30 years ago. The interference patterns from the pipes were found at the horizontal distance of 88 meters (290 feet) and 192 meters (630 feet). However, some conductive areas were found in the subsurface between these pipe patterns. These conductive areas may be originated from saline fluids that leaked from the pipes during previous petroleum activities. The image also indicated that the west side of the image was more conductive than the east. This was correspondent to images TH.A and TH.G which intersected with the survey line TH.C. TH.A image showed more conductive background throughout the domain, and TH.G image had more resistive background electrical resistivity values though it contained significant interference.

TH.D Survey

The results of this survey line were very similar to those of survey line TH.C. The interference patterns from the pipes were also found in this image (Figure 4.4). They were located at 43 meters (140 feet) and 130 meters (430 feet). Some conductive features were found at the bottom of the ERI image at 70 meters (230 feet) and 260 meters (850 feet) lateral distance along the line.

TH.E Survey

The quality of this dataset was significantly affected by the interference of the utilities and petroleum pipelines (Figure 4.5). The majority of the conductive features found below the utilities and petroleum pipelines were not extended to the bottom of the image, except from a feature located at the horizontal distance of 137 meters (450 feet). This conductive feature appeared to connect to a conductive feature at depth.

TH.F Survey

A significant number of conductive features were found in this image (Figure 4.6). Several lower resistivity anomalies at the shallow depth were found near the west and east ends. Especially, the conductive feature on the east side was similar to a pattern which interfered a metal pipe, but other conductive features found in the image may be originated from saline fluid.

TH.G Survey

The survey line TH.G was the longest ERI survey line which was extended the full cable length of 550 m (1804 ft). This was the worst quality dataset due to several buried petroleum pipe lines both parallel and perpendicular to the ERI survey line (Figure 4.7). Most of the conductive features were found near surface. However, some of conductors were extended to depth, one at 219 meters (720 feet) and a second at 475 meters (1560 feet) laterally. Without confirmation drilling, these conductive features at depth cannot conform whether they were originated from saline impact or from interference from metal pipes.

TH.H Survey

The image indicated that area of a potential saline impact was located at 15 meters (50 feet) below the land surface, and it extended to the bottom of the image at more than 45 meters (150 feet) below the land surface (Figure 4.8). Overall the east side of the image was more conductive than the west side of image.

Figure 4.1: Electrical Resistivity Image TH. A

Figure 4.2: Electrical Resistivity Image TH. B

Figure 4.3: Electrical Resistivity Image TH. C

West　　　　　　　　　　　　　　　　　　　　　　East

ERI Line TH. G

Depth (m)

Distance (m)

Resistivity (ohm-m)

Legend	
	Suspected Pipe — Unknown Use
	Oil gathering System (Active/Abandoned)
	Natural Gas Gathering System
	Water Injection System
	Line Intersection
	Barbed Wire Fence with Wood Posts

30　　　29

31　　　32

Figure 4.4: Electrical Resistivity Image TH. D
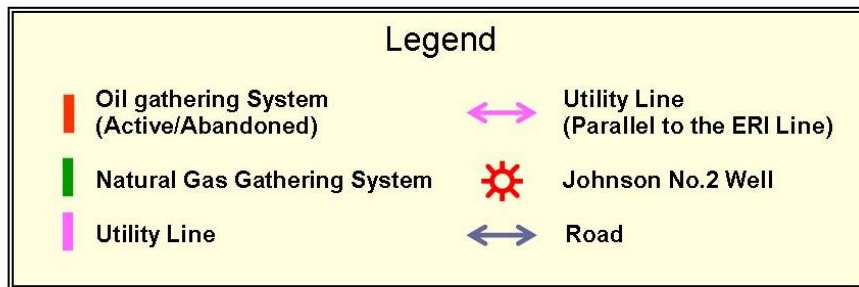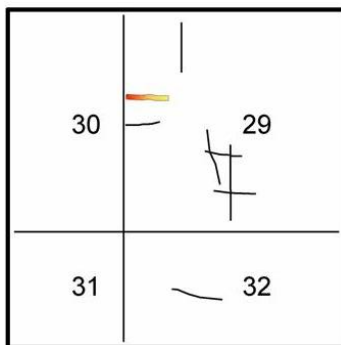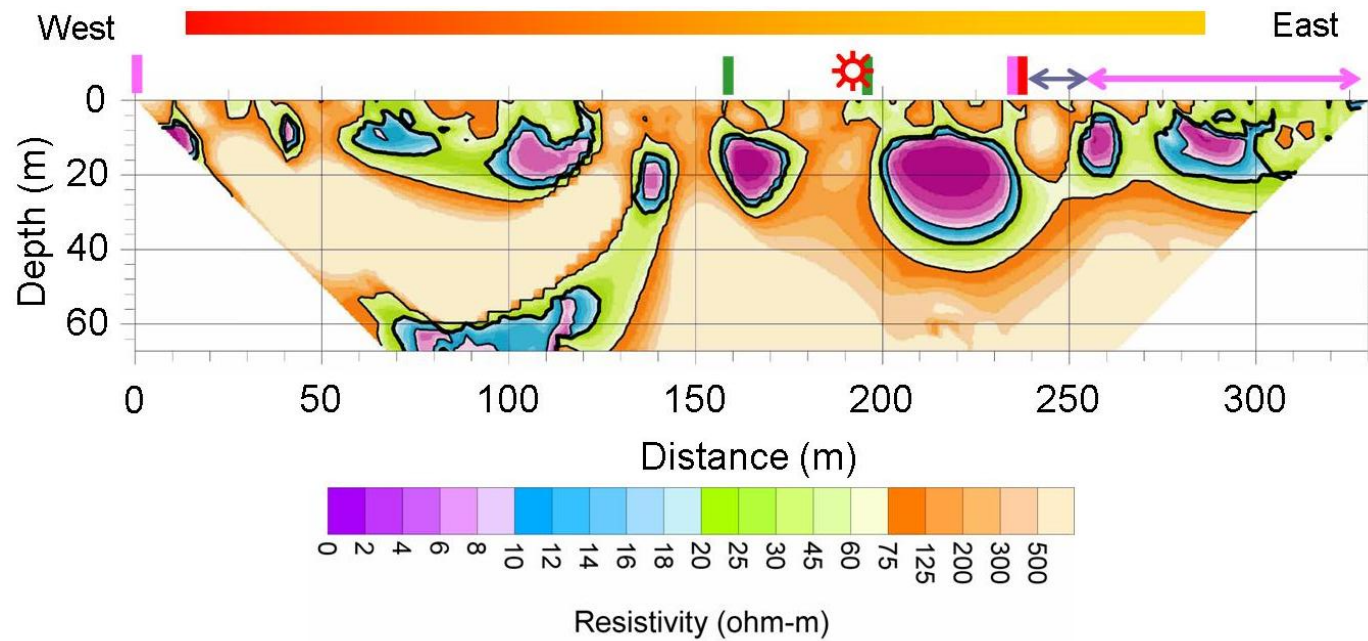
Figure 4.5: Electrical Resistivity Image TH. E
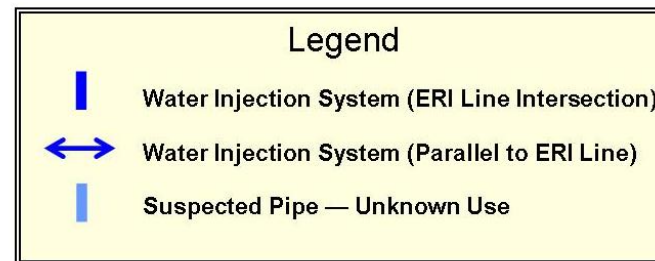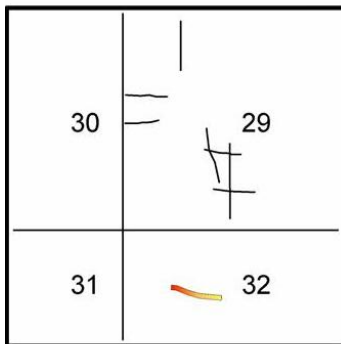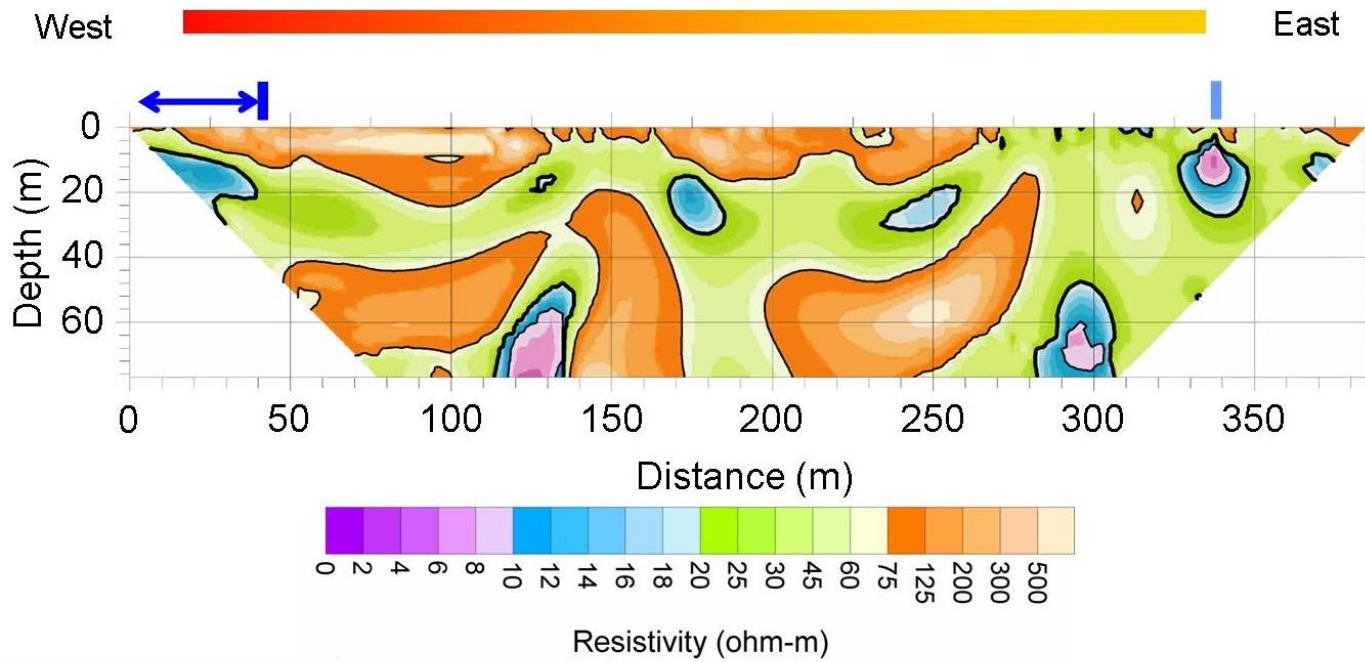
Figure 4.6: Electrical Resistivity Image TH. F

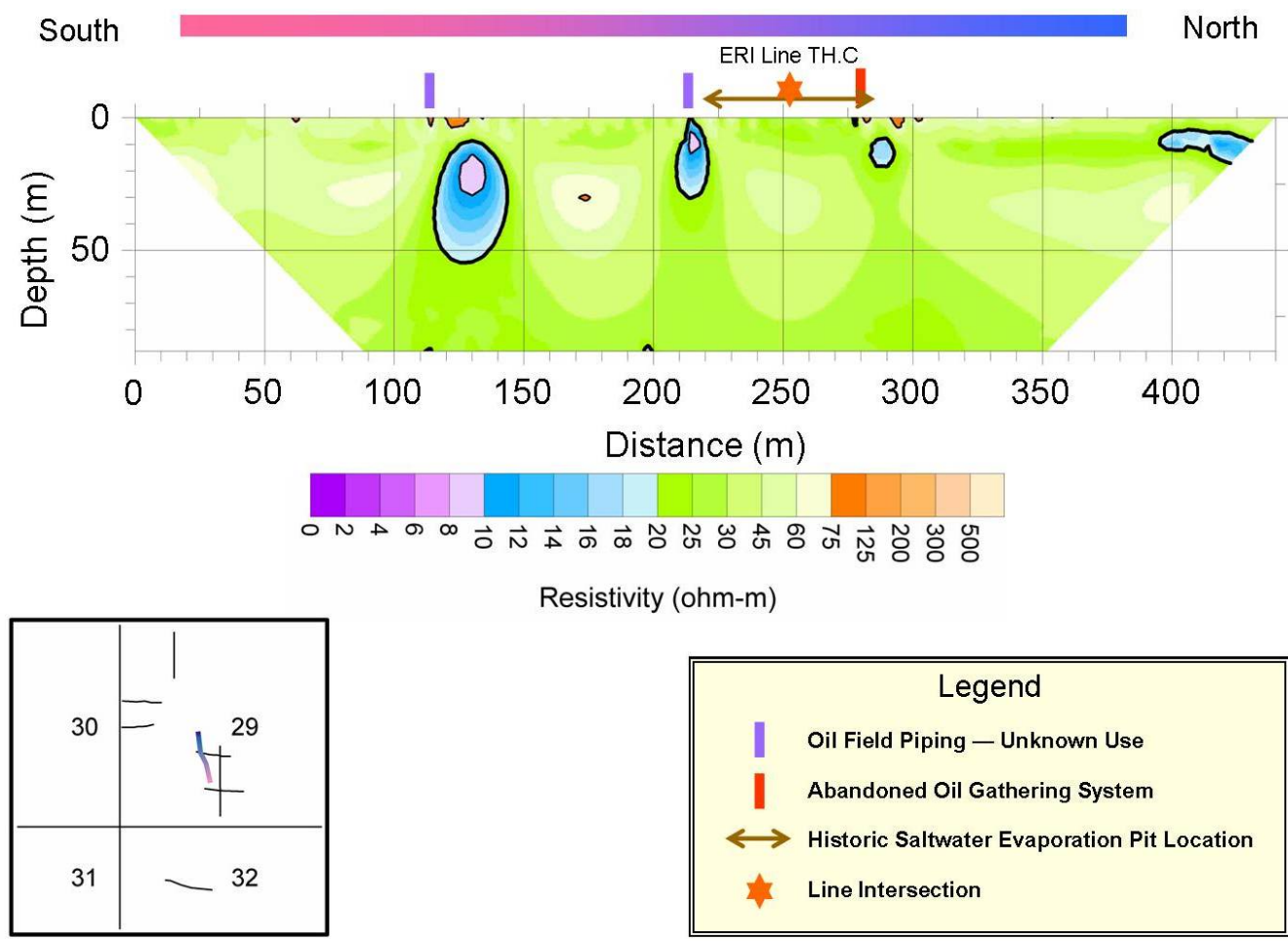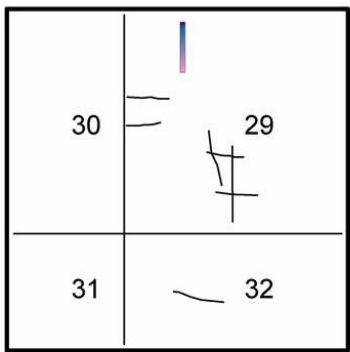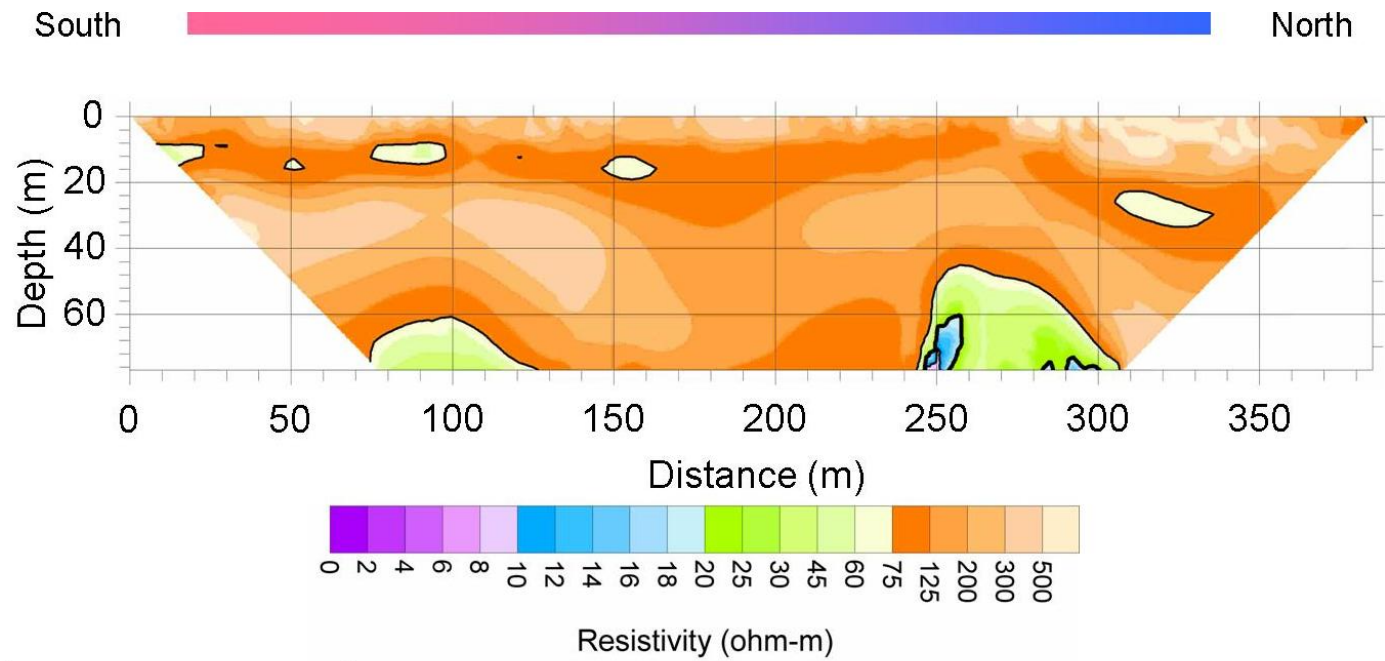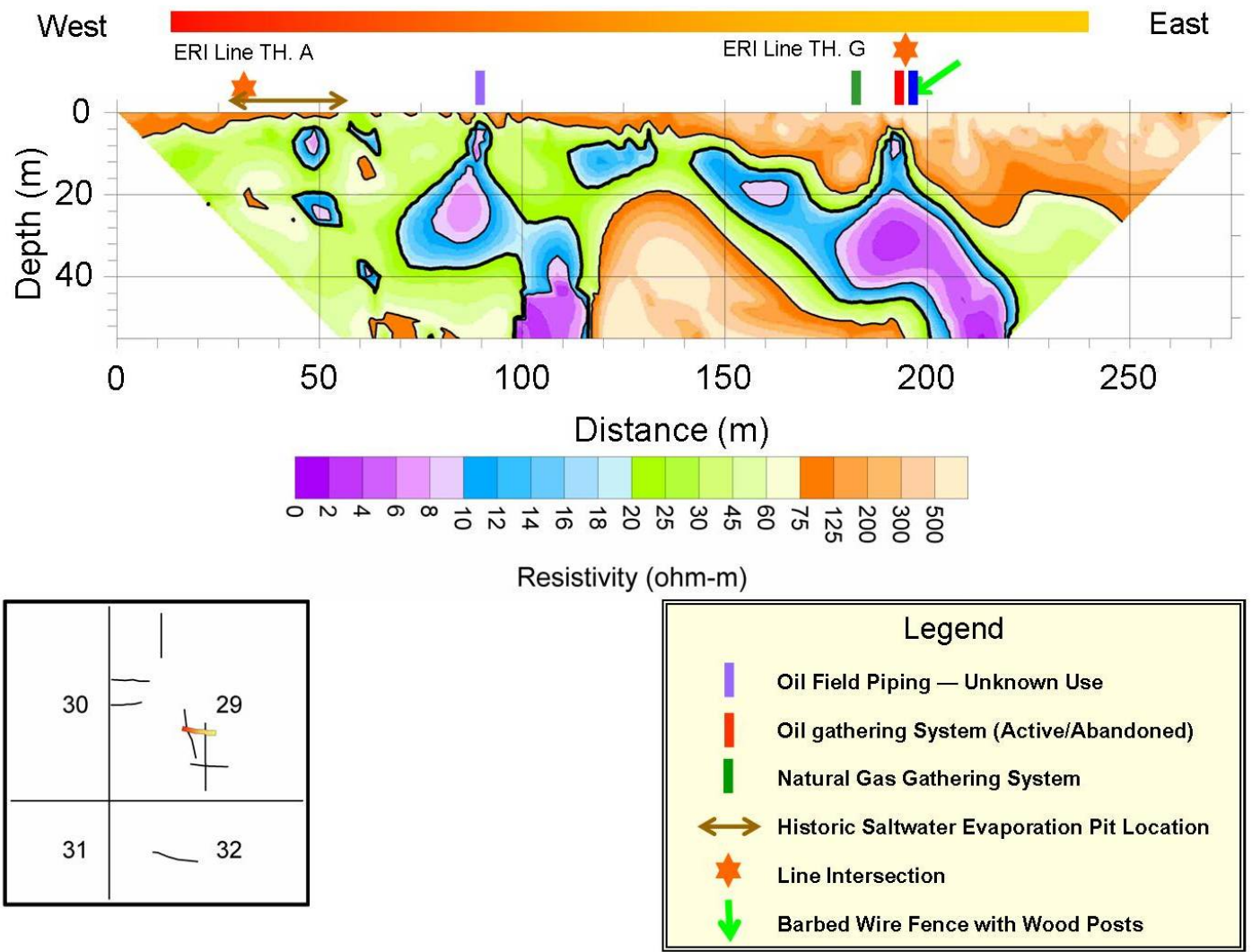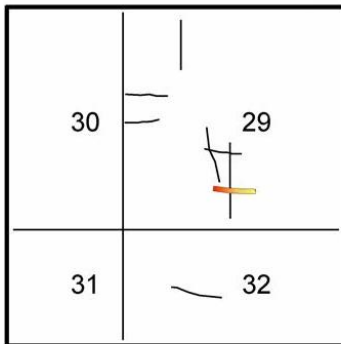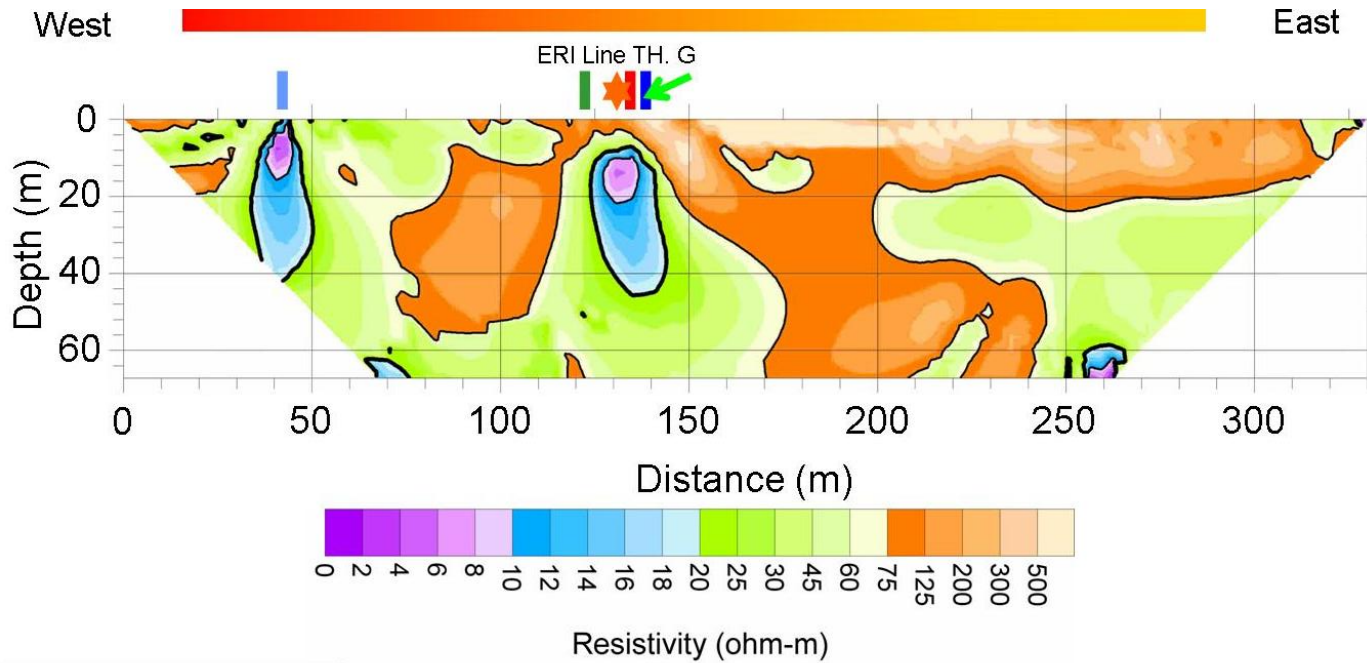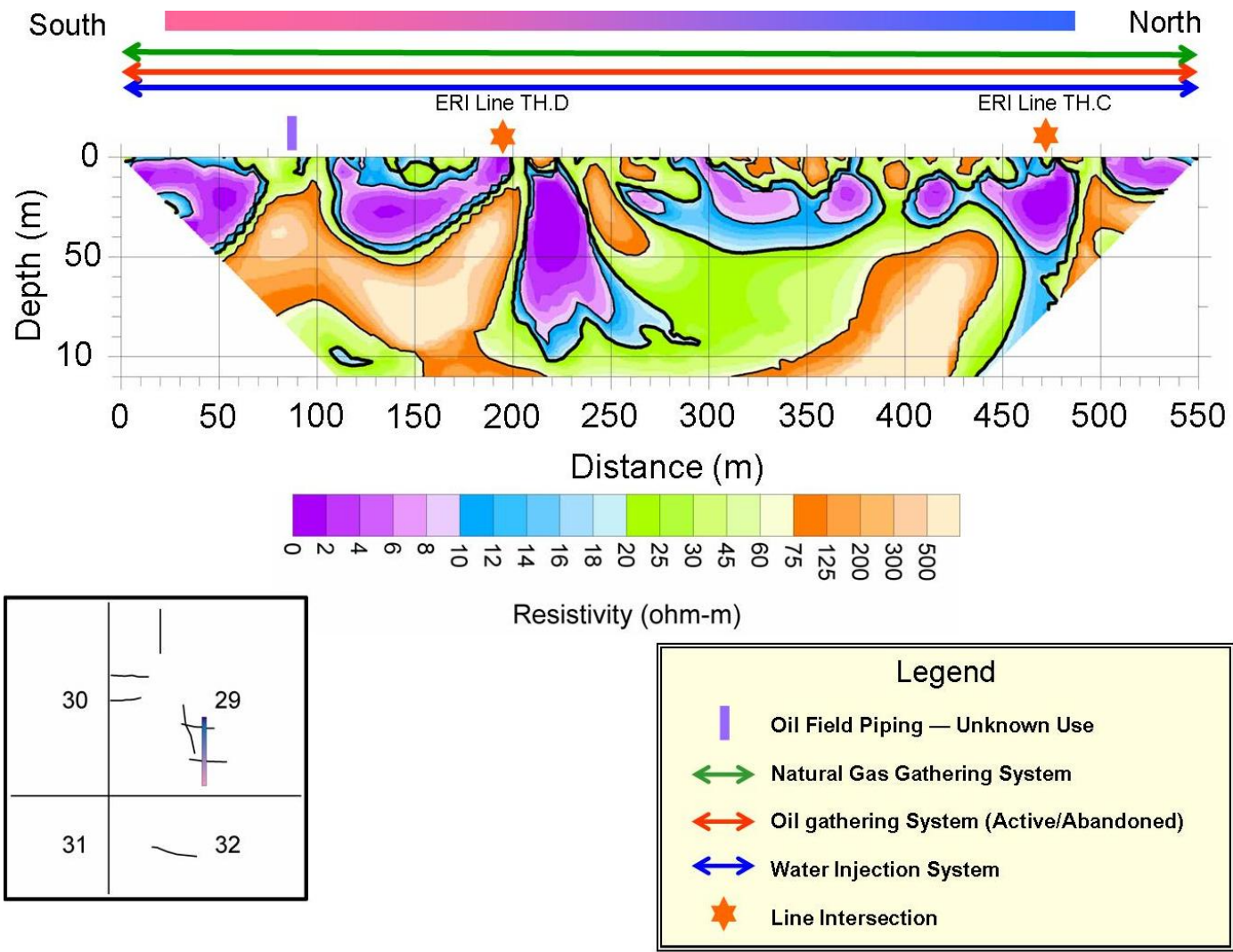**Figure 4.7: Electrical Resistivity Image TH. G**
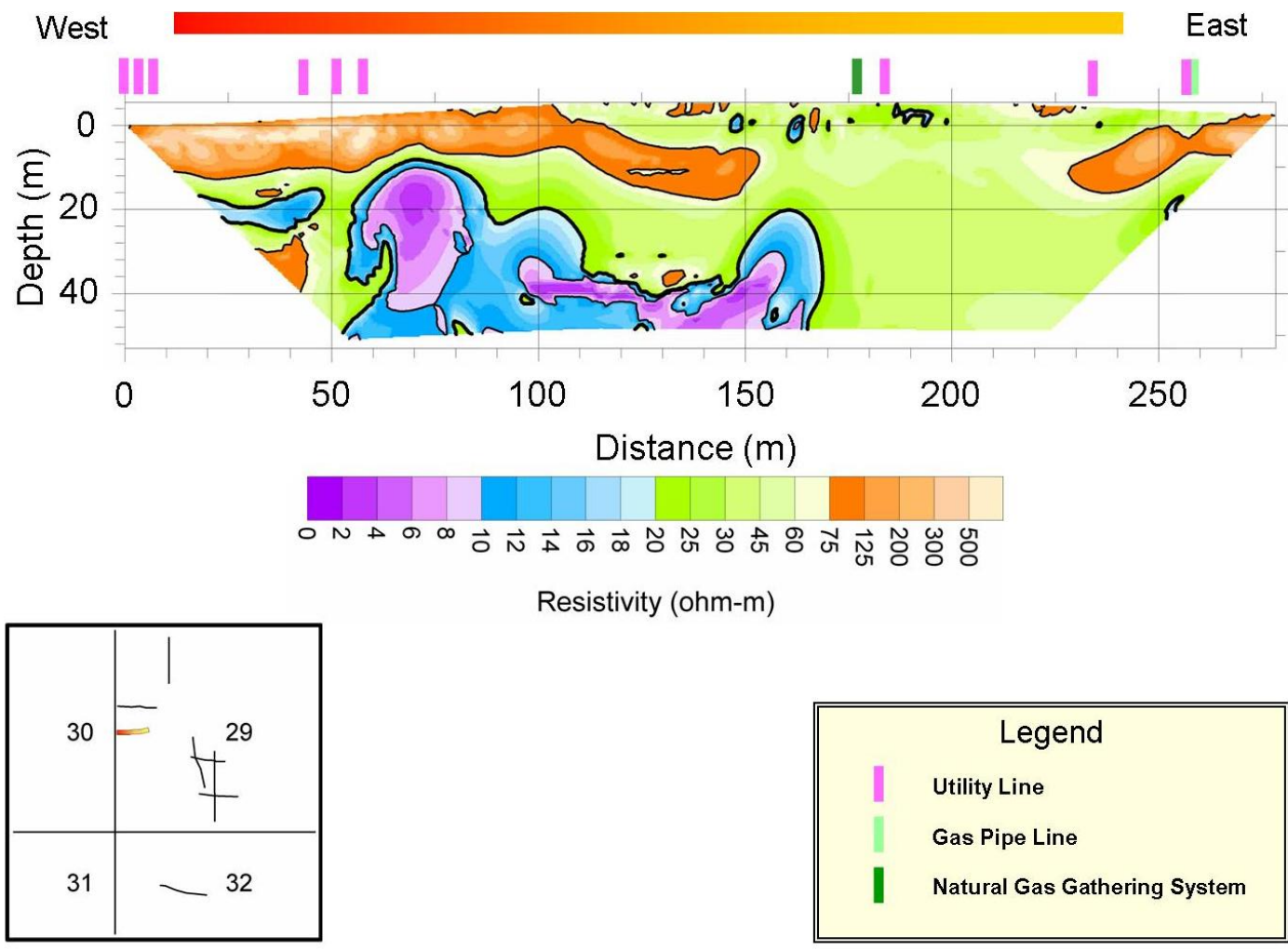
Figure 4.8: Electrical Resistivity Image TH. H

<u>Magnetometer Result</u>

The Magnetometer survey was conducted along the ERI line TH.A. High total magnetic field values were observed at two locations along the survey line (Figure 4.10). One was located approximately at 135 meters (443 feet), and another was located approximately at 220 meters (722 feet). This indicated that at least two conductive objects existed along the TH.A survey line. Furthermore, a strong trough was found lateral location at 290 meters (950 feet).

Gas/petroleum pipe line makers were found in the field while the magnetometer survey was conducted (Figure 4.9). The locations of makers were strongly matched with the horizontal locations of the magnetic field anomalies. The possible source of the lower magnetic field anomaly was not found during the field survey. However, the position of lower anomaly could correlate with the location of the historic saltwater evaporation pit which located approximately 10 meters (33 feet) south of the anomaly (Figure 4.10).

Figure 4.9: Petroleum Pipeline Marker Found in the Field
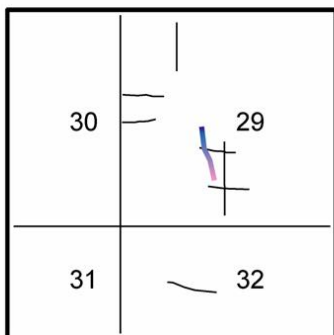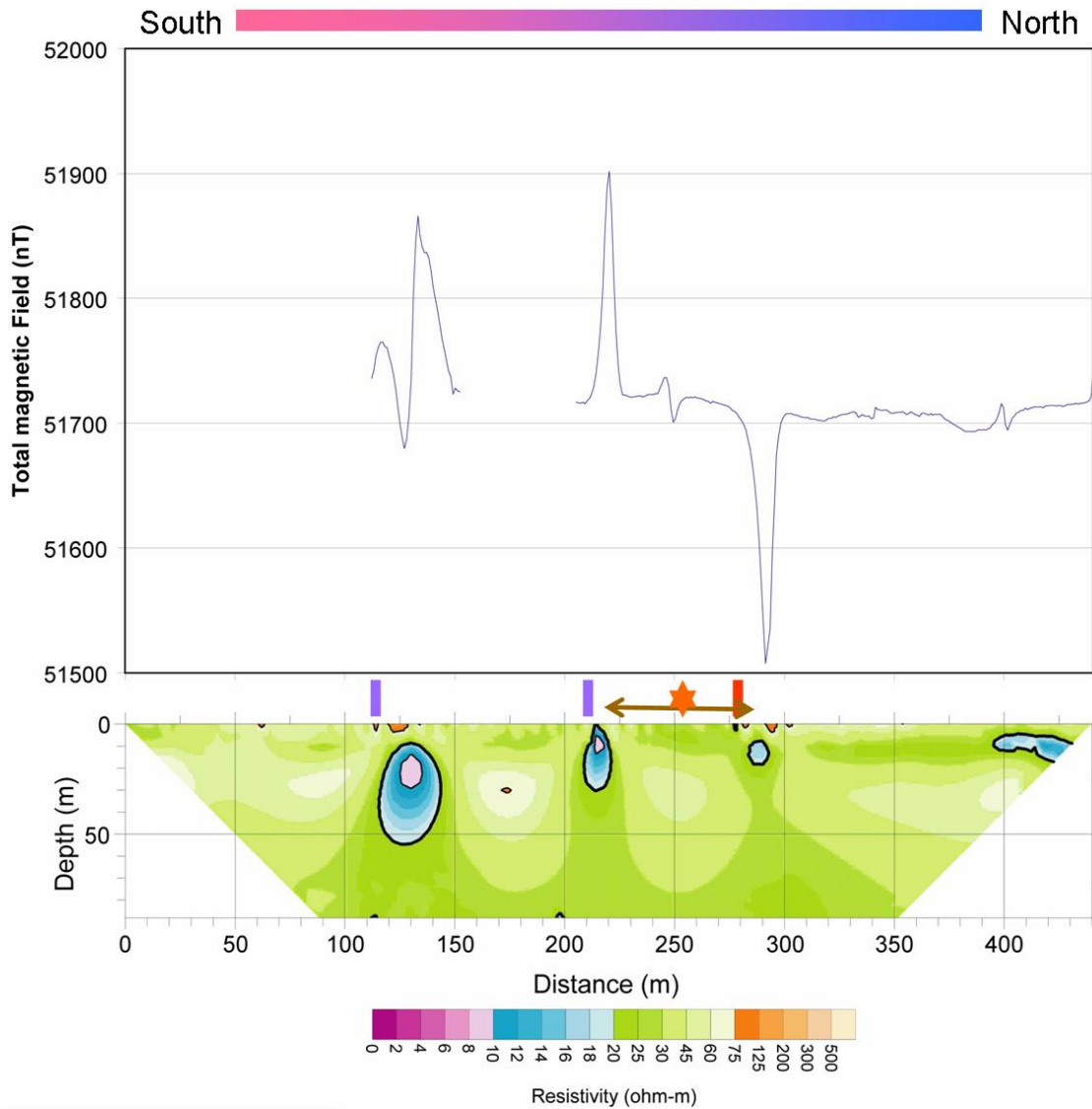
Figure 4.10: Magnetometer Survey Result along the ERI Line TH.A

Electrical Resistivity Model Results

The forward models are employed with both the Halihan/Fenstemaker and the Wenner methods to determine anticipated pipe patterns in ERI datasets. The results from the ERI forward models indicated that conductive features (i.e. metal pipe, utilities, and saline fluid) in the subsurface could be located and distinguished. The results of the forward models were applied to a-prior inversion models of with known and unknown pipe locations.

ERI Forward Modeling

The forward inversion models were saved and plotted as XZ data (horizontal location, depth, resistivity) to quantify the conductive pipe and fluid signatures. Each XZ file was plotted in three graph types, which were horizontal electrical resistivity profiles, vertical electrical resistivity profiles, and vertically averaged horizontal electrical resistivity profiles. The results of each model are described as follows.

Resistivity Forward Model 1 – Single Pipe

The results of resistivity forward model 1, a single pipeline intersecting an ERI line at a right angle illustrated several characteristics. The vertically averaged horizontal electrical resistivity profile plotted the average electrical resistivity values at the different depths of the same horizontal distance so that over all the general tendency of thehorizontal electrical resistivity could be observed. The results from the Halihan/Fenstemaker model demonstrated that a pipe domain corresponded to troughs of the lowest resistivity value (Figure 4.11A; Appendix A, Figures A.1-A.8). As the model

pipe resistivities were increased from 1 to 20 Ω·m, the same tendency was observed across all images. This tendency also did not change with changing in background resistivities, electrode spacing and the location of the model pipe. When the difference between the model pipe resistivity value and the background resistivity value was higher, a significant peak appeared at two cells next to the model pipe domain. The stronger peak appeared on the side of the closest electrode. The results from the Wenner method showed similar results as the results from the Halihan/Fenstemaker method, which the locations of lowest resistivity values corresponded to the model pipe location regardless of differences in electrode spacings, background resistivities, and pipe locations. However, the strong peaks were not observed with the Wenner method (Figure 4.11B; Appendix B, Figure B.1-B.8).
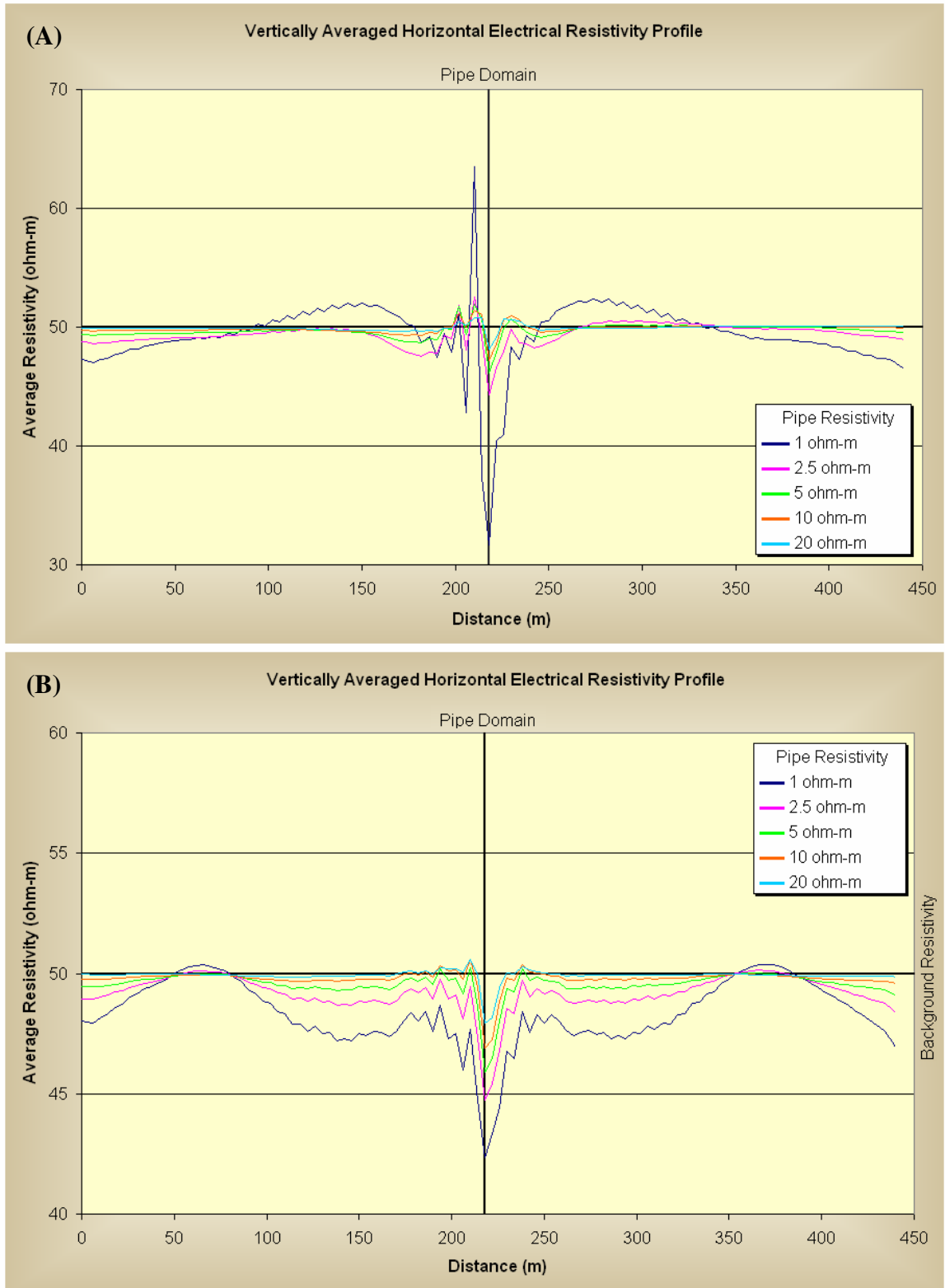
Figure 4.11: Vertically Averaged Horizontal Electrical Resistivity Profile of Forward Model 1
Pipe Domain: 218 m; Background Resistivity: 50 ohm-m; Electrode Spacing: 8 m
(A) The Halihan/Fenstemaker Method (B) The Wenner Method

69

The graphs of the horizontal electrical resistivity profile were composed of various depths adjacent to the cell which the model pipe located (Figure 4.12). Just as the results from the vertically averaged horizontal electrical resistivity profile, the lowest resistivity values from the horizontal electrical resistivity profile matched with the model pipe domain in both methods. However, some of the lowest resistivity points which had similar values were adjoining each other (Figure 4.13A). Moreover, multiple troughs which resemble pipes in their appearance were sometimes found near the model pipe domain. When differences among the resistivity values of those troughs were small, these multiple troughs could be difficult for determining the pipe location (Figure 4.13B). The former issue frequently occurred in the Halihan/Fenstemaker method; the latter issue was occasionally found in the both method.

The depth of the lowest resistivity values had a notable pattern in the Halihan/Fenstemaker method. It was recognized that most of the lowest resistivity values were located at a domain which one cell below where the actual model pipe was placed. However, forward models with 1 $\Omega \cdot m$ model pipe resistivity and 100 $\Omega \cdot m$ background resistivity contained the lowest resistivity values at a domain which two cells below the model pipe location. This tendency was consistent through the forward model 1 despite different settings. While the results from the Halihan/Fenstemaker method had a consistent pattern, the Wenner had different pattern in terms of the depth of the lowest resistivity values. The depths of the lowest resistivity values were found at either one cell below or on the surface of the model pipe location. Also, the lowest resistivity depth decreased as the background resistivity and the model pipe resistivity values were closer (Table 4.1).

70
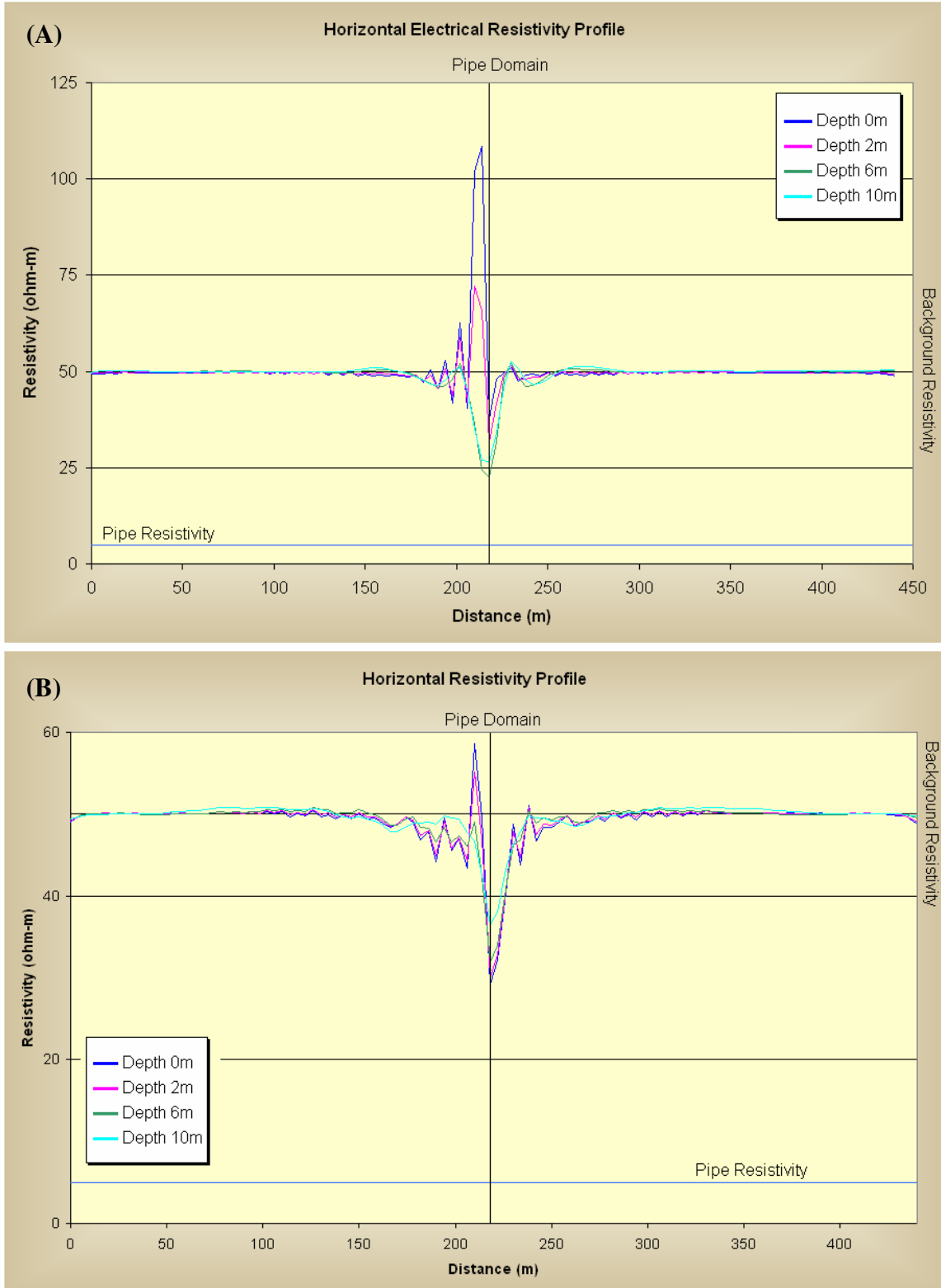
Figure 4.12: Horizontal Electrical Resistivity Profiles
Pipe Domain: 218 m; Background Resistivity: 50 ohm-m; Pipe Resistivity:
5 ohm-m; Electrode Spacing: 8 m
(A) The Halihan/Fenstemaker Method (B) The Wenner Method

71

(A)

Horizontal Electrical Resistivity Profile

Adjoining data points have similar resistivity values

(B)

Horizontal Electrical Resistivity Profile

Pipe Domain

Figure 4.13: Common Issues in the Horizontal Electrical Resistivity Profiles
(A)   Example of adjoining data points with similar resistivity values
(Halihan/Fenstemaker Method; Pipe Domain: 218 m; Background Resistivity: 50
ohm-m; Pipe Resistivity: 2.5 ohm-m; Electrode Spacing: 8 m, Depth: 6 m)
(B)   Example of multiple troughs found near the pipe domain (Halihan/Fenstemaker
Method; Pipe Domain: 218 m; Background Resistivity: 100 ohm-m; Pipe Resistivity:
2.5 ohm-m; Electrode Spacing: 8 m, Depth: 2 m)

Electrode Spacing	Model Pipe Resistivity (Ω·m)	Model Pipe Depth – Cell Number	Measured Pipe Depth – Cell Number			
			Halihan/Fenstemaker		Wenner	
			50 Ω·m	100 Ω·m	50 Ω·m	100 Ω·m
5 m	1	1	2	3	2	2
	2.5	1	2	2	0	2
	5	1	2	2	0	0
	10	1	2	2	0	0
	20	1	2	2	0	0
8 m Horizontal Distance at 218 m	1	1	2	3	2	2
	2.5	1	2	2	0	2
	5	1	2	2	0	0
	10	1	2	2	0	0
	20	1	2	2	0	0
8 m Horizontal Distance at 222 m	1	1	2	3	2	3
	2.5	1	2	2	0	2
	5	1	2	2	0	0
	10	1	2	2	0	0
	20	1	2	2	0	0
10 m	1	1	2	3	2	2
	2.5	1	2	2	0	2
	5	1	2	2	0	0
	10	1	2	2	0	0
	20	1	2	2	0	0

Table 4.1: Model Pipe Depth Profile in Resistivity Forward Model 1
Note: Model grid cells numbered from top down. Cell zero is the top boundary of the model grid.

The vertical electrical resistivity profile of forward model 1 (single pipe) indicated that percent error values of model pipe resistivity tended to decrease as the pipe resistivity values were closer to the background resistivity value (Figure 4.14; Table 4.2). Similarly, when the difference between pipe resistivity values and background resistivity values were small, the percent error values of modeled background resistivity also decreased (Figure 4.14; Table 4.2). This relationship was observed, regardless of differences in electrode spacings, background resistivities, and pipe locations. The results with the Wenner method indicated similar results as the Halihan/Fenstemaker method. However, the vertical electrical resistivity profiles with the Wenner method

were inclined to shift the background resistivity values. Therefore, the percentage errors of the pipe resistivity error with the Wenner method were much greater than that of the Halihan/Fenstemaker method.

Figure 4.14: Vertical Electrical Resistivity Profiles
Pipe Domain: 218 m; Background Resistivity: 50 ohm-m; Electrode Spacing: 8 m
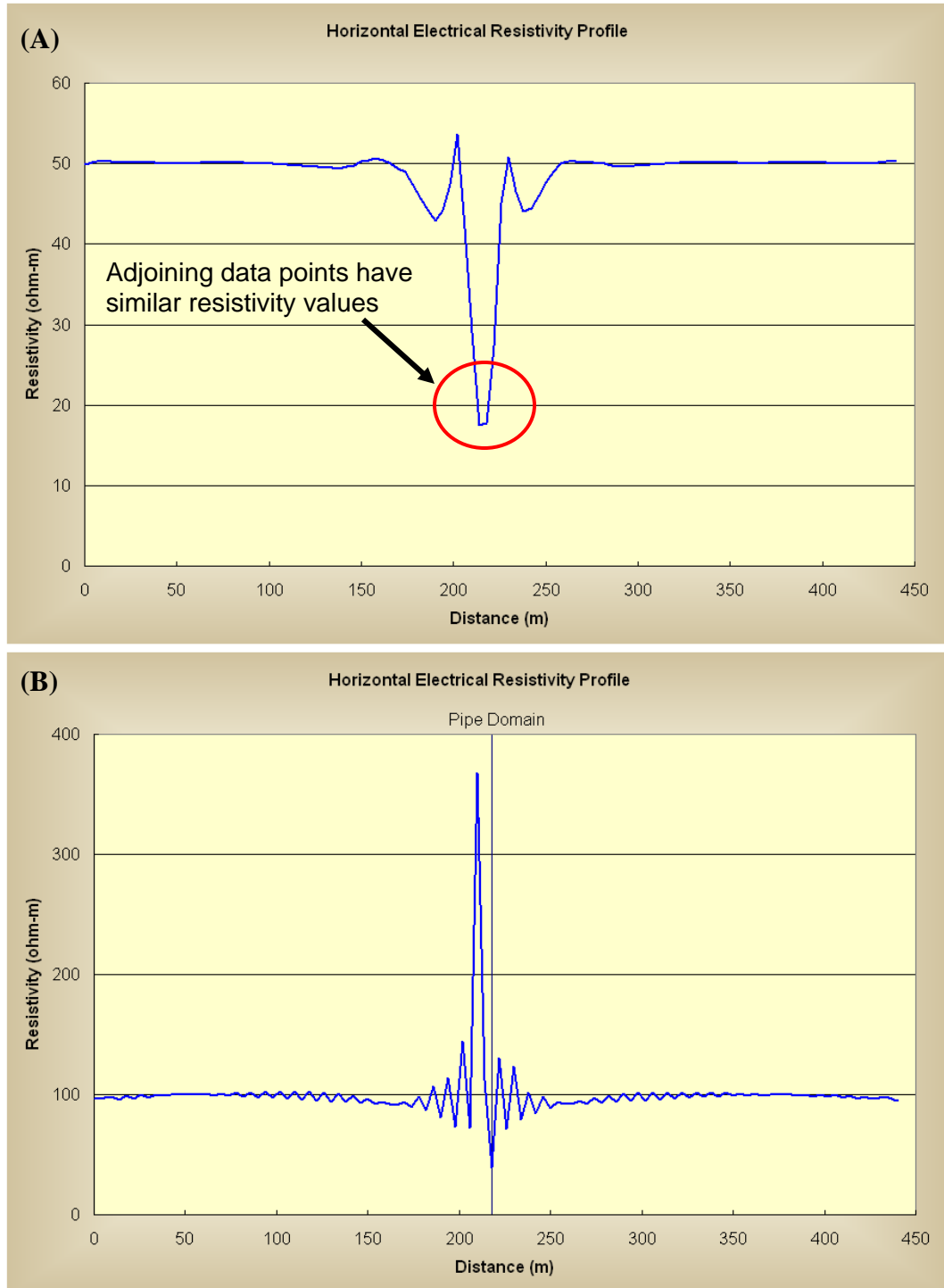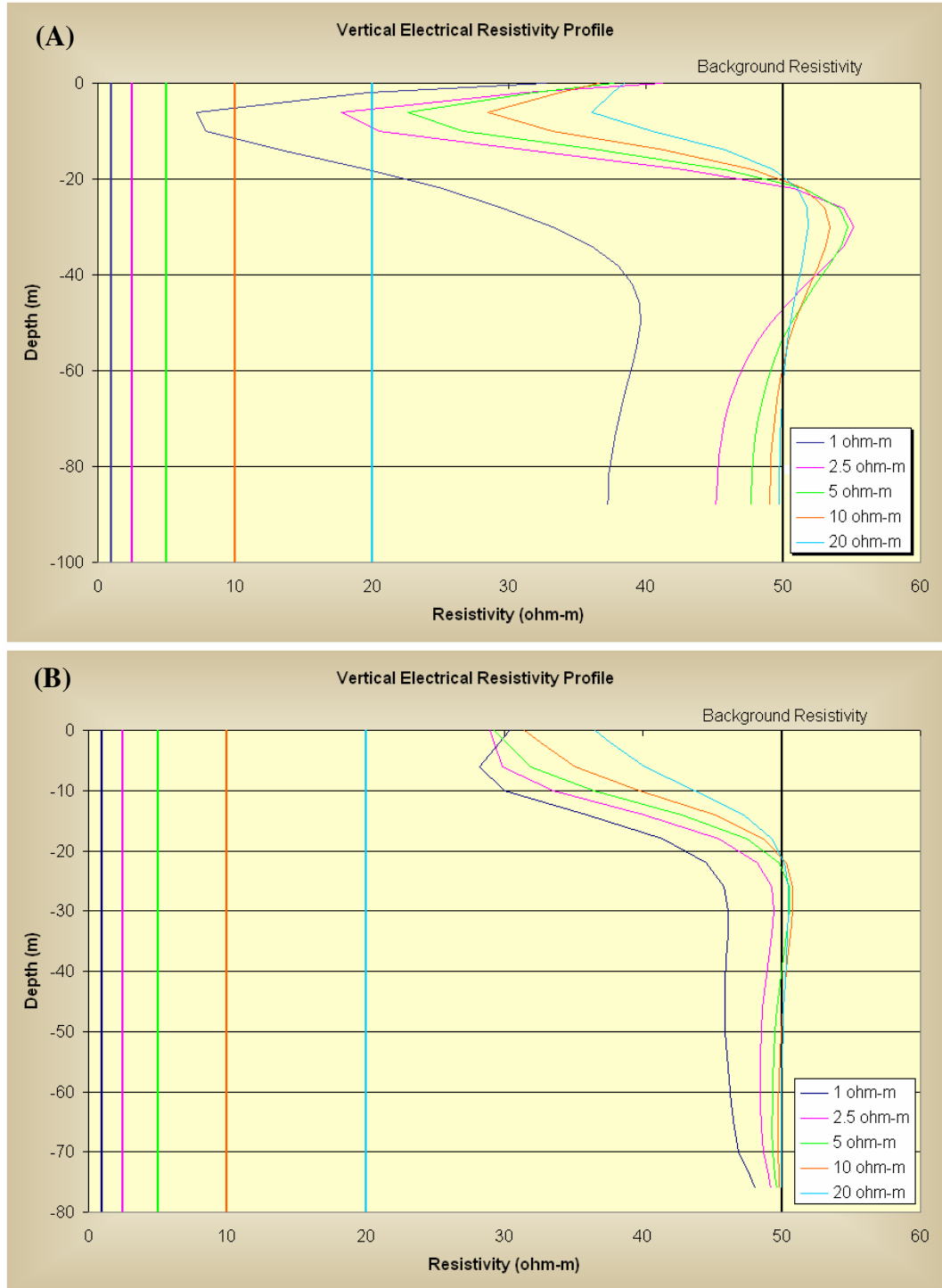(A) The Halihan/Fenstemaker Method (B) The Wenner Method

(A)

Model Pipe Resistivity (Ω·m)	Range of Pipe Resistivity Error (%)	Average Pipe Resistivity Error (%)	Background Resistivity Error Range (%)	Average Background Resistivity Error (%)
1	619.6 – 630.5	624.0	25.6 – 26.1	25.7
2.5	600.1 – 614.2	608.3	9.8 – 10.6	10.0
5	354.2 – 346.1	350.8	4.8 – 5.3	4.9
10	181.5 – 185.3	183.7	1.9 – 2.3	2.1
20	79.5 – 80.6	80.1	0.6 – 0.7	0.6

(B)

Model Pipe Resistivity (Ω·m)	Range of Pipe Resistivity Error (%)	Average Pipe Resistivity Error (%)	Background Resistivity Error Range (%)	Average Background Resistivity Error (%)
1	692.5 – 731.5	719.0	25.6 – 26.1	40.63
2.5	537.6 – 988.0	656.6	9.8 – 10.6	20.97
5	600.1 – 614.2	608.3	4.8 – 5.3	10.04
10	346.1 – 354.2	350.8	2.0 – 2.3	4.92
20	181.5 – 185.3	183.7	0.6 – 0.7	2.08

(C)

Model Pipe Resistivity (Ω·m)	Range of Pipe Resistivity Error (%)	Average Pipe Resistivity Error (%)	Background Resistivity Error Range (%)	Average Background Resistivity Error (%)
1	2712.7 – 2745.6	2724.1	3.8 – 4.0	3.9
2.5	1057.4 – 1069.0	1060.7	1.5 – 1.6	1.6
5	485.4 – 543.1	501.6	0.7 – 0.8	0.8
10	214.45 – 217.9	215.4	0.3 – 0.4	0.4
20	82.4 – 83.5	82.7	0.11 – 0.13	0.1

(D)

Model Pipe Resistivity (Ω·m)	Range of Pipe Resistivity Error (%)	Average Pipe Resistivity Error (%)	Background Resistivity Error Range (%)	Average Background Resistivity Error (%)
1	5367.8 – 5387.2	5378.9	7.2 – 7.0	7.1
2.5	2175.6 – 2202.0	2184.6	3.1 – 3.2	3.1
5	1057.4 – 1069.0	1060.7	1.5 – 1.6	1.6
10	485.3 – 492.3	487.1	0.75 – 0.81	0.8
20	214.5 – 217.9	215.4	0.3 – 0.4	0.4

Table 4.2: Percentage Error in Forward Model 1
(A) Background Resistivity of 50 Ω·m with the Halihan/Fenstemaker Method
(B) Background Resistivity of 100 Ω·m with the Halihan/Fenstemaker Method
(C) Background Resistivity of 50 Ω·m with the Wenner Method
(D) Background Resistivity of 100 Ω·m with the Wenner Method

Resistivity Forward Model 2 – Single Pipe at Small Angle

The electrical resistivity forward model 2, a model of a single pipe which is crossing ERI with angle was replicated by placing two conductive cells adjacent in the model. Results of resistivity forward model 2 resembled the results from the resistivity forward model 1. As in model 1, most of the pipe domain corresponded to troughs of the lowest resistivity values in the vertically averaged horizontal electrical resistivity profile. The graph of the background resistivity value of 100 Ω·m and the model pipe resistivity value of 1 Ω·m in the Halihan/Fenstemaker method was the only one case which this tendency did not apply; conversely, all graphs from the Wenner method had good correlation the pipe domain with the lowest resistivity values (Figure 4.15; Appendix A, Figures A.9-A.10; Appendix B, Figures B.9-B.10). All graphs of the vertically averaged electrical resistivity profile were divided nearly symmetrically through the pipe location.
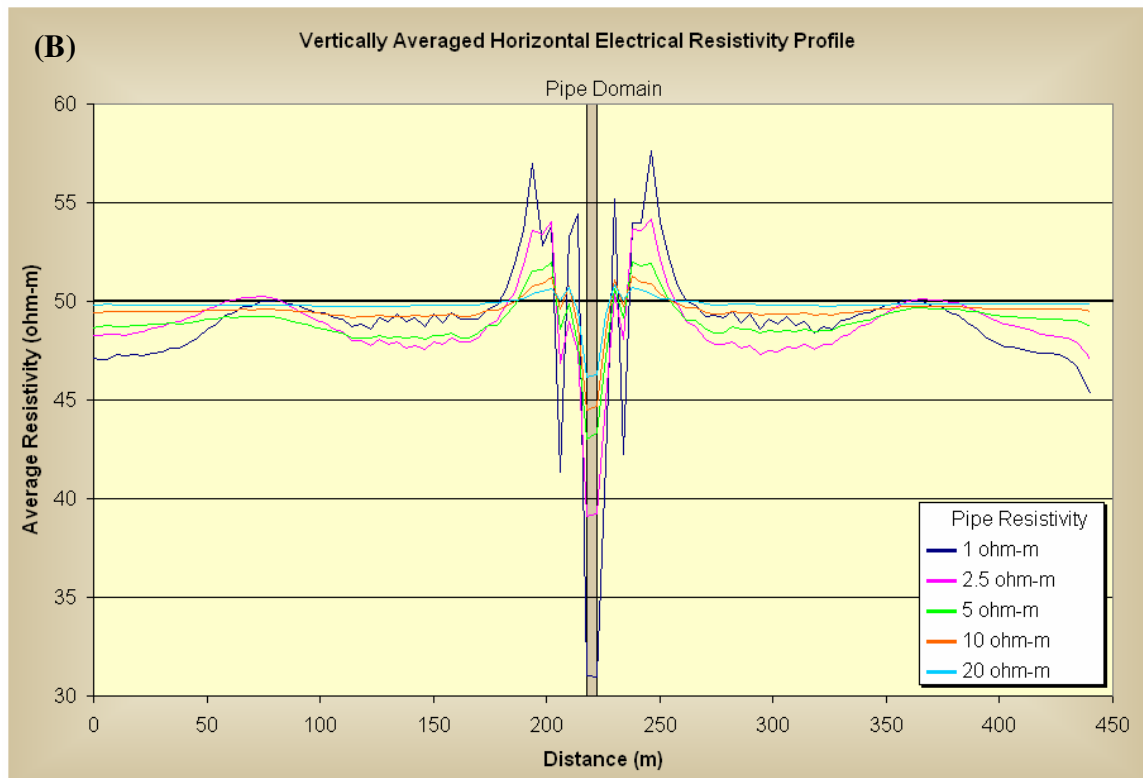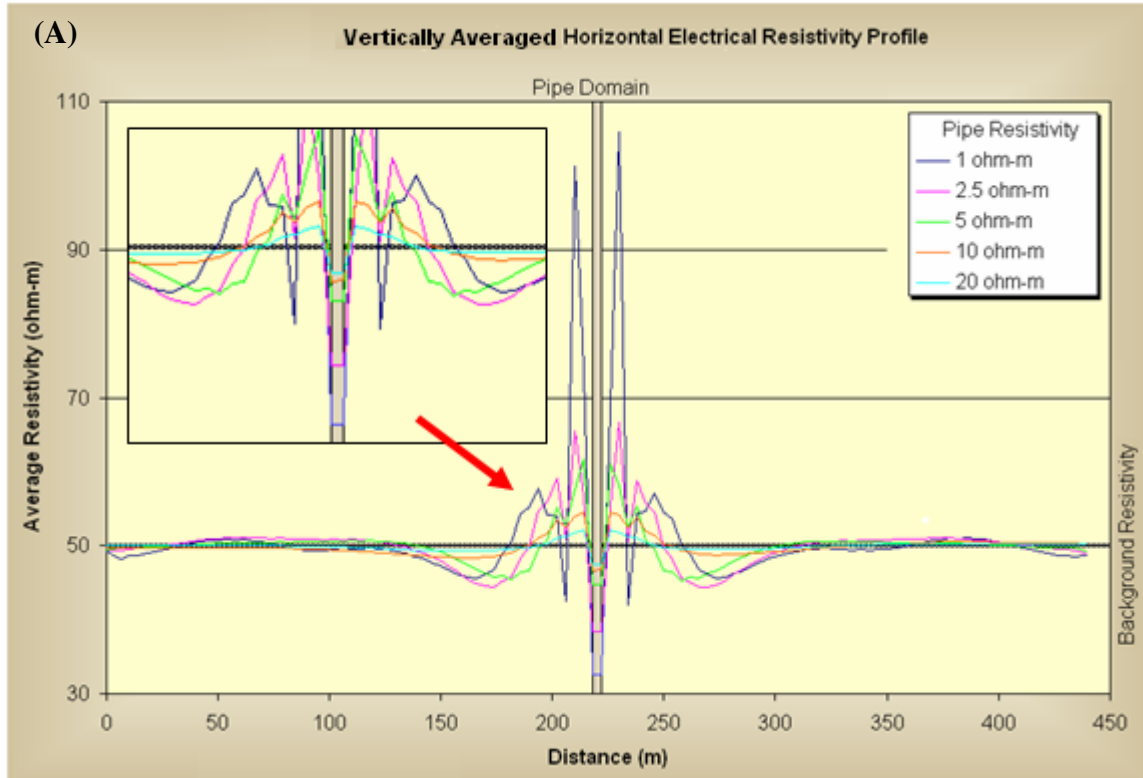
Figure 4.15: Vertically Averaged Electrical Resistivity Profile of Forward Model 2
Pipe Domain: 218-222m; Background Resistivity: 50 ohm-m; Electrode Spacing: 8 m
(A) The Halihan/Fenstemaker Method (B) The Wenner Method

78

The results of the vertically averaged horizontal electrical resistivity profiles were similar to those from the resistivity forward model 1. The model pipe domain passed through the lowest resistivity values in the graph. The bottoms of troughs in the horizontal electrical resistivity profile were somewhat flatter than those of the vertically averaged horizontal electrical resistivity profiles (Figure 4.16). Also, the multiple troughs were found as in resistivity forward model 1. However, the intervals between these troughs were big enough to distinguish.
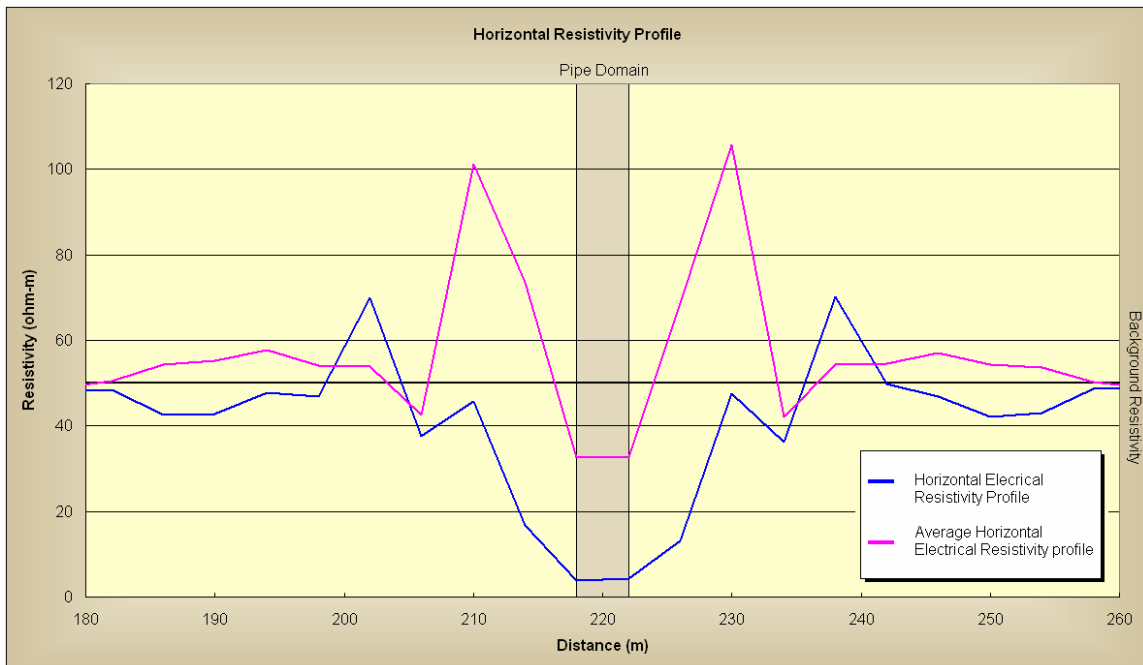
Figure 4.16: Common Issue in the Horizontal Electrical Resistivity Profiles in the Resistivity Model 2
The bottom of trough of Horizontal electrical resistivity profile is flatter than that of the vertically averaged horizontal electrical resistivity profile

Unlike the resistivity forward model 1, both the Halihan/Fenstemaker and the Wenner methods did not have any noticeable pattern in the vertical depth of the lowest resistivity (Table 4.3). The depths of the lowest resistivity with the Halihan/Fenstemaker

79

method were either 2 or 3 cells (6 or 10 meters) while the upper cell (0 or 6 meters) were

common with the Wenner method.

	Model Pipe Resistivity (Ω·m)	Model Pipe Depth – Cell Number	Measured Pipe Depth – Cell Number			
			Halihan/Fenstemaker		Wenner	
			50 Ω·m	100 Ω·m	50 Ω·m	100 Ω·m
Horizontal Distance at 218m	1	1	2	2	0	2
	2.5	1	2	2	0	2
	5	1	2	2	0	0
	10	1	3	2	0	0
	20	1	2	3	0	0
Horizontal Distance at 222m	1	1	2	2	2	2
	2.5	1	2	2	0	2
	5	1	2	2	0	0
	10	1	3	2	0	0
	20	1	2	3	0	0

Table 4.3: Model Pipe Depth Profile in Resistivity Forward Model 2
Note: Model grid cells numbered from top down. Cell zero is the top boundary of the
model grid.

The general trend of the vertical electrical resistivity profile of forward model 2

indicated that percent error values of the model pipe resistivity decreased as the pipe

resistivity values were closer to the background resistivity value (Table 4.4).   As

contrasted the resistivity forward model 1 with the forward model 2, the error percentage

of the model pipe resistivity did not have great difference between the two methods. The

background resistivity error percentages were also likely to decrease as difference

between the pipe resistivity values and the background values becoming smaller.

(A)	Model Pipe Resistivity (Ω·m)	Pipe Resistivity Error (%)		Average Pipe Resistivity Error (%)	Background Resistivity Error Range (%)		Average Background Resistivity Error (%)
		218 m	222 m		218 m	222 m	
Background Resistivity 50 ohm-m	1	295.4	326.1	310.8	10.4	10.5	10.5
	2.5	254.3	268.7	261.5	9.2	9.3	9.2
	5	138.4	139.8	139.1	6.8	6.9	6.8
	10	109.2	110.6	109.9	1.5	1.5	1.5
	20	42.8	43.3	43.1	0.6	0.6	0.6
Background Resistivity 100 ohm-m	1	314.1	372.8	343.5	5.7	5.5	5.6
	2.5	259.3	275.5	267.4	11.3	11.4	11.4
	5	254.3	268.7	261.5	9.2	9.3	9.2
	10	138.4	139.8	139.1	6.8	6.9	6.8
	20	109.2	110.6	109.9	1.5	1.5	1.5

(B)	Model Pipe Resistivity (Ω·m)	Pipe Resistivity Error (%)		Average Pipe Resistivity Error (%)	Background Resistivity Error Range (%)		Average Background Resistivity Error (%)
		218 m	222 m		218 m	222 m	
Background Resistivity 50 ohm-m	1	315.2	290.0	302.6	20.8	20.9	20.8
	2.5	252.2	300.8	276.5	8.3	8.4	8.3
	5	191.5	231.8	211.6	3.4	3.4	3.4
	10	73.3	88.1	80.7	1.3	1.3	1.3
	20	27.2	31.0	29.1	0.3	0.3	0.3
Background Resistivity 100 ohm-m	1	413.8	394.9	404.3	32.5	32.4	32.5
	2.5	345.4	328.6	337.0	16.6	16.6	16.6
	5	252.2	300.8	276.5	8.3	8.4	8.3
	10	191.5	231.8	211.6	3.4	3.4	3.4
	20	73.3	88.1	80.7	1.3	1.3	1.3

Table 4.4: Percentage Error in Forward Model 2
(A) The Halihan/Fenstemaker Method
(B) The Wenner Method

Resistivity Forward Model 3 – Single Pipe at Low Angle

The electrical resistivity forward model 3, a model of a single pipe which is crossing ERI with even lower angle than resistivity forward model 2 was replicated by placing four adjacent conductive cells. Results of resistivity forward model 3 were similar to the results from the resistivity forward model 2. As the electrical resistivity model 2, most of the model pipe domain corresponded to troughs of the lowest resistivity value in the vertically averaged horizontal electrical resistivity profile. Although two cells which were located in the middle of the model pipe domain (i.e. horizontal distance of 218 and 222m) always had the lowest electrical resistivity values, the edges of the domain (i.e. horizontal distance of 214 and 226 meters) were not always the lowest values (Figure 4.17). This was more common with the Halihan/Fenstemaker than the Wenner method.
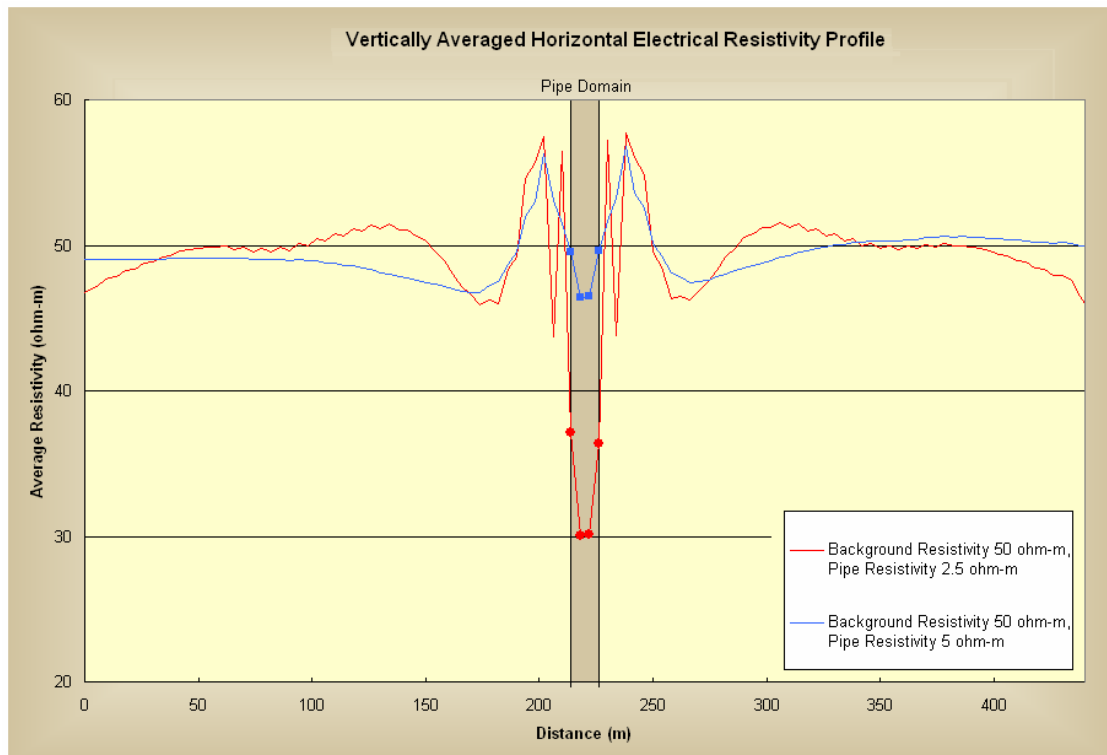
Figure 4.17: Common Problem Found in the Resistivity Forward Model 3
(The Halihan/Fenstemaker Method; Electrode Spacing: 8 m; Pipe Domain: 214 to 226m)

The lowest four data points in the horizontal electrical resistivity profiles were always found with in the model pipe domains. Similar to the resistivity forward model 1 and 2, the results of the Halihan/Fenstemaker method showed that the majority of the lowest resistivity data points found within the model pipe domains were located at one cell below the model pipe location except some of the lowest resistivity values were found two cells below the model pipe location. However, no depth pattern was found from the results of the Wenner method (Table 4.5).

	Model Pipe Resistivity (Ω·m)	Model Pipe Depth – Cell Number	Measured Pipe Depth – Cell Number			
			Halihan/Fenstemaker		Wenner	
			50 Ω·m	100 Ω·m	50 Ω·m	100 Ω·m
Horizontal Distance at 214m	1	1	2	2	4	4
	2.5	1	2	2	3	3
	5	1	2	2	2	3
	10	1	2	2	2	2
	20	1	2	2	0	2
Horizontal Distance at 218m	1	1	2	2	3	3
	2.5	1	2	2	0	3
	5	1	2	2	0	0
	10	1	2	3	0	0
	20	1	2	2	0	0
Horizontal Distance at 222m	1	1	2	2	3	3
	2.5	1	2	2	0	3
	5	1	2	2	0	0
	10	1	3	3	0	0
	20	1	2	2	0	0
Horizontal Distance at 226m	1	1	2	2	3	4
	2.5	1	2	2	3	3
	5	1	2	2	2	3
	10	1	2	2	2	2
	20	1	2	2	0	2

Table 4.5: Model Pipe Depth Profile in Resistivity Forward Model 3
Note: Model grid cells numbered from top down. Cell zero is the top boundary of the model grid.

The percent error values of the model pipe resistivity in the vertical electrical resistivity profiles decreased as the pipe resistivity values were closer to the background

resistivity value without regard to the Halihan/Fenstemaker or the Wenner methods (Table 4.6). The pipe resistivity error percentage values from the Halihan/Fenstemaker method had lower values. The background resistivity error percentage values were also likely to decrease as the gap between the pipe resistivity values and the background values became lesser. The background resistivity error percentage values from both methods were very similar to each other.

(A)	Pipe Resistivity ($\Omega\cdot$m)	Pipe Resistivity Error (%)				Background Resistivity Error (%)			
		214 m	218 m	222 m	226 m	214 m	218 m	222 m	226 m
Background Resistivity 50 ohm-m	1	242.8	145.9	155.8	199.9	19.5	19.5	19.5	19.5
	2.5	156.1	156.1	156.1	156.1	11.8	11.8	11.8	11.8
	5	148.6	148.6	148.6	148.6	6.7	6.7	6.7	6.7
	10	107.9	107.9	107.9	107.9	2.0	2.0	2.0	2.0
	20	61.0	61.0	61.0	61.0	0.2	0.2	0.2	0.2
Background Resistivity 100 ohm-m	1	441.4	175.0	200.7	314.0	31.0	31.3	31.4	31.1
	2.5	200.8	121.2	127.7	167.2	16.4	16.6	16.6	16.4
	5	156.1	96.0	100.8	151.2	11.8	12.0	12.0	11.9
	10	148.6	132.4	134.2	149.9	6.7	6.6	6.6	6.6
	20	107.9	66.1	67.0	106.9	2.0	1.9	1.8	1.9

(B)	Pipe Resistivity ($\Omega\cdot$m)	Pipe Resistivity Error (%)				Background Resistivity Error (%)			
		214 m	218 m	222 m	226 m	214 m	218 m	222 m	226 m
Background Resistivity 50 ohm-m	1	940.2	475.5	474.3	957.0	17.4	17.9	18.0	17.5
	2.5	605.5	210.7	241.6	596.0	7.5	7.7	7.8	7.6
	5	413.9	213.0	231.5	409.3	2.3	2.4	2.4	2.3
	10	201.9	104.6	109.1	201.4	0.7	0.7	0.7	0.7
	20	84.3	48.1	48.8	83.9	0.2	0.2	0.2	0.2
Background Resistivity 100 ohm-m	1	1023.6	393.8	377.6	938.1	31.9	32.8	32.8	32.0
	2.5	885.8	420.9	422.4	854.5	14.7	15.2	15.2	14.8
	5	605.5	210.7	241.6	596.0	7.5	7.7	7.8	7.6
	10	413.9	213.0	231.5	409.3	2.3	2.4	2.4	2.3
	20	201.9	104.6	109.1	201.4	0.7	0.7	0.7	0.7

Table 4.6: Percentage Error in Forward Model 3
(A) The Halihan/Fenstemaker Method
(B) The Wenner Method

Resistivity Forward Model 4 – Pipe with Surrounding Insulators

The resistivity forward model 4 was composed of one conductive cell and four insulators. The resistivity values of insulators were 10, 100, and 1000 times of the background resistivity values. In this model, the vertically averaged horizontal electrical resistivity profiles were plotted separately by the insulator values (Appendix A, Figures A.13-A.18; Appendix B, Figures B.13-B.18). Similar to the previous forward models, the model pipe domains matched with the lowest resistivity values. However, when the resistivity values of the insulator were getting higher and the difference between the background resistivity and the model pipe resistivity values were closer, the model pipe features tended to be hidden by the rebound from the insulator features. Particularly, the results from the Wenner method strongly demonstrated this tendency.

The graphs of horizontal resistivity profile showed some differences between the two methods. The results from the Halihan/Fenstemaker method were very similar to the results of the previous forward models. The lowest resistivity values were likely to be correlated with the model pipe domain. However, the depth where the model pipe placed (i.e. top model cell, 2 meters in depth), and at the top model boundary (i.e. 0 meter in depth) it tended to show multiple troughs which had similar resistivity values. The graphs of 6 meter depth, one cell below the model pipe location, were inclined to have a single significant trough which was easy to match with the model pipe domain. However, similar to the vertically averaged horizontal electrical resistivity profile of this model, the troughs were getting undistinguished as the insulators values became larger and the model pipe resistivity values and the background resistivity values became closer. Although the results from the Wenner method did not show any significant trough at the

model pipe domain (Figure 4.18), the graphs of the depth at 2 and 3 cells (6 and 10 meters) occasionally illustrated some notable troughs at the model pipe location, especially when the difference between the model pipe and the background resistivity was larger.
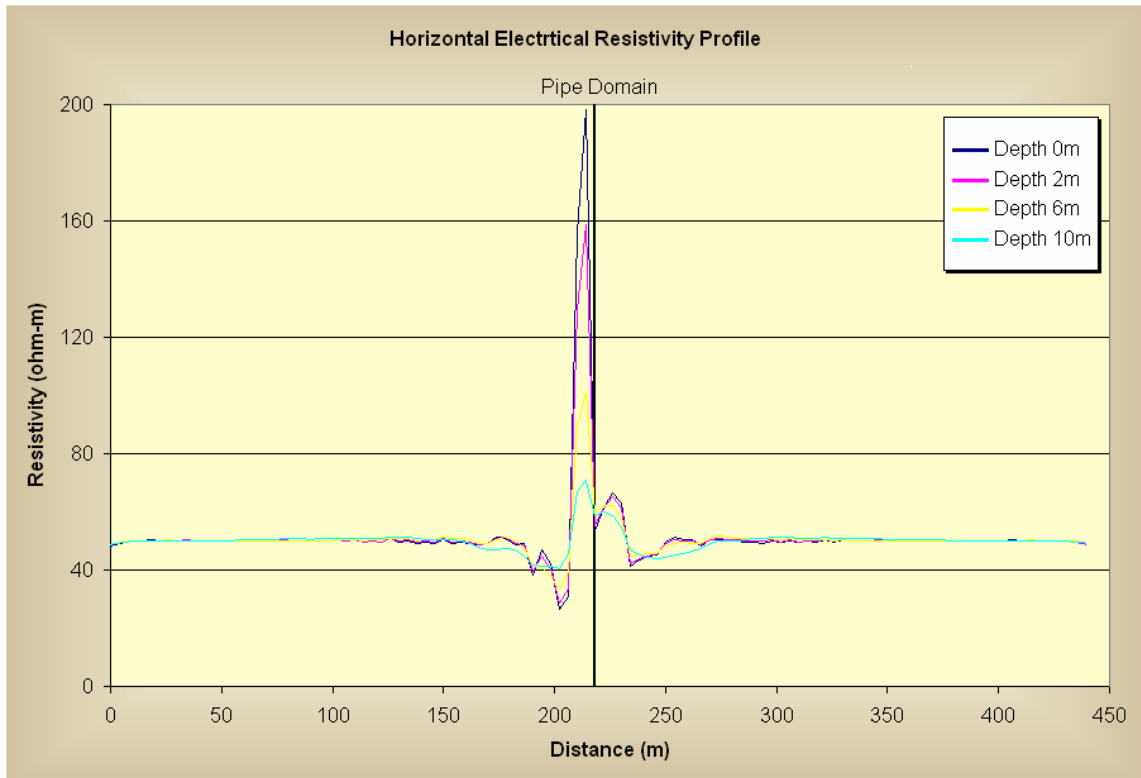

Figure 4.18: Common Failure Found in the Vertically Averaged Horizontal Electrical Resistivity with the Wenner Method
(Background Resistivity: 50 ohm-m, Pipe Resistivity: 20 ohm-m, Insulator Resistivity: 50000 ohm-m)

The depth of the lowest resistivity values with the Halihan/Fenstemaker method became shallower as the background and the model pipe resistivity values were getting closer (Table 4.7). The depth where the model pipe was placed never contained the lowest resistivity values. Unlike the Halihan/Fenstemaker method, the lowest resistivity depth in the graphs of the Wenner method did not show any obvious pattern (Table 4.7).

	Model Pipe Resistivity (Ω·m)	Model Pipe Depth – Cell Number	Measured Pipe Depth – Cell Number			
			Halihan/Fenstemaker		Wenner	
			50 Ω·m	100 Ω·m	50 Ω·m	100 Ω·m
Insulator 10x Background Resistivity	1	1	3	3	3	4
	2.5	1	2	2	3	3
	5	1	2	2	14	3
	10	1	0	2	15	14
	20	1	0	0	51	15
Insulator 100x Background Resistivity	1	1	3	3	3	4
	2.5	1	2	2	3	3
	5	1	2	2	14	3
	10	1	0	2	15	14
	20	1	0	0	15	15
Insulator 1000x Background Resistivity	1	1	3	3	4	4
	2.5	1	2	3	3	3
	5	1	2	2	3	3
	10	1	0	2	14	15
	20	1	0	0	15	15

Table 4.7: Model Pipe Depth Profile in Resistivity Forward Model 4
Note: Model grid cells numbered from top down. Cell zero is the top boundary of the model grid.

When the background resistivity was 50 Ω·m, the percent error values of the model pipe resistivity in the vertical electrical resistivity profiles decreased as the pipe resistivity values were getting closer to the background resistivity values in both methods (Table 4.8). This pattern was not observed, when the background resistivity was 100 Ω·m. The background resistivity error percentage values also declined as the difference between the pipe resistivity values and the background values became lesser. The background resistivity error percentage values from both methods were very similar to each other.

(A)	Model Pipe Resistivity (Ω·m)	Pipe Resistivity Error (%)		Background Resistivity Error (%)	
		50 Ω·m	100 Ω·m	50 Ω·m	100 Ω·m
Insulator 10x Background Resistivity	1	808.0	397.3	41.31	43.95
	2.5	386.9	525.9	24.92	36.75
	5	266.4	386.9	16.64	24.92
	10	156.4	266.4	11.36	16.64
	20	39.0	156.4	8.07	11.37
Insulator 100x Background Resistivity	1	577.3	280.2	43.95	42.53
	2.5	387.5	347.8	36.75	27.68
	5	267.6	238.9	24.92	19.80
	10	139.6	267.6	16.64	14.72
	20	25.5	139.6	11.37	11.64
Insulator 1000x Background Resistivity	1	569.5	261.7	42.53	44.54
	2.5	387.8	339.4	27.68	42.99
	5	267.7	387.8	19.80	33.70
	10	138.9	154.4	14.72	19.80
	20	24.6	138.9	11.64	14.72

(B)	Model Pipe Resistivity (Ω·m)	Pipe Resistivity Error (%)		Background Resistivity Error (%)	
		50 Ω·m	100 Ω·m	50 Ω·m	100 Ω·m
Insulator 10x Background Resistivity	1	3355.50	2258.70	8.11	24.55
	2.5	1743.56	2809.28	2.03	6.98
	5	870.90	1743.56	1.31	2.04
	10	389.70	870.91	0.99	1.31
	20	145.78	389.70	0.84	0.99
Insulator 100x Background Resistivity	1	2258.70	3511.60	24.55	8.31
	2.5	2809.28	1641.92	6.98	4.79
	5	1743.56	867.78	2.04	1.52
	10	870.91	387.97	1.31	1.21
	20	389.70	144.90	0.99	1.09
Insulator 1000x Background Resistivity	1	3511.60	2218.80	8.31	24.28
	2.5	1641.92	1615.32	4.79	13.86
	5	867.78	1641.90	1.52	4.79
	10	387.97	867.77	1.21	1.52
	20	144.90	387.97	1.09	1.21

Table 4.8: Percentage Error in Forward Model 4
(A) The Halihan/Fenstemaker Method
(B) The Wenner Method

Resistivity Forward Model 5 – Vertical Conductive Brine

The vertically averaged horizontal electrical resistivity graphs of the forward model 5 behaved similar to those of the forward model 1. The results from the Halihan/Fenstemaker method demonstrated that a pipe domain corresponded to troughs of the lowest resistivity value (Appendix A, Figures A.19-A.20). Although the strength of troughs were getting insignificant as the model pipe resistivities were increased from 1 to 20 $\Omega \cdot$m, the same tendency was observed across all images. This tendency also observed with the Wenner method.

The graphs of horizontal resistivity profile showed some differences between the two methods. Some of the horizontal electrical resistivity graphs from the Halihan/Fenstemaker method did not show the correlation which the lowest resistivity values matched with the model conductive fluid domain. The lowest resistivity values were found either at horizontal distance of 218 m where the model conductive fluid was placed, or at horizontal distance of 214 m which was one cell next to the target cell (Table 4.9A). The depth which had the lowest resistivity values also did not show any patterns. On one hand, the results from the Halihan/Fenstemaker method did not indicate any pattern in the horizontal electrical resistivity profiles; on the other hand, the results from the Wenner method indicated some pattern. The lowest resistivity values were always found at the horizontal distance of 218 m. Moreover, the depth of the lowest resistivity values was likely to decrease as the resistivity values of the model conductive fluid came closer to those of background (Table 4.9).

(A)

Resistivity (Ω·m)		Horizontal Distance of the Lowest Resistivity (m)	Depth of the Lowest Resistivity – Cell Number	Measured Resistivity Value (Ω·m)
BG*	Fluid			
50	1	214	5	1.38
	2.5	218	3	4.03
	5	214	2	12.80
	10	218	2	21.18
	20	218	2	31.06
100	1	214	3	1.81
	2.5	214	3	3.98
	5	218	3	8.06
	10	218	3	16.21
	20	218	2	42.36

(B)

Resistivity (Ω·m)		Horizontal Distance of the Lowest Resistivity (m)	Depth of the Lowest Resistivity – Cell Number	Measured Resistivity Value (Ω·m)
BG*	Fluid			
50	1	218	5	3.89
	2.5	218	3	20.97
	5	218	2	29.53
	10	218	2	32.57
	20	218	0	36.25
100	1	218	5	5.29
	2.5	218	5	9.17
	5	218	3	41.95
	10	218	2	59.06
	20	218	2	65.14

Table 4.9: Horizontal and Vertical Locations of the Lowest Resistivity (Forward Model 5)   BG*=Background

(A) The Halihan/Fenstemaker Method (B) The Wenner Method
Note: Model grid cells numbered from top down. Cell zero is the top boundary of the model grid.

Resistivity Forward Model 6 – Cone Shaped Brine

The vertically averaged horizontal electrical resistivity graphs of the forward model 6 were very similar to those of previous forward models. The results from both the Halihan/Fenstemaker and the Wenner method demonstrated that a pipe domain corresponded to troughs of the lowest resistivity value (Appendix A, Figures A.21-A.22). The strength of the trough behaved similar to the forward model 5; the magnitude of

troughs became insignificant as the model pipe resistivities were increased from 1 to 20 Ω·m, the same tendency was observed across all images. Overall, the troughs of the forward model 6 were more gently dipping than those of the forward model 5.

The results from the horizontal resistivity profile showed very similar results as the resistivity forward model 5 in terms of the horizontal distance where the lowest resistivity values were found. The graphs from the Halihan/Fenstemaker method did not show the correlation which the lowest resistivity values matched with the model conductive fluid domain (Table 4.10A). The depth which had the lowest resistivity values also did not show any patterns with this method. However, the lowest resistivity values in the graphs of the Wenner method were always located at the cell which was the surface location of the model conductive fluid (Table 4.10B).

(A)

Resistivity (Ω·m)		Horizontal Distance of the Lowest Resistivity (m)	Depth of the Lowest Resistivity – Cell Number	Measured Resistivity Value (Ω·m)
BG*	Fluid			
50	1	214	12	0.27
	2.5	214	21	0.91
	5	218	23	2.91
	10	214	4	7.21
	20	218	14	19.84
100	1	210	14	0.19
	2.5	218	12	0.78
	5	214	21	1.83
	10	218	23	5.82
	20	214	4	14.42

(B)

Resistivity (Ω·m)		Horizontal Distance of the Lowest Resistivity (m)	Depth of the Lowest Resistivity – Cell Number	Measured Resistivity Value (Ω·m)
BG*	Fluid			
50	1	218	5	7.36
	2.5	218	5	8.14
	5	218	5	9.56
	10	218	7	17.71
	20	218	6	24.34
100	1	218	5	3.87
	2.5	218	5	4.40
	5	218	5	16.28
	10	218	5	19.11
	20	218	7	35.41

Table 4.10: Horizontal and Vertical Locations of the Lowest Resistivity (Forward Model 6)   BG*=Background
(A) The Halihan/Fenstemaker Method (B) The Wenner Method
Note: Model grid cells numbered from top down. Cell zero is the top boundary of the model grid.

Resistivity Forward Model 7 – Pipe with Vertical Brine

The results of the resistivity forward model 7 were very similar to those of the forward model 5. Shapes of the vertically averaged horizontal electrical resistivity profiles were almost identical each other except the lowest resistivity values of the forward model 7 were slightly higher than those of the forward model 5 (Appendix A, Figures A.23-A.24; Appendix B, Figures B.23-B.24). The horizontal distances of the lowest resistivity values also showed similar pattern as the forward model 5 (Table 4.11).

(A)

Resistivity (Ω·m)			Horizontal Distance of the Lowest Resistivity (m)	Depth of the Lowest Resistivity – Cell Number	Measured Resistivity Value (Ω·m)
BG*	Pipe	Fluid			
50	1	2.5	214	3	2.72
	2.5	5	218	3	6.31
	5	10	214	2	16.99
	10	20	218	2	25.05
100	1	2.5	218	6	2.73
	2.5	5	214	3	5.97
	5	10	218	3	12.62
	10	20	214	2	33.97

(B)

Resistivity (Ω·m)			Horizontal Distance of the Lowest Resistivity (m)	Depth of the Lowest Resistivity – Cell Number	Measured Resistivity Value (Ω·m)
BG*	Pipe	Fluid			
50	1	2.5	218	4	7.02
	2.5	5	218	2	28.11
	5	10	218	2	30.09
	10	20	218	0	31.73
100	1	2.5	218	6	8.27
	2.5	5	218	3	40.15
	5	10	218	2	56.23
	10	20	218	2	60.18

Table 4.11: Horizontal and Vertical Locations of the Lowest Resistivity (Forward Model 7)   BG*=Background

(A) The Halihan/Fenstemaker Method   (B) The Wenner Method
Note: Model grid cells numbered from top down. Cell zero is the top boundary of the model grid.

Resistivity Forward Model 8 – Pipe with Cone Shaped Brine

The results of the resistivity forward model 8 were similar to those of the forward model 6. Shapes of the vertically averaged horizontal electrical resistivity graphs were almost indistinguishable each other except the lowest resistivity values of the forward model 8 were slightly higher than those of the forward model 5 (Appendix A, Figures A.25-A.26; Appendix B, Figures B.25-B2.6). The horizontal distances of the lowest resistivity values with the Halihan/Fenstemaker method could observe some pattern unlike the forward model 6 (Table 4.12). The lowest resistivity values were always

found at horizontal distance of 214 meters which was one cell next to the model

conductive fluid was placed at the surface.

(A)

Resistivity (Ω·m)			Horizontal Distance of the Lowest Resistivity (m)	Depth of the Lowest Resistivity – Cell Number	Measured Resistivity Value (Ω·m)
BG*	Pipe	Fluid			
50	1	2.5	214	21	0.87
	2.5	5	214	23	2.68
	5	10	214	3	5.98
	10	20	214	3	17.40
100	1	2.5	214	21	0.75
	2.5	5	214	21	1.77
	5	10	214	23	5.35
	10	20	214	3	11.95

(B)

Resistivity (Ω·m)			Horizontal Distance of the Lowest Resistivity (m)	Depth of the Lowest Resistivity – Cell Number	Measured Resistivity Value (Ω·m)
BG*	Pipe	Fluid			
50	1	2.5	218	5	8.12
	2.5	5	218	5	9.56
	5	10	218	7	18.04
	10	20	218	6	24.88
100	1	2.5	218	5	14.95
	2.5	5	218	5	16.27
	5	10	218	5	19.12
	10	20	218	7	36.08

Table 4.12: Horizontal and Vertical Locations of the Lowest Resistivity (Forward Model 8)   BG*=Background
(A) The Halihan/Fenstemaker Method (B) The Wenner Method
Note: Model grid cells numbered from top down. Cell zero is the top boundary of the model grid.

A-priori Inversion Model

The original purpose of the *a-priori* inversion models was to evaluate the effect of

pipes to determine if they were leaking. However, the currently available resistivity

modeling software did not have ability to control complicated *a-priori* inversion models.

Therefore, the only simple *a-priori* inversion models were constructed based on the

single pipe, forward model 1.

Figure 4.19 and Appendix C, Figures C.1-C.4 show the horizontal electrical resistivity profiles with the Halihan/Fenstemaker method. A target depth of these graphs was one cell below the model pipe cell (i.e. centered at 6 meters depth). The target depth was selected based on the results from the previous forward models. A significant behavior was observed from the results of the *a-priori* inversion model. The pipe resistivity of 5 ohm-m was set as the benchmark in these models. As the pipe resistivity values decreased, the resistivity values at the pipe location increased and vice versa, as the pipe resistivity values increased, the resistivity values at the pipe location decreased (Figure 4.19). Although the intensity of the peaks in the graphs of the Halihan/Fenstemaker was stronger, the same results were observed with the Wenner Method (Appendix D, Figures D.1-D.4).
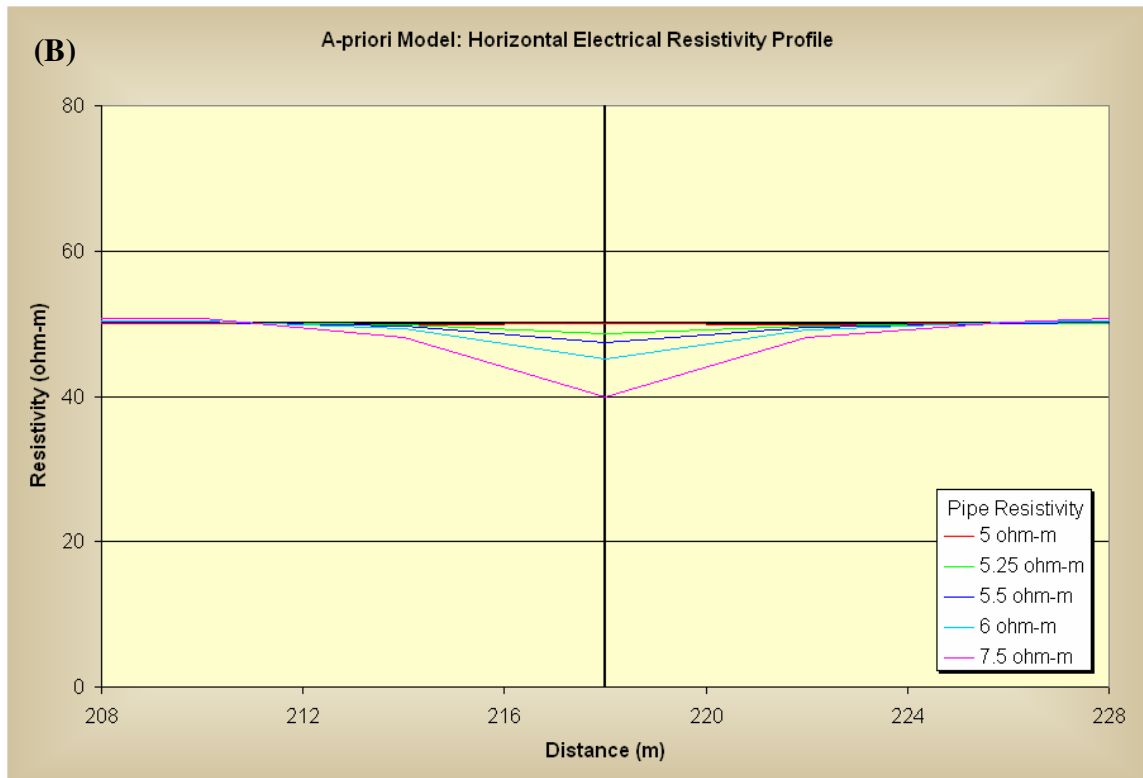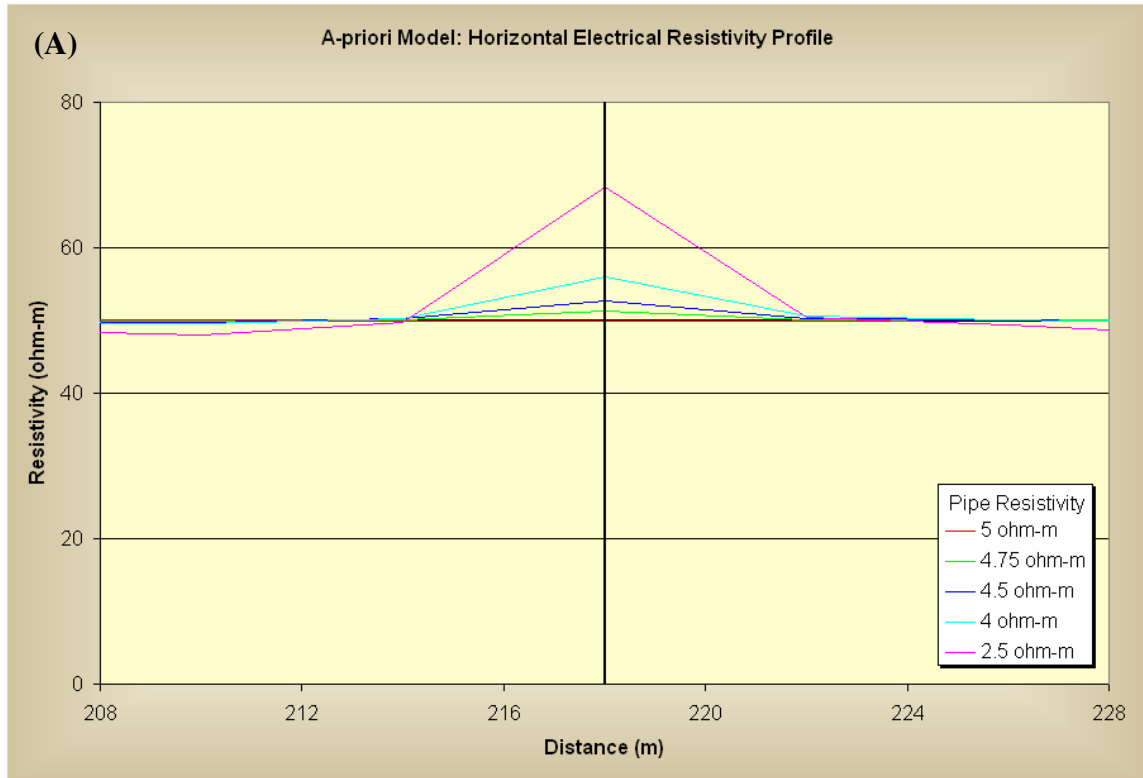
Figure 4.19: *A-priori* **Inversion Model: Horizontal Electrical Resistivity Profile with the Halihan/Fenstemaker Method at 2nd Cell Model Depth (6 m)**
(A) A case which the model pipe resistivity values are lower than 5 Ω·m
(B) A case which the model pipe resistivity values are high are than 5 Ω·m

The Application of the Forward Modeling to the Field Data

Appendix E provides the results of the vertically averaged horizontal resistivity profiles for the field data. The Y axes of the graphs which represent the resistivity values in ohm-meters were converted to logarithmic scale because some field datasets contained a large range of values.

The ERI survey line TH.A was the only survey line which the application of the forward modeling to the field data worked well (Appendix E.1). The troughs of the vertically averaged horizontal electrical resistivity profile matched the locations of petroleum pipelines which were found both in the field and on a pipeline map. Furthermore, the vertically averaged horizontal electrical resistivity profile of TH.A was also well correlated with the magnetometer survey results. The location of the low magnetic field found lateral location at 290 meters (950 feet) matched to the lower resistivity value at same horizontal location. However, no pipeline maker was observed during the field survey unlike the other two pipeline locations.

The graphs from ERI line TH.B did not show any significant troughs (Appendix E, Figure E.2). Although the lowest resistivity value could be correlated with a conductive feature which was found at the bottom of the ERI image, it was not outstanding enough to correlate.

The ERI survey lines TH.C and TH.D showed very similar results (Appendix E, Figures E.3 and E.4). The ERI images and the vertically averaged horizontal electrical resistivity profiles suggested that west side of the survey line was more conductive than the east. Although some pipe-like signatures observed in the results images could be correlated with some troughs found in the resistivity profiles, the signatures in the

vertically horizontal electrical resistivity profiles were not significant enough to correlated with the conductive features found in the ERI images.

Some of the troughs found in the vertically averaged horizontal electrical resistivity profiles could matched conductive features found in an ERI line image of TH.E (e.g. the horizontal distance of 10 m, 140 m, 200 m, and 220 m). While the horizontal distance between 60 and 120 meters showed the conductive features in the ERI image, the vertically averaged horizontal electrical resistivity profile had very high resistivity values in same location (Appendix E, Figure E. 5)

Conductive features found in the ERI image of TH.F were fairly correlated with troughs in the vertically averaged horizontal electrical resistivity profile. Some conductive signatures which located under the high resistivity feature which were found in the ERI image (e.g. the lateral location at 170 m and 250 m) did not show significant troughs in the vertically averaged horizontal electrical resistivity profile.

The ERI image of TH.G contained conductive features across the entire image. Some of the lowest resistivity in the image could be correlated with the troughs of the lowest resistivity values in the vertically averaged horizontal electrical resistivity profile of TH.G (e.g. the lateral location at 320 m and 470 m). However, other conductive signatures found in the image could not be correlated with the vertically averaged horizontal electrical resistivity profile.

No significant trough was found in the vertically averaged horizontal electrical resistivity profile of TH.H. The lateral locations at which pipelines and utilities were found in the field did not show any significant trough in the profile.

CHAPTER V

DISCUSSION

The behavior of conductive materials in ERI data from the results of the forward models are discussed in this chapter. The field data collected from Edmond, Oklahoma are compared to the modeling results. Finally, implication from the results of *a-priori* inversion model and the possible future work related to identification of leaking pipes are discussed.

Forward Modeling

In most cases, the vertically averaged horizontal resistivity profile was the most useful interpretation method to spot the location of conductive materials in subsurface because the troughs in those graphs were easy to distinguish. The case where a pipe is not perpendicular to the ERI line sometimes caused troughs in the vertically averaged electrical resistivity profile that did not match with the conductive cell domains. This can be solved by observing the location of a mirror plane because the graphs tend to be almost symmetrical when a conductive object is crossing the ERI line with some angles (e.g. forward model 2 and 3). Another case where the model pipe location was obscured was with the resistivity forward model 4 which contained a pipe surrounding by insulators. The highly resistive objects near the conductive pipe could create troughs to keep the model calculations in equilibrium.

As the result, the true location of the pipe could be hidden. The case of an insulator inside of a pipe was not evaluated as the pipe would provide the conductive element and perform as model 1 demonstrated.

The comparison the forward model 5 with 7, or the forward model 6 with 8 showed that the vertically averaged horizontal electrical resistivity profiles were approximately identical to single pipe models with more conductive pipes (Figure 5.1). As the resistivity of the pipe is not known in the field in advance, this result indicated that the forward models could not be an effective aid to distinguish a pipe(s) from conductive fluids leaking from the pipe unless there was significant lateral transport.
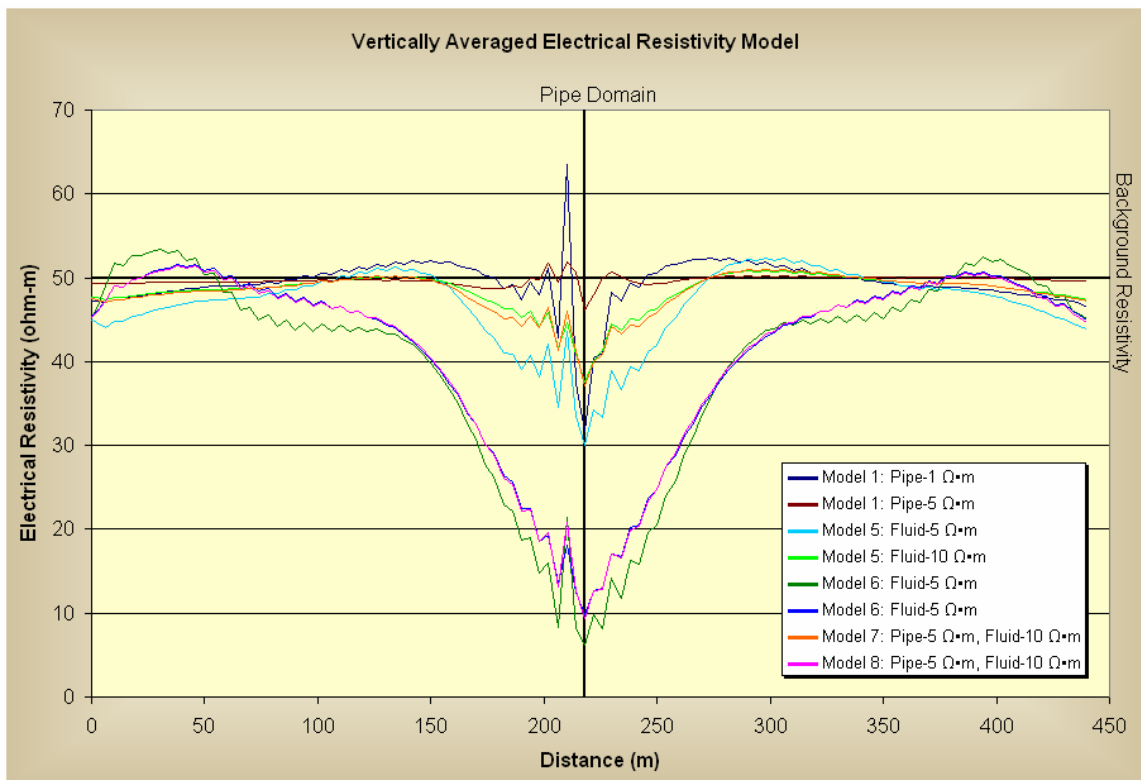
Figure 5.1: Vertically Averaged Horizontal Electrical Resistivity of Model 1, 5, 6, 7, and 8 with the Halihan/Fenstemaker Method
Pipe Domain: 218 m; Background Resistivity: 50 ohm-m; Electrode Spacing: 8 m

Although the graphs of the horizontal electrical resistivity profiles showed the similar results as the vertically averaged electrical resistivity profiles, it was more difficult to locate the conductive domain because the troughs were not outstanding in some cases. Additionally, the horizontal electrical resistivity profiles within the same graphs were varied with the depths, which prevented from locating the conductive objects in subsurface. As the results from the horizontal electrical resistivity graphs, the cells, either above or below the actual location of the conductive object tended to have the lowest resistivity values. However, no definite pattern of the depth was observed.

The results of the vertical electrical resistivity profiles indicated that the percent error tended to increase as the difference between the conductive object and the background resistivity value was getting larger. Therefore, it is harder to find out the true resistivity values of both the background and the conductive objects when the difference of their resistivity values is larger.

The Application of the Forward Modeling to the Field Data

The application of the vertically averaged horizontal electrical resistivity profiles to the actual field data is shown in Appendix E (Figures E.1 to E.8). The ERI survey line TH.A was the only survey line which the application of the forward modeling to the field data apparently worked well (Appendix E, Figure E.1). The troughs of the vertically averaged horizontal electrical resistivity profile could match to the petroleum pipelines which were found both in the field and on a pipeline map. Furthermore, the vertically averaged horizontal electrical resistivity profile of TH.A was also well correlated with the magnetometer survey results. The location of the low magnetic field found lateral

location at 290 meters (950 feet) matched to the lower resistivity value at same horizontal location. However, any pipeline maker was not observed during the field survey unlike other two pipes. The possible reason of the lower magnetic field could be occurred by removing earth around the area and infilling with earth which has different magnetic property since the area of the historic saltwater evaporation pit was located relatively close to the location of the lower magnetic anomaly (e.g. 10 meters / 33 feet south of the anomaly). Moreover, because the location of the salt evaporation pit was determined from the aerial photo taken in 1965, and the magnetometer survey was not simultaneously conducted with the ERI line TH.A survey, those locations were not definite.

The ERI survey lines TH.C and TH.D showed very similar results. The ERI images and the vertically averaged horizontal electrical resistivity profiles suggested that west side of the survey line was more conductive than the east. Although some pipe-like signatures were observed in the results images, and some troughs were found in the resistivity profiles, the signatures in the resistivity profiles were not clear enough to conform as pipes.

Many of the ERI survey lines had to be conducted adjacent to utility and petroleum pipes which affected the quality of the dataset since the survey were conducted in an urban setting. For that reason, the method of using the vertically averaged horizontal electrical resistivity profiles did not work well. The survey line TH.G was a good example of poor quality dataset. Because many petroleum pipelines were running almost parallel across the entire survey line in the site TH.G, the vertically averaged horizontal profile by itself could not show definite location or orientation of the pipes.

The results of the forward modeling application to the field data indicated that to be successful to apply this method has to have the following factors:

1. The vertically averaged horizontal electrical resistivity profile method works well when the background resistivity of the survey area is nearly homogeneous. A reason which this method worked well with the survey line TH.A could be because TH.A had relatively steady background resistivity values comparing to other survey lines.

2. The extremely high resistivity values caused by natural variations (e.g. massive fine grained tight sandstone) can act as insulator. In this case, the resistivity signatures can be hidden. TH.E was a good example of this case (Appendix E, Figure E.5). Some of the low conductive area which was appeared in the ERI image did not have strong troughs on the vertically averaged horizontal electrical resistivity profile (e.g. the horizontal distance of 100 meter / 330 feet).

3. Pipes which across ERI survey lines can be at angles lower than 90° but cannot be completely parallel to the lines. The survey line TH.G was a good example of this case (Appendix D, Figure D.7). The entire graph contains relatively low resistivity values at the shallow depth, which did not give significant resistivity signatures on the vertically averaged horizontal electrical resistivity profile.

A-priori Inversion Model

The original purpose of *a-priori* inversion model was to evaluate the effect of pipes to determine whether conductive fluid was leaking out from them or not. The limitation of the 2D electrical resistivity model software, which resistivity values of

conductive cells could not maintain *a-priori* values when the geometry was complicated prevented completing this objective.

As discussed in the previous chapter, the graph of the horizontal electrical resistivity profile did not show any peak or trough at the modeled pipe location when the estimated pipe resistivity value was exactly same as the actual pipe resistivity ($5\Omega \cdot m$). When the estimation was lower than actual, a peak appeared in the graph, and vice versa, the higher estimation resistivity value caused an appearance of the trough. Additionally, the intensity of peaks or troughs indicated how the estimated pipe resistivity value was closer to the actual value. When the difference between the estimated resistivity values and the actual values were larger, the peak or trough became more outstanding. The results of the single pipe *a-priori* inversion model indicated that the resistivity values of conductive pipes could be detectable by evaluating the intensity of peaks or troughs in the horizontal electrical resistivity profile.

The work also showed that in regions where pipes have been out of service for 30 or more years, conductive signatures remain in the subsurface. If these are signatures generated during previous petroleum production activities, it indicates two potential interpretation problems. First, a conductive signature in the vadose zone may have been deposited decades earlier and is not the source of an active leak in an area. Secondly, a source deposited long ago can be flushed from the vadose zone due to changes in surface drainage due to develop of former petroleum producing areas.

Future Work

Possible future work related to discerning conductive pipe and fluid in ERI image

could be conducted with development of electrical resistivity model software. In particular, 2D electrical resistivity model software could be designed to hold *a-priori* values to allow for pipe modeling of field data. If the software were available, it might be possible to determine the location of leaking conductive fluid from a pipe by using *a-priori* pipe resistivity values in field ERI data.

Distinguishing saline fluids with various chemical compositions might be possible by examining the relationships between saline fluids with different chemical compositions and their electrical resistivity properties. However, if each saline fluids from different sources do not have any significant electrical resistivity differences, it is not possible to distinguish between saline fluids with resistivity.

Applying a large amount de-icing chemicals, usually salt (sodium chloride), onto roads during winter seasons is common in some regions. Although the study area of this investigation did not have this problem, an investigation related to this problem is important to observe if result ERI line images from those de-icing regions could be affected by the road salt.

CHAPTER VI

CONCLUSIONS

The primary purpose of the study was to determine the efficiency of the advanced ERI field surveys with 2D electrical resistivity forward and *a-priori* inversion modeling to delineate the area of saline impact on ground water. Because the study area was in an urban area where two petroleum fields were located, multiple utilities and petroleum pipelines were present in the ground. The hypothesis was constructed based on the presence of pipe lines and their status as competent or leaking.

A total of eight ERI survey lines were taken adjacent to the Thunderhead Hills Addition where the saline impact in ground water was found. In addition to the field data, 252 forward models and 36 *a-priori* inversion models of resistivity were conducted. All ERI images from the field except TH.B contained some conductive features near the pipes or utilities which were located based on field observations and the pipeline location map. The ERI images alone could not indicate conclusively whether the pipes were competent or leaking conductive fluid. The forward models were constructed as an aid to characterize pipe behaviors. Although the vertically averaged horizontal electrical resistivity profiles from the forward models could provide presence of pipes and their locations, the heterogeneity in the field limited the application of the forward modeling to the data collected in the field.

Moreover, the forward models did not separate the pipes from conductive fluid, which were shown in the results of comparison the forward model 5 with 7 and the forward model 6 with 8. To solve this problem, *a-priori* inversion models were performed. However, because of the limitation in the available 2D electrical resistivity model software, the complicated *a-priori* inversion models could not be constructed. Further study with *a-priori* inversion models seems promising.

BIBLIOGRAPHY

Advanced Geosciences, Inc. 2004. Instruction Manual for EarthImager 2D Version 1.7.4. Resistivity and IP Inversion Software. P.O. Box 201087, Austin, Texas 78720. Tel. (512) 335-3338, Fax (512) 258-9958, www.agiusa.com.

Aristodemou, E. and Thomas-Betts, A., 2000. DC resistivity and induced polarisation investigations at a waste disposal site and its environments. Journal of Applied Geophysics, 44(2-3): 275-302.

Borradaile, G.J., 2003. Statistics of earth science data : their distribution in time, space, and orientation /. Springer, Berlin, New York 351 pp.

Christenson, S. and Havens, J.S., 1998. Ground-water-quality assessment of the Central Oklahoma Aquifer; summary of investigations, U. S. Geological Survey Water-Supply Paper. U. S. Geological Survey : Reston, VA, United States, United States, pp. 1-179.

Christenson, S.C., Morton, R.B. and Mesander, B.A., 1992. Hydrogeologic maps of the central Oklahoma aquifer, Oklahoma / U.S. Department of the Interior, U.S. Geological Survey Hydrologic investigations atlas ; HA-724, pp. Scale 1:250,000 ; U.T.M. proj. 6 maps on 3 sheets : photocopy ; 55 x 36 cm., sheets 86 x 112 cm., folded in envelope 33 x 26 cm.

Edwards, D.A., 1992. The protection of the municipal water well-field serving the City of Edmond, Oklahoma using wellhead protection area delineation, Oklahoma State University, Stillwater, 1-222 pp.

Ground Water Protection Council, 2005. Quality Assurance Project Plan Assessment of Oil Field Activities, Non-point Source Pollusion and Water Quality in the Spring Creek Watershed and the City of Edmond Municipal Well Field. Ground Water Protection Council, FY2002 319(h) Project 8: pp. 27.

Haihan, T. and T. Fenstemaker, 2004. Proprietary Electrical Resistivity Imaging Method. 2.0 ed. Oklahoma State University Office of Intellectual Property, Stillwater, OK.

Halihan, T., Paxton, S., Graham, I., Fenstemaker, T. and Riley, M., 2005. Post-remediation evaluation of a LNAPL site using electrical resistivity imaging. Journal of Environmental Monitoring: JEM, 7(4): 283-287.

Heran, W.D., Green, G.N. and Stoeser, D.B., 2003. A digital geologic map database for the state of Oklahoma. In: G.N. Green and D.B. Stoeser (Editors), Open-File Report 03-247 - U. S. Geological Survey. U. S. Geological Survey: Reston, VA, United States, United States.

Hibbs, B.J., 1989. Investigation of a brine contaminated aquifer in southeastern Hitchcock County, Nebraska emphasizing the conjunctive use of geophysical and geochemical methods of pollutant detection.

Jakosky, J.J., 1950. Exploration geophysics. Trija Pub. Co., Los Angeles, 1195pp.

Kearey, P., Brooks, M. and Hill, I., 2002. An introduction to geophysical exploration. Blackwell Science, Malden, MA 262 pp.

Koehler, J.A., 1988. Electrical resistivity as an approach to evaluating brine contamination of groundwater in the Walker oil field, Ottawa County, Michigan.

Reynolds, J.M., 1997. An introduction to applied and environmental geophysics. John Wiley & Sons, New York, 796 pp.

Roberts, J.W. and Spitz, D.S., 2001. Characterizing and Mapping the Regional Base of an Underground Source of Drinking Water in Central Oklahoma Using Open-Hole Geophysical Logs and Water Quality Data, Ground Water Protection Research Foundation, Oklahoma City, 40 pp.

Schwartz, F.W. and Zhang, H., 2003. Fundamentals of Ground Water. John Wiley & Sons, New York, 592 pp.

Swesnik, R.M., 1952. The fractured nature of the West Edmond Hunton reservoir, central Oklahoma. Oil and Gas Journal, 50(46): 176.

Van Nostrand, R. and Cook, K.L., 1966. Interpretation of resistivity data. Geological Survey Professional paper; 499. U.S. Govt. Print. Off., Washington, pp. 310.

Whittecar, G.R., 2005. Delineation of saltwater intrusion through a coastal borrow pit by resistivity survey. Environmental & Engineering Geoscience, 11: 209.

Wilson, S.R., 2006. The applicability of earth resistivity methods for saline interface definition. Journal of Hydrology, 316: 301.

Wood, P.R. and Burton, L.C., 1968. Ground-water resources in Cleveland and Oklahoma counties. In: L.C. Burton (Editor), Circular 71 - Oklahoma Geological Survey. University of Oklahoma : Norman, OK, United States, United States, pp. 1-75.

APPENDICES

APPENDIX A

Vertically Averaged Horizontal Electrical Resistivity Profiles for Forward Model
1 to 8 with the Halihan/Fenstemaker Method
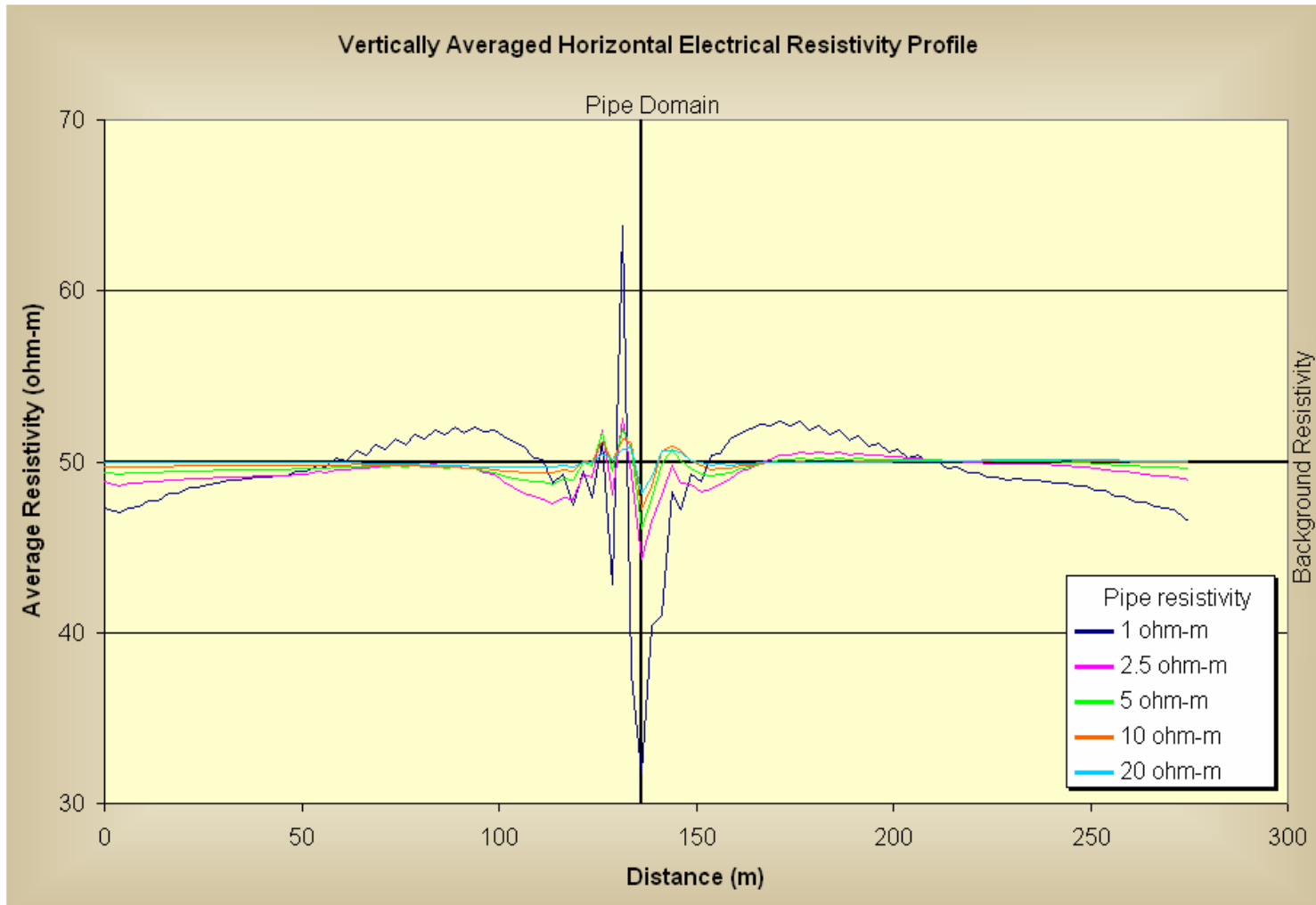
Figure A.1: Forward Electrical Resistivity Model 1 – Single Pipe
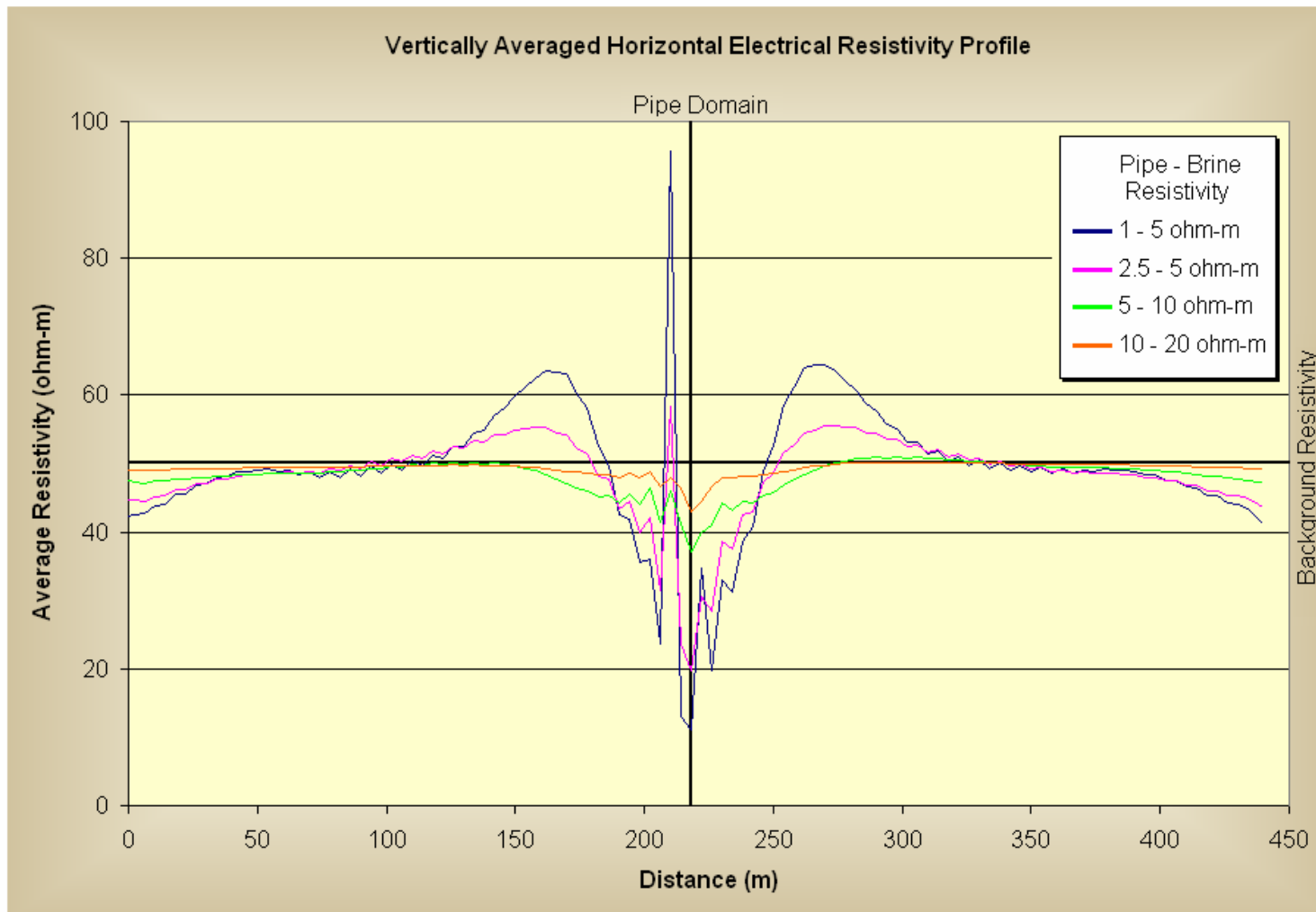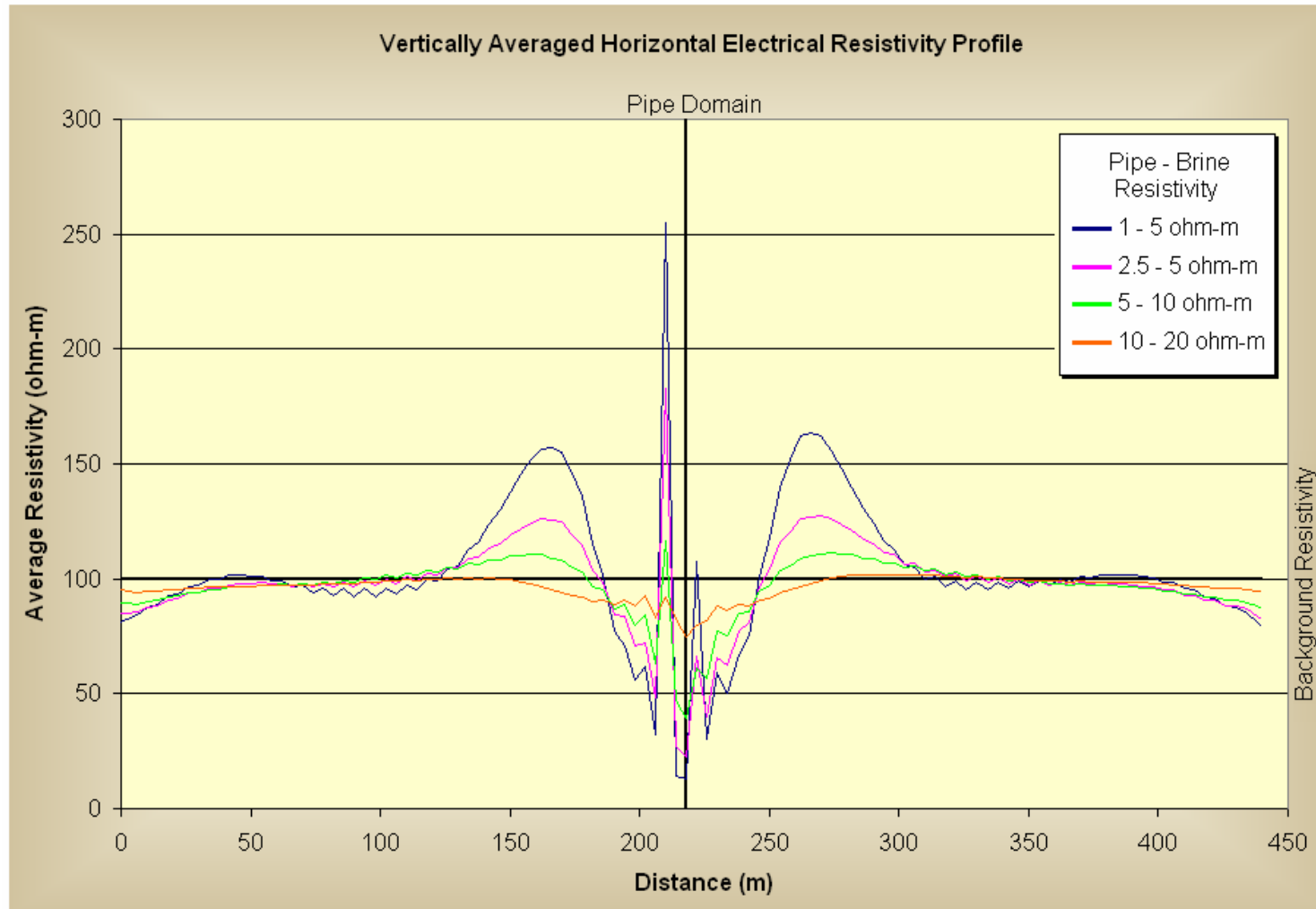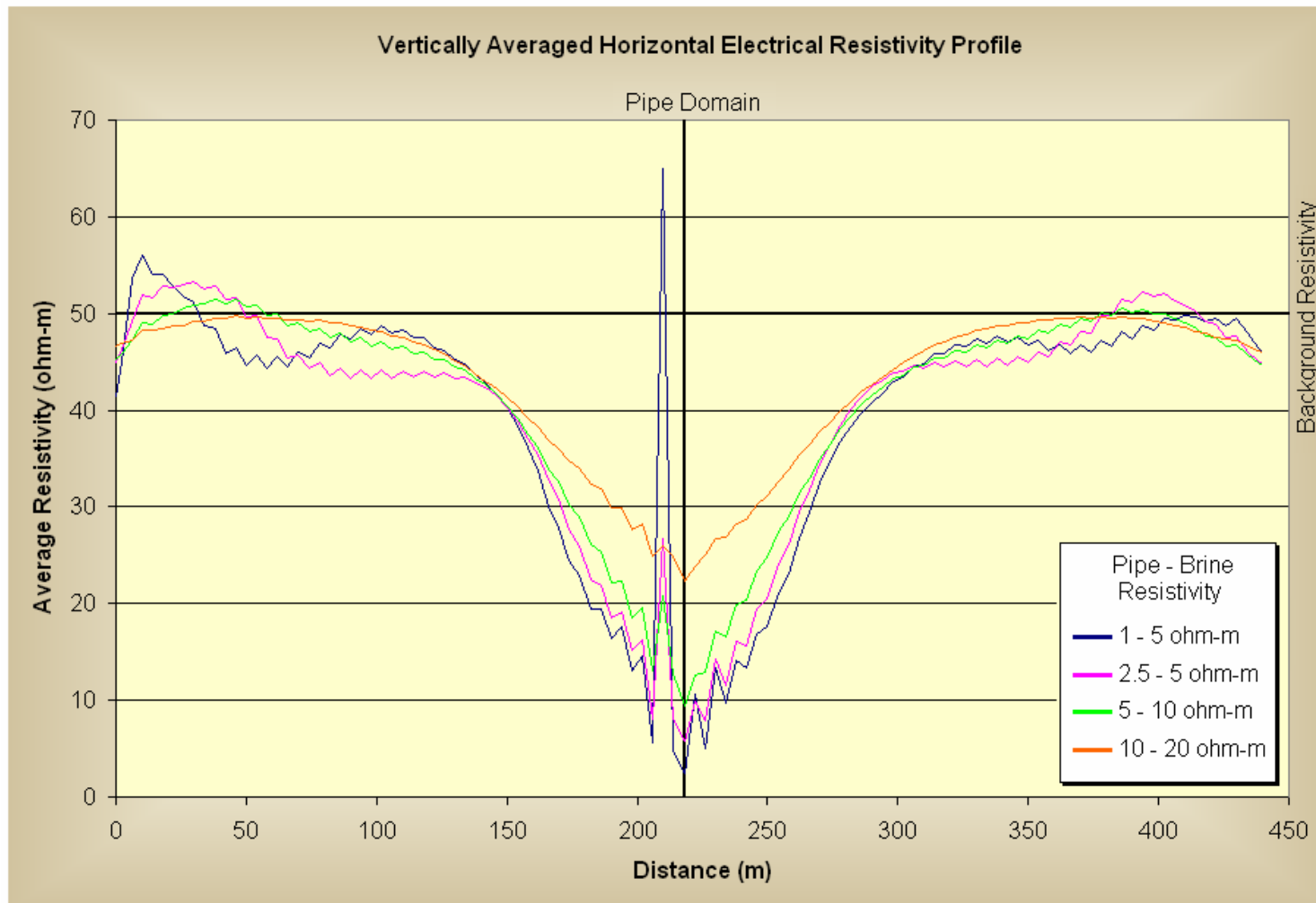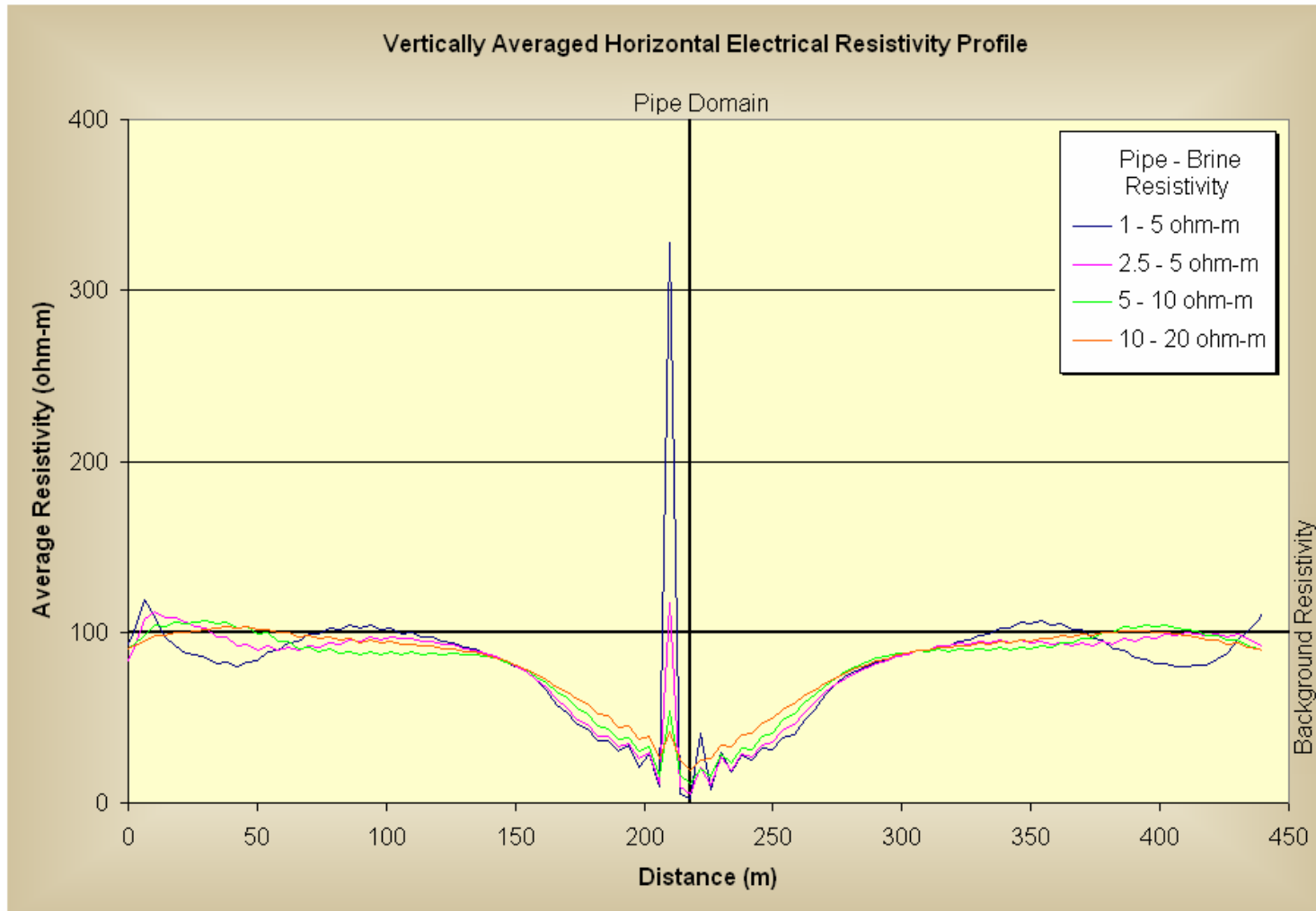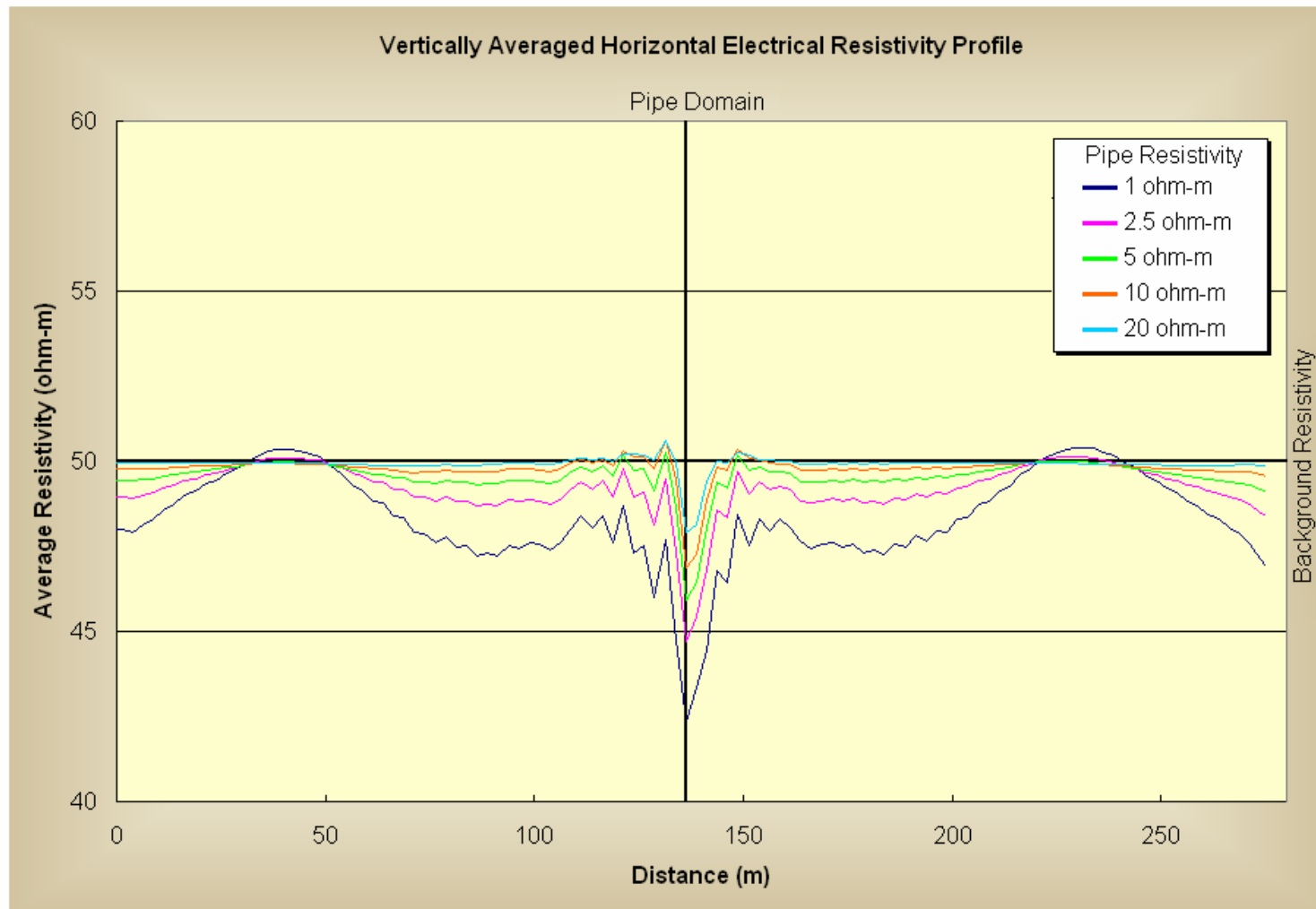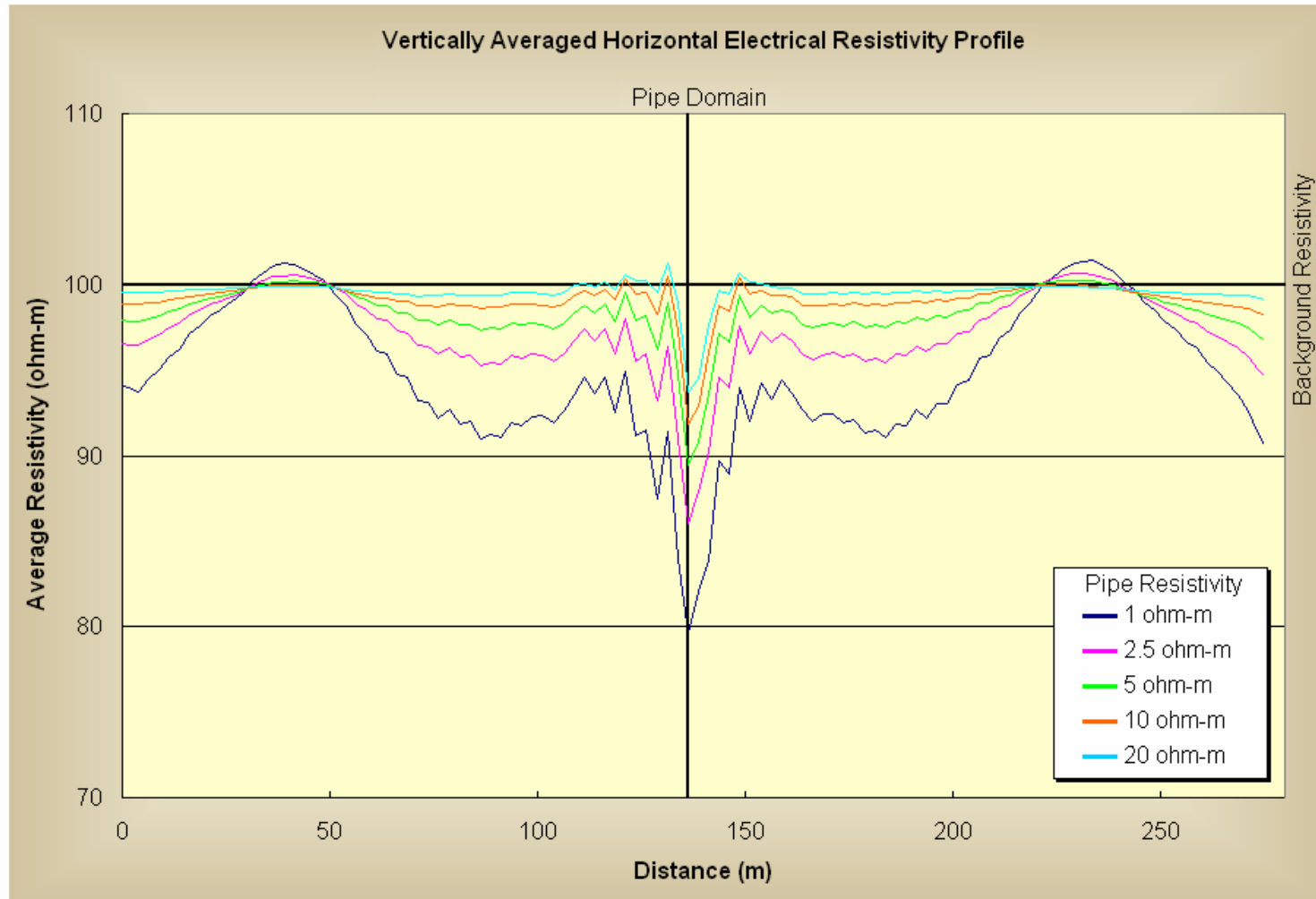Background Resistivity: 50 ohm-m, Electrode Spacing: 5 m, Pipe Location: 218 m

Figure A.2: Forward Electrical Resistivity Model 1 – Single Pipe
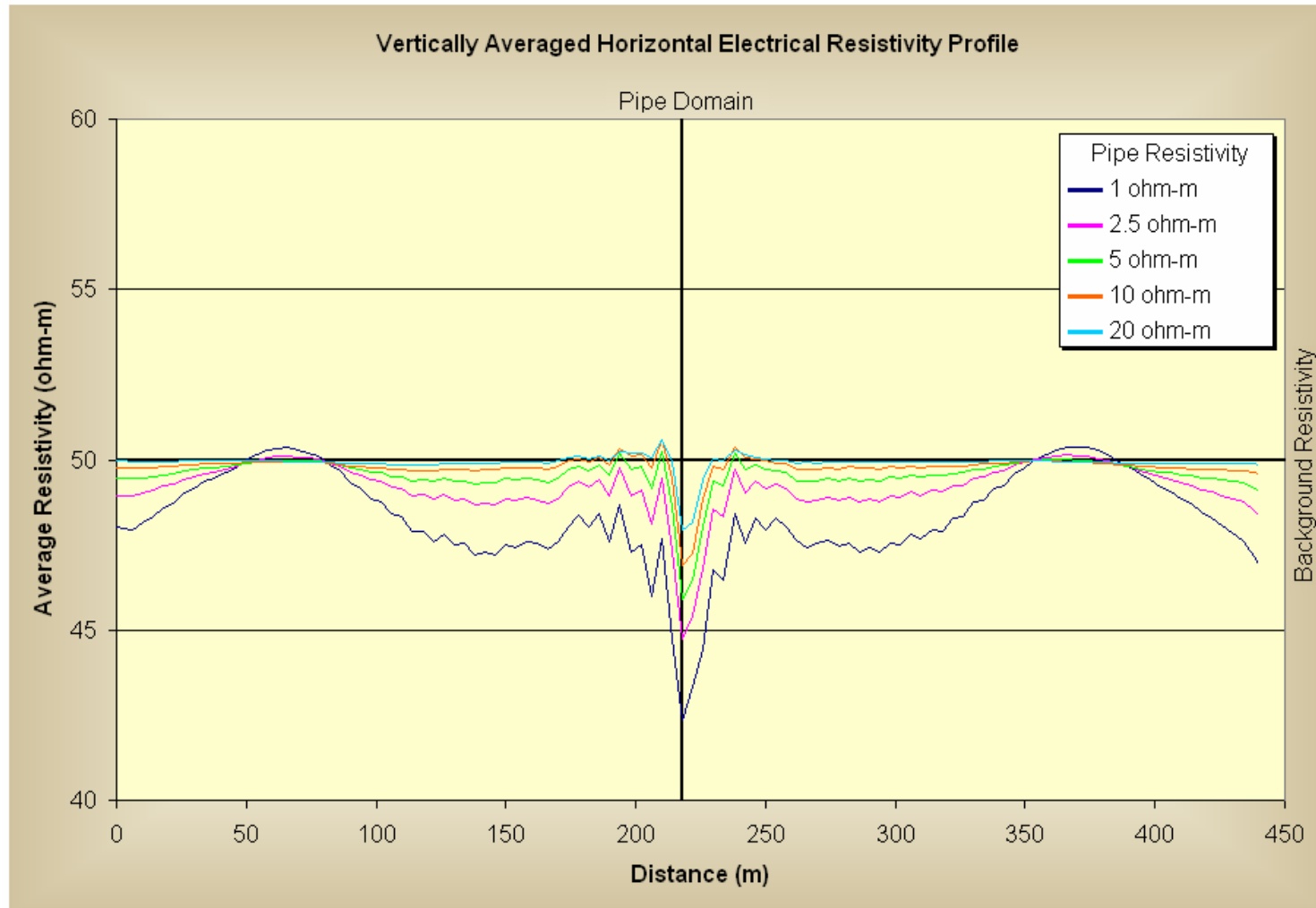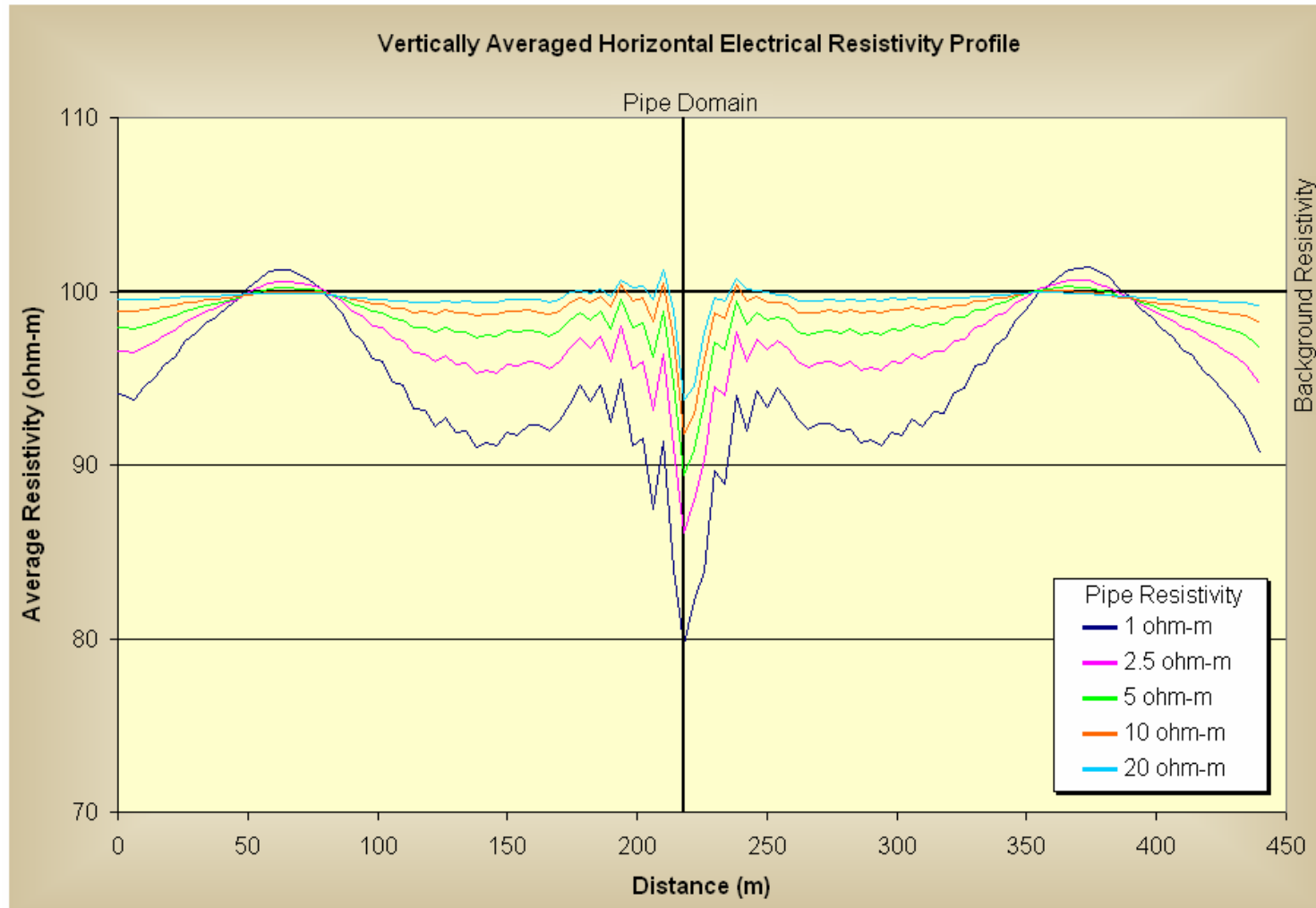Background Resistivity: 100 ohm-m, Electrode Spacing: 5 m, Pipe Location: 218 m
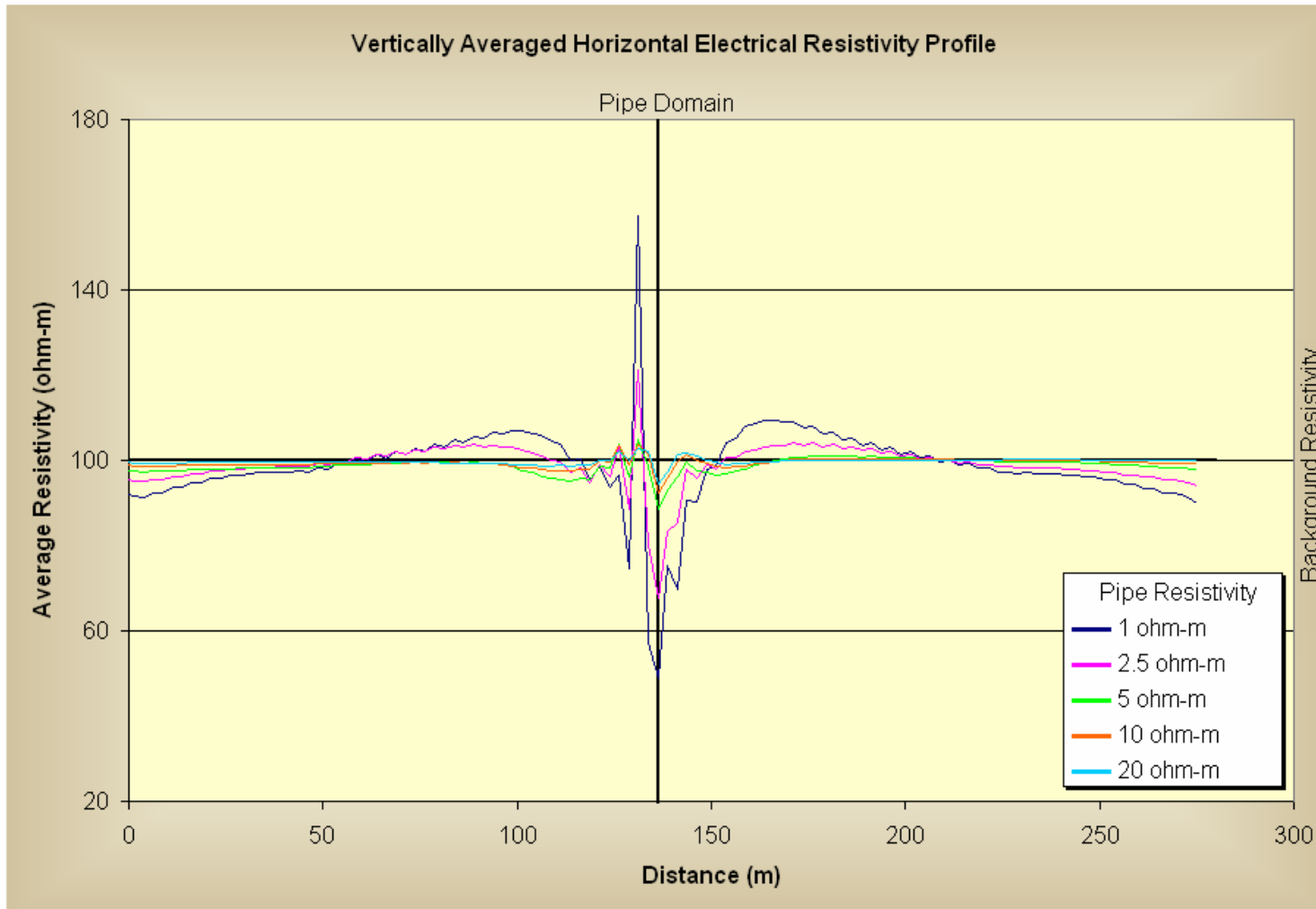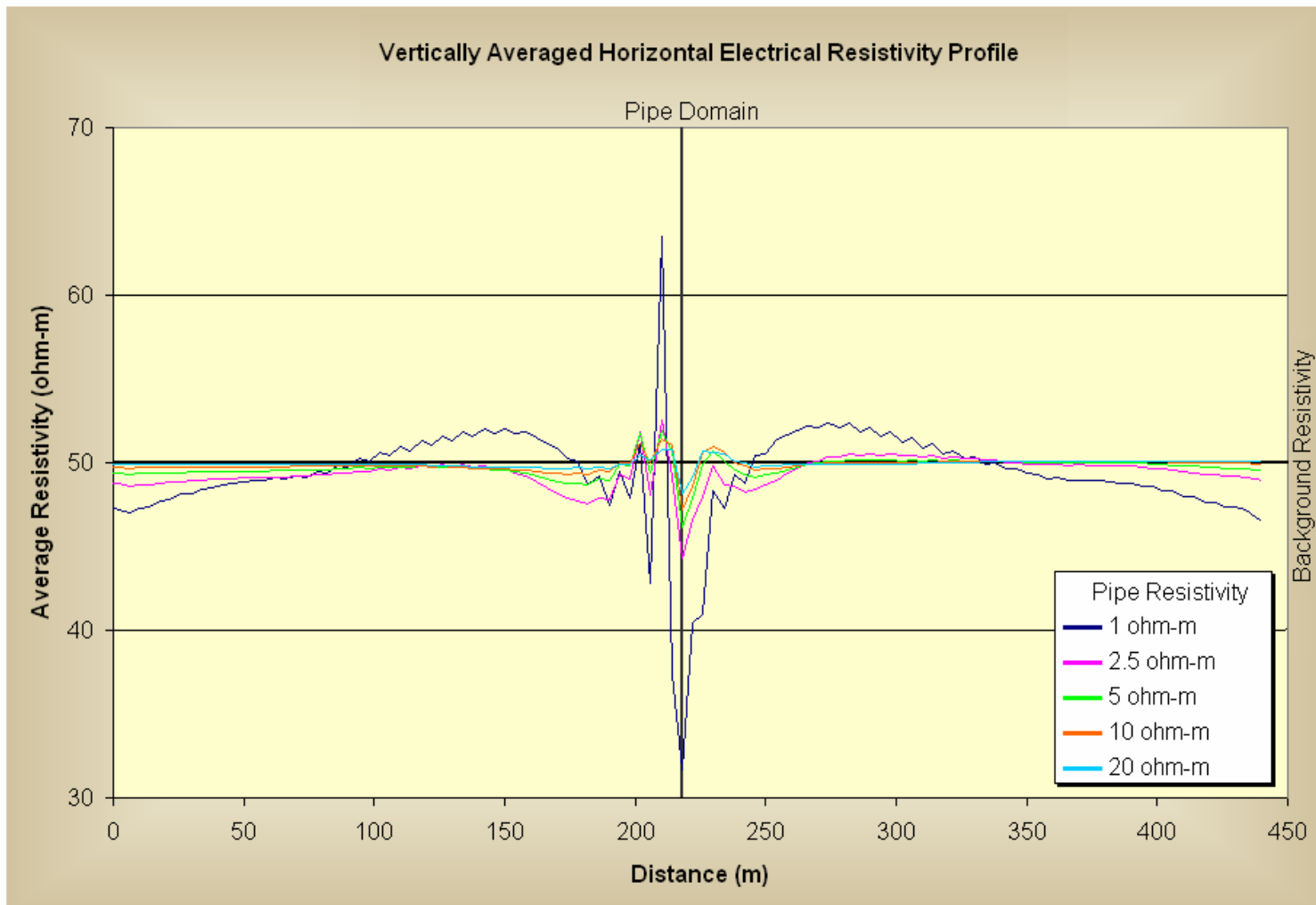
Figure A.3: Forward Electrical Resistivity Model 1 – Single Pipe
Background Resistivity: 50 ohm-m, Electrode Spacing: 8 m, Pipe Location: 218 m
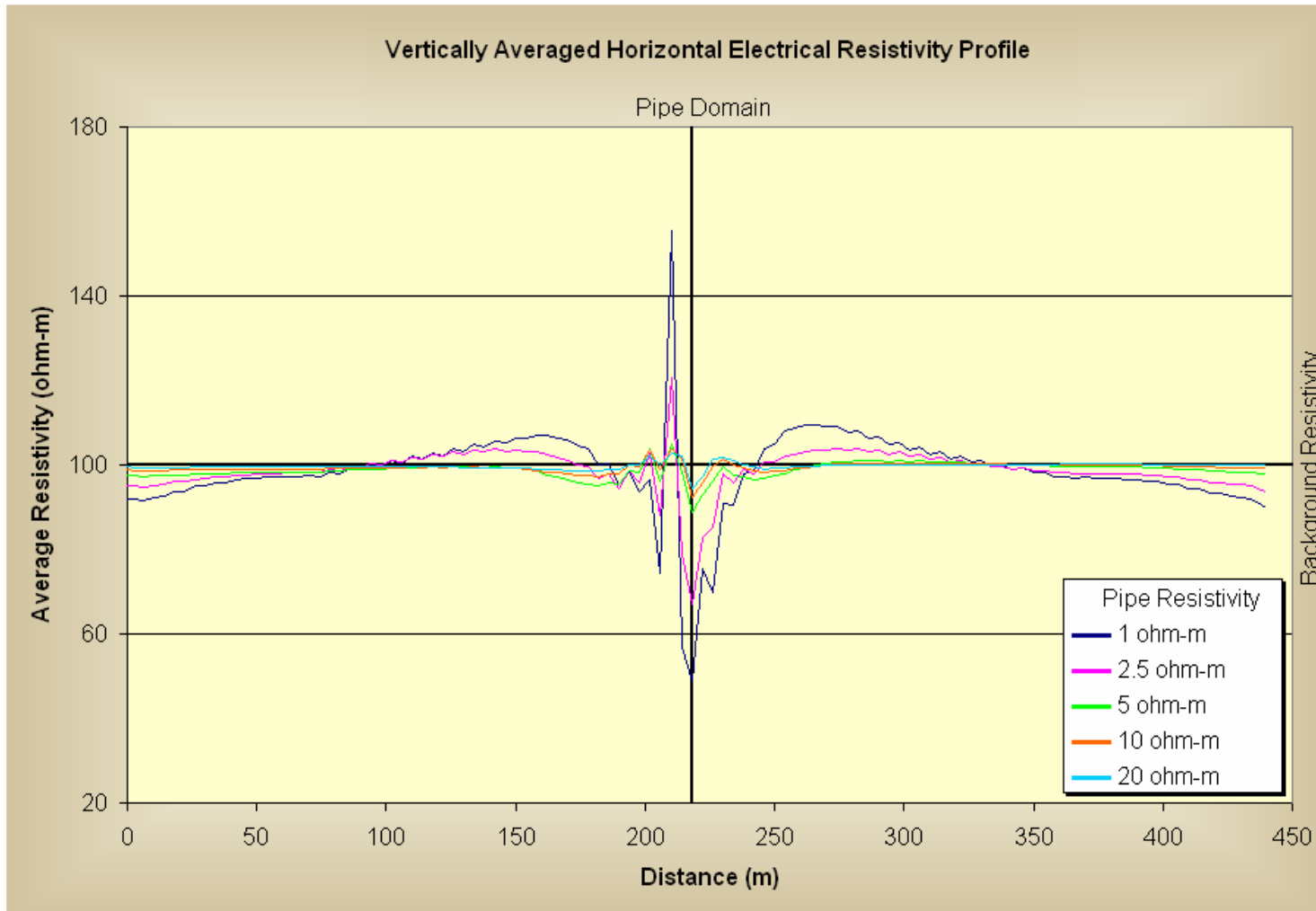
Figure A.4: Forward Electrical Resistivity Model 1 – Single Pipe
Background Resistivity: 100 ohm-m, Electrode Spacing: 8 m, Pipe Location: 218 m
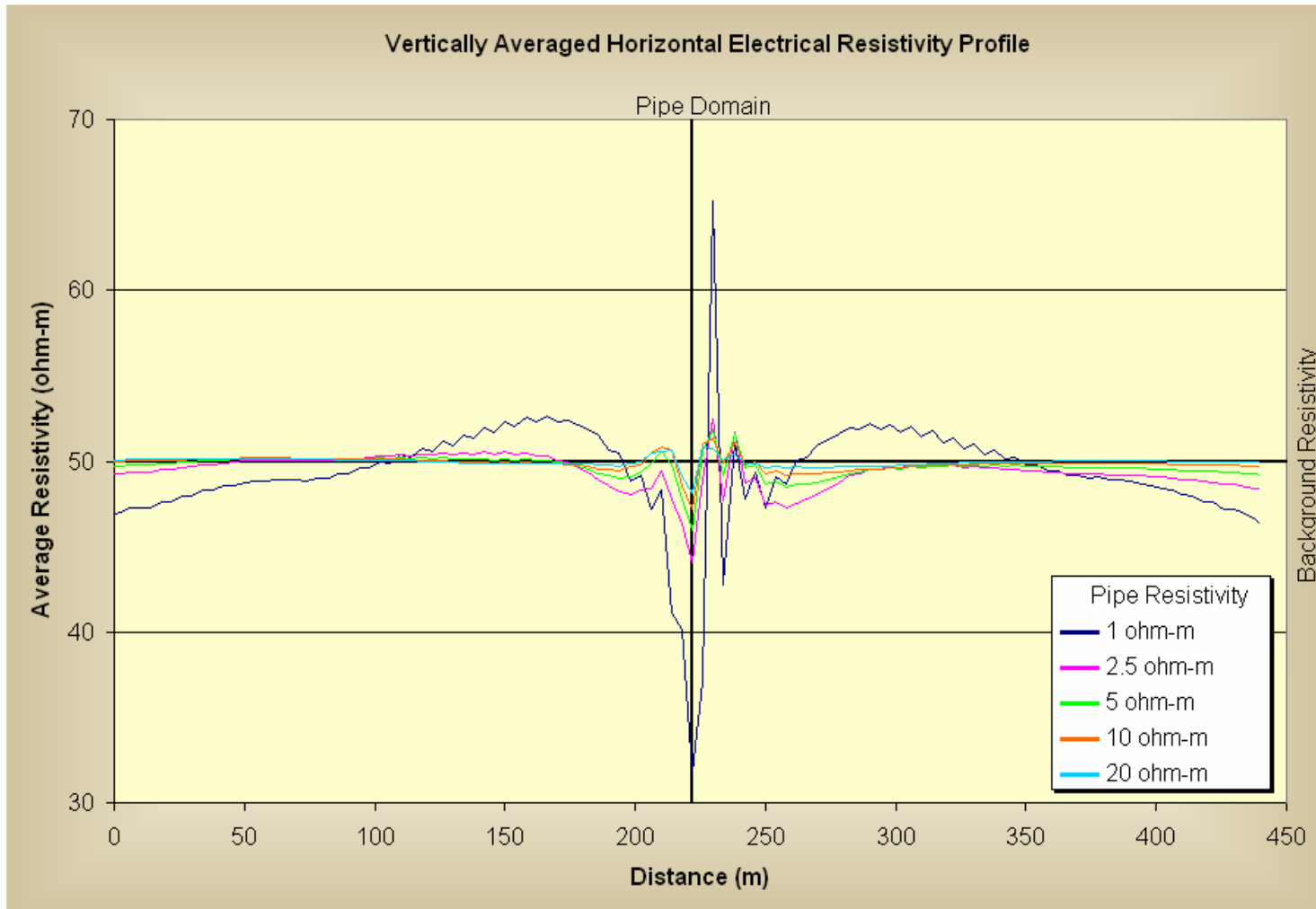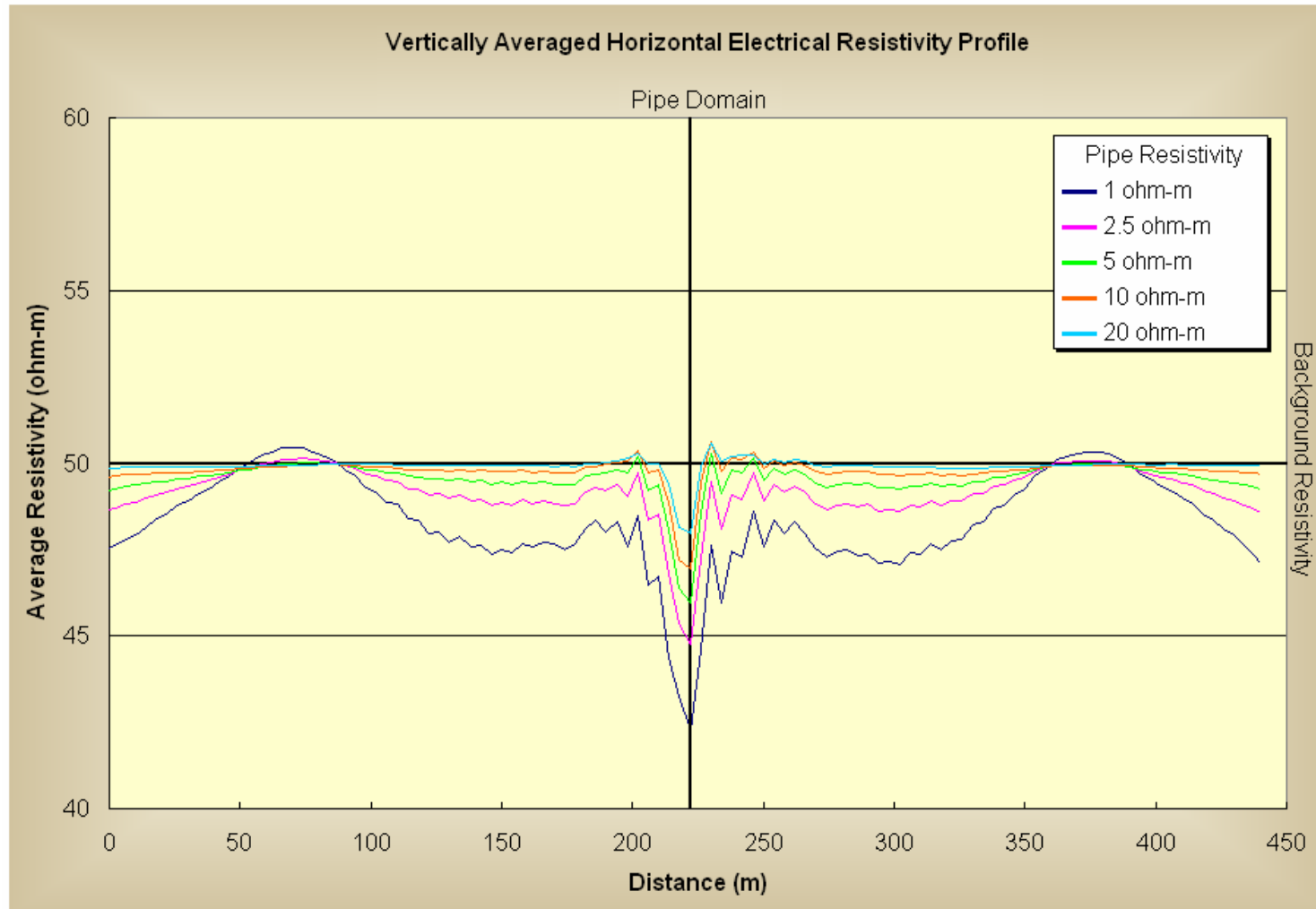
Figure A.5: Forward Electrical Resistivity Model 1 – Single Pipe
Background Resistivity: 50 ohm-m, Electrode Spacing: 8 m, Pipe Location: 222 m
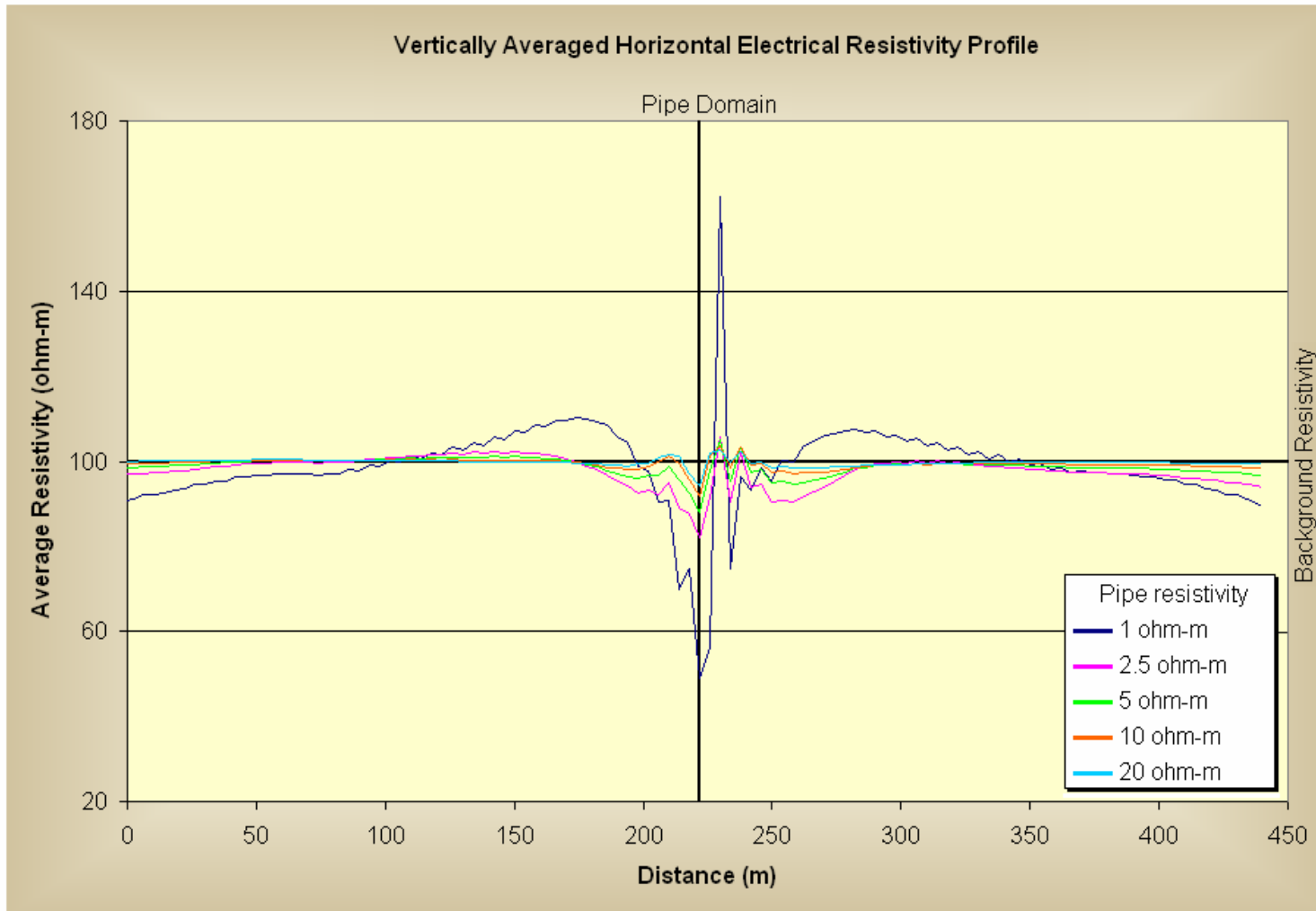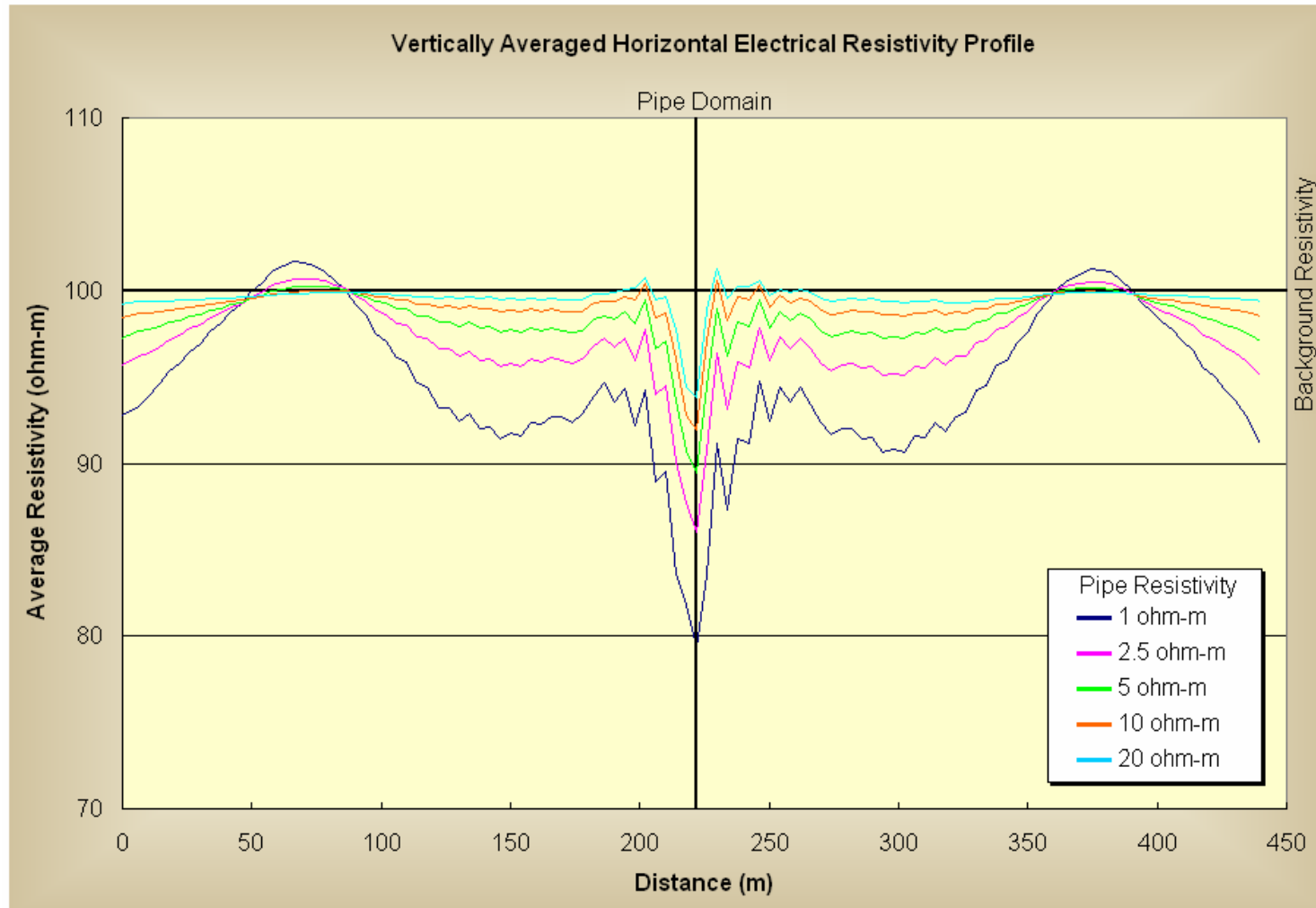
Figure A.6: Forward Electrical Resistivity Model 1 – Single Pipe
Background Resistivity: 100 ohm-m, Electrode Spacing: 8 m, Pipe Location: 222 m
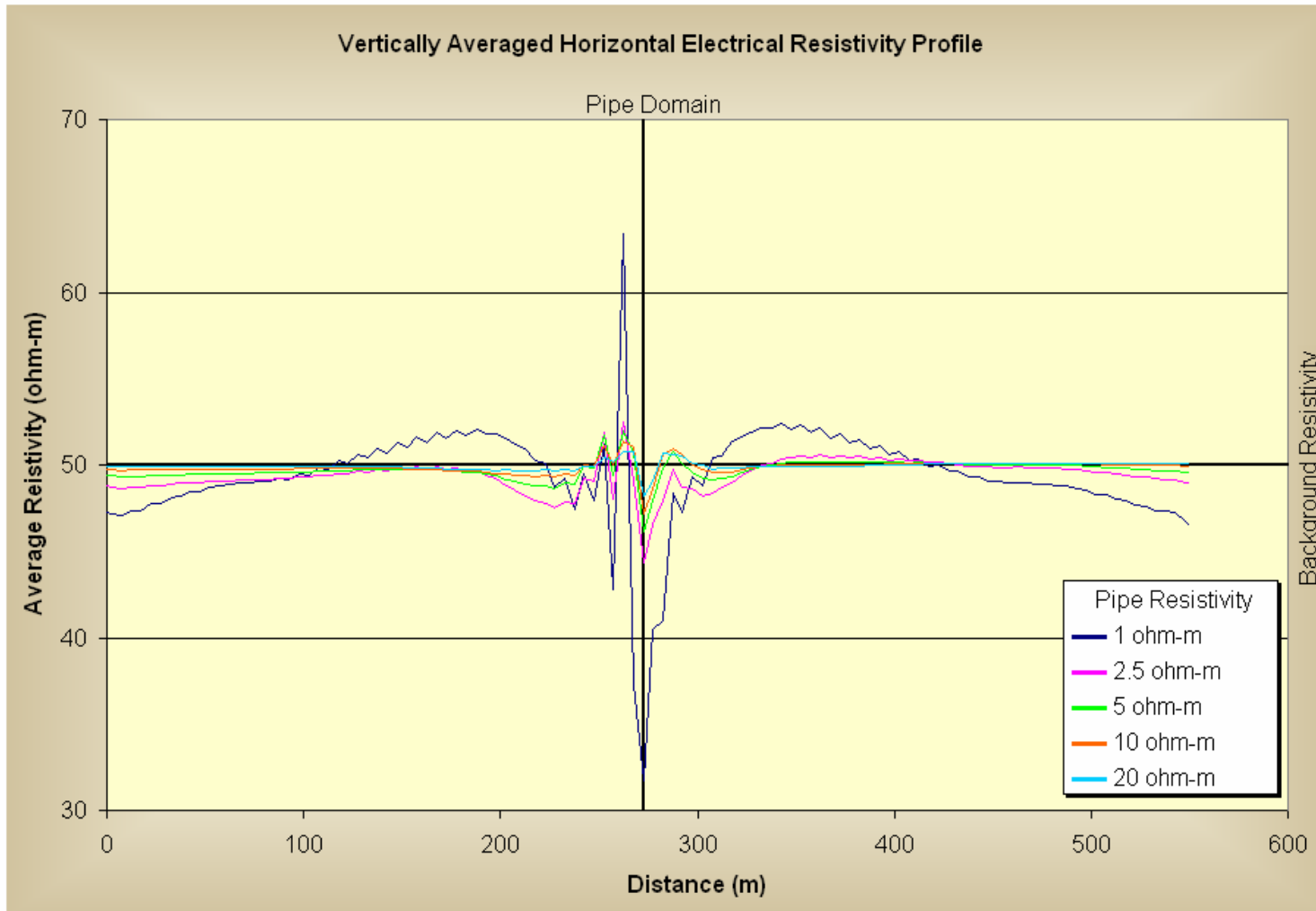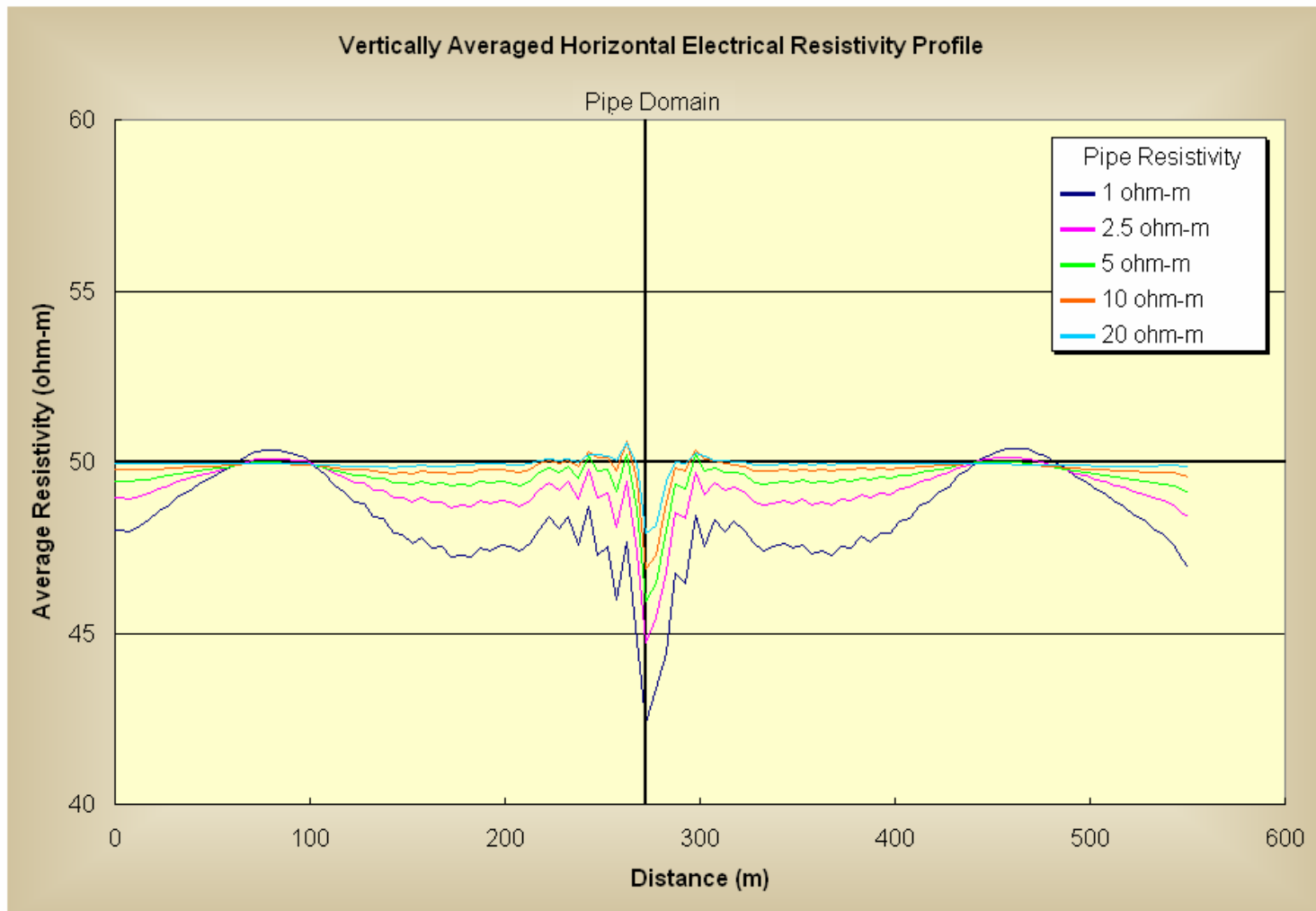
Figure A.7: Forward Electrical Resistivity Model 1 – Single Pipe
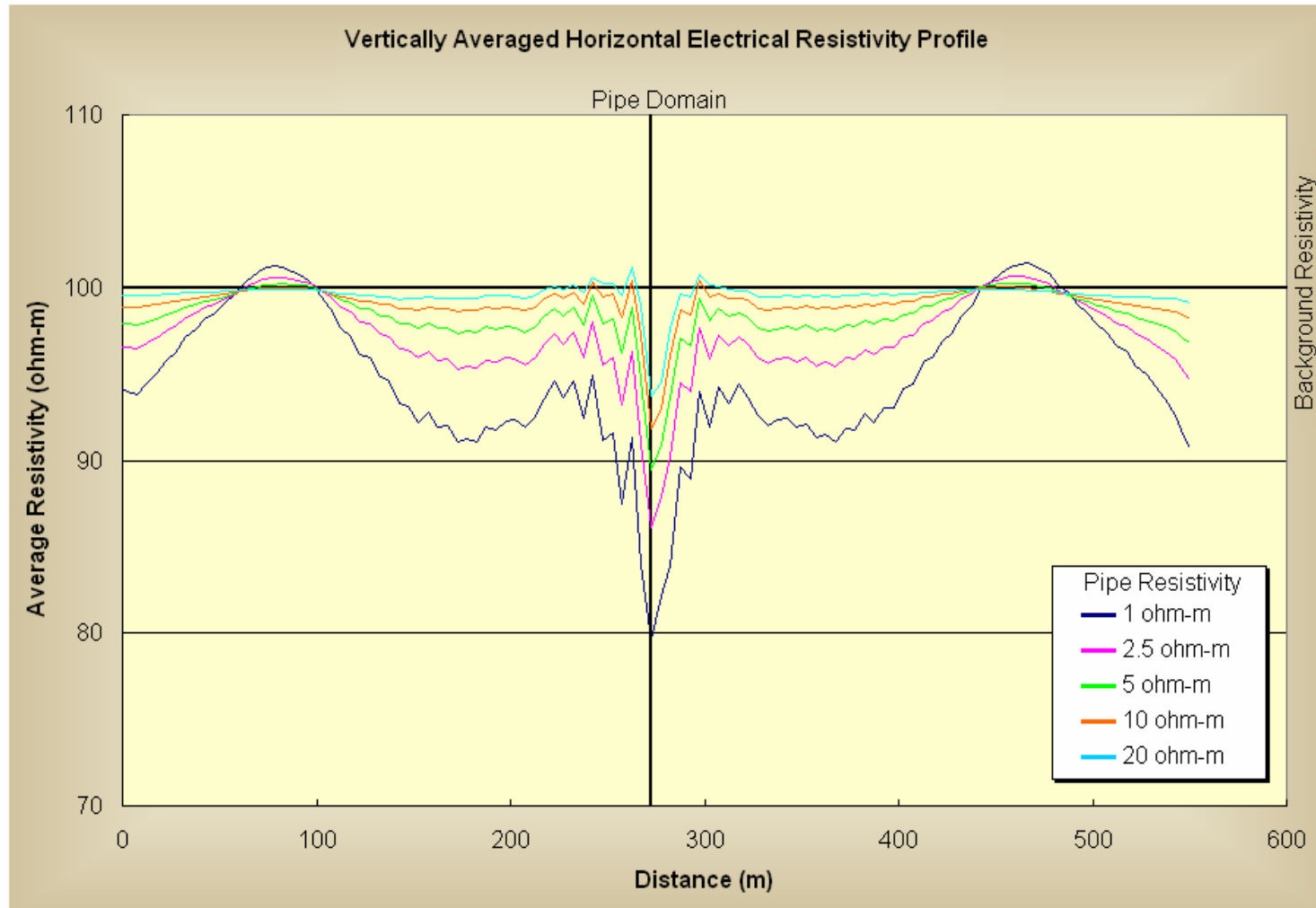Background Resistivity: 50 ohm-m, Electrode Spacing: 10 m, Pipe Location: 218 m
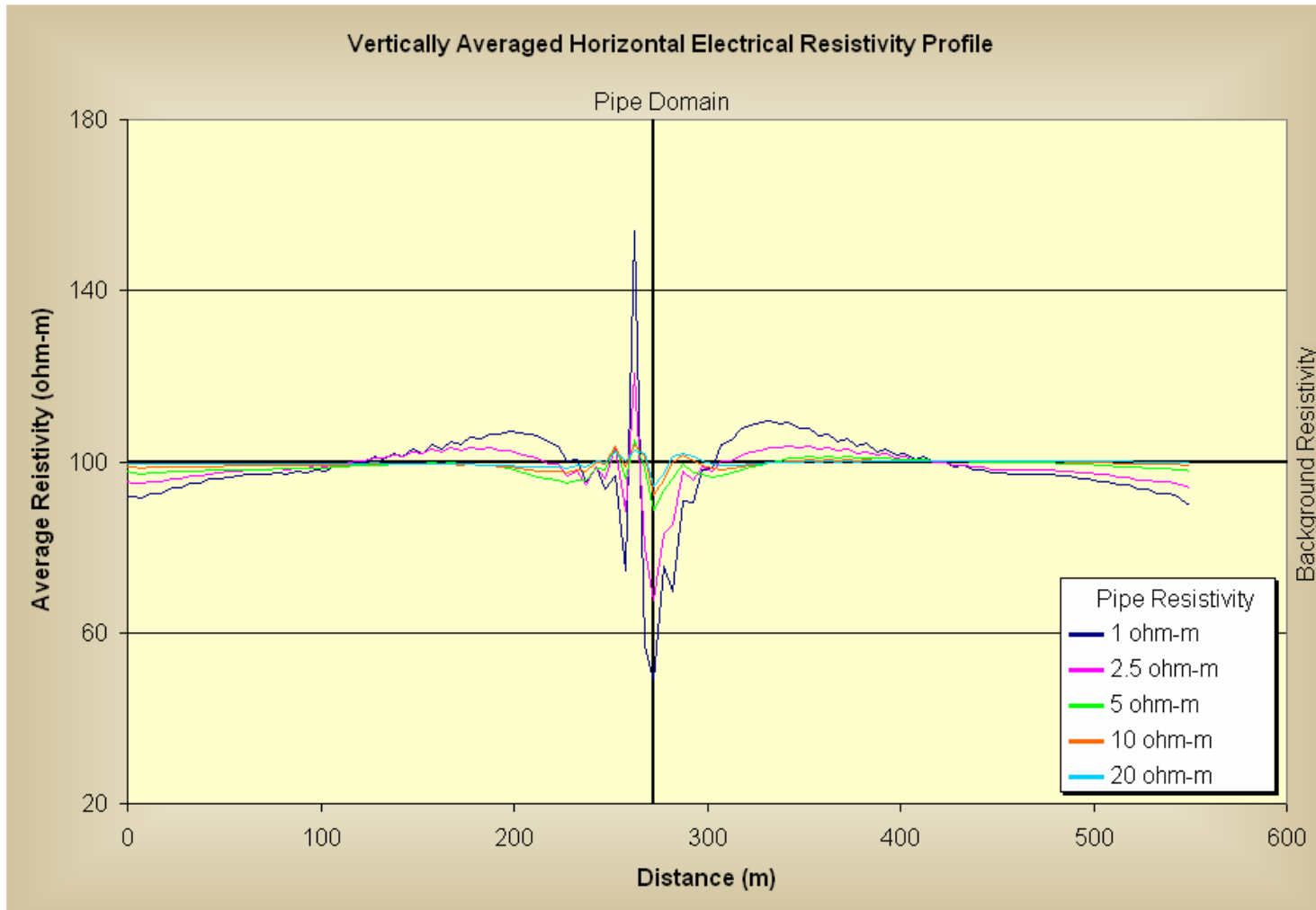
Figure A.8: Forward Electrical Resistivity Model 1 – Single Pipe
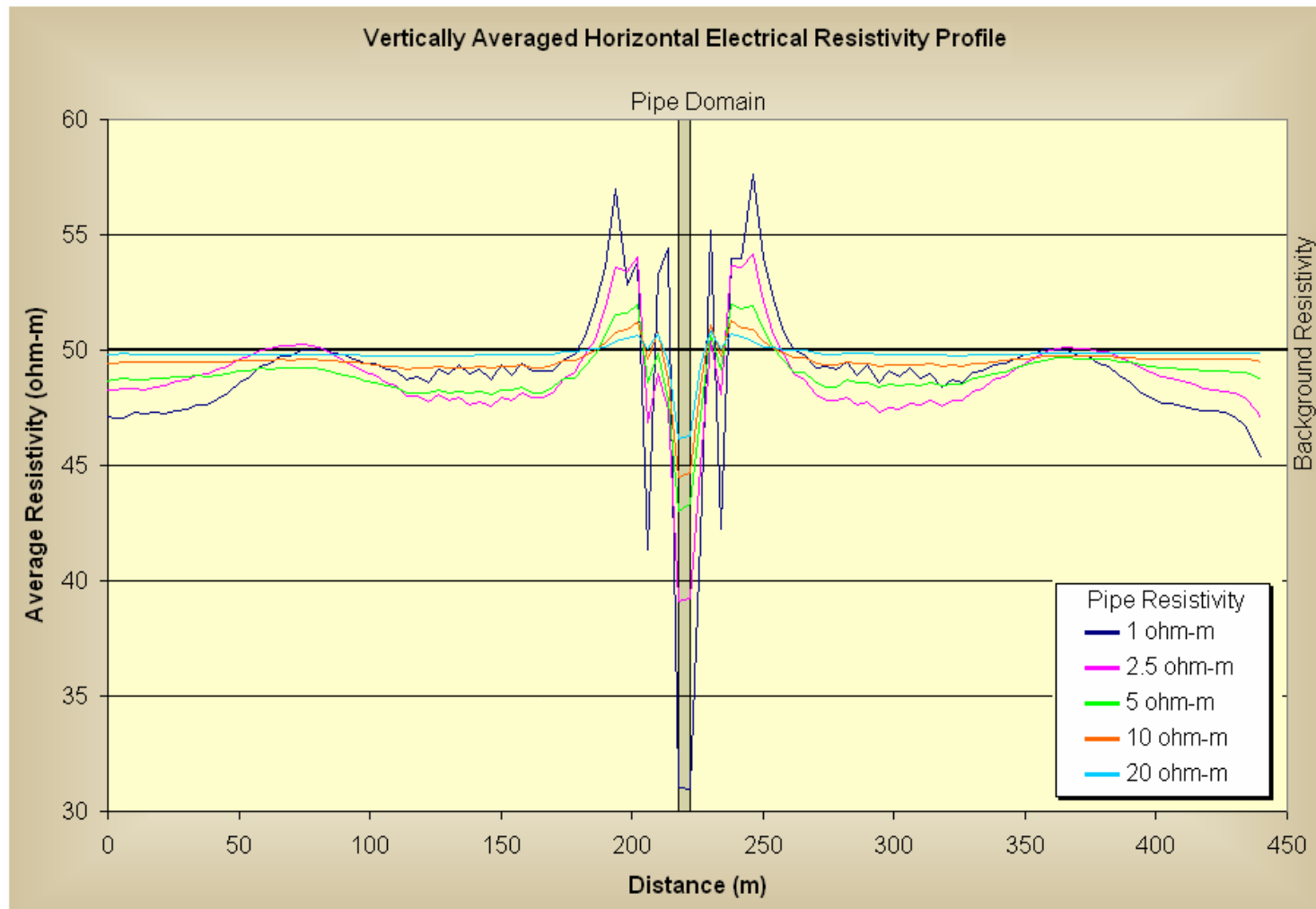Background Resistivity: 100 ohm-m, Electrode Spacing: 10 m, Pipe Location: 218 m
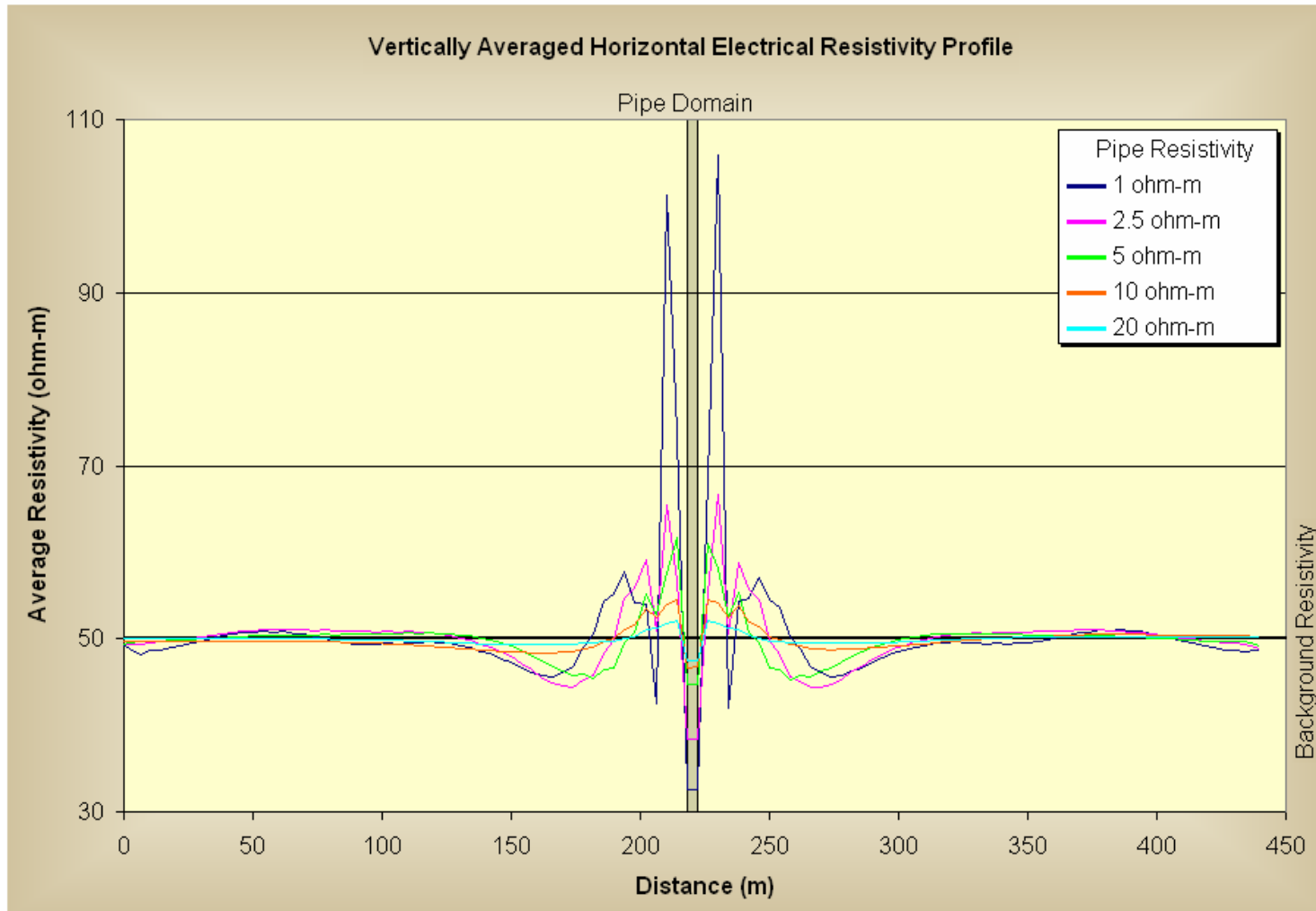
Figure A.9: Forward Electrical Resistivity Model 2 – Single Pipe at Small Angle
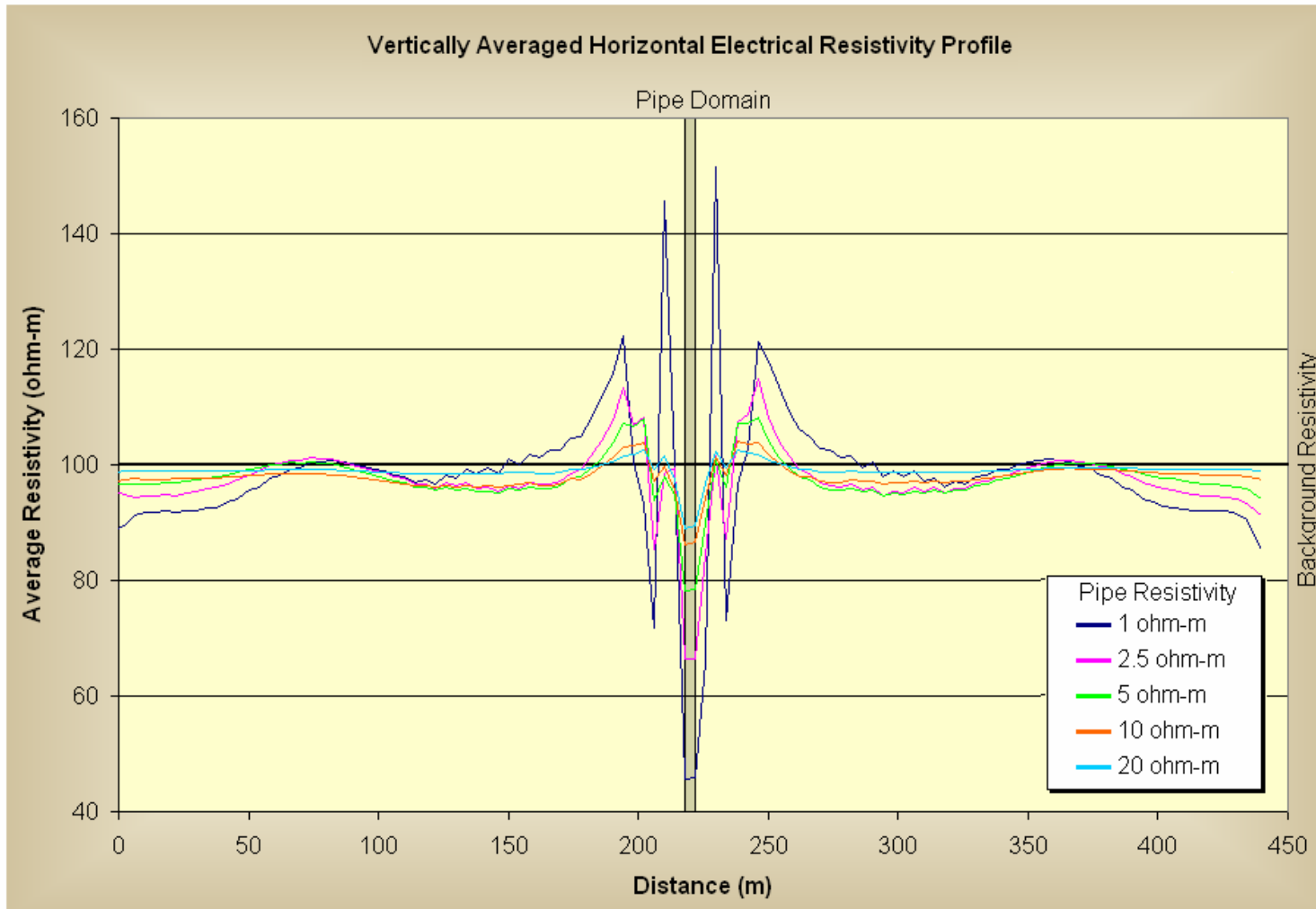Background Resistivity: 50 ohm-m, Electrode Spacing: 8 m, Pipe Location: 218 m
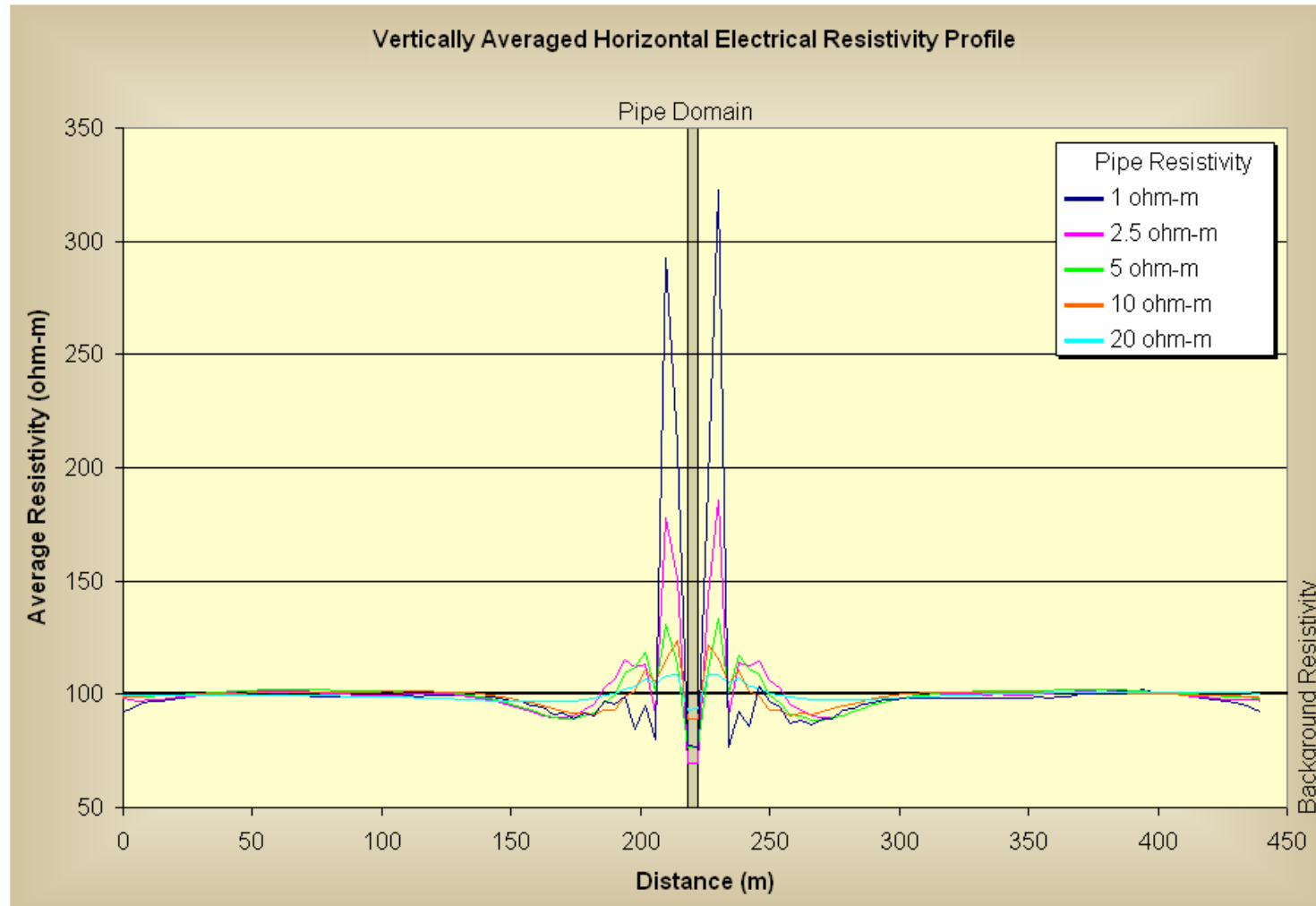
Figure A.10: Forward Electrical Resistivity Model 2 – Single Pipe Inter at Small Angle
Background Resistivity: 100 ohm-m, Electrode Spacing: 8 m, Pipe Location: 218 m
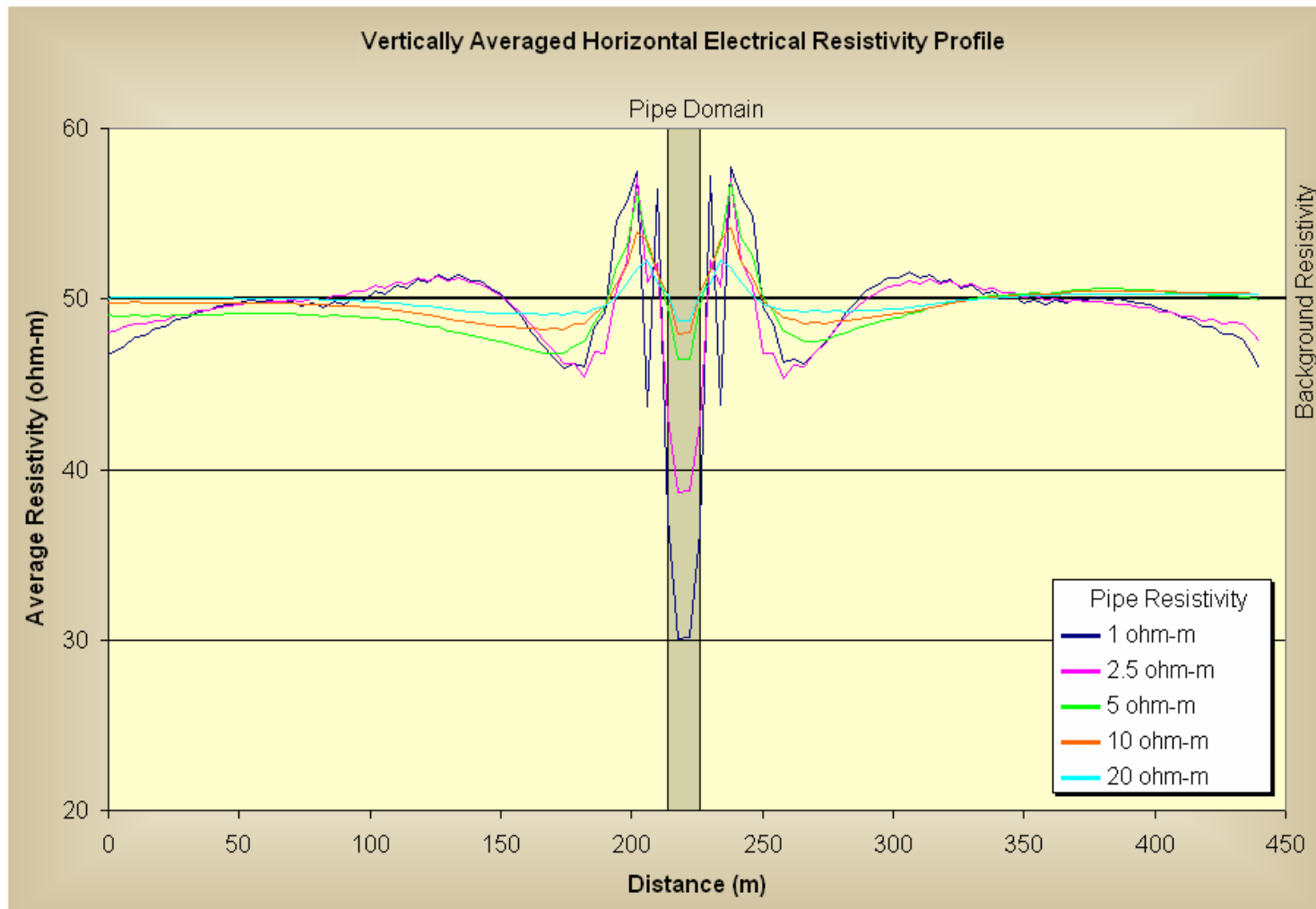
Figure A.11: Forward Electrical Resistivity Model 3 – Single Pipe at Low Angle
Background Resistivity: 50 ohm-m, Electrode Spacing: 8 m, Pipe Location: 218 m
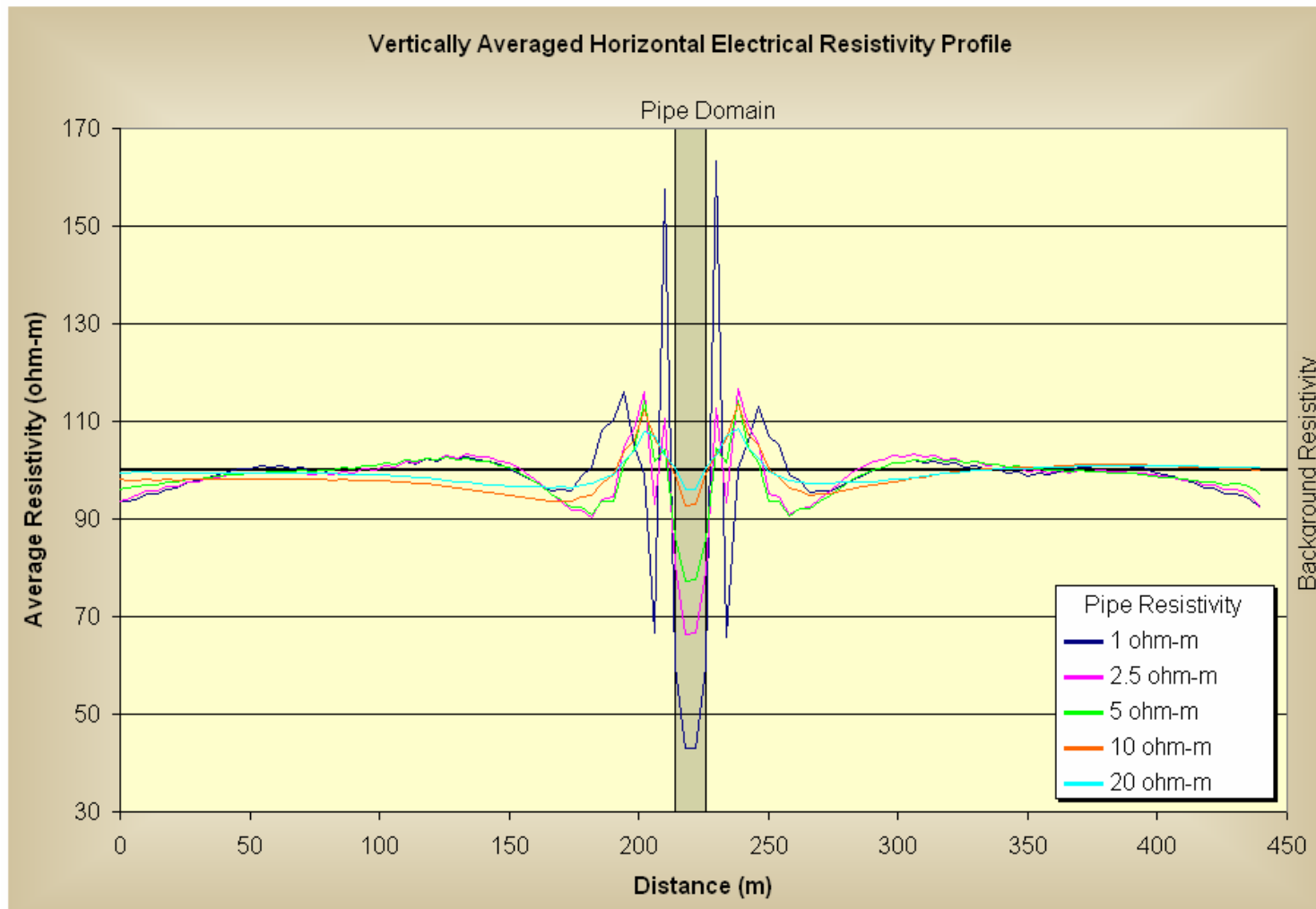
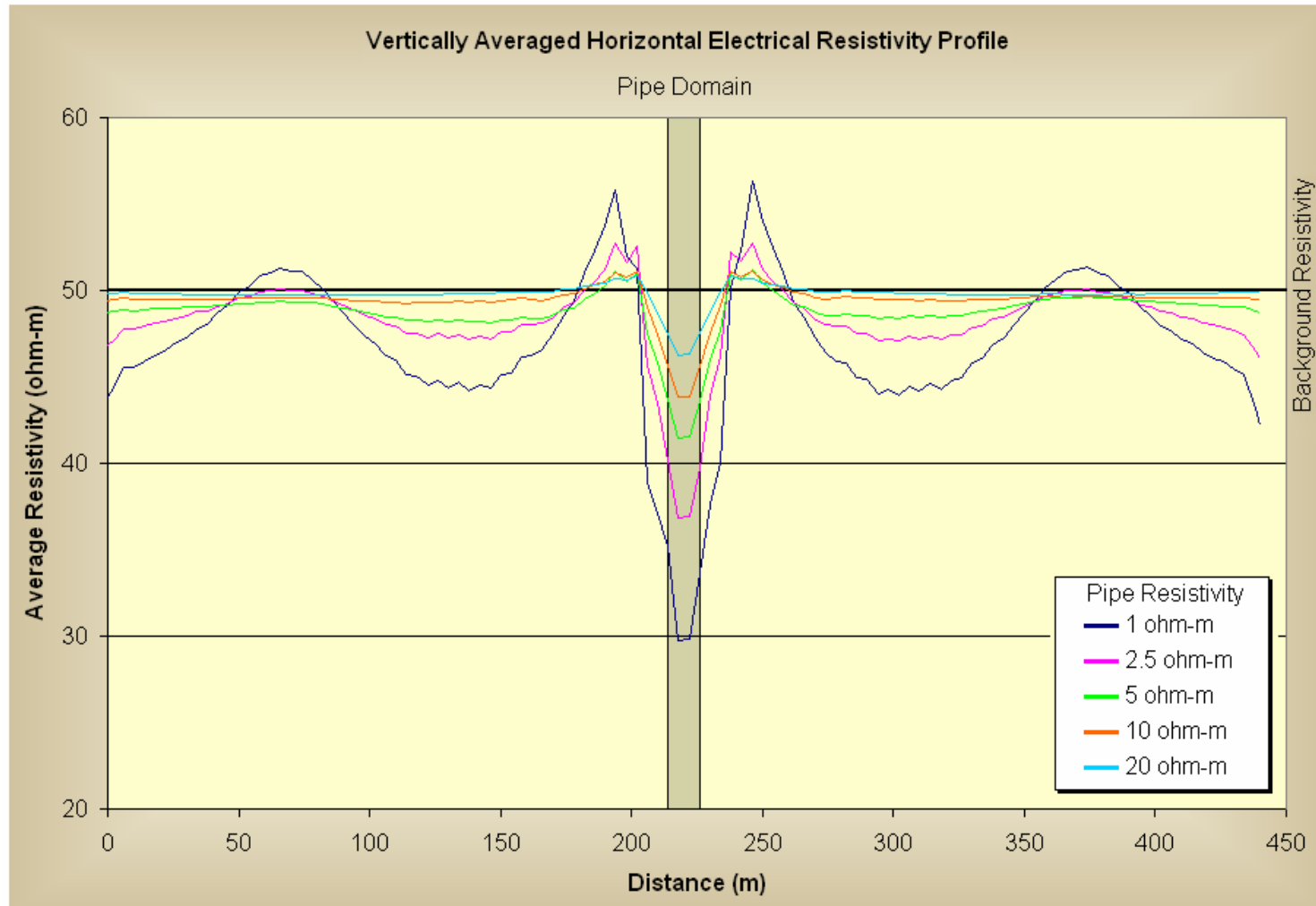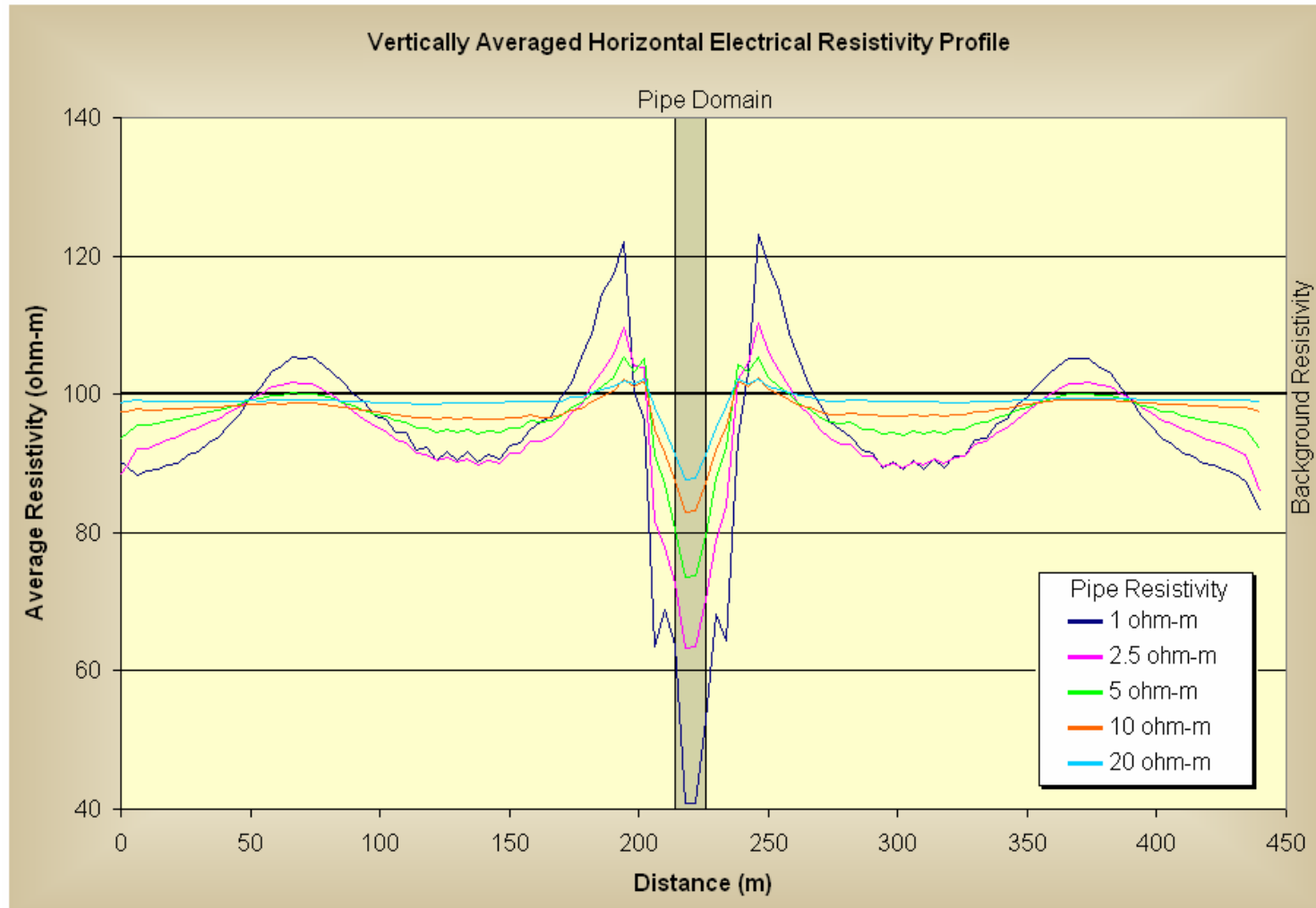**Figure A.12: Forward Electrical Resistivity Model 3 – Single Pipe at Low Angle**
Background Resistivity: 100 ohm-m, Electrode Spacing: 8 m, Pipe Location: 218 m
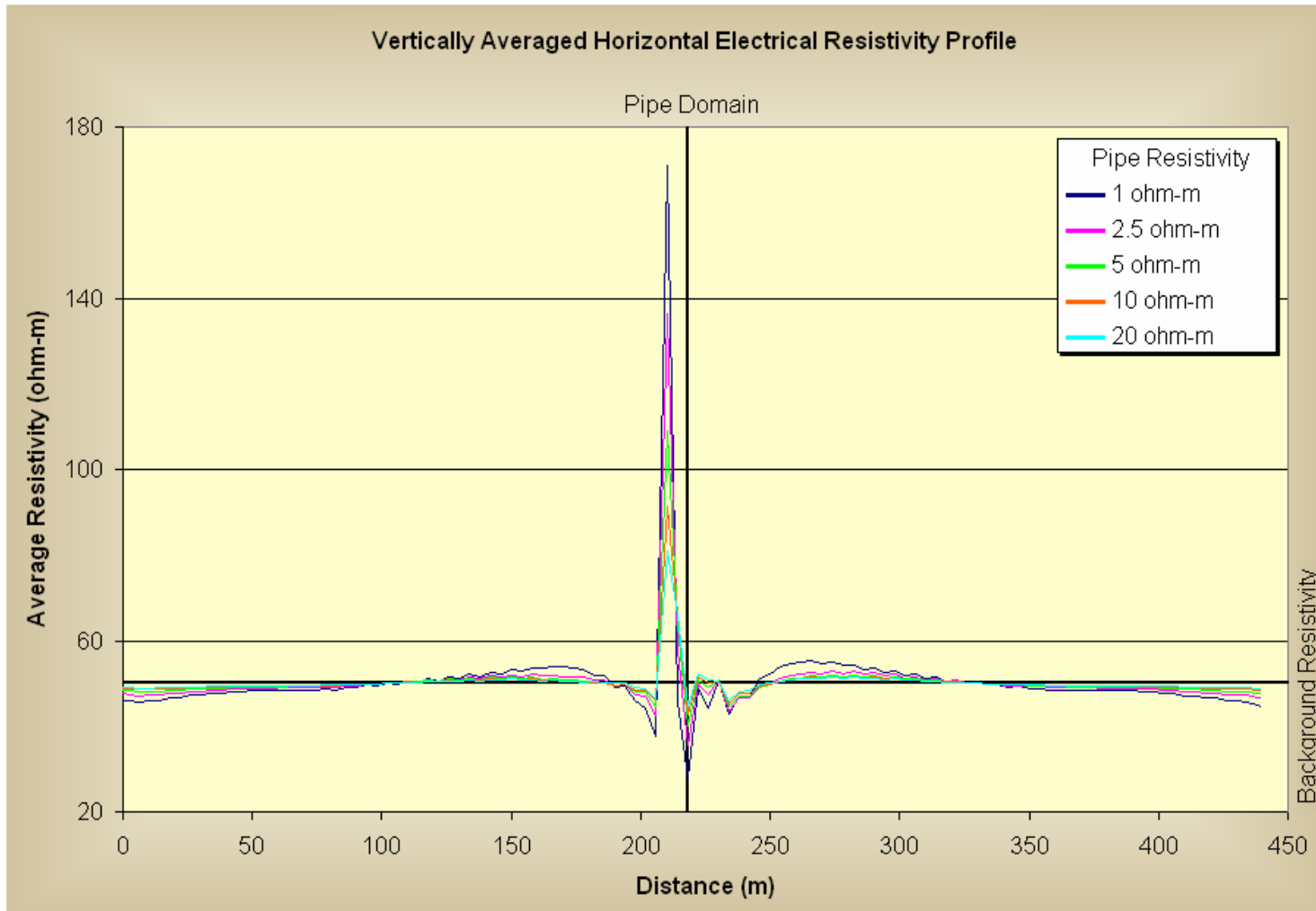
Figure A.13 Forward Electrical Resistivity Model 4 – Single Pipe with Surrounding Insulators
Background Resistivity: 50 ohm-m, Insulator Resistivity: 500 ohm-m, Electrode Spacing: 8 m, Pipe Location: 218 m
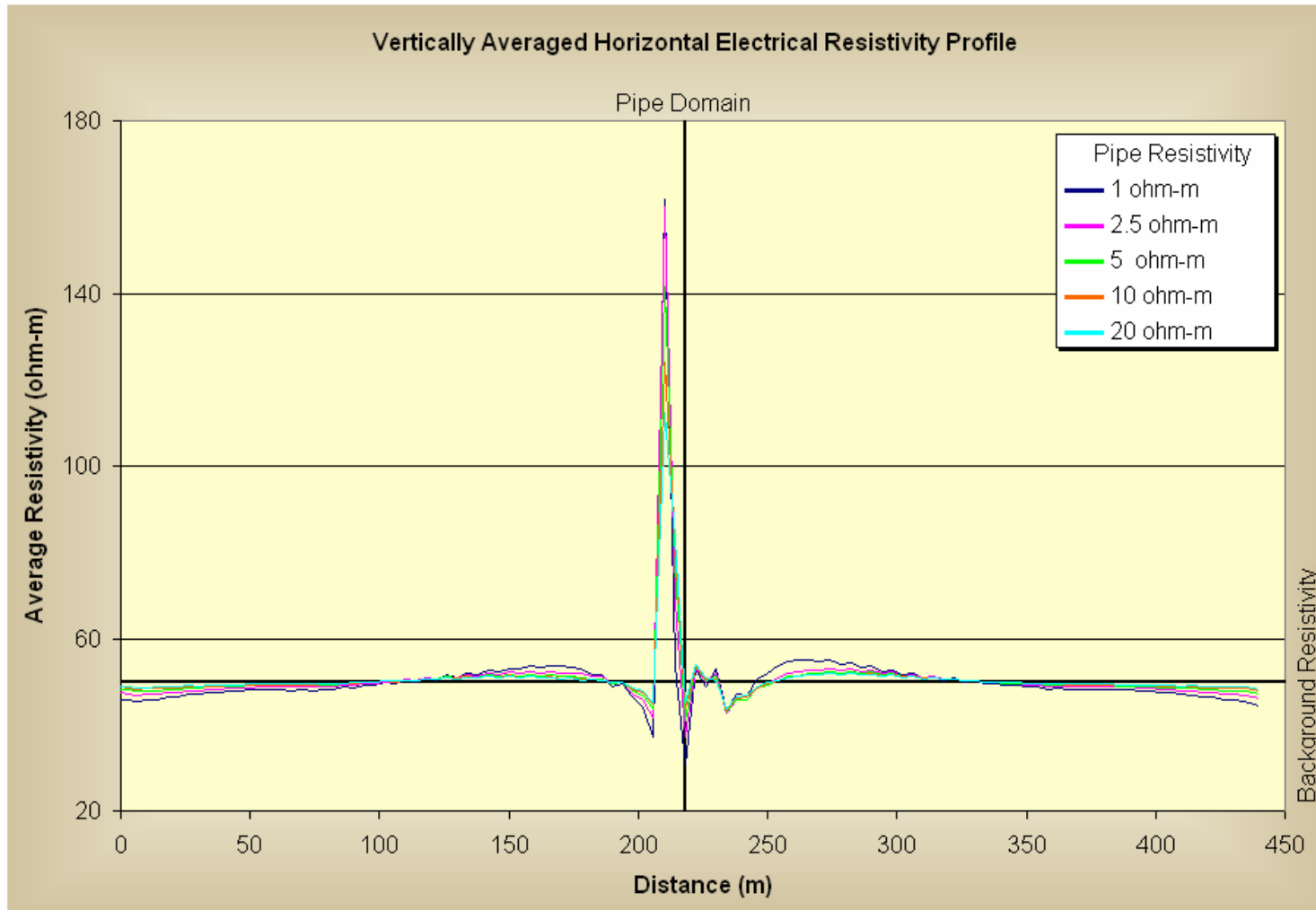
Figure A.14 Forward Electrical Resistivity Model 4 – Single Pipe with Surrounding Insulators
Background Resistivity: 50 ohm-m, Insulator Resistivity: 5000 ohm-m, Electrode Spacing: 8 m, Pipe Location: 218 m
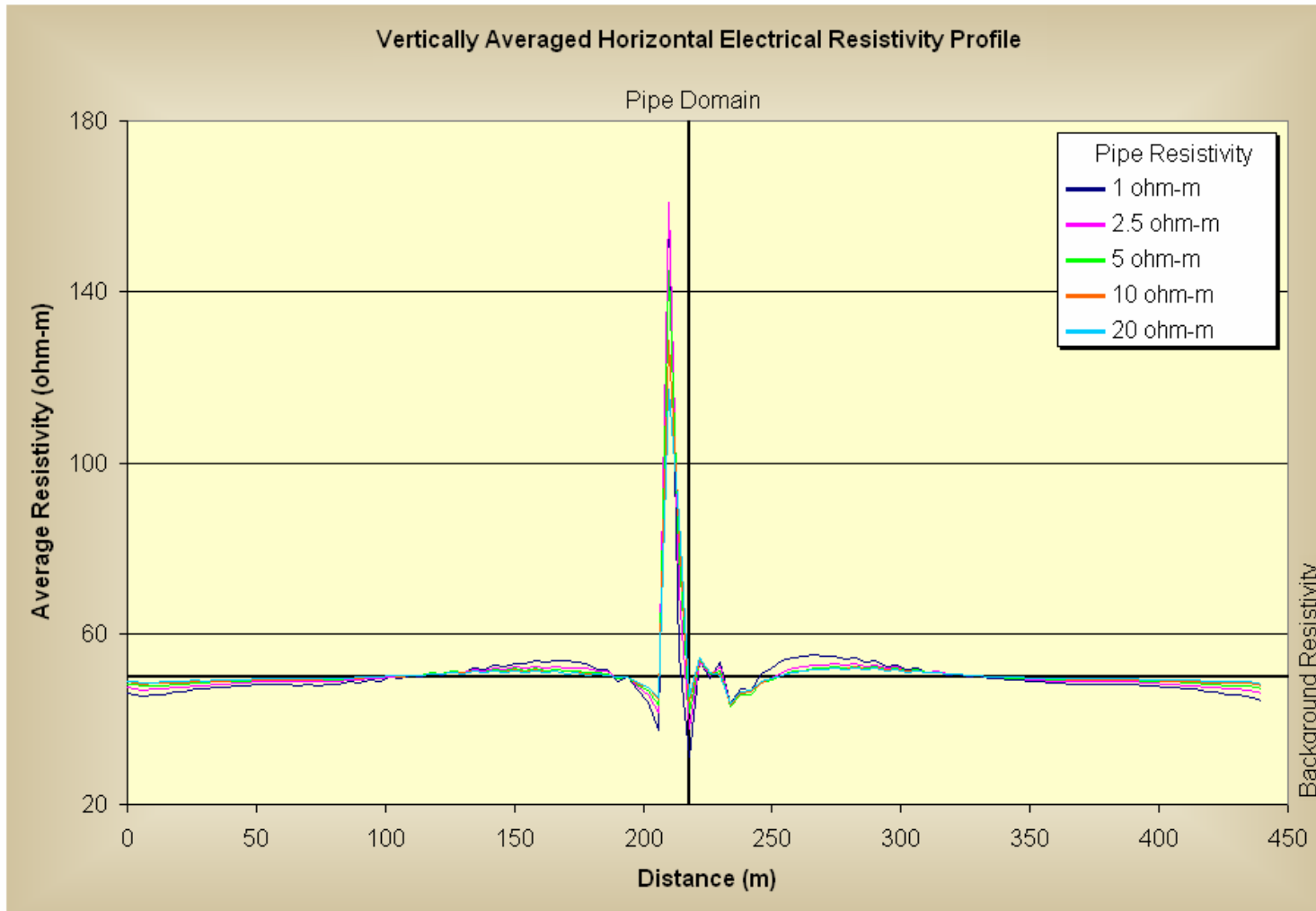
Figure A.15 Forward Electrical Resistivity Model 4 – Single Pipe with Surrounding Insulators
Background Resistivity: 50 ohm-m, Insulator Resistivity: 50000 ohm-m, Electrode Spacing: 8 m, Pipe Location: 218 m
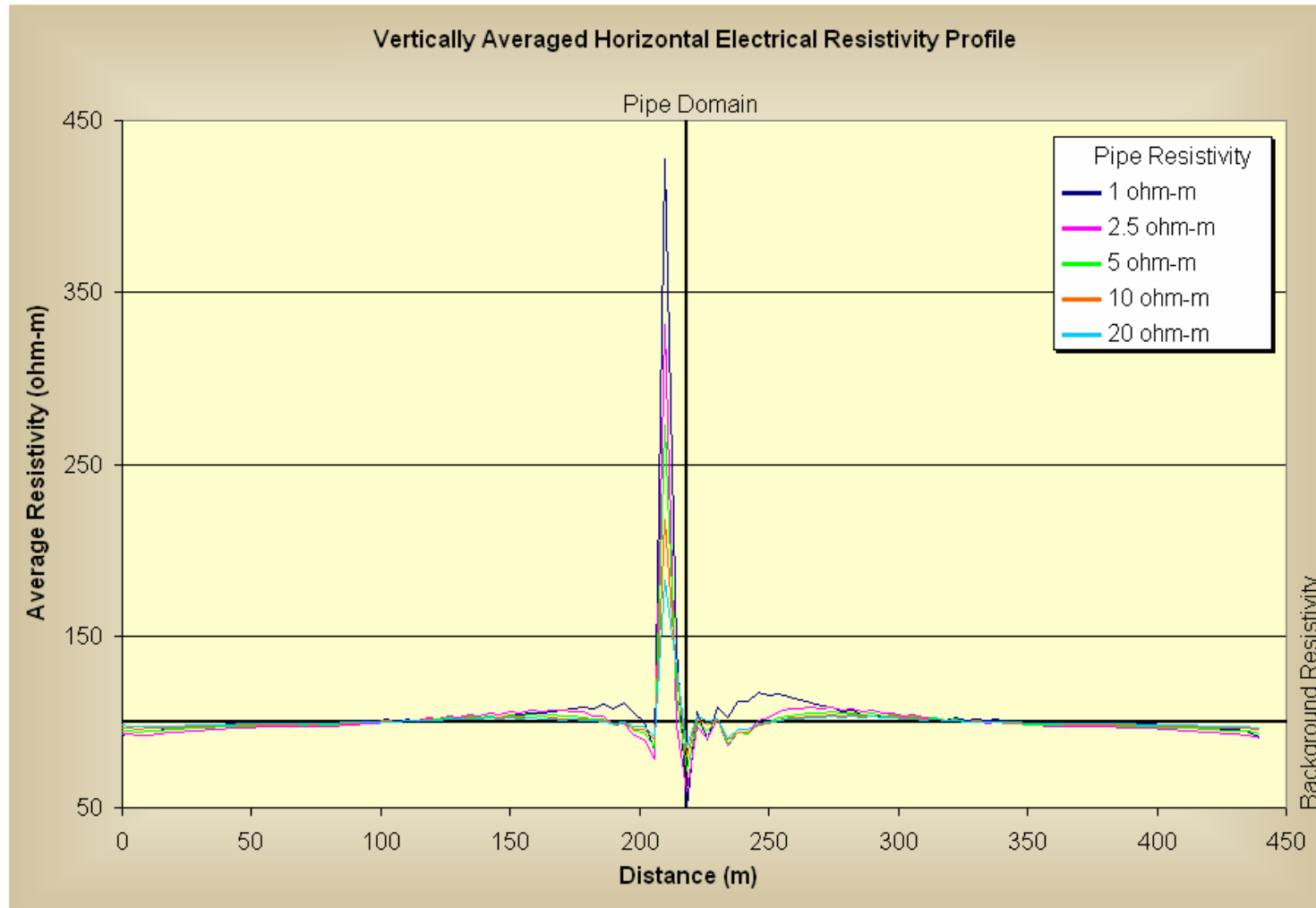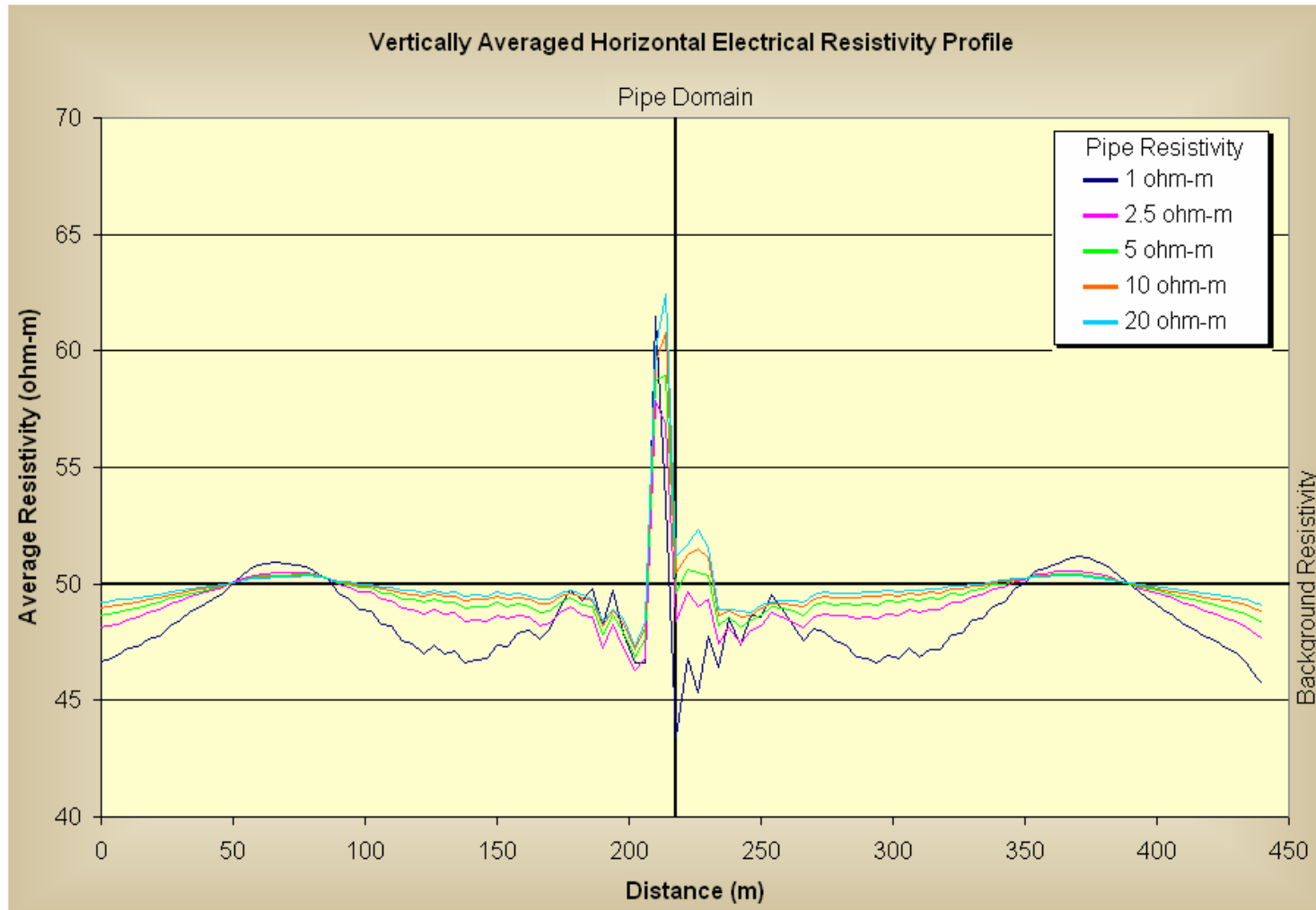
Figure A.16 Forward Electrical Resistivity Model 4 – Single Pipe with Surrounding Insulators
Background Resistivity: 100 ohm-m, Insulator Resistivity: 1000 ohm-m, Electrode Spacing: 8 m, Pipe Location: 218 m
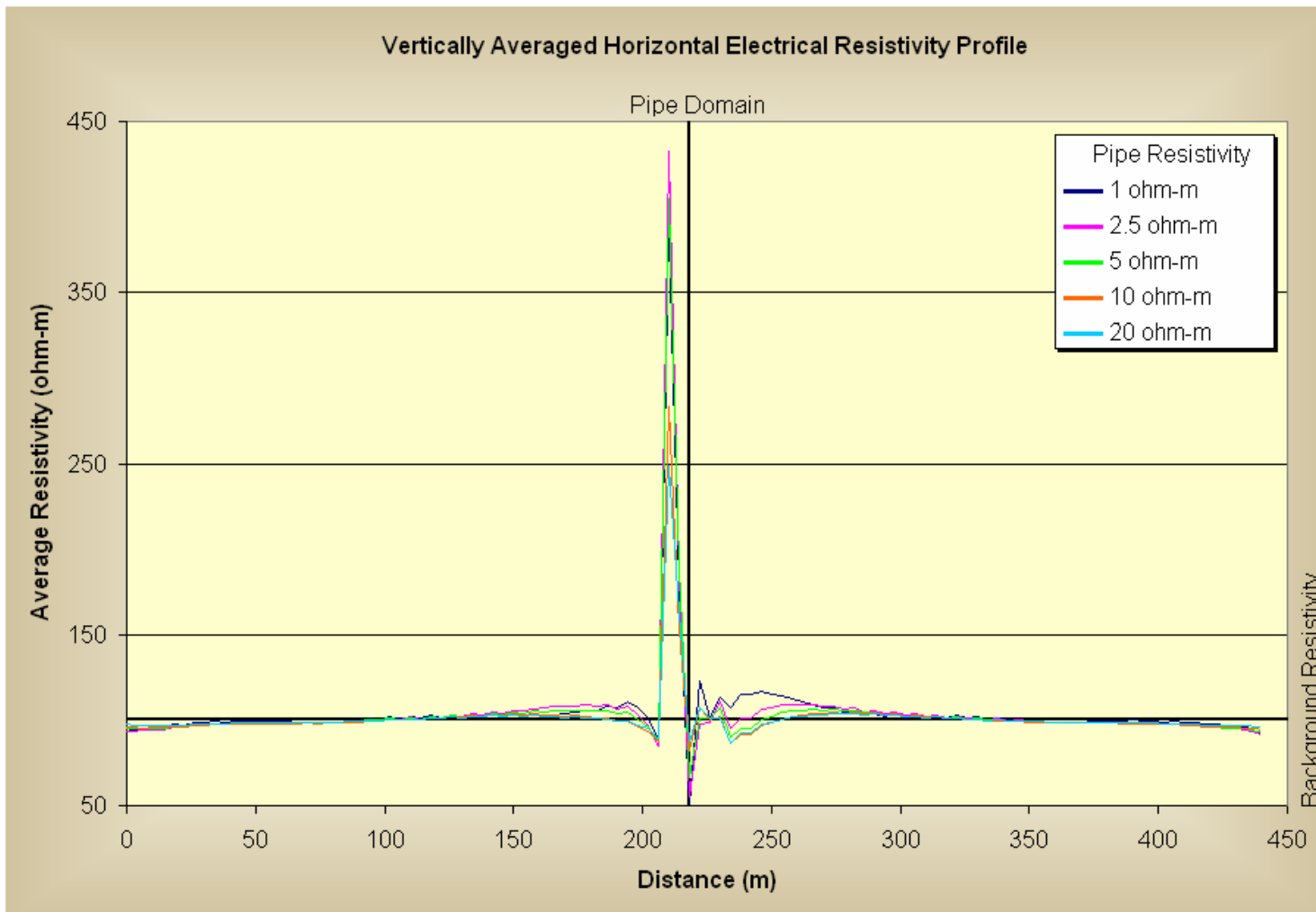
Figure A.17 Forward Electrical Resistivity Model 4 – Single Pipe with Surrounding Insulators
Background Resistivity: 100 ohm-m, Insulator Resistivity: 10000 ohm-m, Electrode Spacing: 8 m, Pipe Location: 218 m
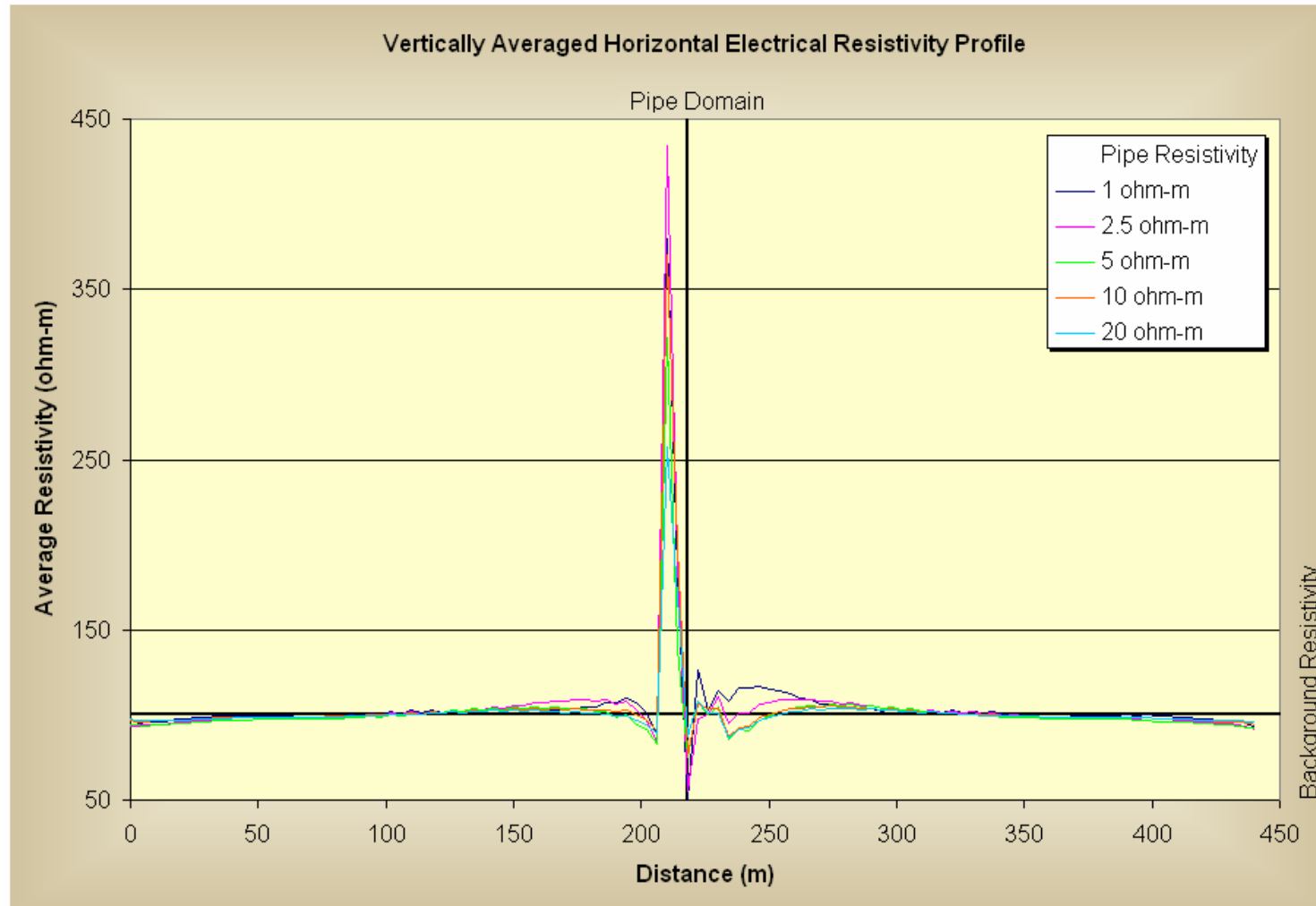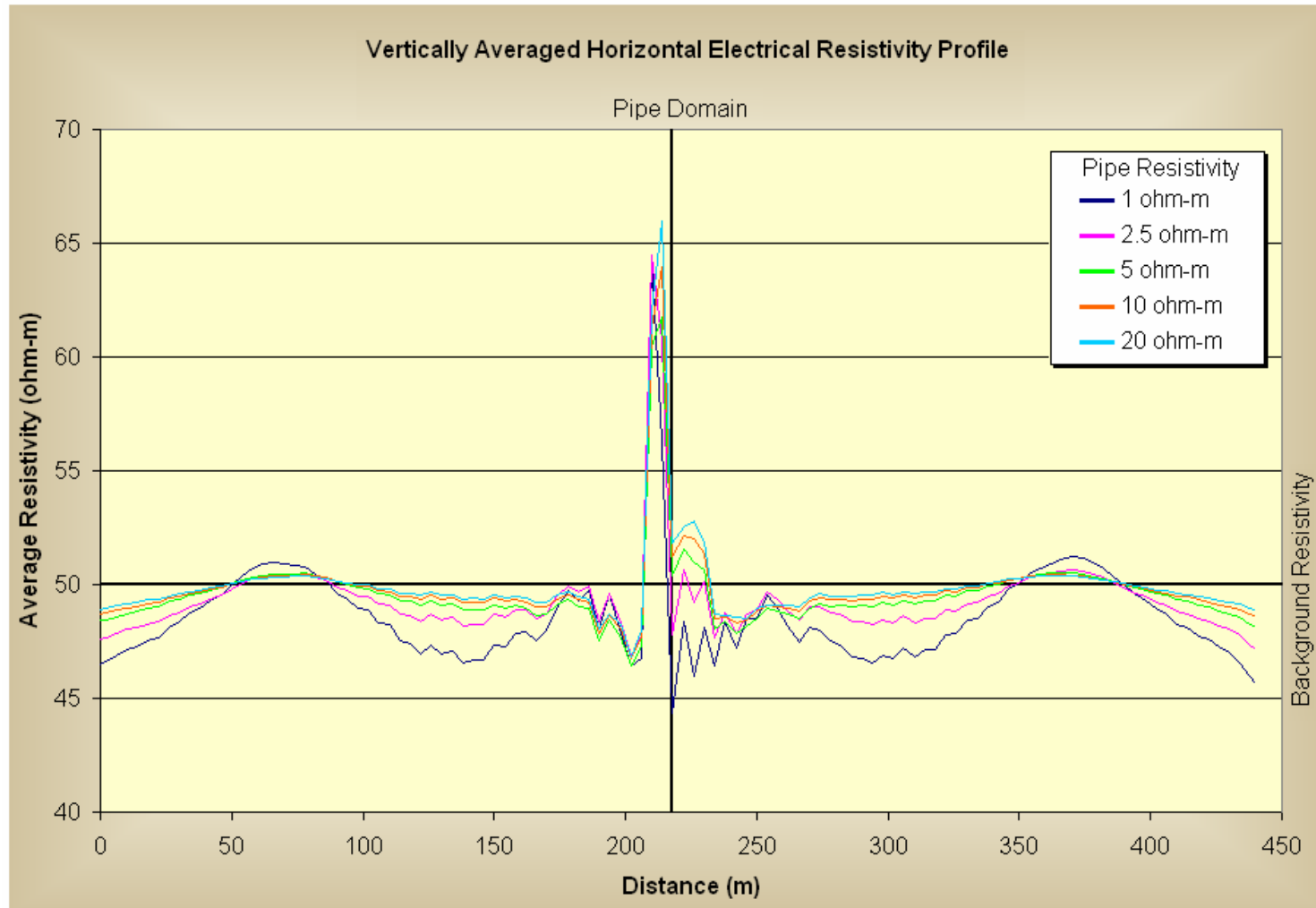
Figure A.18 Forward Electrical Resistivity Model 4 – Single Pipe with Surrounding Insulators
Background Resistivity: 100 ohm-m, Insulator Resistivity: 100000 ohm-m, Electrode Spacing: 8 m, Pipe Location: 218 m
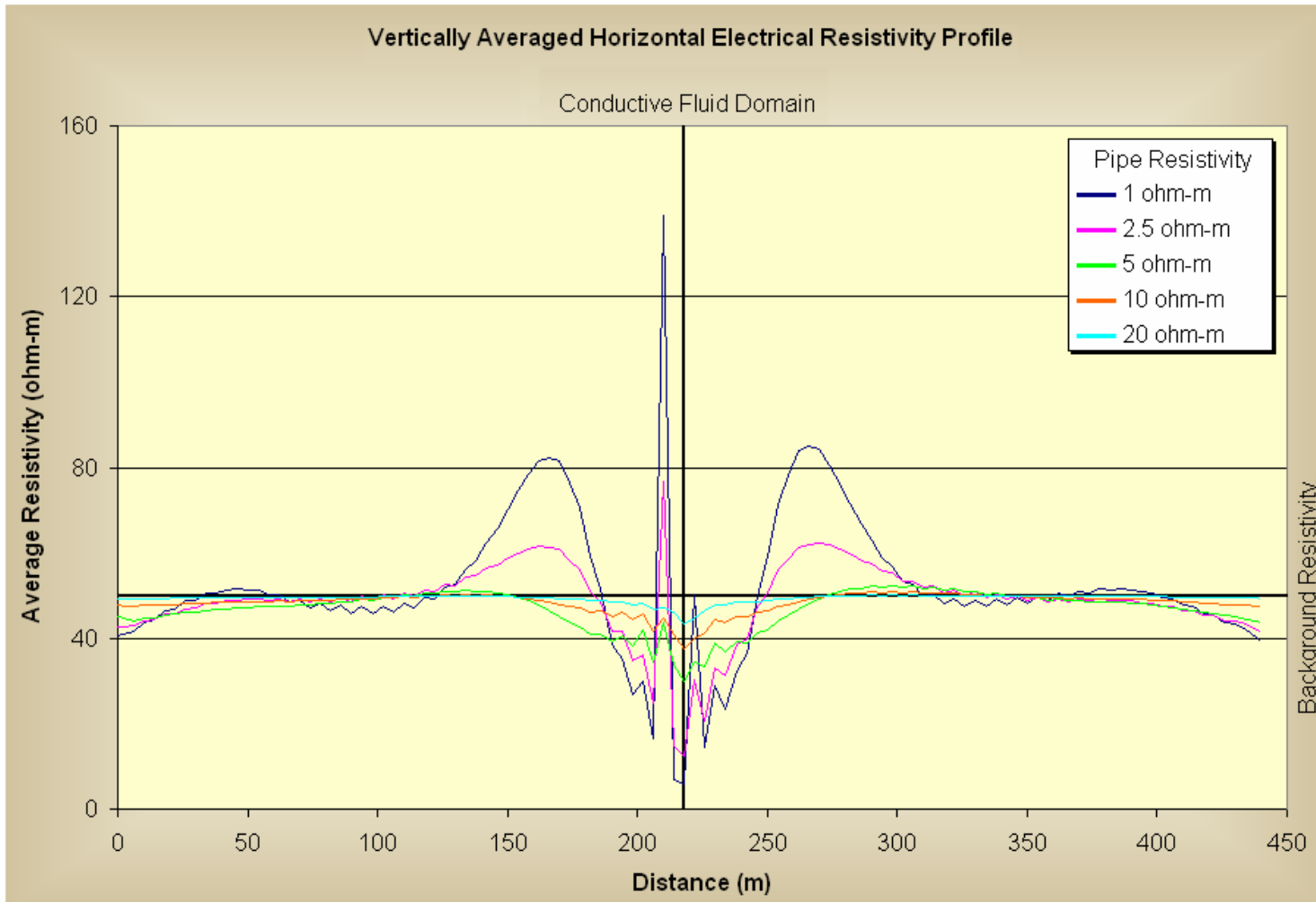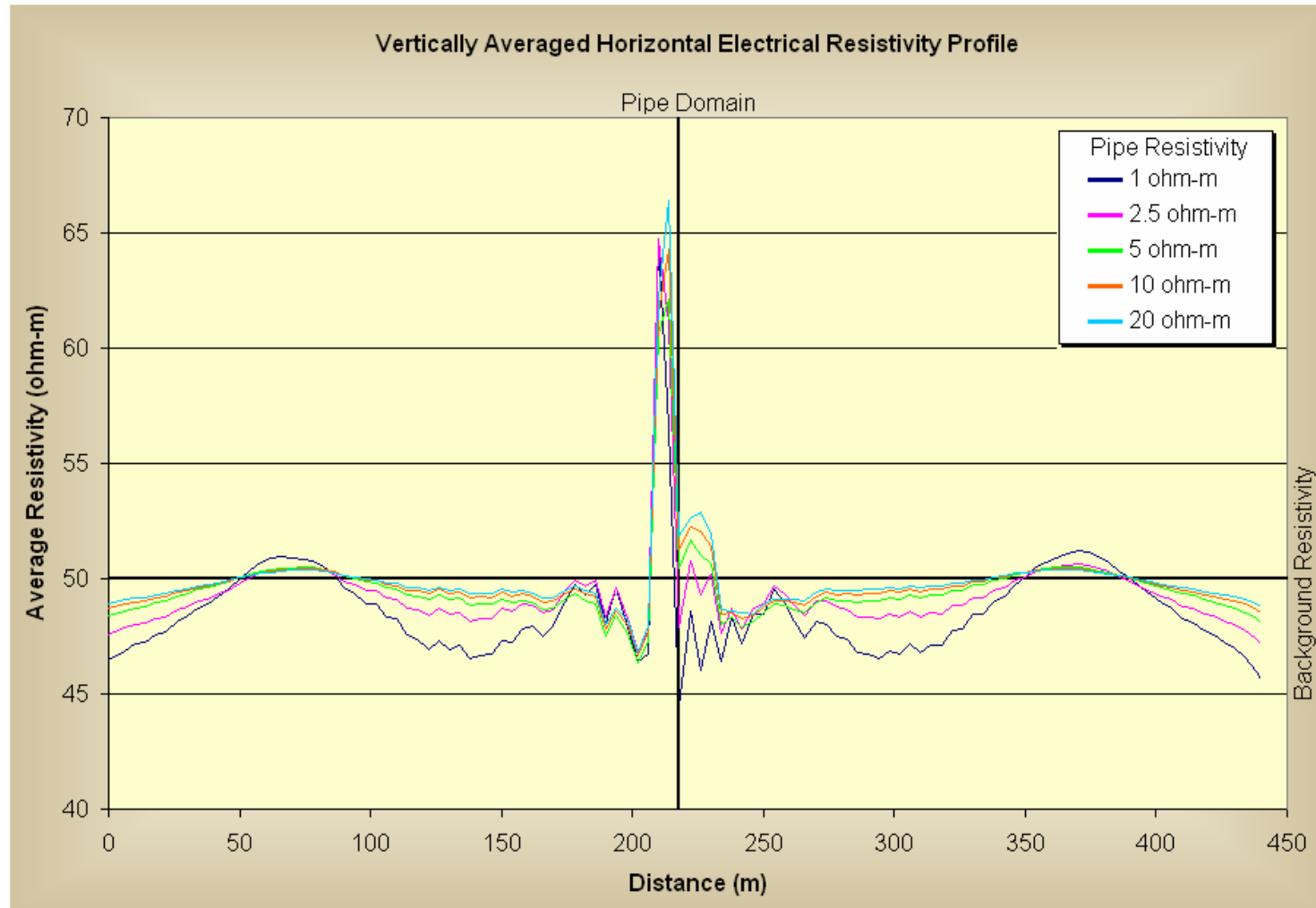
Figure A.19: Forward Electrical Resistivity Model 5 –Vertical Conductive Brine
Background Resistivity: 50 ohm-m, Electrode Spacing: 8 m, Pipe Location: 218 m
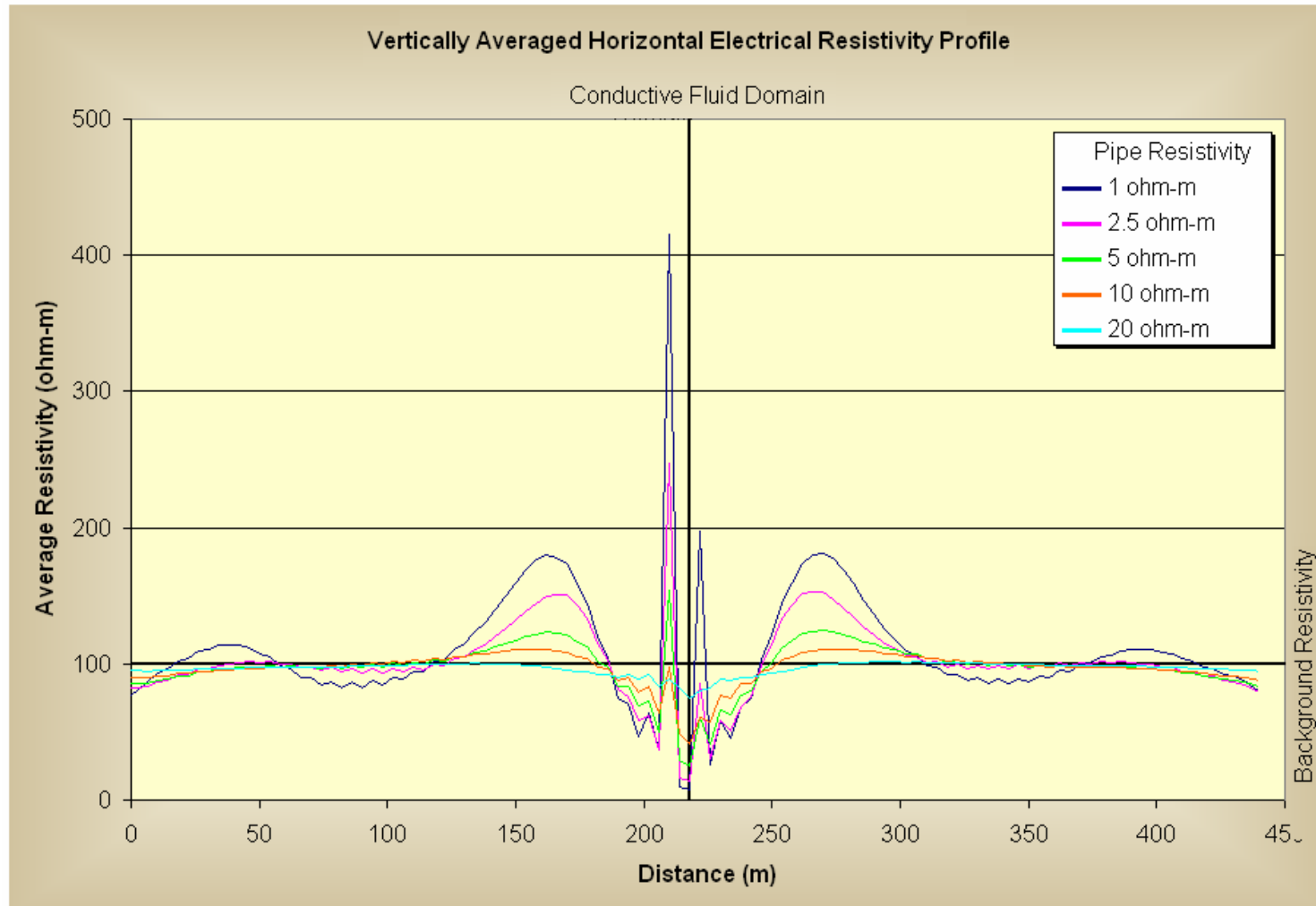
Figure A.20: Forward Electrical Resistivity Model 5 – Vertical Conductive Brine
Background Resistivity: 100 ohm-m, Electrode Spacing: 8 m, Pipe Location: 218 m
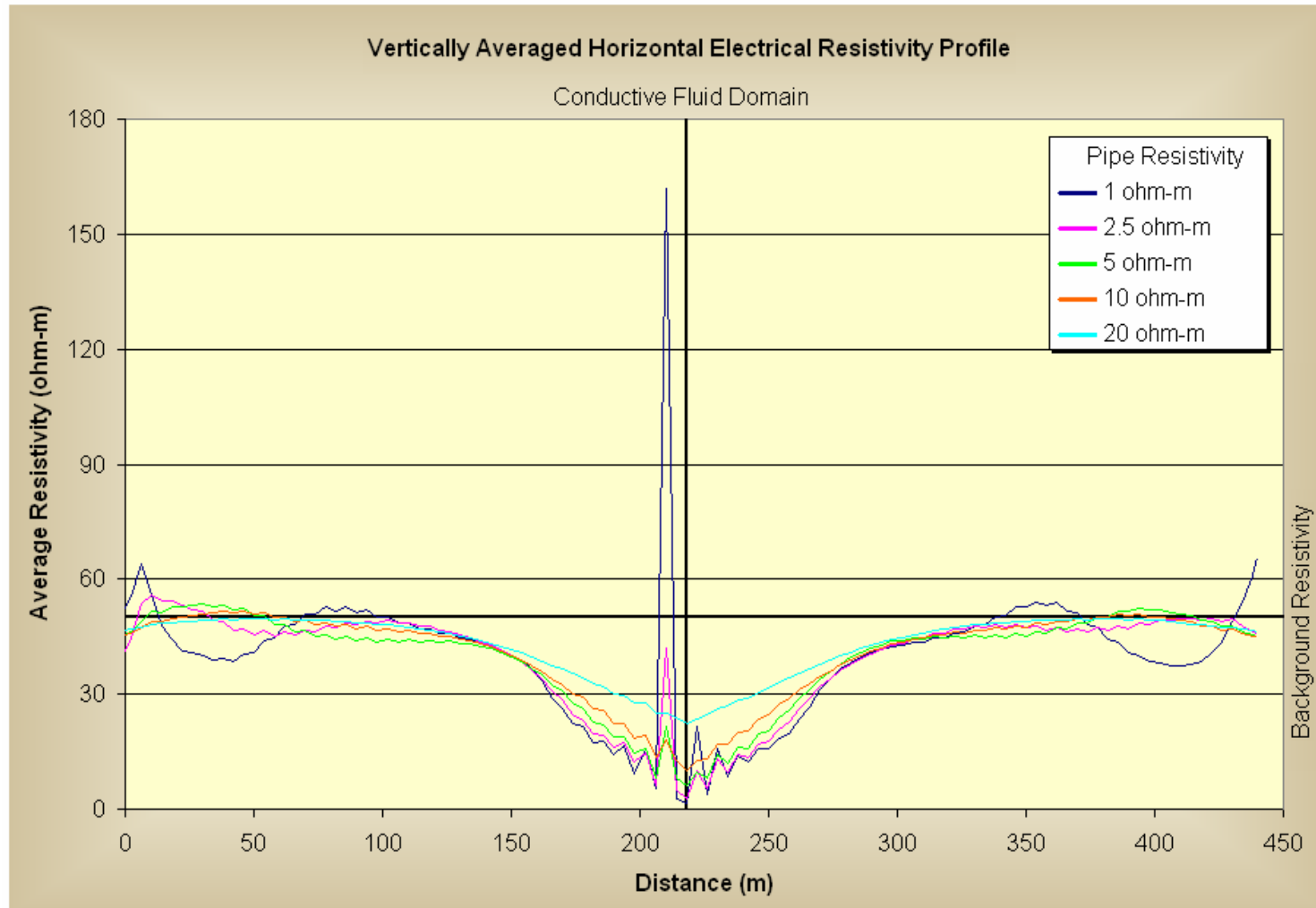
Figure A.21: Forward Electrical Resistivity Model 6 – Cone Shaped Brine
Background Resistivity: 50 ohm-m, Electrode Spacing: 8 m, Pipe Location: 218 m
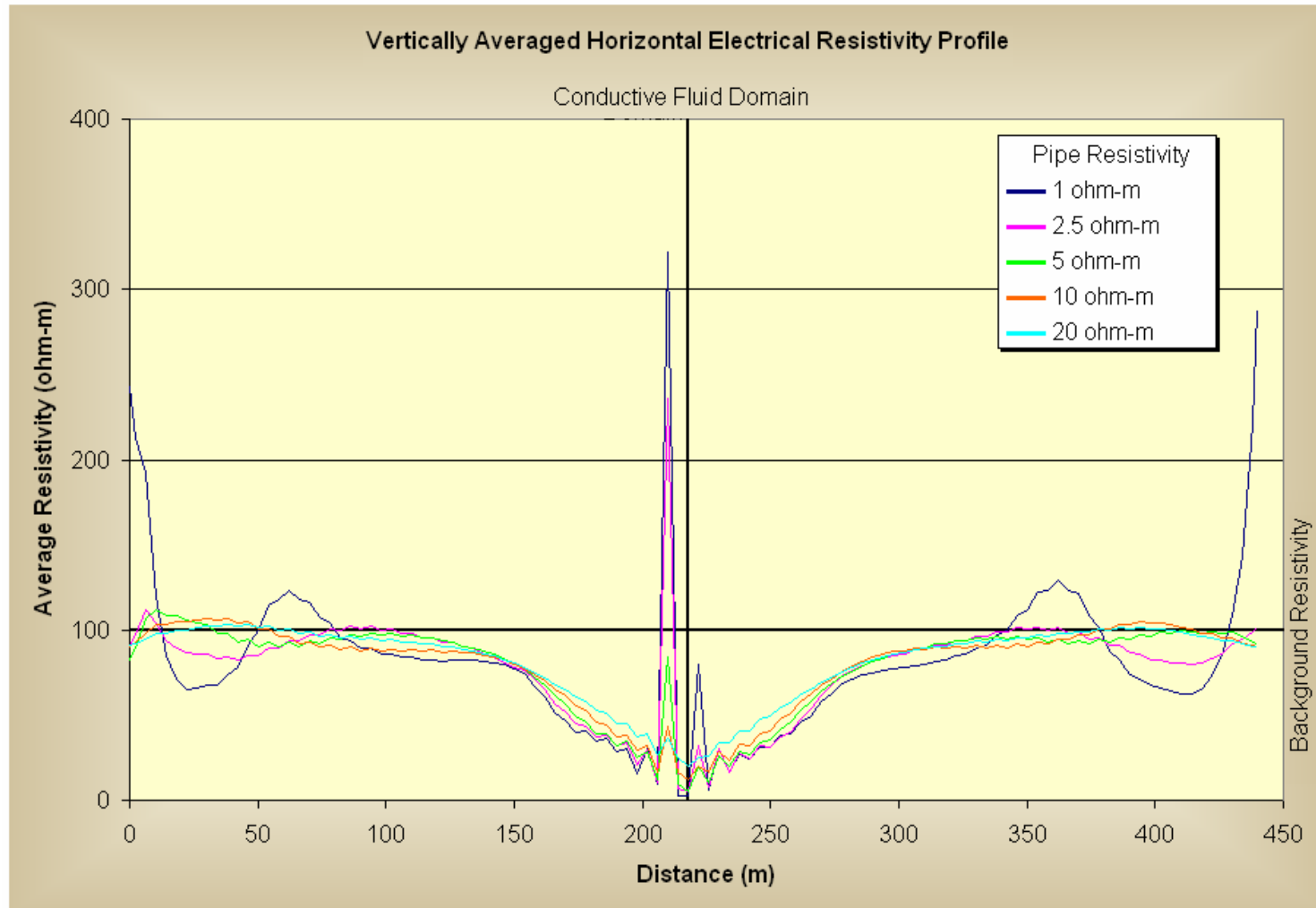
Figure A.22: Forward Electrical Resistivity Model 6 – Cone Shaped Brine
Background Resistivity: 100 ohm-m, Electrode Spacing: 8 m, Pipe Location: 218 m

Figure A.23: Forward Electrical Resistivity Model 7 – Pipe with Vertical Brine
Background Resistivity: 50 ohm-m, Electrode Spacing: 8 m, Pipe Location: 218 m

Figure A.24: Forward Electrical Resistivity Model 7 – Pipe with Vertical Brine
Background Resistivity: 100 ohm-m, Electrode Spacing: 8 m, Pipe Location: 218 m

Figure A.25: Forward Electrical Resistivity Model 8 – Pipe with Cone Shaped Brine
Background Resistivity: 50 ohm-m, Electrode Spacing: 8 m, Pipe Location: 218 m

Figure A.26: Forward Electrical Resistivity Model 6 – Pipe with Cone Shaped Brine
Background Resistivity: 100 ohm-m, Electrode Spacing: 8 m, Pipe Location: 218 m

APPENDIX B

Vertically Averaged Horizontal Electrical Resistivity Profiles for Forward Model
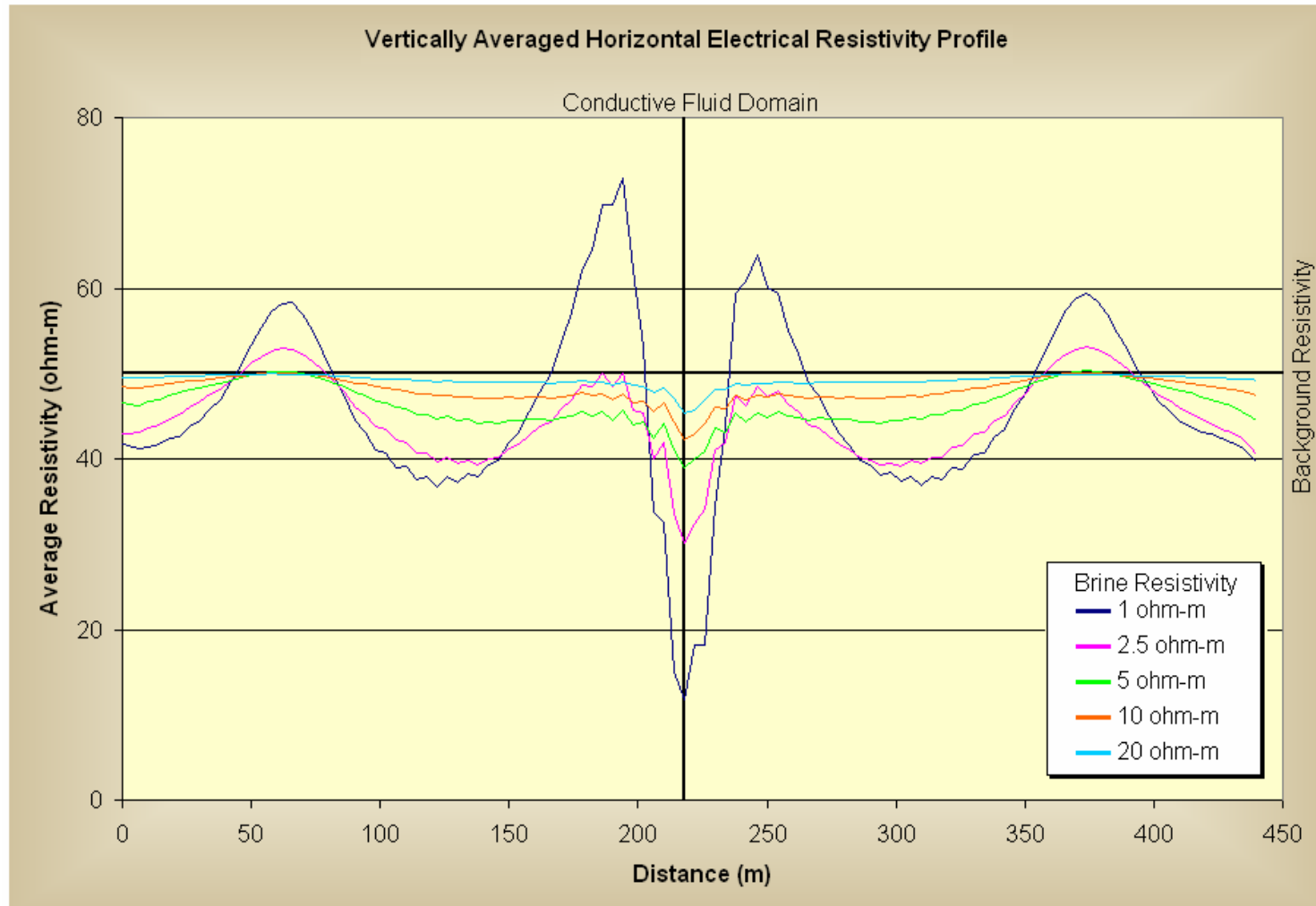1 to 8 with the Wenner Method

Figure B.1: Forward Electrical Resistivity Model 1 – Single Pipe
Background Resistivity: 50 ohm-m, Electrode Spacing: 5 m, Pipe Location: 218 m
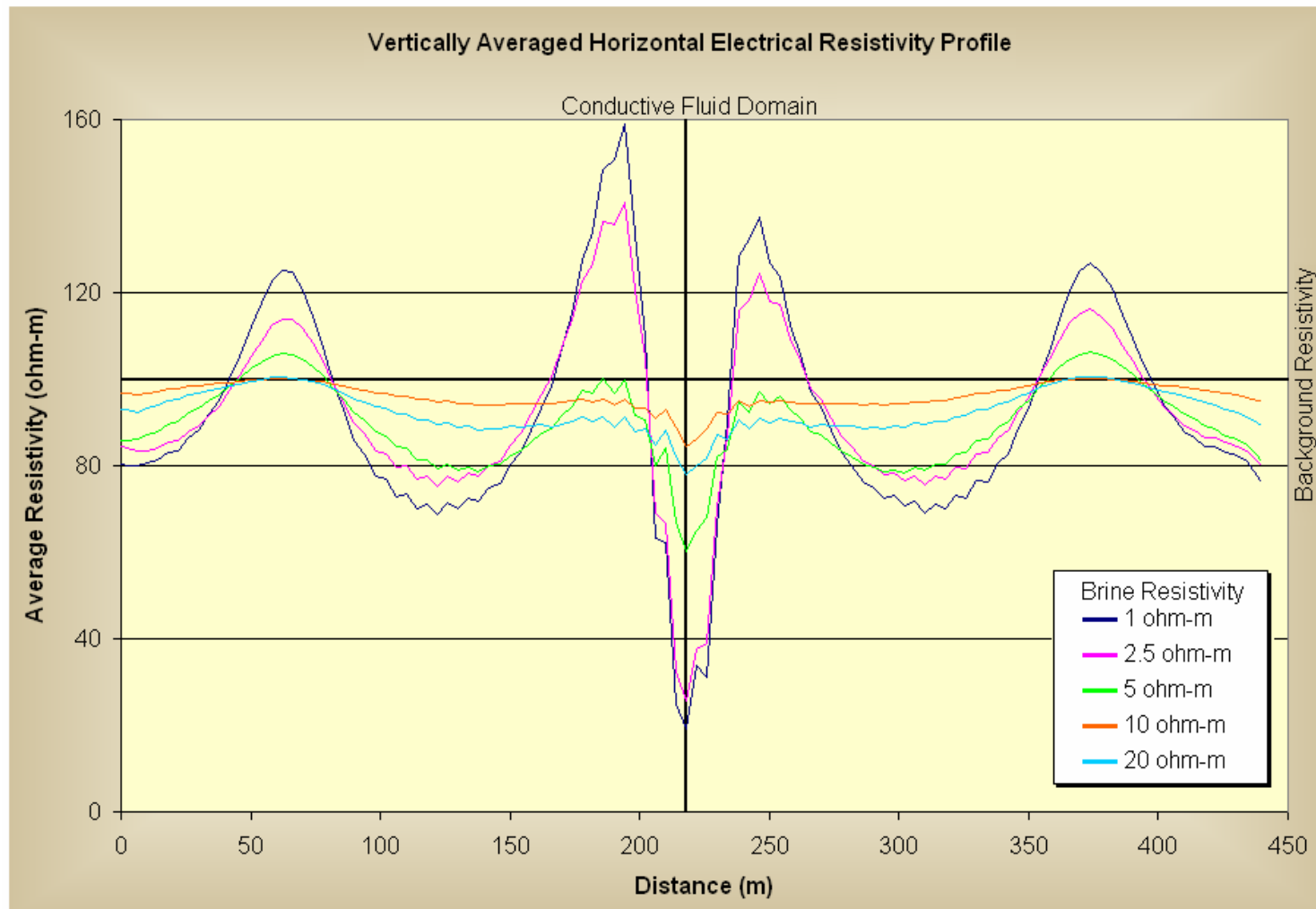
Figure B.2: Forward Electrical Resistivity Model 1 – Single Pipe
Background Resistivity: 100 ohm-m, Electrode Spacing: 5 m, Pipe Location: 218 m

Figure B.3: Forward Electrical Resistivity Model 1 – Single Pipe
Background Resistivity: 50 ohm-m, Electrode Spacing: 8 m, Pipe Location: 218 m

Figure B.4: Forward Electrical Resistivity Model 1 – Single Pipe
Background Resistivity: 100 ohm-m, Electrode Spacing: 8 m, Pipe Location: 218 m
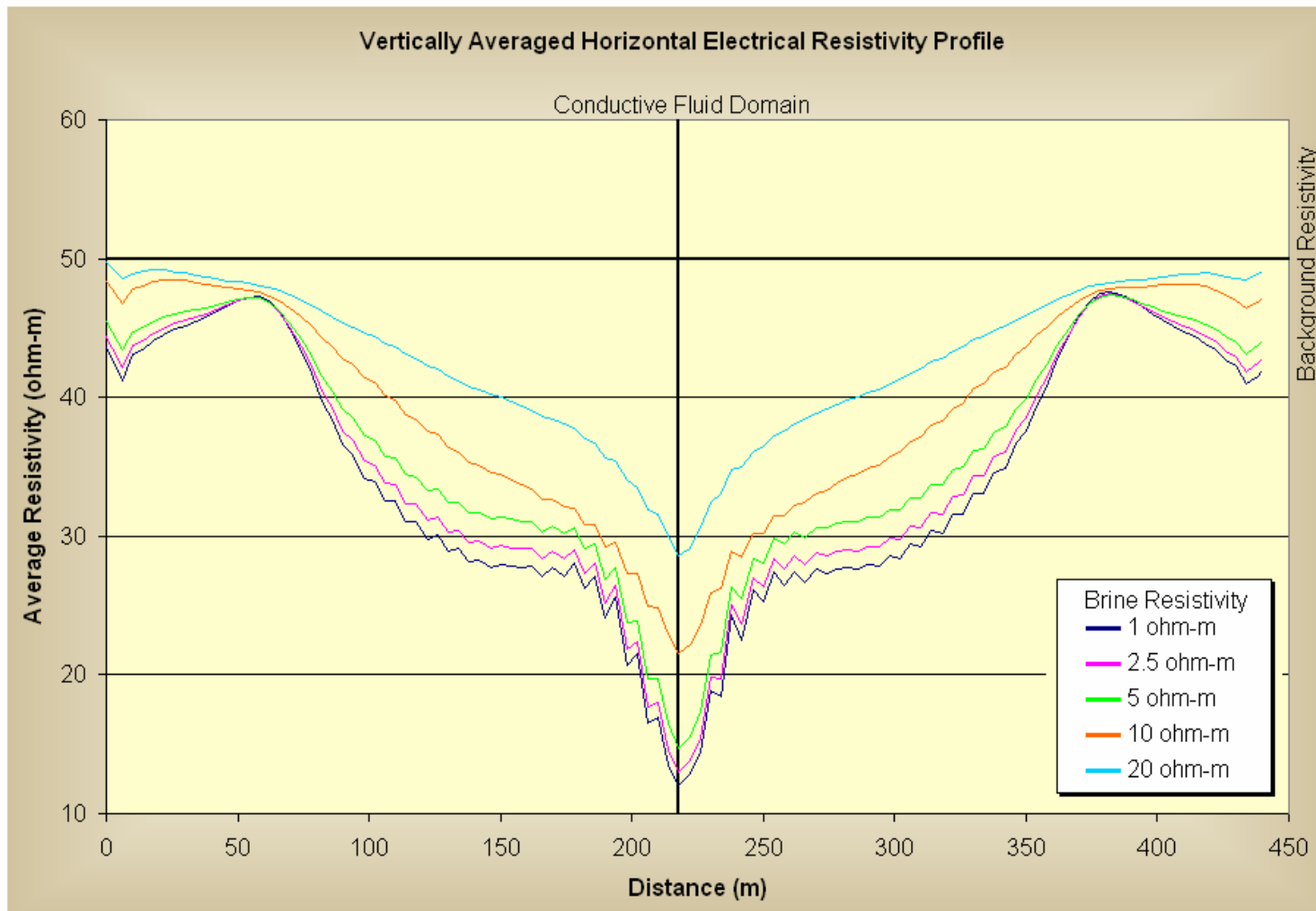
Figure B.5: Forward Electrical Resistivity Model 1 – Single Pipe
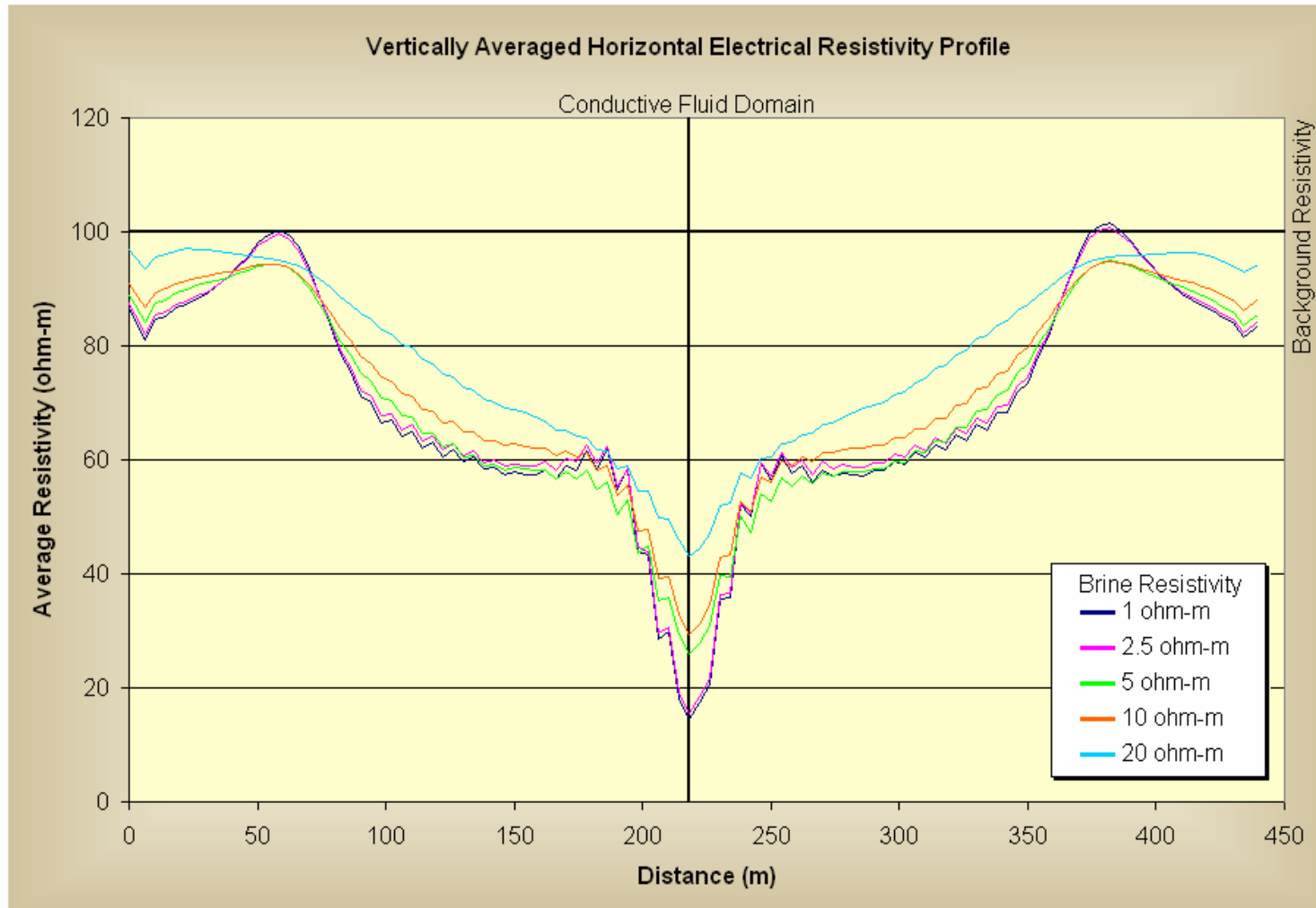Background Resistivity: 50 ohm-m, Electrode Spacing: 8 m, Pipe Location: 222 m

Figure B.6: Forward Electrical Resistivity Model 1 – Single Pipe
Background Resistivity: 100 ohm-m, Electrode Spacing: 8 m, Pipe Location: 222 m

Figure B.7: Forward Electrical Resistivity Model 1 – Single Pipe
Background Resistivity: 50 ohm-m, Electrode Spacing: 10 m, Pipe Location: 218 m

Figure B.8: Forward Electrical Resistivity Model 1 – Single Pipe
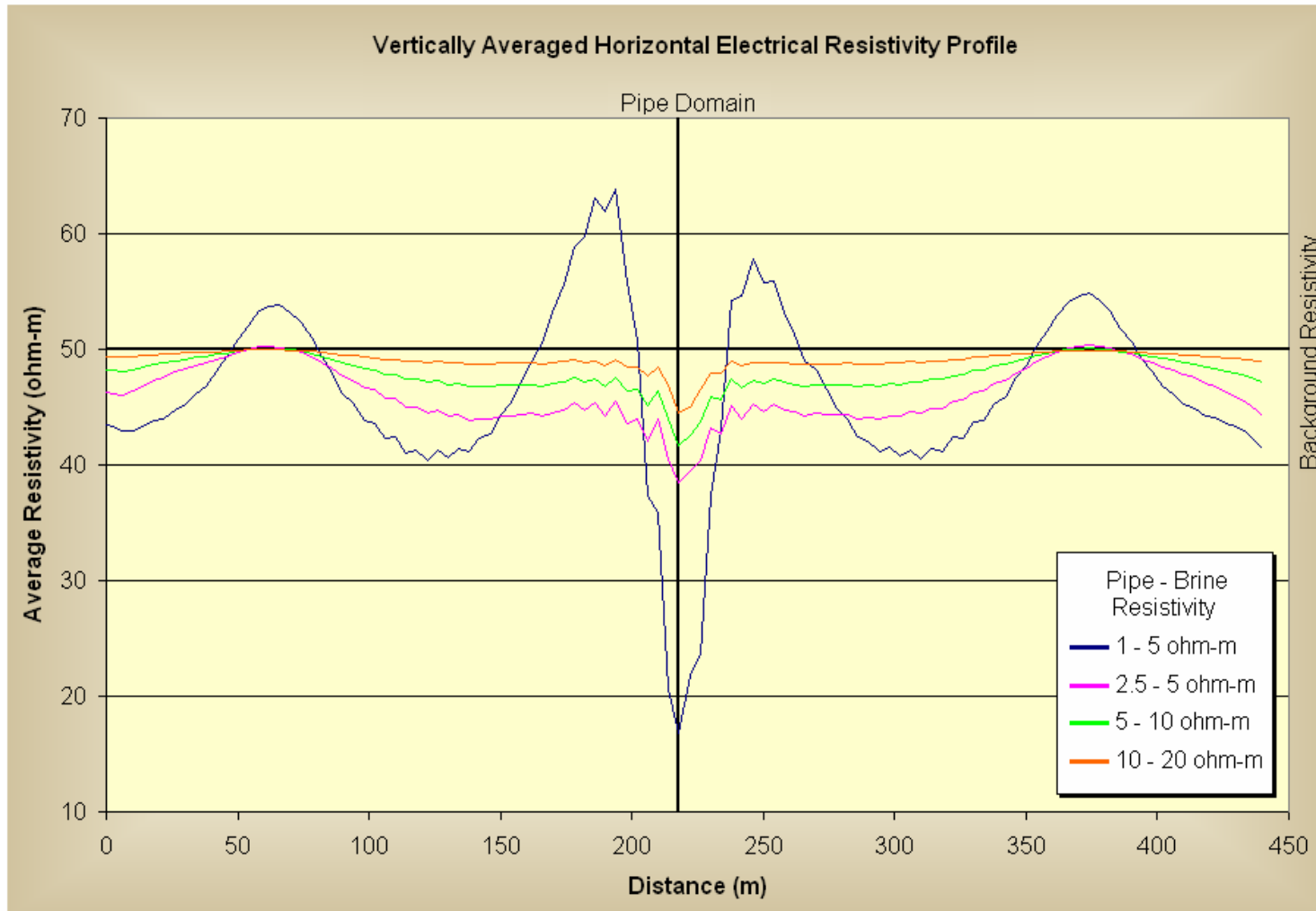Background Resistivity: 100 ohm-m, Electrode Spacing: 10 m, Pipe Location: 218 m

Figure B.9: Forward Electrical Resistivity Model 2 – Single Pipe at Small Angle
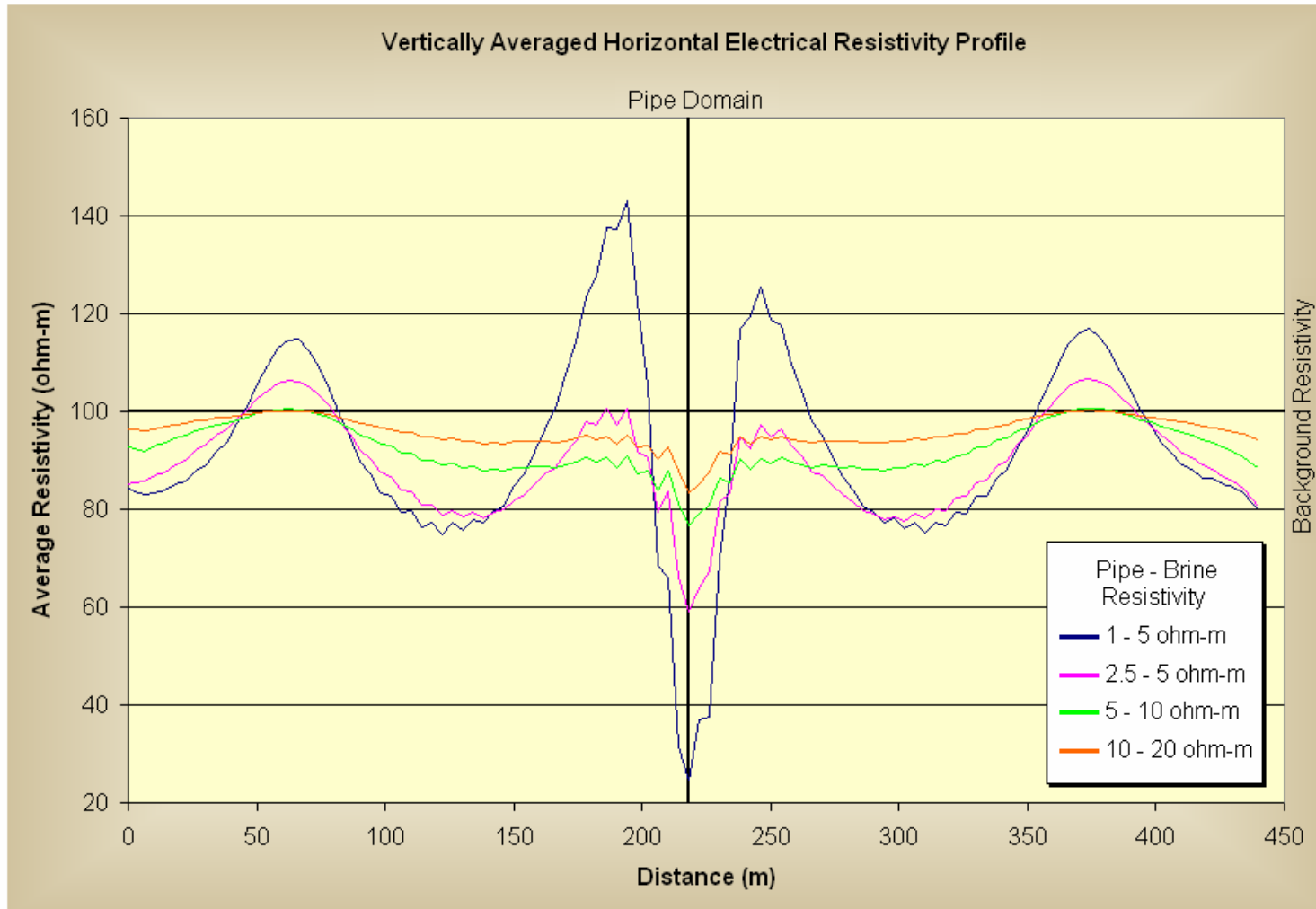Background Resistivity: 50 ohm-m, Electrode Spacing: 8 m, Pipe Location: 218 m

Figure B.10: Forward Electrical Resistivity Model 2 – Single Pipe Single Pipe at Small Angle
Background Resistivity: 100 ohm-m, Electrode Spacing: 8 m, Pipe Location: 218 m

Figure B.11: Forward Electrical Resistivity Model 3 – Single Pipe at Low Angle
Background Resistivity: 50 ohm-m, Electrode Spacing: 8 m, Pipe Location: 218 m

Figure B.12: Forward Electrical Resistivity Model 3 – Single Pipe at Lower Angle
Background Resistivity: 100 ohm-m, Electrode Spacing: 8 m, Pipe Location: 218 m
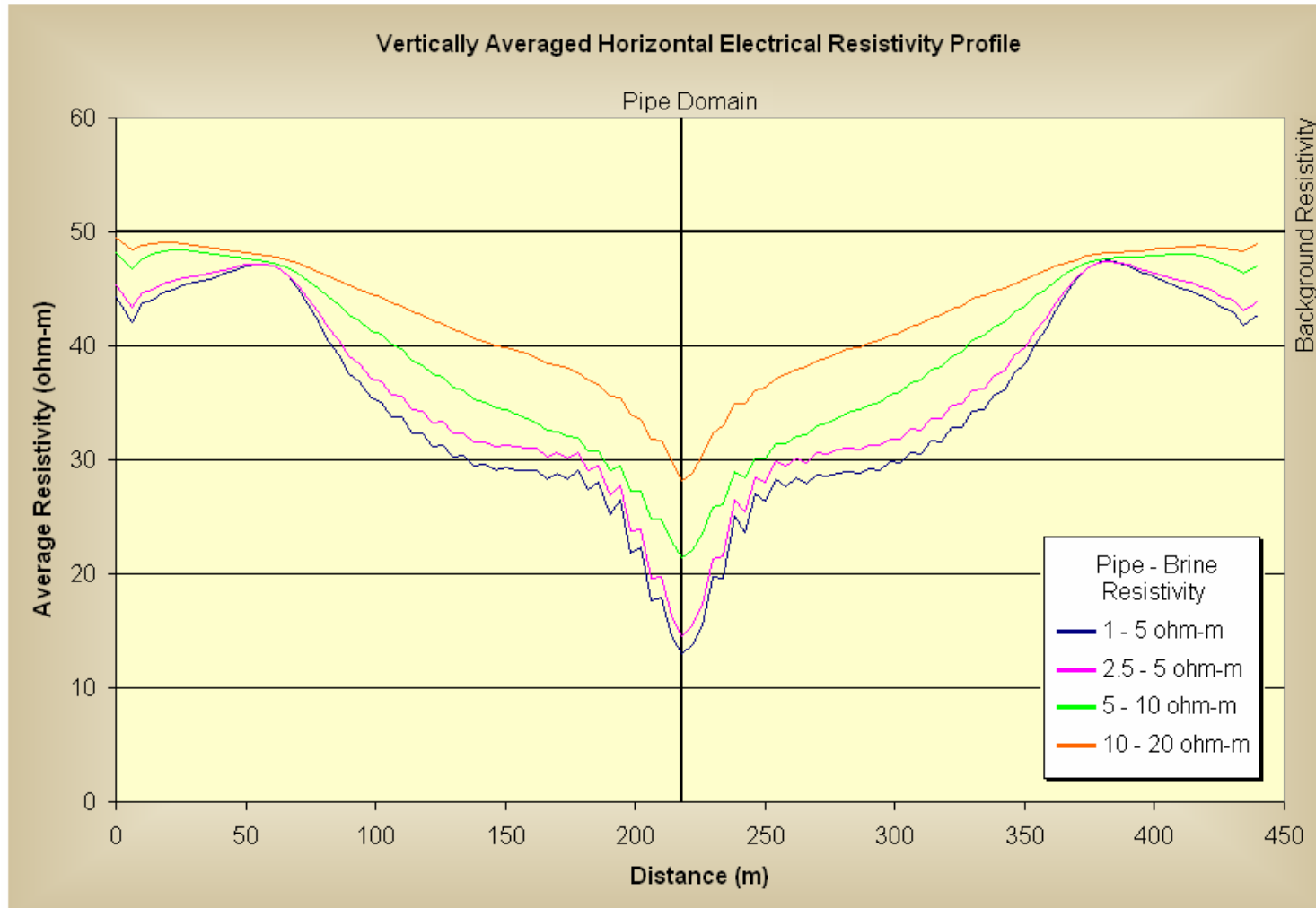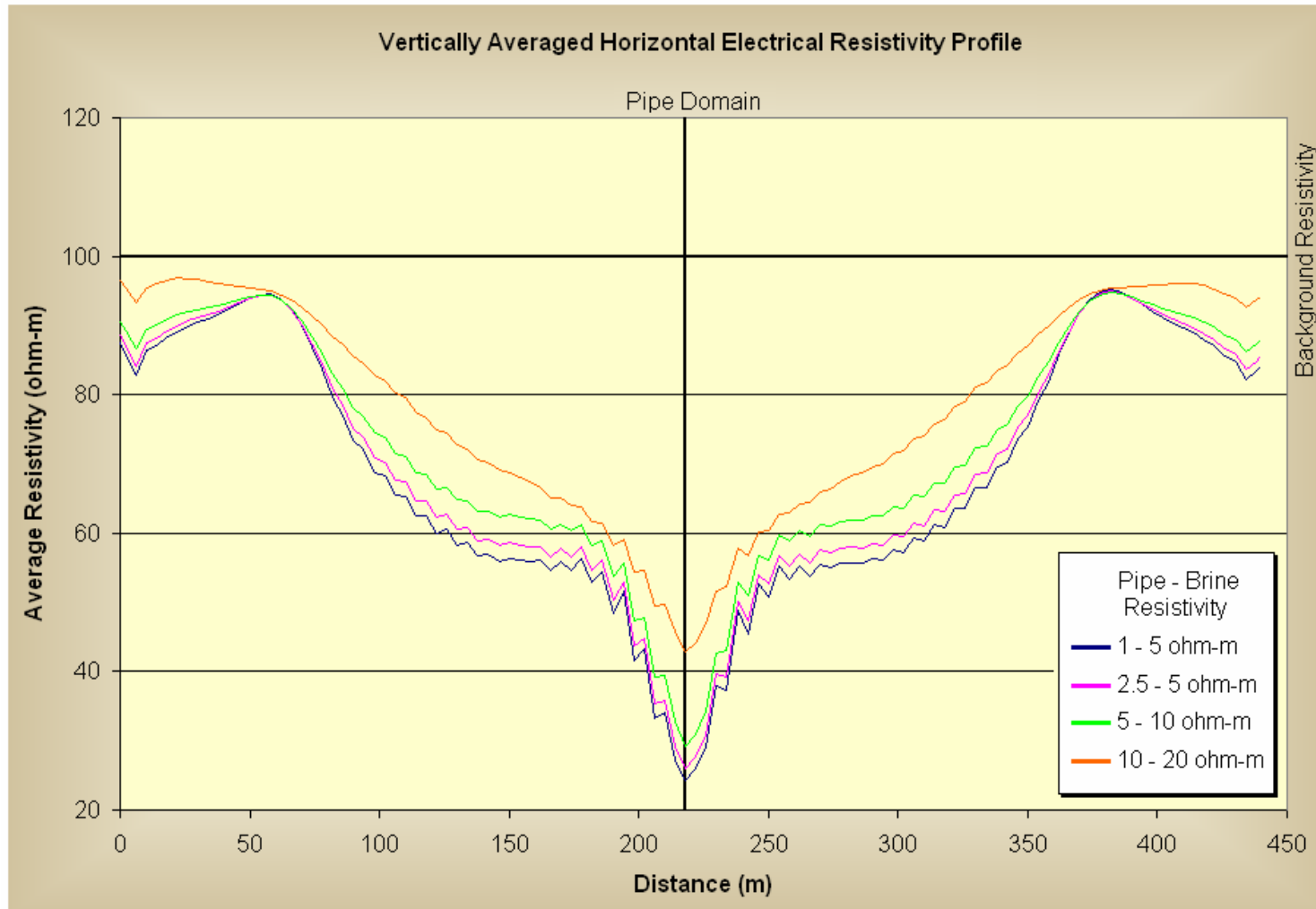
Figure B.13 Forward Electrical Resistivity Model 4 – Single Pipe with Surrounding Insulators
Background Resistivity: 50 ohm-m, Insulator Resistivity: 500 ohm-m, Electrode Spacing: 8 m, Pipe Location: 218 m

Figure B.14 Forward Electrical Resistivity Model 4 – Single Pipe Single Pipe with Surrounding Insulators
Background Resistivity: 50 ohm-m, Insulator Resistivity: 5000 ohm-m, Electrode Spacing: 8 m, Pipe Location: 218 m

Figure B.15 Forward Electrical Resistivity Model 4 – Single Pipe Single Pipe with Surrounding Insulators
Background Resistivity: 50 ohm-m, Insulator Resistivity: 50000 ohm-m, Electrode Spacing: 8 m, Pipe Location: 218 m
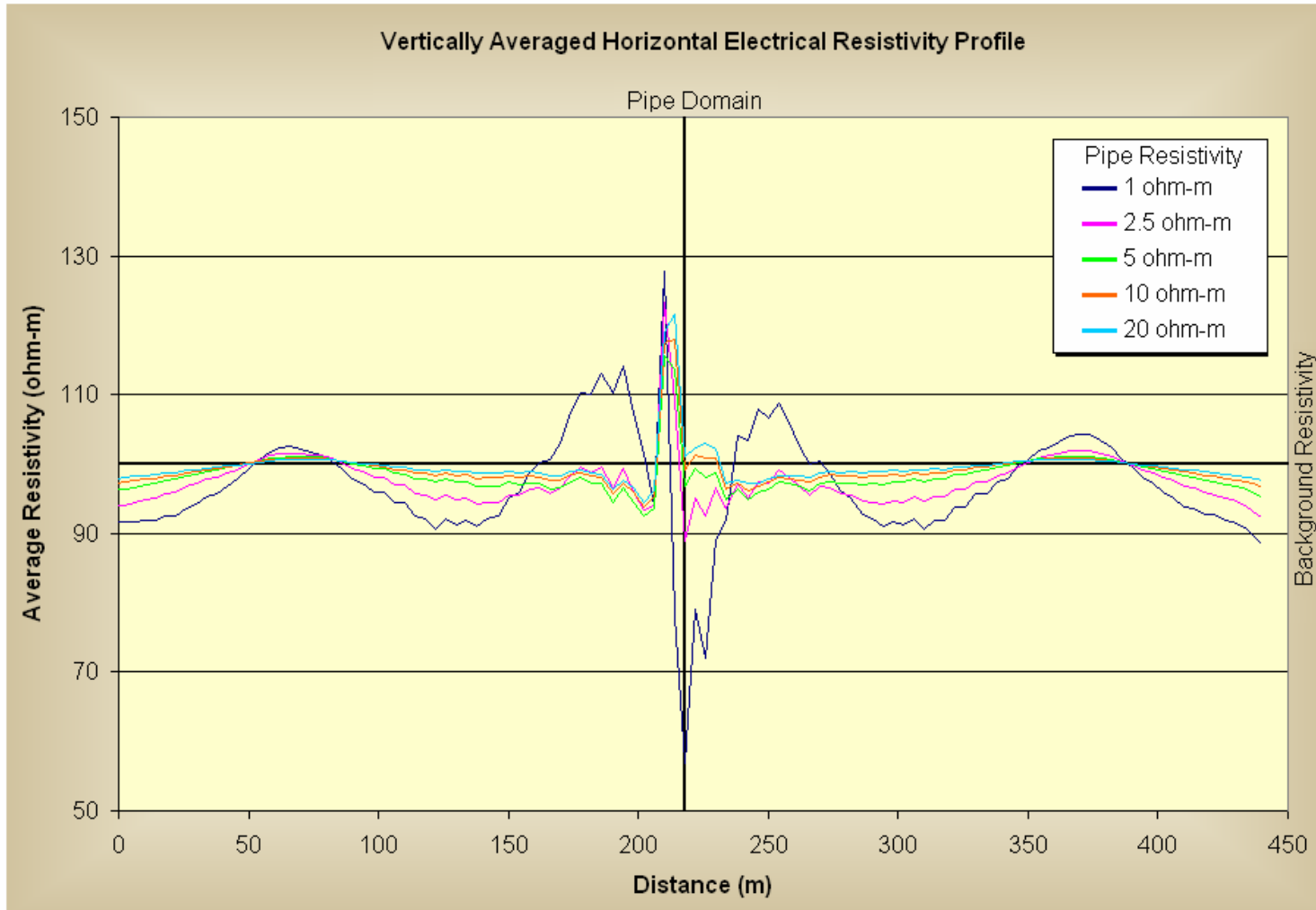
Figure B.16 Forward Electrical Resistivity Model 4 – Single Pipe Single Pipe with Surrounding Insulators
Background Resistivity: 100 ohm-m, Insulator Resistivity: 1000 ohm-m, Electrode Spacing: 8 m, Pipe Location: 218 m
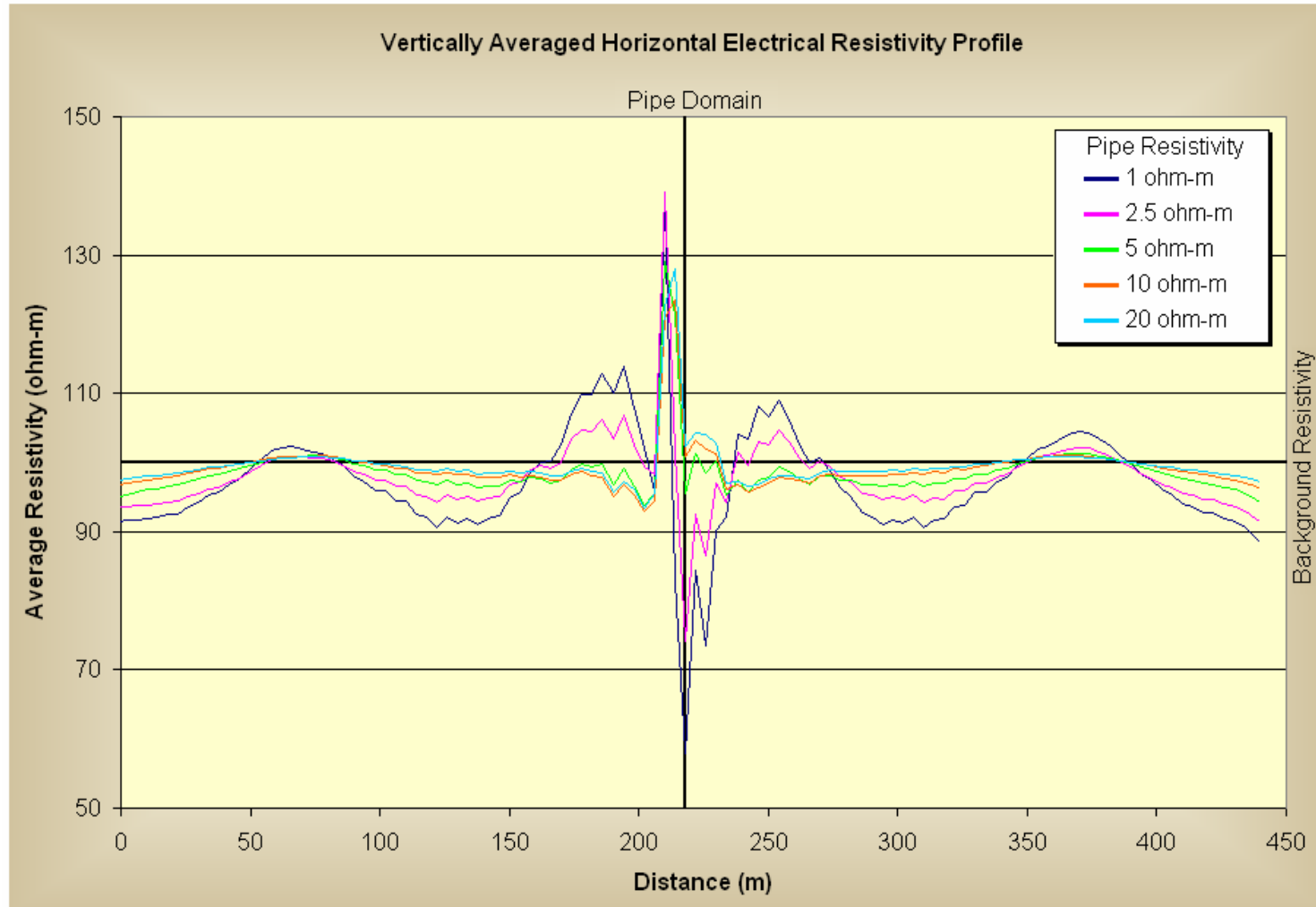
Figure B.17 Forward Electrical Resistivity Model 4 – Single Pipe Single Pipe with Surrounding Insulators
Background Resistivity: 100 ohm-m, Insulator Resistivity: 10000 ohm-m, Electrode Spacing: 8 m, Pipe Location: 218 m
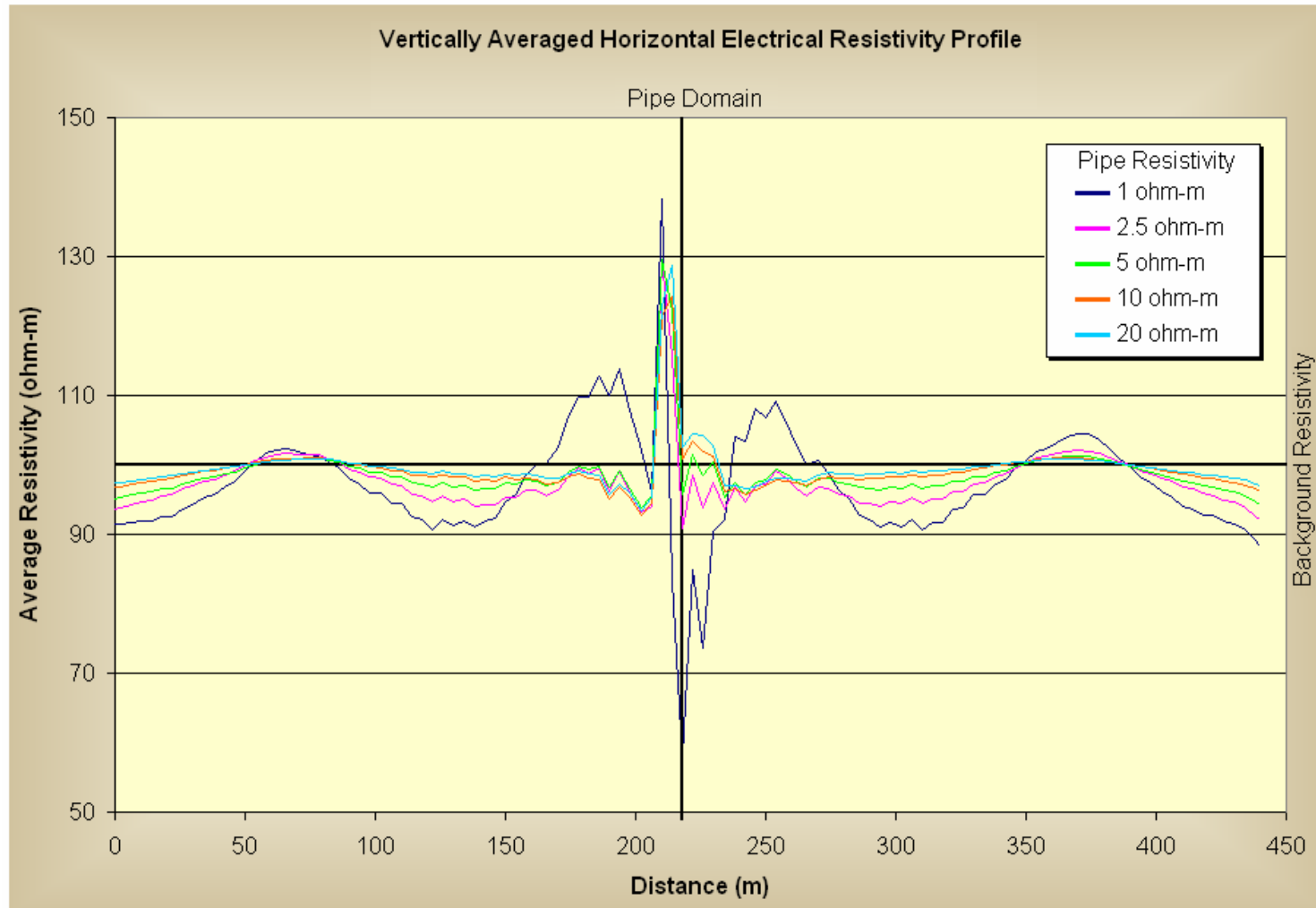
Figure B.18 Forward Electrical Resistivity Model 4 – Single Pipe Single Pipe with Surrounding Insulators
Background Resistivity: 100 ohm-m, Insulator Resistivity: 100000 ohm-m, Electrode Spacing: 8 m, Pipe Location: 218 m

Figure B.19: Forward Electrical Resistivity Model 5 – Vertical Brine
Background Resistivity: 50 ohm-m, Electrode Spacing: 8 m, Pipe Location: 218 m

Figure B.20: Forward Electrical Resistivity Model 5 – Vertical Brine
Background Resistivity: 100 ohm-m, Electrode Spacing: 8 m, Pipe Location: 218 m

Figure B.21: Forward Electrical Resistivity Model 6 – Cone Shaped Brine
Background Resistivity: 50 ohm-m, Electrode Spacing: 8 m, Pipe Location: 218 m

Figure B.22: Forward Electrical Resistivity Model 6 – Cone Shaped Brine
Background Resistivity: 100 ohm-m, Electrode Spacing: 8 m, Pipe Location: 218 m

Figure B.23: Forward Electrical Resistivity Model 7 – Pipe with Vertical Brine
Background Resistivity: 50 ohm-m, Electrode Spacing: 8 m, Pipe Location: 218 m

Figure B.24: Forward Electrical Resistivity Model 7 – Pipe with Vertical Brine
Background Resistivity: 100 ohm-m, Electrode Spacing: 8 m, Pipe Location: 218 m

Figure B.25: Forward Electrical Resistivity Model 8 – Pipe with Cone Shaped Brine
Background Resistivity: 50 ohm-m, Electrode Spacing: 8 m, Pipe Location: 218 m

Figure B.26: Forward Electrical Resistivity Model 8 – Pipe with Cone Shape Brine
Background Resistivity: 100 ohm-m, Electrode Spacing: 8 m, Pipe Location: 218 m

163

APPENDIX C

Horizontal Electrical Resistivity *A-priori* Inversion Model with the Halihan/Fenstemaker
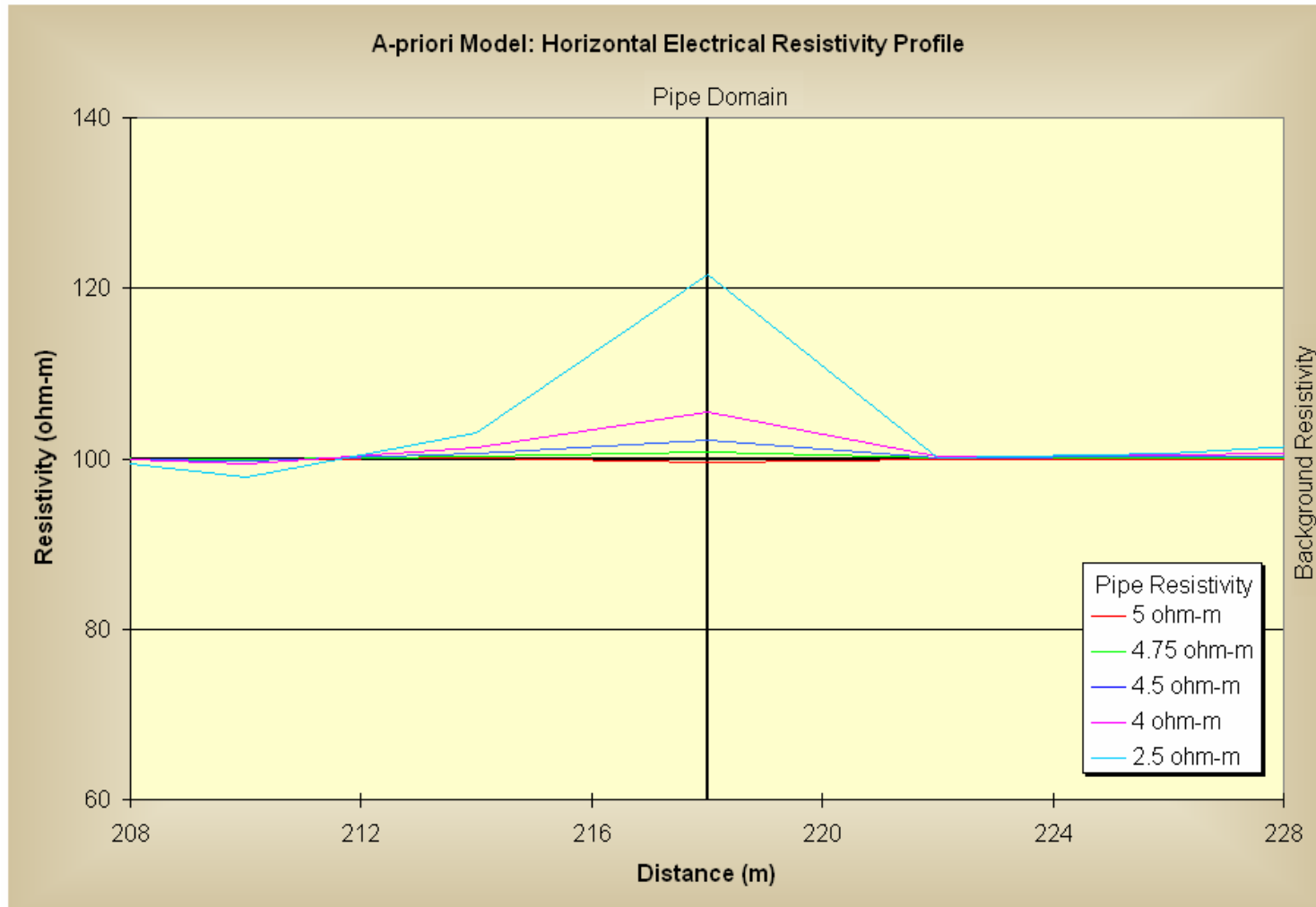Method
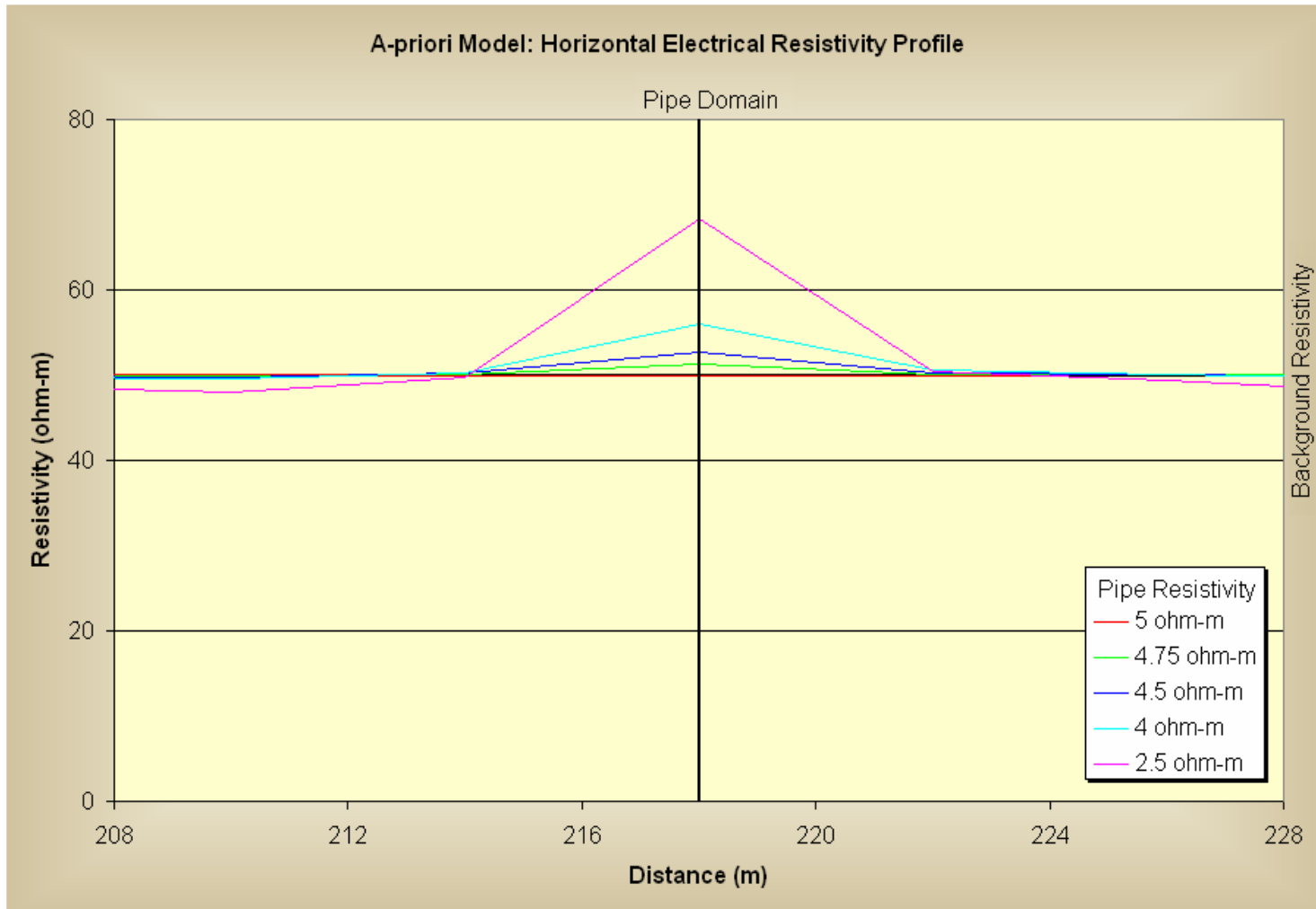
Figure C.1: Horizontal Electrical Resistivity Invert *a-priori* Inversion Model – Lower Resistivity
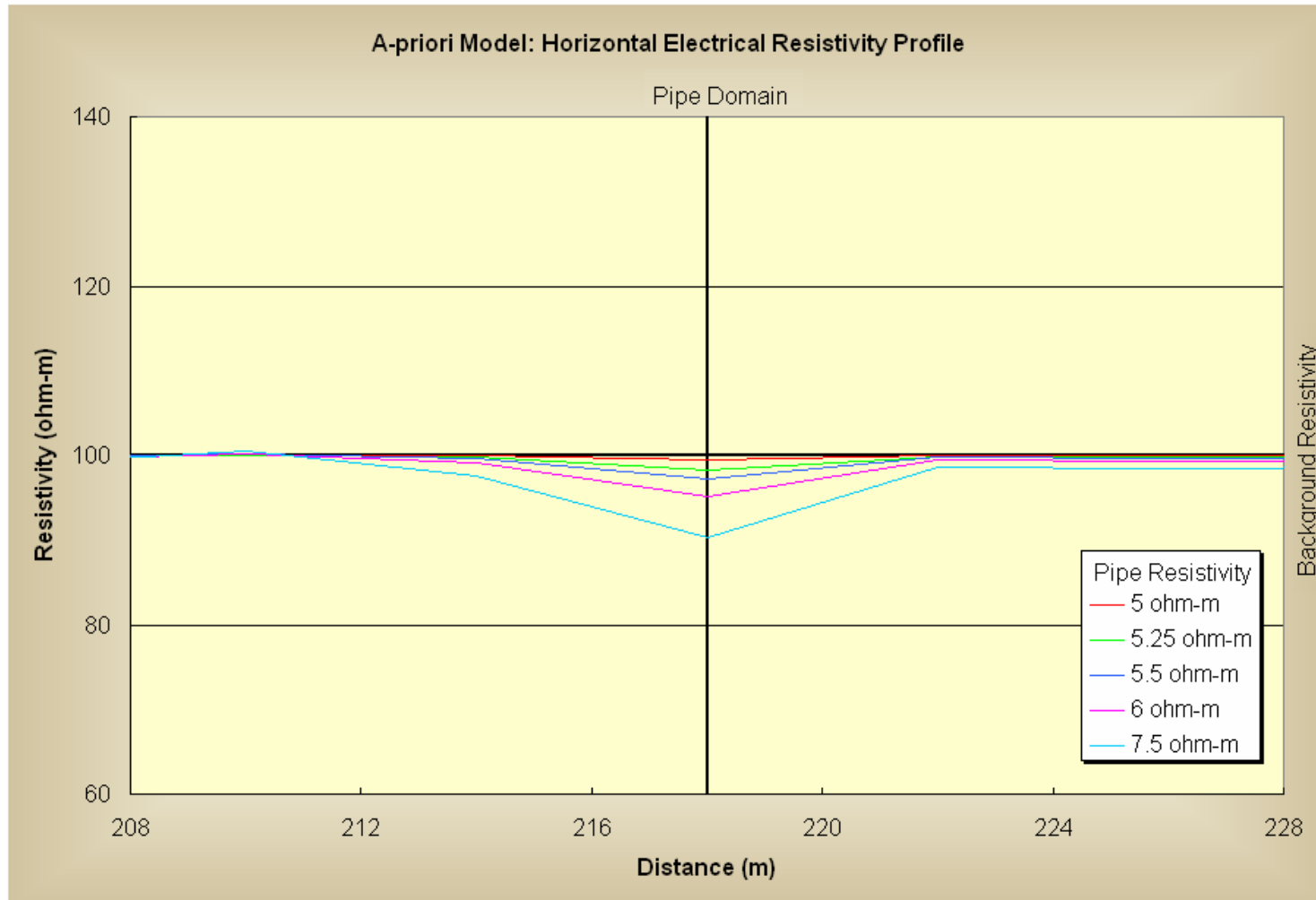Background Resistivity: 50 ohm-m, Electrode Spacing: 8 m, Pipe Location: 218 m
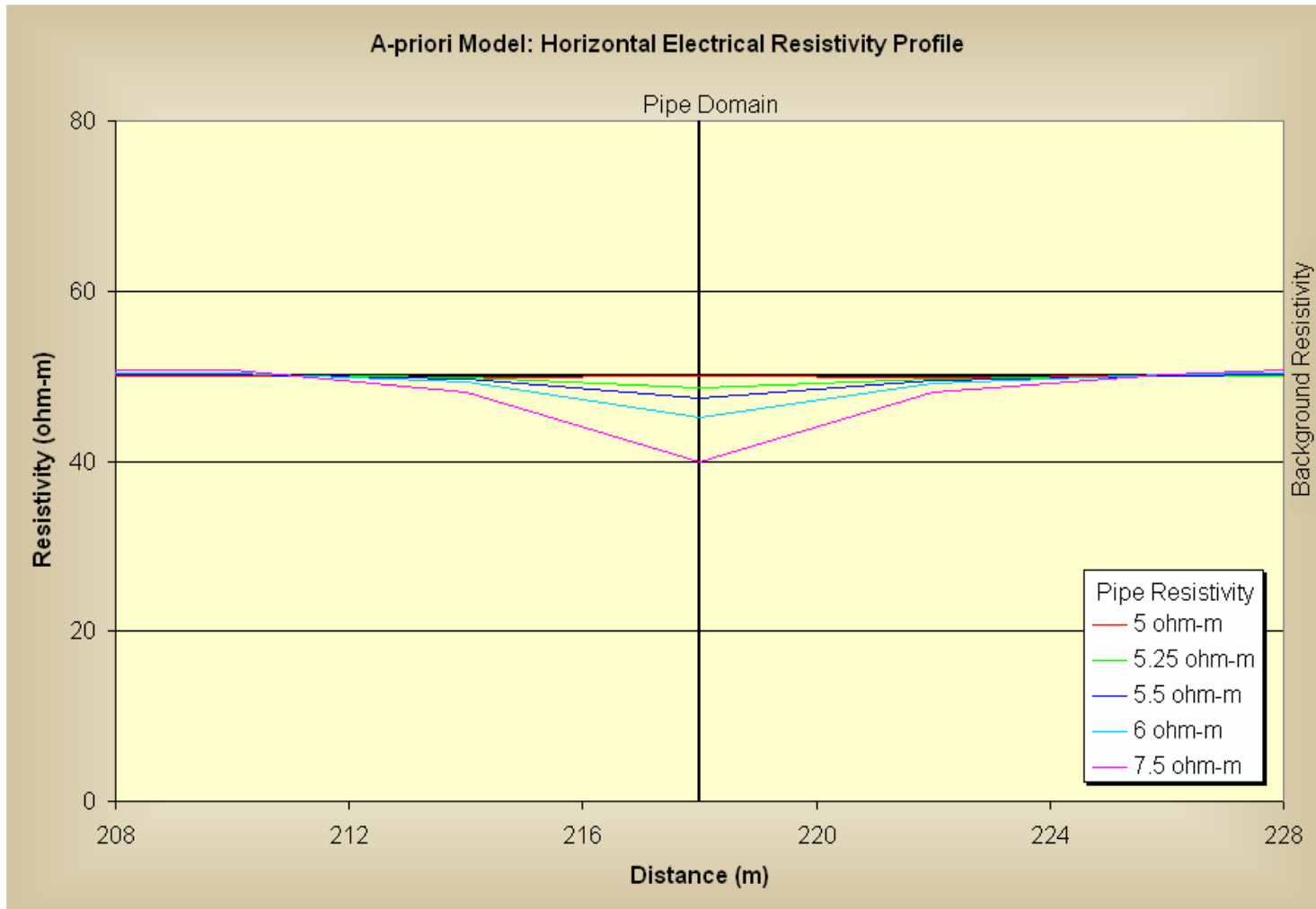
Figure C.2: Horizontal Electrical Resistivity Invert *a-priori* Inversion Model – Higher Resistivity
Background Resistivity: 50 ohm-m, Electrode Spacing: 8 m, Pipe Location: 218 m
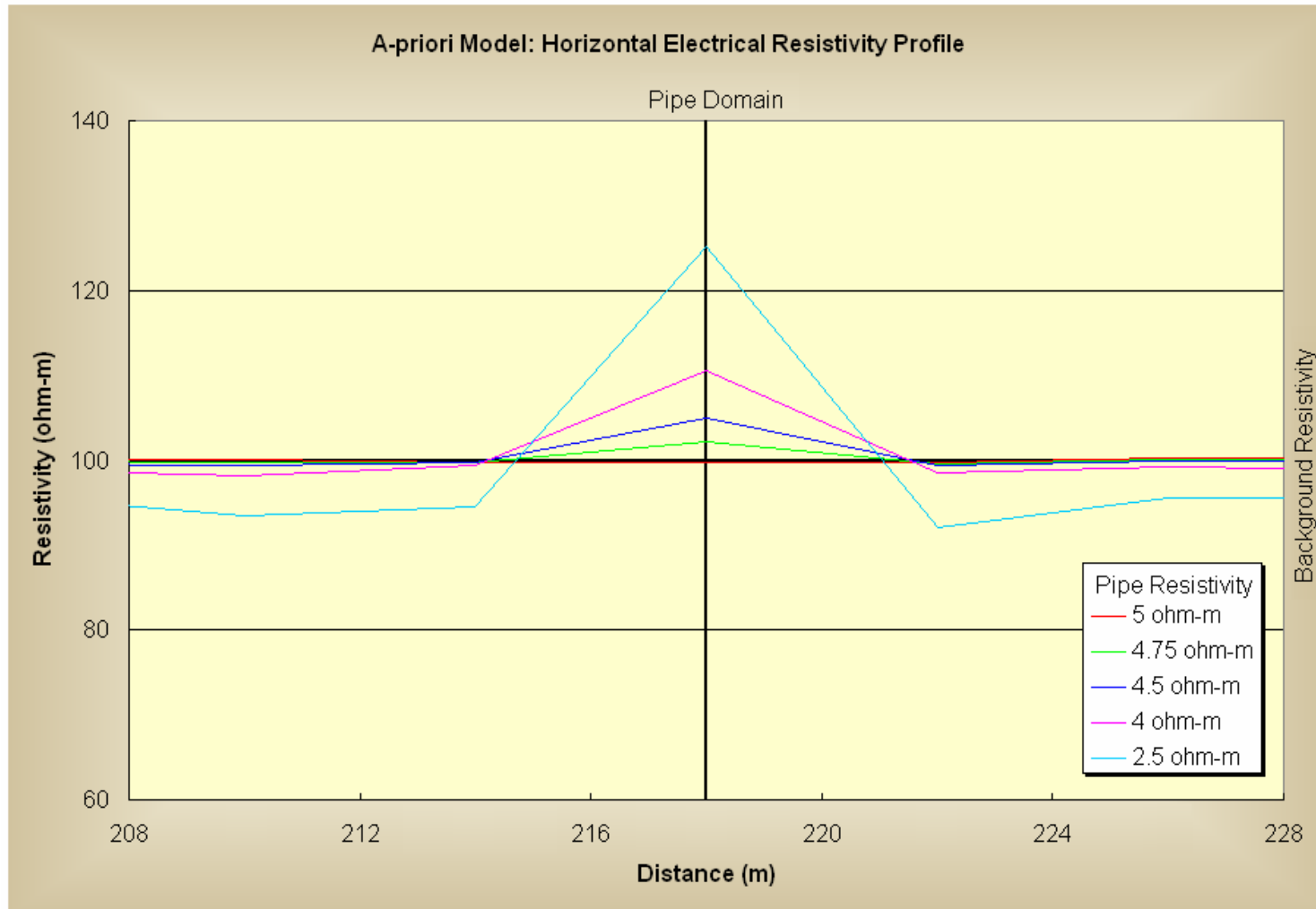
Figure C.3: Horizontal Electrical Resistivity Invert *a-priori* Inversion Model – Lower Resistivity
Background Resistivity: 100 ohm-m, Electrode Spacing: 8 m, Pipe Location: 218 m
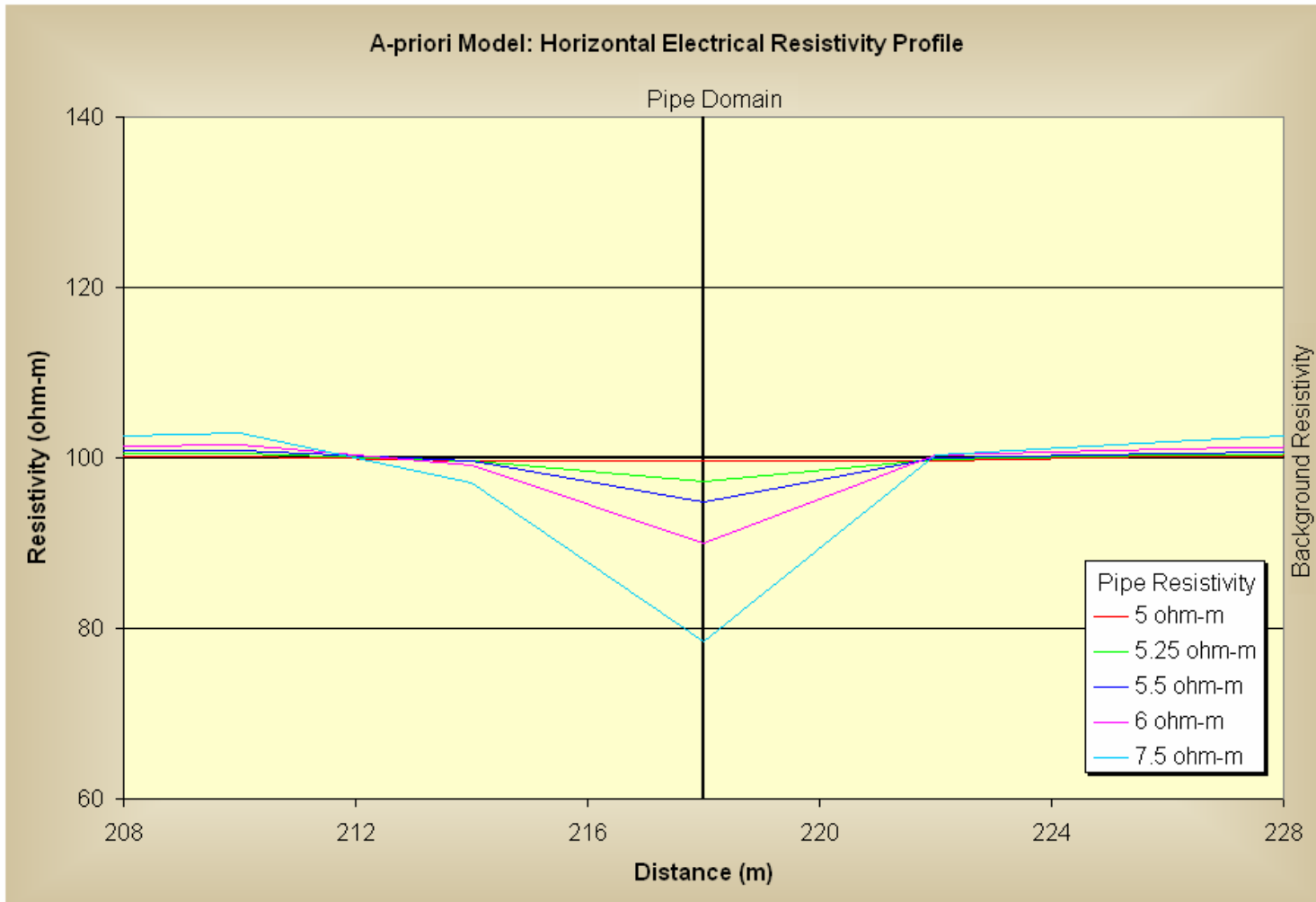
Figure C.4: Horizontal Electrical Resistivity Invert *a-priori* Inversion Model – Higher Resistivity
Background Resistivity: 100 ohm-m, Electrode Spacing: 8 m, Pipe Location: 218 m

APPENDIX D

Horizontal Electrical Resistivity *A-priori* Inversion Model with the Wenner Method
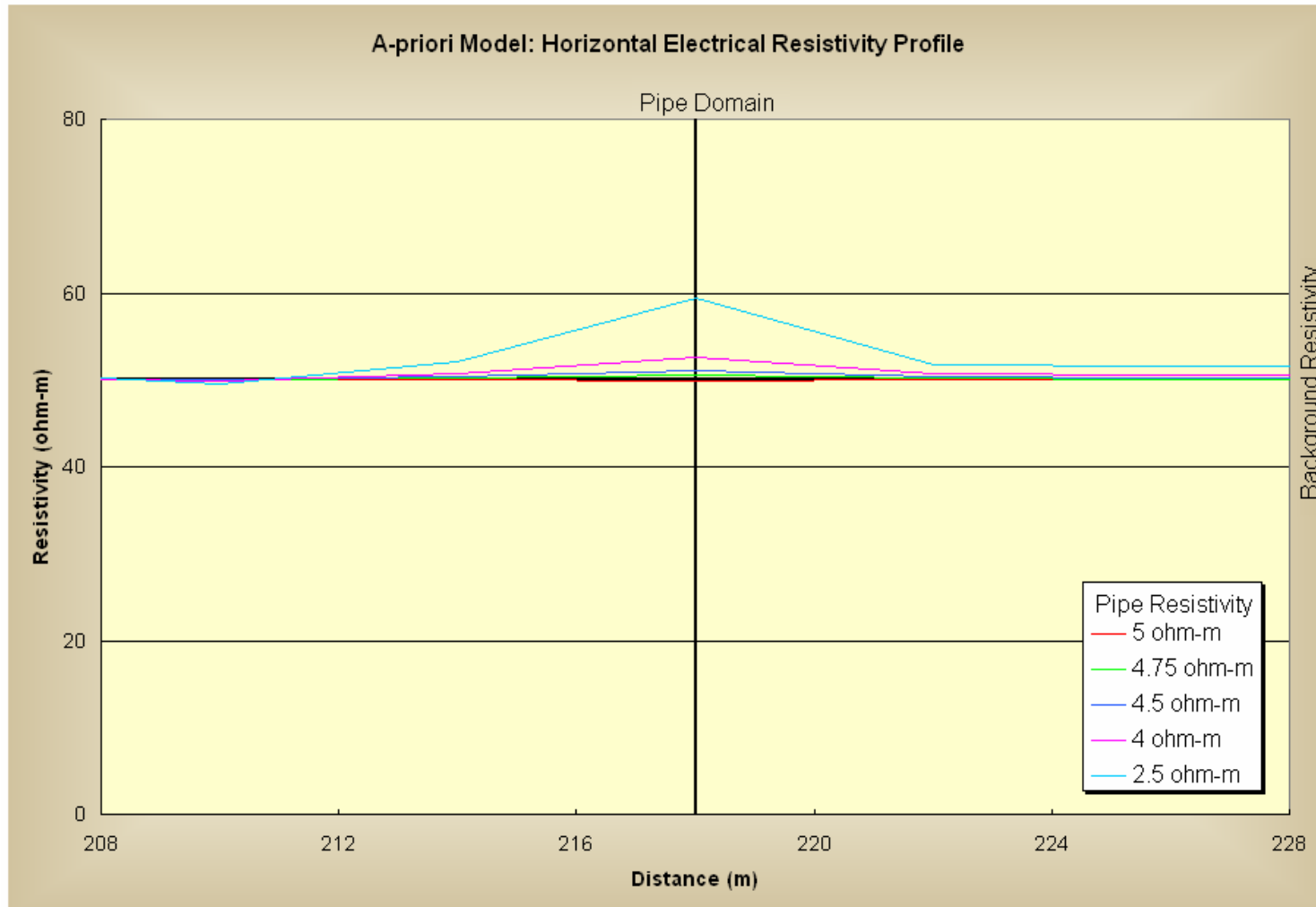
Figure D.1: Horizontal Electrical Resistivity Invert *a-priori* Inversion Model – Lower Resistivity
Background Resistivity: 50 ohm-m, Electrode Spacing: 8 m, Pipe Location: 218 m
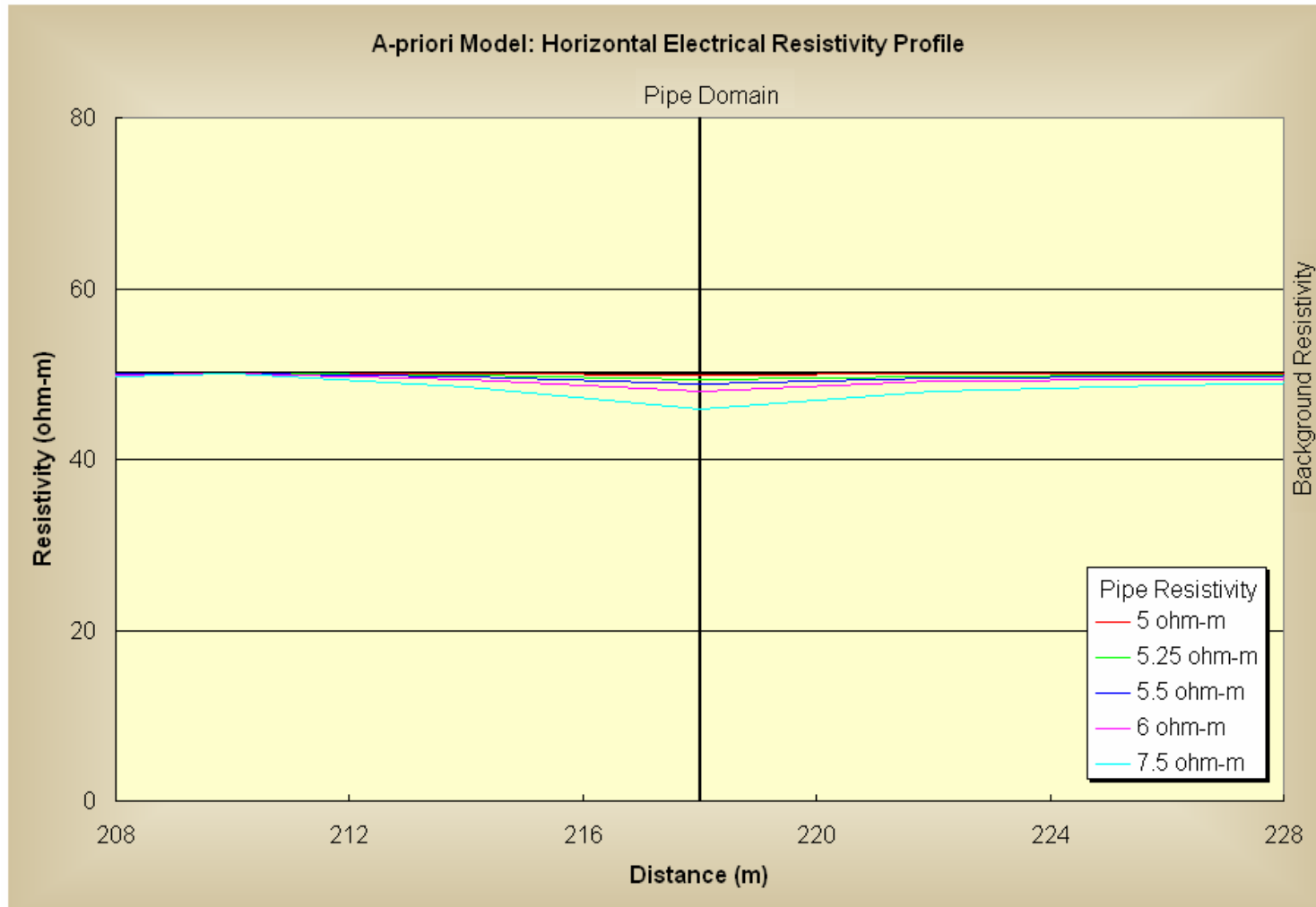
Figure D.2: Horizontal Electrical Resistivity Invert *a-priori* Inversion Model – Higher Resistivity
Background Resistivity: 50 ohm-m, Electrode Spacing: 8 m, Pipe Location: 218 m

Figure D.3: Horizontal Electrical Resistivity Invert *a-priori* Inversion Model – Lower Resistivity
Background Resistivity: 100 ohm-m, Electrode Spacing: 8 m, Pipe Location: 218 m

Figure D.4: Horizontal Electrical Resistivity Invert *a-priori* Inversion Model – Higher Resistivity
Background Resistivity: 100 ohm-m, Electrode Spacing: 8 m, Pipe Location: 218 m

APPENDIX E

Vertically Averaged Horizontal Electrical Resistivity Profiles of the Field Data
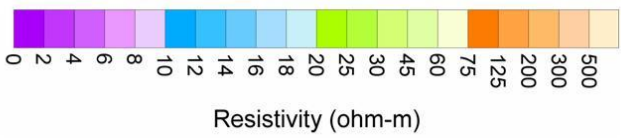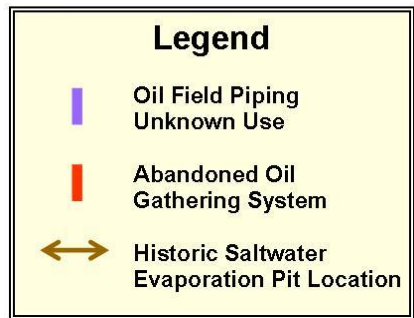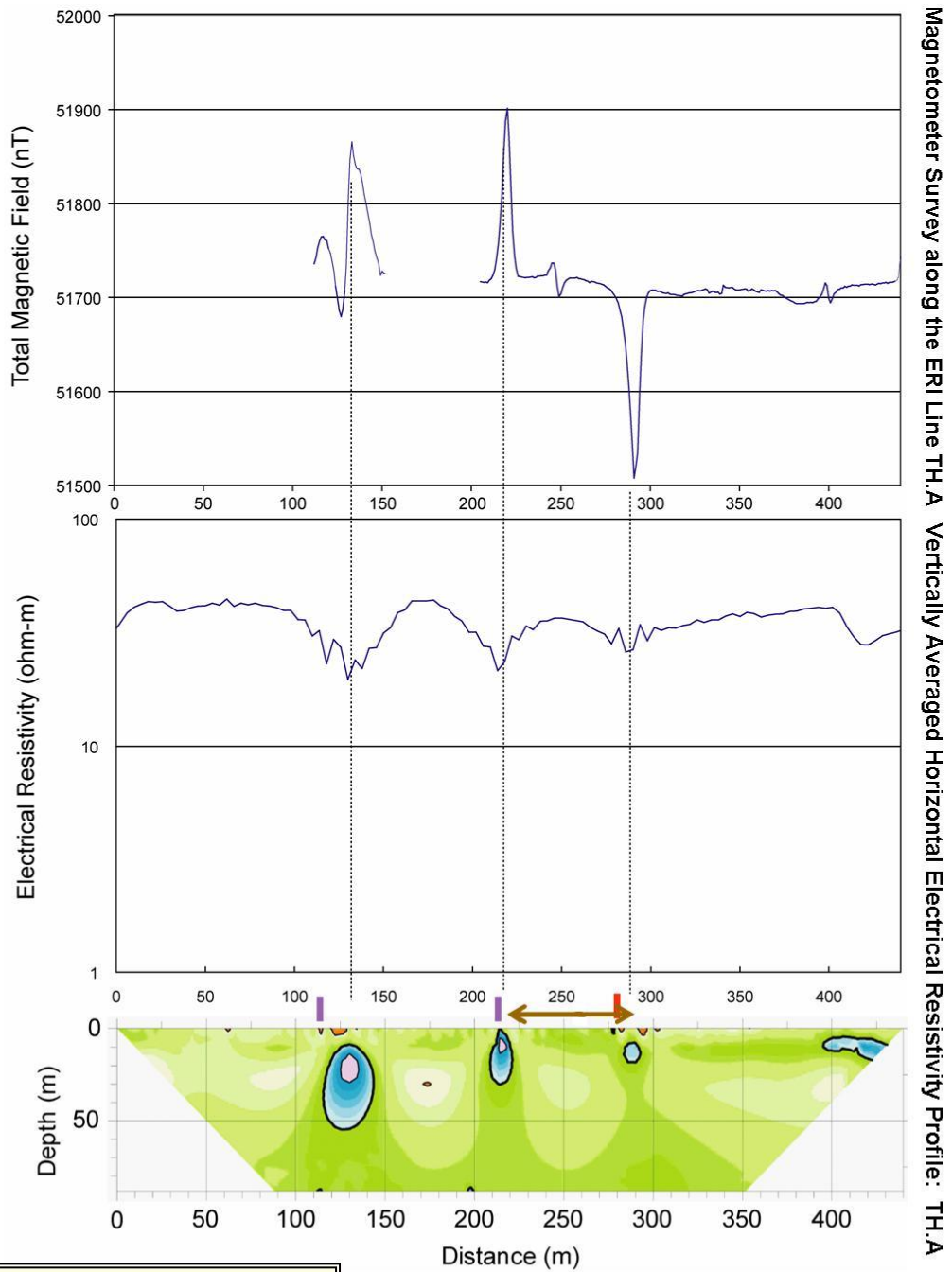
Figure E.1: Vertically Averaged Horizontal Electrical Resistivity Profile of TH.A
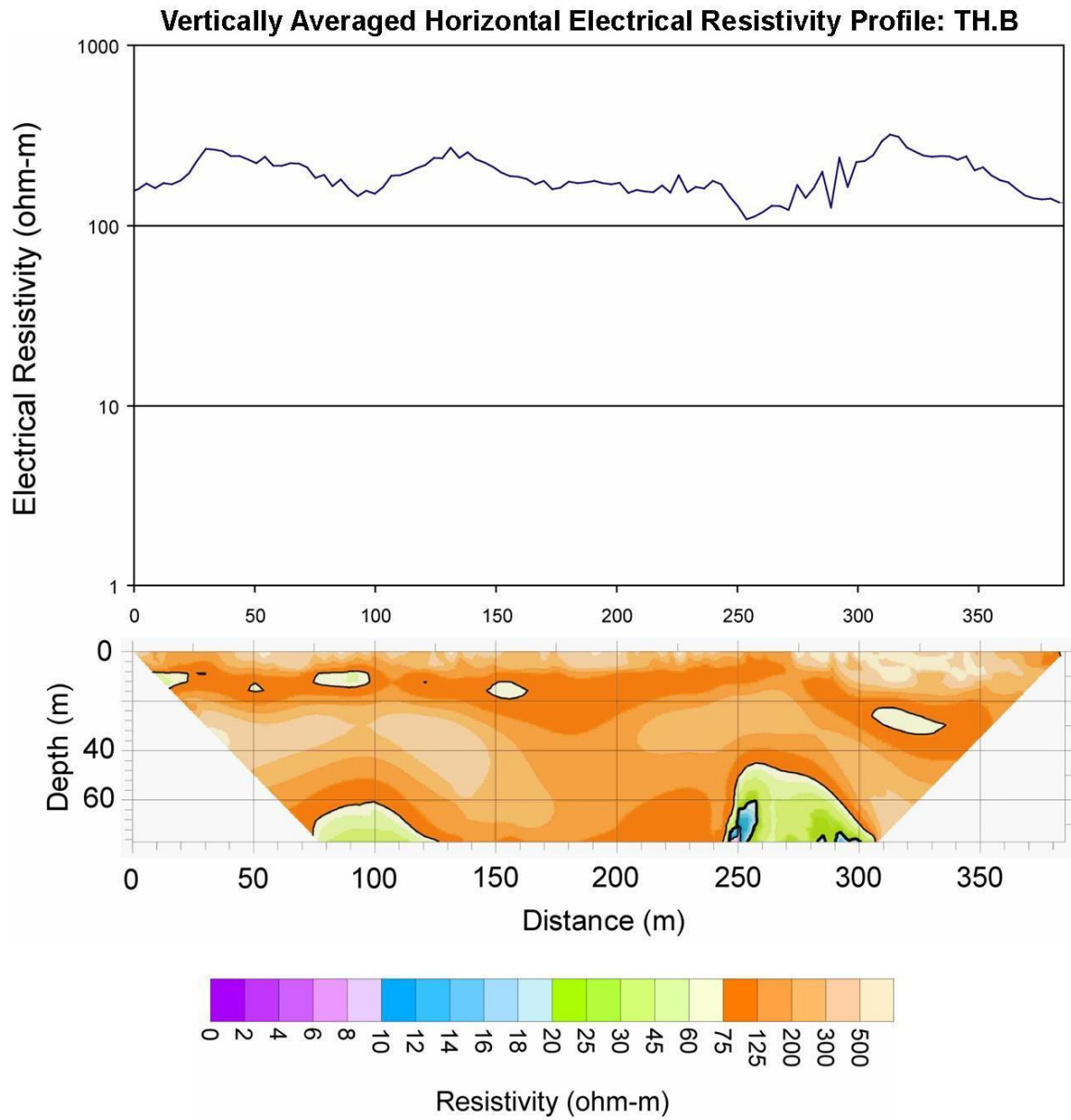
Figure E.2: Vertically Averaged Horizontal Electrical Resistivity Profile of TH.B
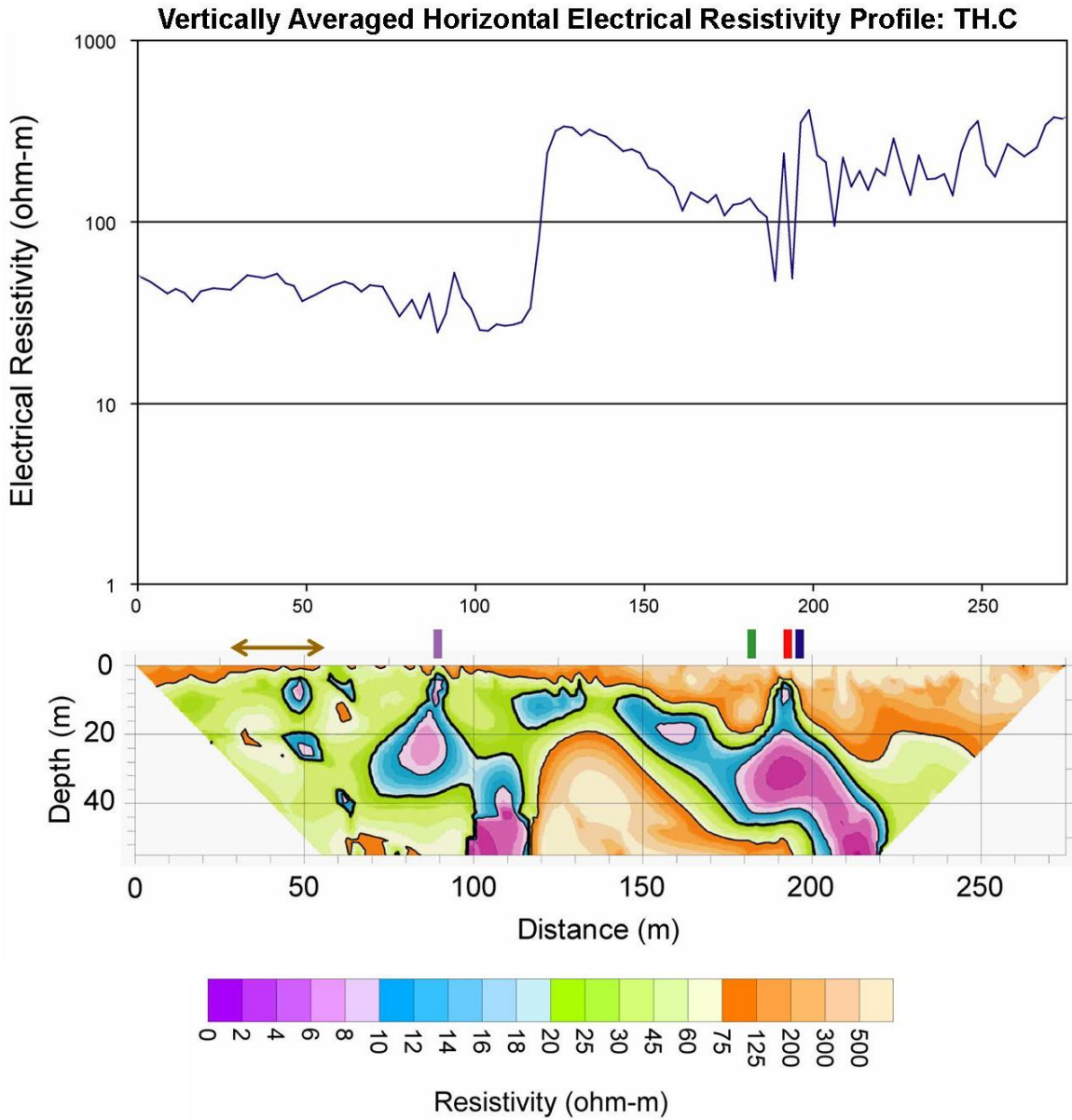
Figure E.3: Vertically Averaged Horizontal Electrical Resistivity Profile of TH.C
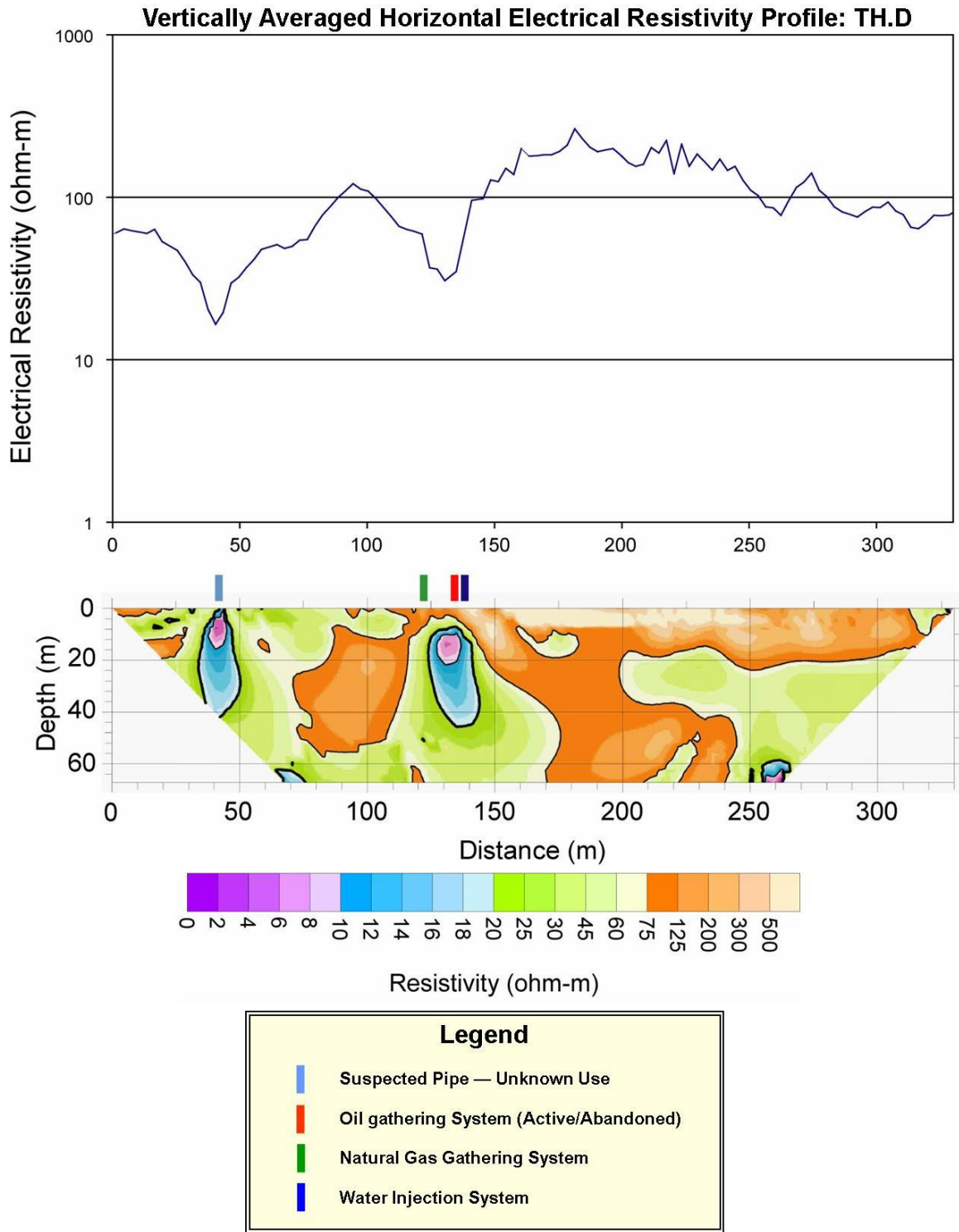
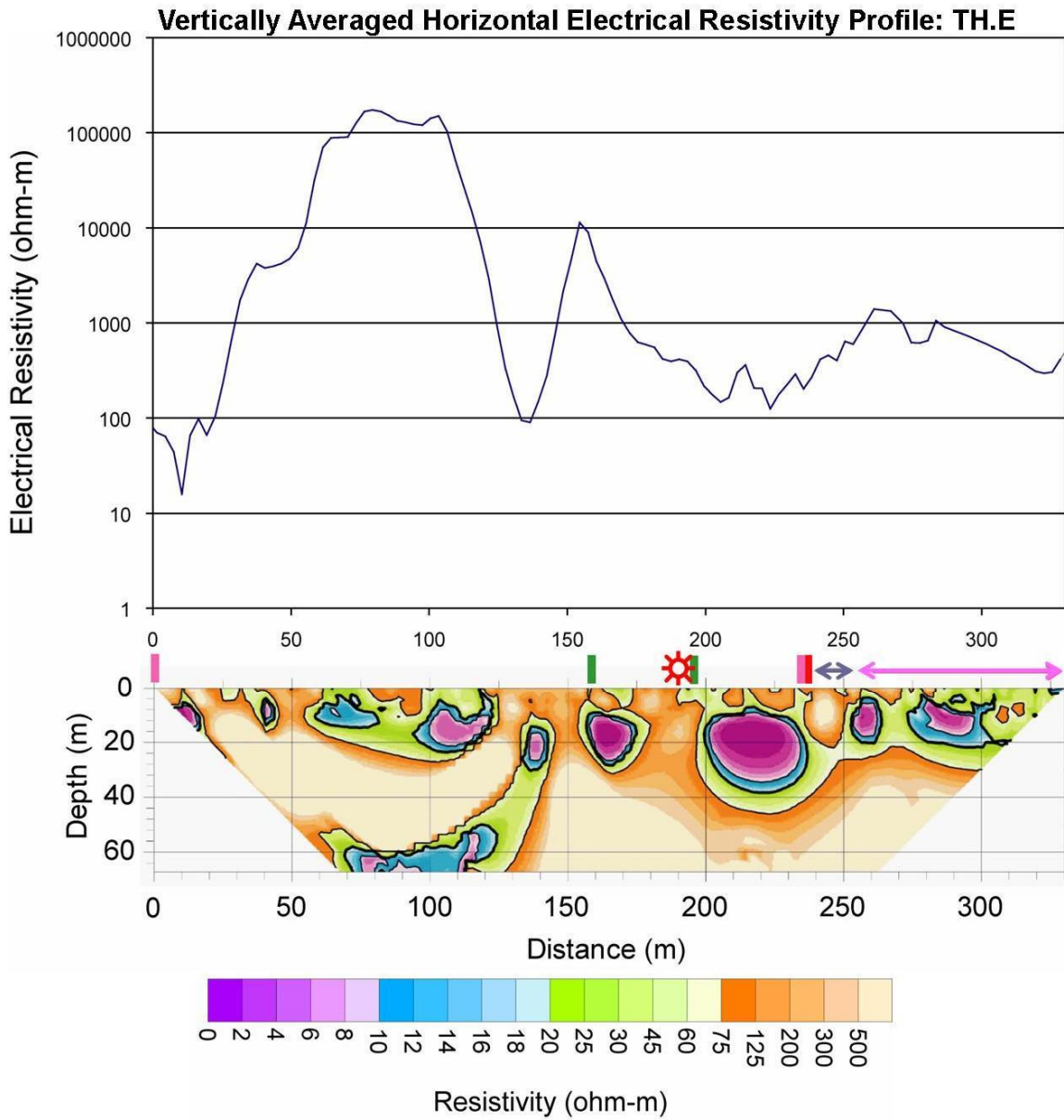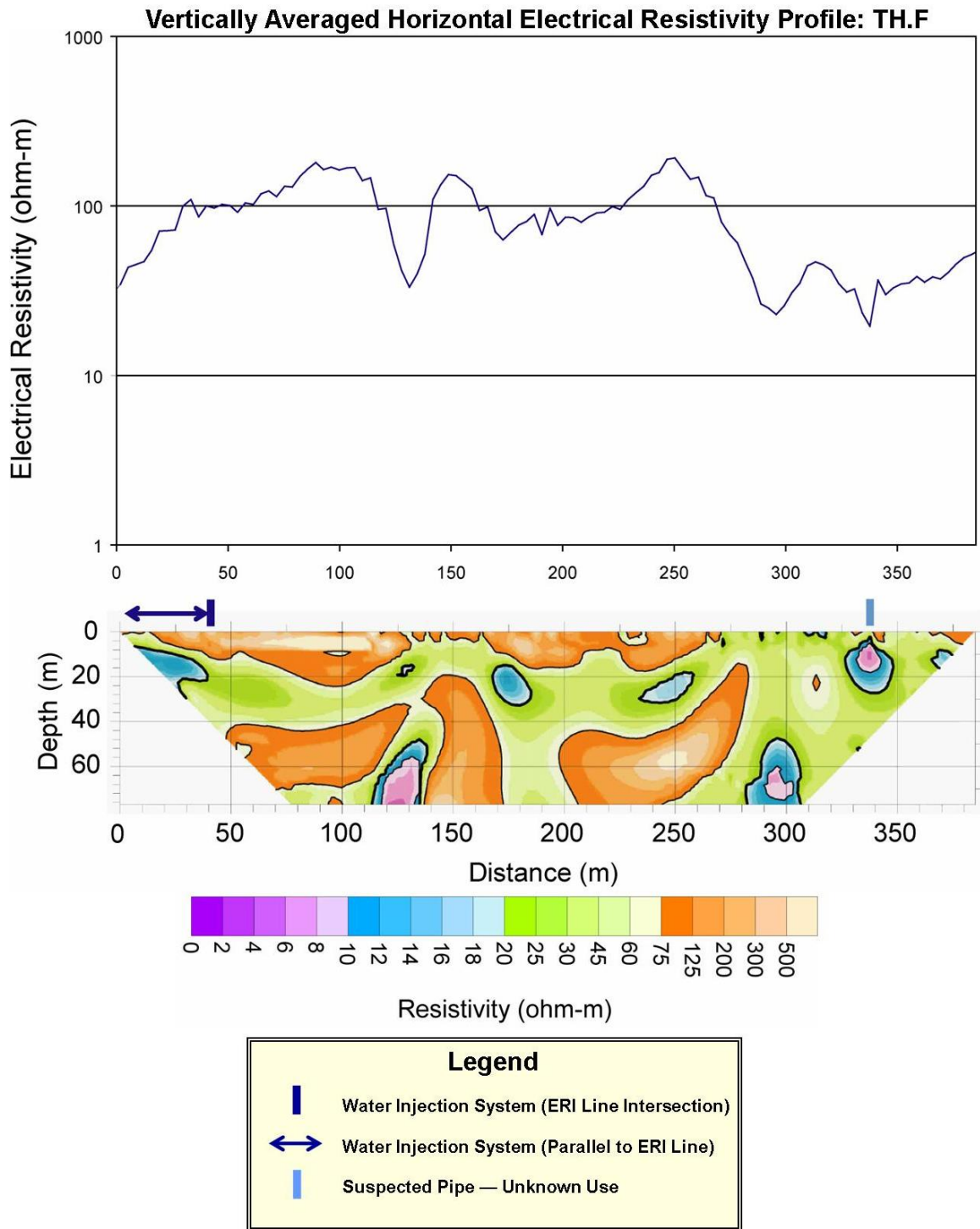**Figure E.4: Vertically Averaged Horizontal Electrical Resistivity Profile of TH.D**

Figure E.5: Vertically Averaged Horizontal Electrical Resistivity Profile of TH.E

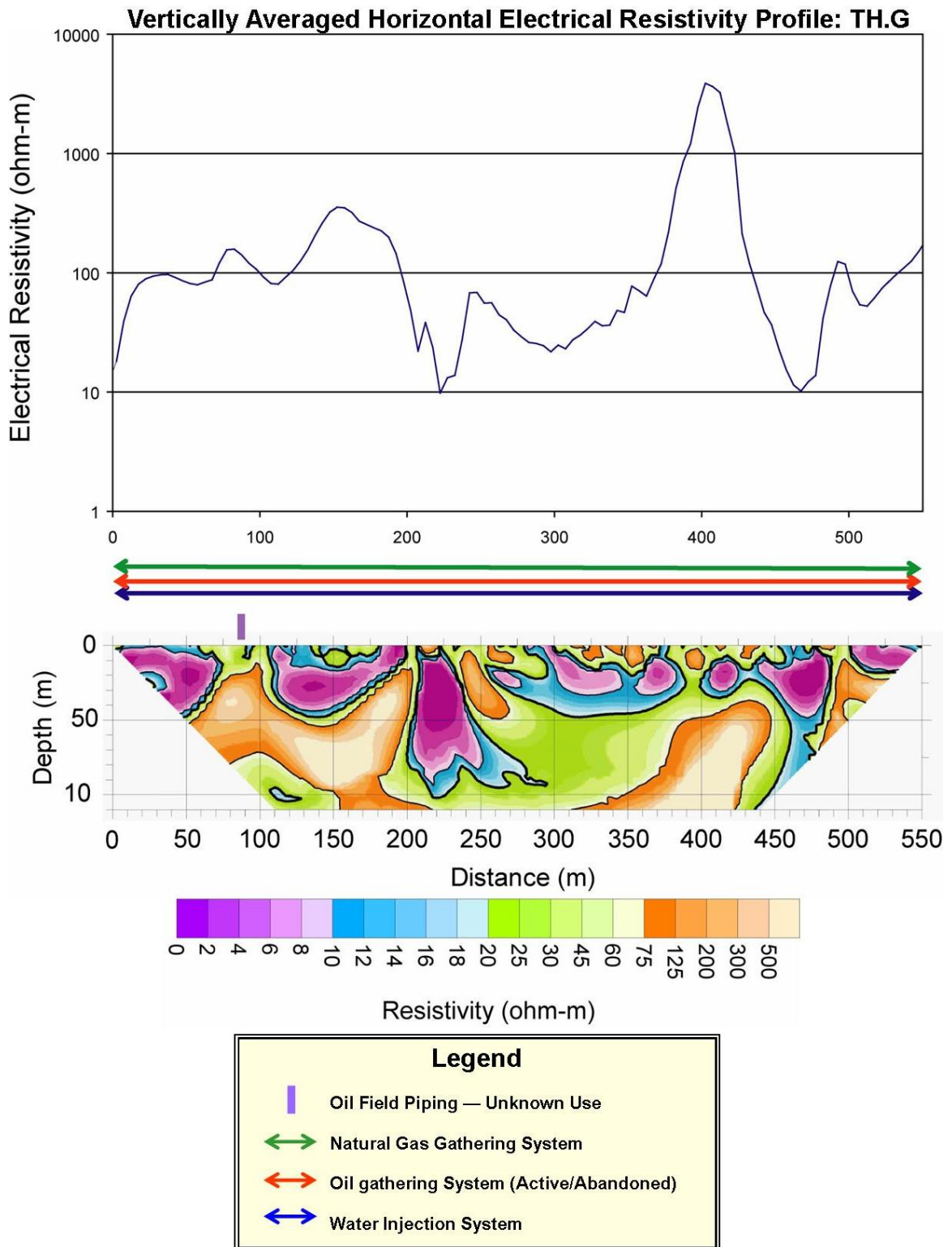**Figure E.6: Vertically Averaged Horizontal Electrical Resistivity Profile of TH.F**

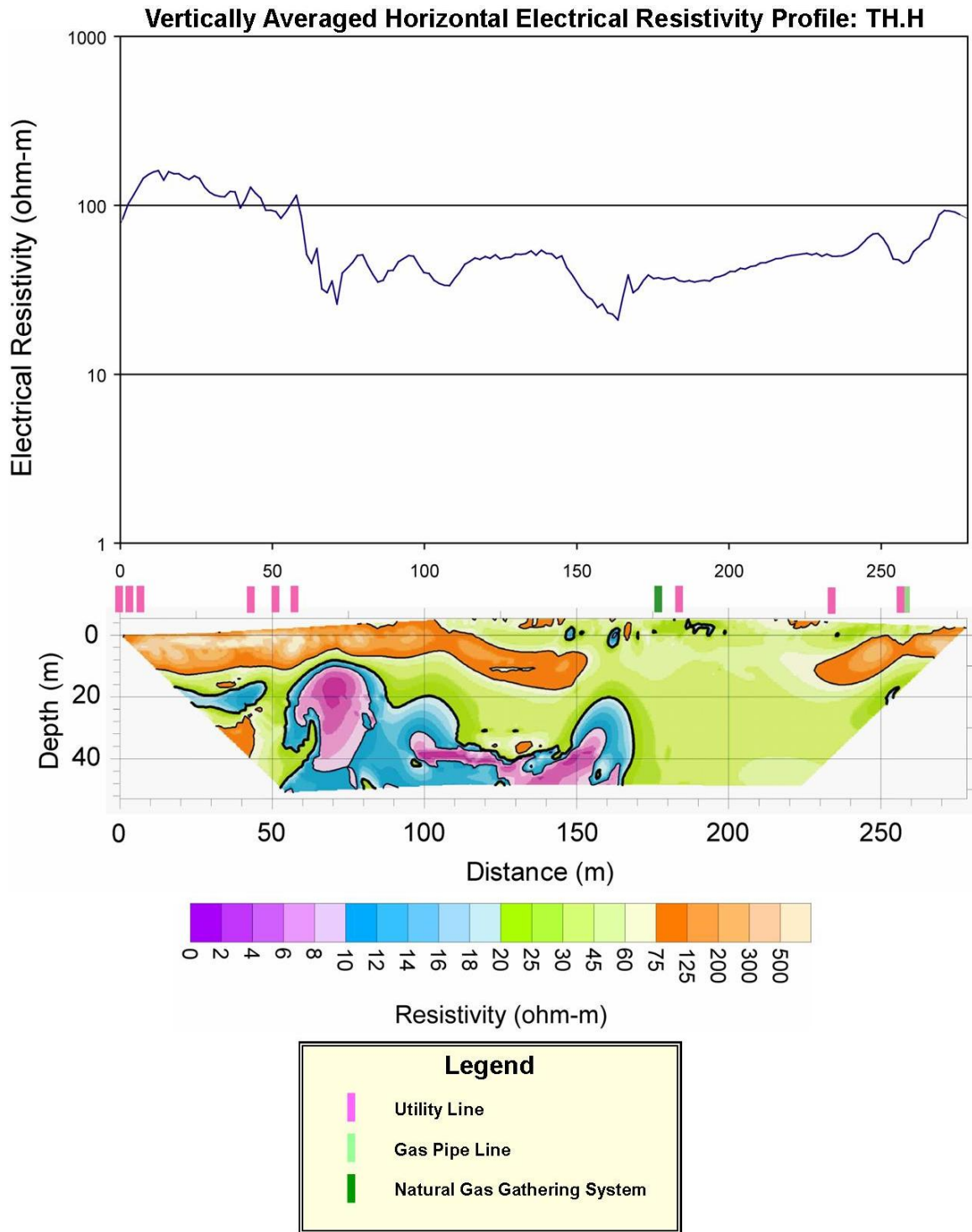**Figure E.7: Vertically Averaged Horizontal Electrical Resistivity Profile of TH.G**

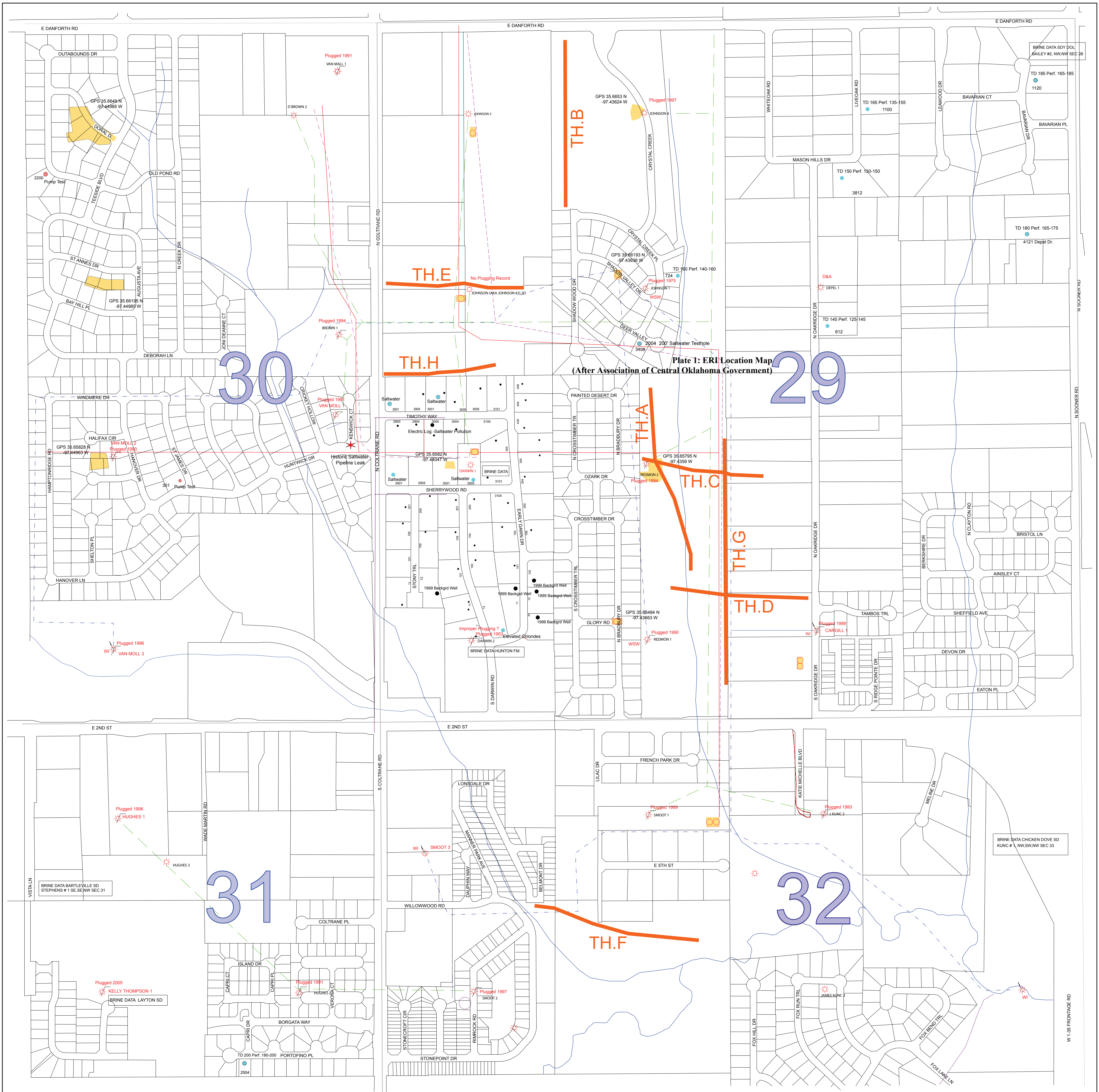**Figure E.8: Vertically Averaged Horizontal Electrical Resistivity Profile of TH.H**
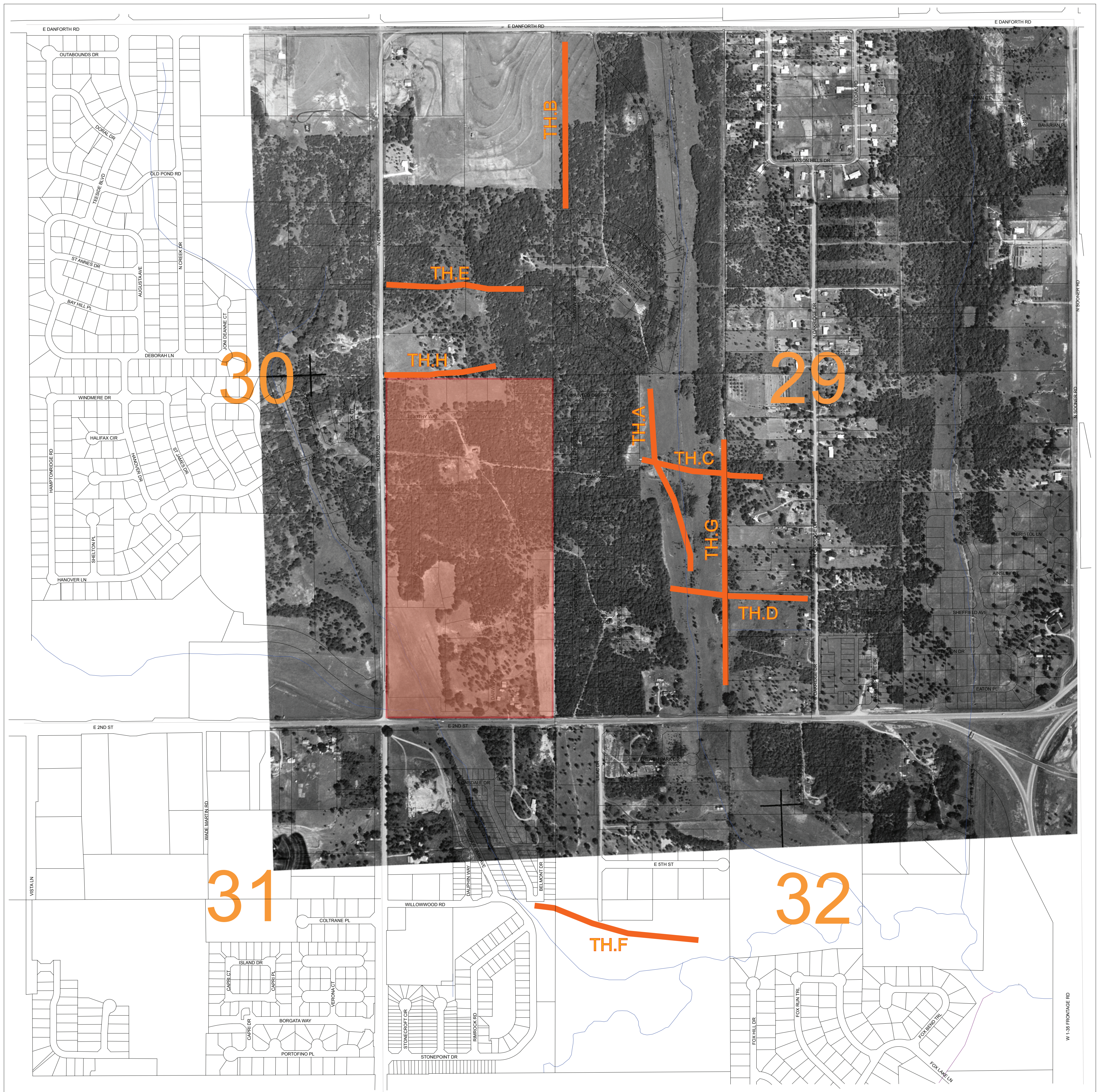
Plate 1: ERI Location Map
(After Association of Central Oklahoma Government)

Legend:

- Abandoned Oil gathering system
- Water Injection System
- Naturall Gas Gathering System
- Active Oil Gathering System
- ERI Survey Line (TH.A ~ TH.H)
- Production Facility (Active/Abandoned)
- Historic Saltwater Evaporation Pit Location
- Confirmed Saltwater Contamination
- Location of Historical Surface Spill
- Thunderhead Hills Addition

0   1000   2000
FEET

N

Plate 1: ERI Location Map
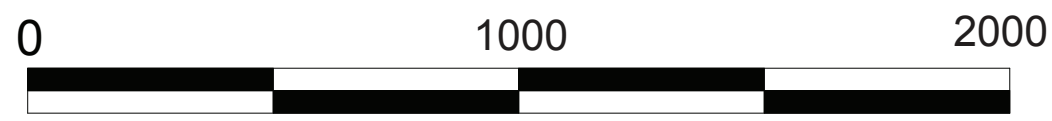**(After Association of Central Oklahoma Government)**

Plate 2: ERI Location with Aerial Photo from 1965
(Aerial Photo supplied by Ace Aerial Photo, OK)

Aerial Photo Taken: 1965

Legend:

ERI Survey Line (TH.A ~ TH.H)

Thunderhead Hills Addition

30

29

TH.B

TH.E

TH.H

TH.A

TH.C

TH.G

TH.D

31

32

TH.F

Aerial Photo Taken: 1-14-2006

Legend:

ERI Survey Line (TH.A ~ TH.H)

Thunderhead Hills Addition

| 30 | 29 |
| 31 | 32 |

0   1000   2000

FEET

N

Plate 3: ERI Location with Aerial Photo from 2006
(Aerial Photo Supplied by Ace Aerial Photo, OK)
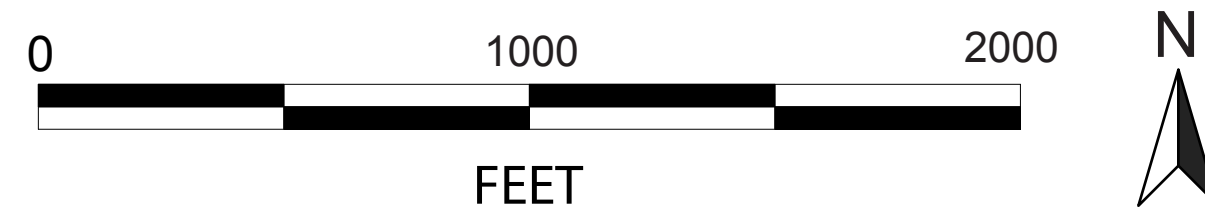
VITA

Emiko Konishi

Candidate for the Degree of

Master of Science

Thesis: USE OF ERI TO FIND THE SOURCE OF SALINE IMPACTS IN EDMOND, OKLAHOMA

Major Field: Geology

Biographical:

Personal Data: Born in Tokyo, Japan, on December 24, 1981, the daughter of Yasutaka and Terumi Konishi

Education: Graduated from Kaichi Gakuen High School, Saitama, Japan in March 2000. Received Bachelor of Science degree in Geology from Oklahoma State University, Stillwater, Oklahoma in December 2004. Completed the requirements for the Master of Science degree with a major in Geology at Oklahoma State University in 2007.

Experience: Employed by Oklahoma State University, Stillwater, OK from January 2007 to December 2007 as a graduate teaching laboratory assistant, from May 2006 to December 2006 as a graduate research assistant, and from January 2004 to May 2007 as a graduate teaching assistant in the Department of Geology.

Professional Memberships: American Association of Petroleum Geologists, Golden Key International Honour Society, The Honor Society of Phi Kappa Phi, The Geological Society of America, The Society of Sigma Gamma Epsilon

Name: Emiko Konishi   Degree: December, 2007

Institution: Oklahoma State University   Location: Stillwater, Oklahoma

Title of Study: USE OF ERI TO FIND THE SOURCE OF SALINE IMPACTS IN
                EDMOND, OKLAHOMA

Pages in Study: 185   Candidate for the Degree of Master of Science

Major Field: Geology

Abstract: Major portions of Edmond, Oklahoma were once covered by oilfields. The
    rapid urbanization of Edmond has caused residential and commercial areas to expand
    over former oil and gas exploration sites. The residential areas have found salt water
    contamination in water supply wells at 150 feet depth. Electrical Resistivity Imaging
    (ERI) was selected as a primary sampling method in this investigation because of its
    portable, economical, and practicable advantages in an urban area. In this study,
    several ERI lines were collected to determine how efficiently advanced ERI
    techniques can delineate the extent and cause of impacted ground water, which may
    be caused by previous and/or active petroleum activities, specifically salt water floods
    and the piping that is used as part of these systems. In addition to the field surveys,
    the forward models are employed to determine anticipated pipe patterns in ERI
    datasets. The results of the forward models were applied into the field data with
    known and unknown pipe locations.

    The ERI survey method was a practical technique to determine anomalous regions of
    the subsurface that have either higher resistivities or lower resistivities than
    surrounding formation materials. However, this method could not immediately
    confirm the composition and/or cause of specific anomalies (i.e., whether anomalies
    are caused by variations in geology/lithology, moisture content changes or other
    naturally occurring heterogeneities; or if they are caused by the presence of impacts
    to soils/groundwater in the subsurface). The resistivity models indicated that
    conductive features (i.e. metal pipe, utilities, and saline fluid) in subsurface could be
    located and distinguished by application of forward and *a-priori* inversion models.

ADVISER'S APPROVAL: Dr. Todd Halihan